STATISTICAL DELAY AND ERROR-RATE BOUNDED QOS PROVISIONING FOR MURLLC OVER 6G MOBILE WIRELESS NETWORKS

A Dissertation

by

JINGQING WANG

Submitted to the Graduate and Professional School of
Texas A&M University
in partial fulfillment of the requirements for the degree of

DOCTOR OF PHILOSOPHY

Chair of Committee,	Xi Zhang
Committee Members,	Erchin Serpedin
	I-Hong Hou
	Andrew Jiang
Head of Department,	Miroslav Begovic

December 2022

Major Subject: Computer Engineering

ABSTRACT

To support increasing demands for real-time multimedia mobile wireless-network data transmissions, there have been considerable the efforts and initiatives from academia, industry, and standard bodies toward guaranteeing very stringent quality-of-service (QoS) requirements, including tightly-bounded end-to-end delay, super-reliability, etc., when designing the next generation mobile wireless networks. Towards this end, massive Ultra-Reliable Low-Latency Communications (mURLLC), as one of the 6G standard traffic services, have received tremendous research attention, while raising several major design issues, including massive connectivity, ultra-low latency, super-reliability, and high energy efficiency. Several promising 6G enablers, such as statistical delay and error-rate bounded QoS provisioning, cell-free (CF) massive multi-input-multi-output (m-MIMO), simultaneous wireless information and power transfer (SWIPT), millimeter wave (mmWave) and Terahertz (THz) band communications, etc., have been developed to support mURLLC. Specifically, due to potential benefits of favorable propagation and channel hardening, CF m-MIMO can significantly enhance QoS performance in terms of achievable data rate and energy efficiency. Moreover, small-packet data communication techniques, such as finite blocklength coding (FBC), has been proposed to support various massive access techniques for reducing access latency and decoding complexity at the receivers while guaranteeing stringent QoS requirements of 6G mURLLC for time-sensitive wireless services. However, how to efficiently integrate the above new techniques for statistical delay and error-rate bounded QoS provisioning in the finite blocklength regime is still a challenging and open problem. In addition, However, how to rigorously and efficiently characterize the stochastic dynamics in terms of statistically upper-bounding FBC-based *both delay* and *error-rate* QoS metrics has been neither well understood nor thoroughly studied before.

To effectively overcome the above-mentioned challenges imposed in supporting 6G mURLLC, in this dissertation we propose to develop the FBC based statistical delay and error-rate bounded QoS provisioning schemes over 6G mobile wireless networks for mURLLC traffic. In particular,

we propose to integrate various 6G promising techniques, such as CF m-MIMO, SWIPT, mmWave and THz-band communication, with FBC for guaranteeing statistical delay and error-rate bounded QoS provisioning. We develop analytical modeling frameworks and controlling mechanisms for statistical delay and error-rate bounded QoS provisioning in the non-asymptotic regime. In addition, we develop a set of new statistical delay and error-rate bounded QoS metrics including delay-bound-violation probability, QoS-exponent function, and the ϵ-effective capacity using FBC over 6G mobile wireless networks. The obtained numerical and simulation results validate and evaluate our proposed schemes for statistical QoS in supporting mURLLC.

ACKNOWLEDGMENTS

First of all, I would like to express my deep appreciation to my Ph.D. advisor Professor Xi Zhang for his guidance and contribution to this research. Without his visionary guidances, deep insights, and the offers of various funding supports, this dissertation would not have been possible. His commitment to top-quality research work through the rigorous efforts impressed me most and will motivate me for my future career. He gives students freedom to conduct research while providing necessary help. Furthermore, he is willing to share his knowledge and career experience with me and encourage me whenever needed.

I would like to express my gratitude to the dissertation committee members, Professor Erchin Serpedin, Professor I-Hong Hou, and Professor Andrew Jiang. I greatly appreciate their precious time and efforts. Their valuable comments and suggestions help me improve the quality of this dissertation.

Furthermore, I would also like to take this opportunity to sincerely thank all my friends and fellow students at Texas A&M University for making my life in College Station enjoyable and memorable. Especially, I would like to express my sincere appreciation to Qixuan Zhu for her friendship, helpful discussion, and kind help on my research. I am also grateful to the Networking and Information Systems Laboratory, Department of Electrical and Computer Engineering, and College of Engineering of Texas A&M University, which have contributed in the academic programs and the excellent research environments.

Finally, but most importantly, this dissertation is dedicated to all of my family members and my parents for their infinite love and support.

The funding for this research was supported in part by Professor Xi Zhang's U.S. National Science Foundation CAREER Award under Grant ECCS-0348694, and his other U.S. National Science Foundation Grants including: CCF-2008975, ECCS-1408601, and CNS-1205726, and his U.S. Air Force Grant: FA9453-15-C-0423.

CONTRIBUTORS AND FUNDING SOURCES

Contributors

This work was supported by a dissertation committee consisting of Professor Xi Zhang, Professor Erchin Serpedin, and Professor I-Hong Hou of the Department of Electrical and Computer Engineering and Professor Andrew Jiang of the Department of Computer Science and Engineering.

All other work conducted for the dissertation was completed by the student independently.

Funding Sources

Graduate study was supported by the Dr. R. K. Pandey and Christa U. Pandey'84 Fellowship and Advanced Study Heep Fellowship from Texas A&M University. Graduate study was supported in part by the U.S. National Science Foundation under Grants CCF-2008975, ECCS-1408601, and CNS-1205726, and the U.S. Air Force under Grant FA9453-15-C-0423. Graduate study was also supported in part by the U.S. National Science Foundation under Grants CCF-0939370 and CCF-1908308.

TABLE OF CONTENTS

Page

LIST OF FIGURES

FIGURE Page

1. INTRODUCTION

1.1 Background and Motivations

While 5G mobile wireless networks are being widely deployed around the world, researchers have begun to conceptualize 6G mobile wireless networks to support the unprecedented scenarios with extremely diverse and challenging quality of service (QoS) requirements. Due to the stochastic nature of wireless fading channels, it is challenging to guarantee both reliability and low-latency requirements for delay-sensitive wireless multimedia services over 6G mobile wireless networks. Traditionally, researchers have developed a deterministic network calculus to derive explicit guarantees on the maximum delay for wireless data transmissions. However, deterministic network calculus is not sufficient for characterizing the wireless traffics due to time-varying and stochastic natures of wireless fading channels.

Towards this way, the delay-bounded QoS theory [1–14] has been proposed and developed to characterize queueing behaviors in supporting explosively growing demands of time-sensitive wireless multimedia applications over 5G and the upcoming 6G mobile networks which are defined and detailed in [15–17]. Due to the highly time-varying nature of wireless fading channels, researchers have proposed the concept of *statistical QoS provisioning* [8, 18–22], in terms of effective capacity [12] and delay-bound violation probabilities, in supporting delay-sensitive multimedia wireless services over mobile wireless networks. Accordingly, how to further extend and integrate the statistical QoS theory with the emerging wireless techniques to efficiently support and implement the very stringent QoS requirements for mURLLC in 6G wireless networks, including extra-tighter delay bound (< 1 ms), super-reliability ($> 99.99999\%$), super-high spectrum and energy efficiencies, etc., has imposed many new challenging but unsolved problems, which cannot be tackled with traditional techniques.

1.1.1 Statistical Delay and Error-Rate Bounded QoS for mURLLC in the Finite Blocklength Regime

As a new and dominating 6G mobile-networks' service class for time-sensitive traffics, *massive ultra-reliable and low latency communications* (mURLLC) [15, 23–26], which integrate URLLC with massive access, also known as massive connectivity or machine-type communications (mMTC) as one of the main use-cases of 6G wireless networks, require the *massive short-packet data communications* to support time-sensitive 6G wireless multimedia services with high wireless-resource efficiency and low access latency [27]. The major design issue raised by mURLLC is how to support latency-sensitive multimedia transmissions while guaranteeing the reliability bound overtime-varying wireless channels. This implies that the traditional Shannon's theorem with infinite blocklength is no longer feasible under 6G standards. Motivated by this observation, considering finite blocklength data transmissions with non-vanishing decoding error probability, *finite blocklength coding* (FBC) [28–31] has been proposed to support various massive access techniques while reducing the access latency and guaranteeing stringent QoS requirements.

Towards this end, we have developed the statistical QoS provisioning schemes over 6G wireless networks to apply FBC technique for supporting low-latency, reliable-connectivity, and high-scalability requirements by using *short-packet data transmissions* for supporting 6G wireless real-time services [32]. In particular, the maximum achievable coding rate using FBC over additive white Gaussian noise (AWGN) channels has been derived in [33]. The authors of [34] have derived the goodput over AWGN channels and the energy-efficiency spectral-efficiency tradeoff by using recent results of non-asymptotic coding rate. The maximum achievable data rates using FBC over quasi-static multiple-input multiple-output (MIMO) based wireless fading channels with and without the knowledge of channel state information (CSI) have been derived in [35]. The authors of [31] have investigated different properties of channel codes for a given memoryless wireless channel with a non-vanishing decoding error probability. However, although small-packet communications used in FBC-based wireless mobile networks are usually employed for massive access to reduce access latency and decoding complexity, how to upper-bound the decoding error proba-

bility while supporting 6G mURLLC is still a challenging research topic.

Furthermore, there have been a great deal of research works focusing on investigating the QoS controlling mechanisms as well as the performance analyses while guaranteeing the stringent URLLC requirements. The authors of [15] have presented the vision of 6G wireless networks and proposed a new set of service classes and expose their target 6G performance requirements for mURLLC. However, previous research works focus on investigating QoS metrics and controlling mechanisms in terms of the delay-bound violating probability without considering the non-vanishing decoding error probability, which has become a major design issue when designing the next generation wireless network architecture models in supporting mURLLC services. It is crucial to design and measure wireless network architecture models considering both delay and error-rate bounded QoS constraints by defining and identifying new statistical QoS metrics and their analytical relationships, such as delay-bound violation probability, effective capacity, error probability, outage capacity, etc., especially in practical scenarios using FBC. Unlike mechanisms to guarantee the statistical bounded-delay or average delay, how to model statistical delay and error-rate bounded QoS provisioning for a given constrained decoding error probability in the non-asymptotic regime, for supporting 6G mURLLC traffic has not been sufficiently resolved.

1.1.2 Emerging 6G Techniques in Supporting mURLLC

Various advanced 5G beyond and 6G techniques, such as cell-free (CF) massive MIMO (m-MIMO) [36–38], simultaneous wireless information and power transfer (SWIPT) [39, 40], millimeter wave (mmWave) and Terahertz (THz) band communications [41, 42], etc., have been designed to play critically important roles for mURLLC in terms of connecting massive number of mobile devices without imposing congestions, while guaranteeing very stringent QoS requirements, including tightly-bounded end-to-end delay, super-reliability, etc.

1.1.2.1 CF M-MIMO System

To support the massive access imposed by mURLLC, CF m-MIMO [37], where the geographically distributed APs jointly serve a massive number of mobile devices using the same time-

frequency resources, has been developed as a promising 6G network architecture for improving the access reliability while reducing the co-channel interference caused by traditional m-MIMO systems. Traditionally, the optimal power control is performed at the central processing unit (CPU). However, the centralized power-control strategies may jeopardize the system scalability and violate mURLLC requirements as the numbers of APs and mobile users grow significantly. The authors of [43] have proposed scalable and distributed power control policies for CF m-MIMO systems to achieve system scalability and mURLLC as the number of mobile users goes to infinity. The authors of [44] have developed new framework for scalable CF m-MIMO systems, where the complexity and signalling at each AP is finite when connecting a massive number of mobile devices. The system scalability aspects of CF m-MIMO system are analyzed in [45] and a solution is proposed for data processing, network topology, and power control. There are many new challenges, including the channel characteristics, stochastic networking behaviors, and user associations, etc., as compared with traditional m-MIMO systems. It is crucial to design and characterize the delay and reliability performances of the CF m-MIMO system for statistical delay and error-rate bounded QoS provisionings for supporting mURLLC in the finite blocklength regime.

1.1.2.2 SWIPT-Based CF M-MIMO System

One of the challenges that can potentially limit the widespread deployment of mURLLC-enabled 6G wireless networks is the constrained power/battery supply of the mobile devices. To solve this problem, taking advantage of the broadcast nature of radio frequency (RF) wave propagation, SWIPT, which transfers both information and power simultaneously to the mobile devices, has recently gained significant research attention since it can prolong the battery-life of energy-constrained and low-power-supported mobile devices. Unlike in the information and energy transmissions separated receivers, researchers have developed two main low-complexity co-located receiver structures, i.e., the power-splitting (PS) receiver and the time-switching (TS) receiver for enabling SWIPT. In the PS receiver, the power and information transfer to the co-located energy harvesting (EH) and information decoding receivers are simultaneously achieved via a set of power splitting devices. On the other hand, each transmission block is split into two orthogonal time-slots

for information and energy transmissions in the TS receiver. The authors of [46] have conducted a comprehensive survey of the state-of-art techniques based on advances and open issues imposed by SWIPT. The authors of [47] have analyzed the fundamental tradeoff between transmitting energy and information over a single noisy line. In addition, ultra reliable cooperative short packet communication schemes have been investigated in [48] with wireless power transfer (WPT) to support mURLLC.

One of the major bottlenecks for implementing SWIPT is the low harvested energy levels due to the inherent severe end-to-end path-loss at the receiver. Towards this end, the application of conventional co-located m-MIMO techniques, where a large number of collocated antennas are deployed for each AP to simultaneously serve many mobile users in the same time-frequency resource, can enhance the performance of SWIPT in terms of the achievable data rate and energy efficiency due to its benefits of favorable propagation, channel hardening, and aggressive spatial multiplexing gains. In addition, in distributed m-MIMO systems, service antennas are spread out over a large area, which provide with significantly higher probability of coverage than the conventional collocated m-MIMO systems, at the cost of increased backhaul networks overhead. However, the inter-cell interference is becoming the major bottleneck for m-MIMO systems, especially for the dense mobile wireless networks. To resolve the interference issues in current cellular networks, as one of the promising 6G network architectures, CF m-MIMO has been developed to improve the access reliability of massive access while reducing the co-channel interference caused by traditional m-MIMO systems. One of the important features of CF m-MIMO lies in its operating regime: a huge number of single-antenna APs simultaneously and cooperatively serve a relatively smaller number of mobile users, performing computationally simple signal processing at the APs. Due to the closer distance between the APs and mobile devices, integrating SWIPT with CF m-MIMO systems has a significant potential to offer substantially higher coverage probability while minimizing the throughput/energy outage probabilities as compared with the co-located m-MIMO systems.

However, it is challenging to characterize the stochastic networking/queueing behaviors when

being integrated with SWIPT-enabled CF m-MIMO architecture models while guaranteeing mURLLC under statistical delay and error-rate bounded QoS constraints in the non-asymptotic regime. As a result, how to efficiently integrate SWIPT with CF m-MIMO architecture models and accurately upper-bound the delay-bound violation probability while guaranteeing statistical delay and error-rate bounded QoS provisionings still remains as a challenging and open problem over 6G SWIPT-enabled CF m-MIMO mobile wireless networks in the finite blocklength regime.

1.1.2.3 MmWave and THz-band Communication System

The limited available bandwidth for conventional wireless communication systems in the microwave frequency range motivates the exploration of higher frequency bands in supporting statistical delay-bounded QoS provisioning for real-time wireless services in supporting mURLLC. Spurred by the impressive benefits of mmWave techniques, researchers have extensively studied mmWave communication systems over the last decade. Despite the much higher operation frequency, the available bandwidth is less than 10 GHz, which requires the communication systems to achieve a spectral efficiency on the order of 100 bits/second/Hz for supporting 1 Terabit-per-second (Tbps) for 6G wireless network [49, 50]. However, this is several times above the state-of-the-art for wireless communication systems.

To satisfy the increasing demand for higher-speed wireless communication of current wireless systems, Terahertz (0.1–10 THz) band communications and wireless networks [41, 42] have been widely envisioned as the promising 6G wireless techniques to provide wireless mobile devices with an unprecedentedly large bandwidth, ranging from several tens of GHz up to a few THz, while satisfying the increasing demand of 100 Gbps and even 1 Tbps data rates [51], while efficiently supporting stringent QoS requirements. However, the large pathloss and molecular noise introduced by the THz wireless systems may produce transmission errors during the data transmissions. Such errors may result in distorted multimedia signals received. As a result, it is crucial to apply the FBC technique for short-packet data transmissions to support time-sensitive wireless multimedia services while guaranteeing statistical delay and error-rate bounded QoS provisioning in the THz band.

Motivated by the potential of THz technologies, researchers have focused on leveraging the advantages of nanomaterials, such as graphene [52–55], to implement THz communication systems into a set of applications. There has been a limited number of studies on the channel characterisation of THz-band nano-communication systems, which incorporate molecular absorption, spreading loss, and shadowing into a theoretical THz channel model. The authors of [56] have reviewed the current state-of-the-art technologies and applicability of nano communication in biomedical application. The authors of [57] have shown that the large bandwidth in the THz band is susceptible to shadowing and noise. The joint effects of path loss and shadowing for THz wireless channels have been studied in [58]. The channel modelling of the THz wave propagating and the corresponding channel capacity modelling with different power allocation schemes for electromagnetic communications have been studied in [59]. The channel capacity in the THz band is numerically evaluated by using a new THz-band propagation model with different channel molecular compositions and under different power allocation schemes in [60]. Furthermore, the authors of [61] have proposed a integrated MIMO antenna system with THz communications by applying the graphene-based antennas. The authors of [62] have investigated the uplink spectral efficiency of MIMO systems in large scale MIMO scenario and conventional scale MIMO scenario based on the models of single walled carbon nano tubes (SWCNTs). Although there are some studies of the channel models for nano-scale communications in the THz band, how to accurately model and characterize the relationships among THz-band wireless channel, energy consumption, and EH models employing FBC based nano-communication still remains as a major challenge in the THz band while supporting both delay and error-rate bounded QoS provisioning.

1.1.3 Contributions

In this dissertation, to overcome the above mentioned challenges, we propose FBC-based statistical delay and error-rate bounded QoS provisioning schemes to support mURLLC services over 6G mobile wireless networks. The significant research topics/areas to be explored in details in this dissertation include:

- We develop a set of analytical frameworks and controlling mechanisms for statistical delay and error-rate bounded QoS metrics, tradeoff-functions, and control mechanisms including ϵ-effective capacity, delay-bound-violating probability, QoS-exponents functions, and FBC-based outage-capacity in finite blocklength regime.

- We formulate and solve FBC-based ϵ-effective energy-efficiency maximization problem by using iterative algorithm for our proposed statistical delay and error-rate bounded QoS provisioning schemes.

- Given the constrained decoding error probability, we propose and analyze the delay-violation probability function by applying the Mellin transform over both arrival and service processes, while taking into account the statistical delay and error-rate bounded QoS constraints.

- We derive the optimal resource allocation adaptation policies, which play an important role in the system design and performance analyses for statistical delay and error-rate bounded QoS in the finite blocklength regime.

- We quantitatively characterize the fundamental tradeoff between harvested energy and ϵ-effective capacity and formulate and solve the optimal ϵ-effective capacity-energy tradeoff problems.

1.1.4 Dissertation Organization

The rest of this dissertation is organized as follows: Chapter 2 proposes to apply the Mellin transform to analytically model and characterize stochastic QoS performances in terms of both delay and error-rate for CF m-MIMO modeling schemes in the finite blocklength regime. Chapter 3 integrates the mmWave user-centric cell-free m-MIMO system with FBC-HARQ technique over 6G wireless networks for statistical delay and error-rate bounded QoS provisioning. Chapter 4 proposes and develops statistical delay and error-rate bounded QoS provisioning schemes over SWIPT-enabled CF m-MIMO 6G wireless networks using FBC. Chapter 5 develops FBC-EH based optimal resource allocation policies for self-powered nano devices in the THz band over

wireless nano-networks under statistical delay and error-rate bounded QoS constraints. Chapter 6 summarizes the dissertation and point out future research directions.

2. STATISTICAL DELAY AND ERROR-RATE BOUNDED QOS PROVISIONING FOR MURLLC OVER 6G CF M-MIMO MOBILE NETWORKS IN THE FINITE BLOCKLENGTH REGIME *

2.1 Introduction

The statistical delay-bounded QoS theory [8] as well as stochastic network calculus (SNC) [63] have been proposed as a promising technique to support the explosively growing demands of time-sensitive wireless multimedia applications over 6G mobile wireless networks. Accordingly, the concept of *effective capacity* has been proposed to characterize the statistical delay-bounded QoS provisioning of time-sensitive wireless multimedia applications over 6G mobile wireless networks. In addition, mURLLC has been proposed for supporting time-sensitive traffics with *massive short-packet data communications* over 6G mobile wireless networks. We have integrated the statistical QoS provisioning schemes over 6G wireless networks with the FBC technique [30] for supporting stringent mURLLC requirements, including ultra-low latency, ultra-reliability, and high-scalability by using *short-packet data transmissions* [32]. There have been a great deal of research efforts on applying FBC over 6G mobile wireless networks. However, the problems on how to efficiently employ the unique nature of the FBC techniques for supporting statistical delay and error-rate bounded QoS provisioning have been neither well understood, nor thoroughly studied. Consequently, it becomes increasingly important to develop the modeling frameworks and corresponding analytical techniques for the fundamentally charactering the statistical delay and error-rate bounded QoS provisioning theory.

As a new and dominating type of time/error-sensitive services over 6G wireless networks, mURLLC has attracted substantial research attention while imposing many new challenges not encountered before. Towards this end, various advanced promising 6G techniques, such as the CF

m-MIMO [36], have been designed to play critically important roles in supporting extremely stringent mURLLC requirements in terms of connecting massive number of mobile devices without imposing congestions. Researchers have shown that the CF m-MIMO framework can support full scalability at the cost of a modest performance loss compared to the conventional form of the massive MIMO system. However, it is challenging to characterize the stochastic networking behaviors when being integrated with CF m-MIMO schemes while guaranteeing mURLLC under statistical delay and error-rate bounded QoS constraints using FBC. As a result, how to accurately upper-bound the delay violation probability while guaranteeing statistical delay and error-rate bounded QoS provisionings for supporting mURLLC still remains as a challenging and open problem over 6G CF m-MIMO mobile wireless networks.

To effectively overcome the above-mentioned challenges, in this chapter we propose to apply the Mellin transform to analytically model and characterize stochastic QoS performances in terms of both delay and error-rate for CF m-MIMO modeling schemes in the *finite blocklength regime*. In particular, we develop the CF m-MIMO based system models across Rician wireless fading channels in the finite blocklength regime. Furthermore, we propose and analyze the delay-violation probability function by applying the Mellin transform over both arrival and service processes, while taking into account the statistical delay and error-rate bounded QoS constraints. We also formulate and solve the delay-violation probability minimization problem for our proposed CF m-MIMO modeling schemes in the finite blocklength regime. Also conducted is a set of simulations to validate and evaluate our proposed schemes for statistical delay and error-rate bounded QoS provisioning over 6G CF m-MIMO mobile wireless networks.

The rest of this chapter is organized as follows: Section 2.2 establishes FBC based CF m-MIMO system models across Rician wireless channels. Section 2.3 derives and analyzes the Mellin transform over arrival/service processes as well as an upper bound on the delay violation probability in the finite blocklength regime. Section 2.4 analyzes the delay performance and formulates and solves the delay violation probability minimization problem for statistical delay and error-rate bounded QoS provisioning in the finite blocklength regime. Section 2.5 evaluates and analyzes the

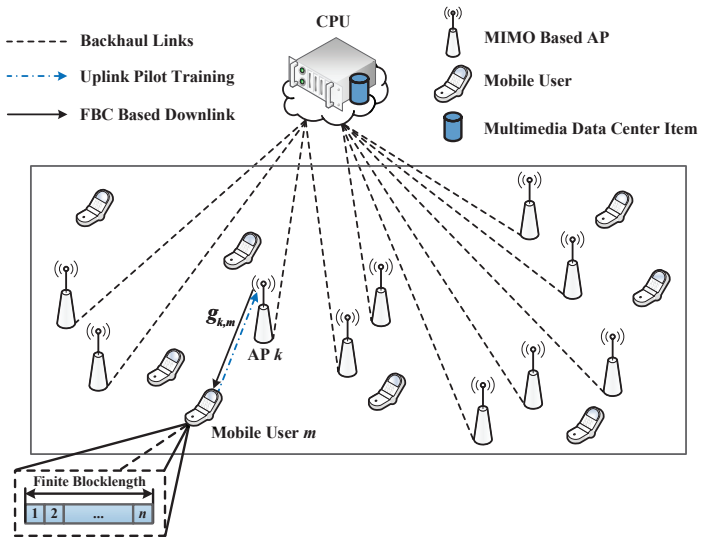

Figure 2.1: The system architecture model for 6G CF m-MIMO mobile wireless networks in the finite blocklength regime.

system performance for our proposed FBC based CF m-MIMO schemes. This chapter concludes with Section 2.6.

2.2 The CF M-MIMO Based System Models

Consider a CF m-MIMO network model, where each mobile user is served by coherent joint transmissions from all APs, as shown in Fig. 2.1. Assume that there are K_{a} randomly located APs over a large area and K_{u} mobile users. Assume that each AP is equipped with N_{T} antennas, while each mobile user is equipped with a single antenna. In addition, time division duplexing (TDD) mode is assumed to be operated over our proposed 6G CF m-MIMO mobile wireless networks. All APs are connected to a CPU through backhaul links. Define n_{p} as the number of channel uses for uplink pilot training symbols and n_{d} as the number of channel uses reserved for downlink data transmissions. Defining n as the total number of channel uses for both uplink pilot training and downlink data transmission phases, we have $n = n_{\mathrm{p}} + n_{\mathrm{d}}$.

2.2.1 Massive MIMO Based Rician Wireless Fading Channel Model

Considering the propagation effects, the channel's impulse response vector, denoted by $\boldsymbol{h}_{k,m} \in \mathbb{C}^{N_{\mathrm{T}} \times 1}$, between mobile user m and AP k over Rician massive MIMO based wireless fading channel model can be characterized as follows:

$$\boldsymbol{h}_{k,m} = \sqrt{\beta_{k,m}} \boldsymbol{g}_{k,m} \tag{2.1}$$

where $\beta_{k,m}$ represents the large-scale propagation that includes pathloss and shadowing effects and $\boldsymbol{g}_{k,m}$ represents the small-scale multipath fading effect which can be modeled using Rician distribution [64] as follows:

$$\boldsymbol{g}_{k,m} = \sqrt{\frac{\kappa}{\kappa+1}} \overline{\boldsymbol{g}}_{k,m} + \sqrt{\frac{1}{\kappa+1}} \widetilde{\boldsymbol{g}}_{k,m} \tag{2.2}$$

where $\boldsymbol{g}_{k,m}$ consists of the component $\overline{\boldsymbol{g}}_{k,m}$ representing the line of sight (LOS) signals and a Rayleigh distributed random component $\widetilde{\boldsymbol{g}}_{k,m}$ representing the non-line-of-sight (NLOS) signals, and $\kappa > 0$ is the Rician factor. Note that $\kappa = 0$ corresponds to a Rayleigh fading channel, while $\kappa \to \infty$ corresponds to non-fading channel. We can rewrite the Rician massive MIMO based wireless fading channel model as follows:

$$\boldsymbol{h}_{k,m} = \sqrt{\frac{\kappa}{\kappa+1}} \overline{\boldsymbol{h}}_{k,m} + \sqrt{\frac{1}{\kappa+1}} \widetilde{\boldsymbol{h}}_{k,m} \tag{2.3}$$

where $\overline{\boldsymbol{h}}_{k,m} \triangleq \overline{\boldsymbol{g}}_{k,m} \beta_{k,m}$ and $\widetilde{\boldsymbol{h}}_{k,m} \triangleq \widetilde{\boldsymbol{g}}_{k,m} \beta_{k,m}$.

2.2.2 Uplink Pilot Training and Channel Estimation

Define the pilot training sequence for mobile user m as $\boldsymbol{\phi}_m^{n_{\mathrm{p}}} = \left[\phi_m^{(1)}, \ldots, \phi_m^{(n_{\mathrm{p}})}\right] \in \mathbb{C}^{1 \times n_{\mathrm{p}}}$ and $\left\|\boldsymbol{\phi}_m^{n_{\mathrm{p}}}\right\|^2 = 1$, where $\|\cdot\|$ denotes the Euclidean norm. During the uplink pilot training phase, we derive the received signal, denoted by $\mathbf{Y}_k^{n_{\mathrm{p}}} \in \mathbb{C}^{N_{\mathrm{T}} \times n_{\mathrm{p}}}$, for transmitting n_{p} pilot data blocks from

mobile user m to AP k as in the following equation:

$$\mathbf{Y}_k^{n_\mathrm{p}} = \sum_{m=1}^{K_\mathrm{u}} \sqrt{n_\mathrm{p}\mathcal{P}_\mathrm{p}}\boldsymbol{h}_{k,m}\boldsymbol{\phi}_m^{n_\mathrm{p}} + \mathbf{N}_k \tag{2.4}$$

where $\mathcal{P}_\mathrm{p}$ is the uplink pilot transmit power at the mobile users and $\mathbf{N}_k \in \mathbb{C}^{N_\mathrm{T}\times n_\mathrm{p}}$ is the AWGN matrix with zero mean and covariance $\mathbf{I}_{N_\mathrm{T}}$ where $\mathbf{I}_{N_\mathrm{T}}$ is the identity matrix of size N_T. We assume that the LOS component $\overline{\boldsymbol{h}}_{k,m}$ given in Eq. (2.3) is perfectly known at both the APs and mobile users. Accordingly, we only need to estimate the NLOS Rayleigh-distributed random component. As a result, the received matrix, denoted by $\widetilde{\mathbf{Y}}_k^{n_\mathrm{p}}$, for the NLOS channel estimation can be derived as follows:

$$\widetilde{\mathbf{Y}}_k^{n_\mathrm{p}} = \sum_{m=1}^{K_\mathrm{u}} \sqrt{\frac{n_\mathrm{p}\mathcal{P}_\mathrm{p}}{\kappa+1}}\widetilde{\boldsymbol{h}}_{k,m}\boldsymbol{\phi}_m^{n_\mathrm{p}} + \mathbf{N}_k. \tag{2.5}$$

Then, by projecting the received signal $\widetilde{\mathbf{Y}}_k^{n_\mathrm{p}}$ onto $\boldsymbol{\phi}_m^{n_\mathrm{p}}$, we obtain:

$$\widetilde{\boldsymbol{y}}_k^{n_\mathrm{p}} = \widetilde{\mathbf{Y}}_k^{n_\mathrm{p}}\left(\boldsymbol{\phi}_m^{n_\mathrm{p}}\right)^H = \sqrt{\frac{n_\mathrm{p}\mathcal{P}_\mathrm{p}}{\kappa+1}}\widetilde{\boldsymbol{h}}_{k,m} + \sum_{\substack{m'=1\\ m'\neq m}}^{K_\mathrm{u}} \sqrt{\frac{n_\mathrm{p}\mathcal{P}_\mathrm{p}}{\kappa+1}}\widetilde{\boldsymbol{h}}_{k,m'} + \widetilde{\boldsymbol{n}}_k \tag{2.6}$$

where $(\cdot)^H$ represents the conjugate transpose of a vector and $\widetilde{\boldsymbol{n}}_k \triangleq \mathbf{N}_k\left(\boldsymbol{\phi}_m^{n_\mathrm{p}}\right)^H$ is an independent and identically distributed (i.i.d.) Gaussian vector with zero mean and covariance $\mathbf{I}_{N_\mathrm{T}}$. Denote by $\widetilde{\mathbf{H}}_k \triangleq \left[\widetilde{\boldsymbol{h}}_{k,1},\ldots,\widetilde{\boldsymbol{h}}_{k,K_\mathrm{u}}\right]$ the NLOS component of the channel's impulse response matrix between AP k and all mobile users. Define $\mathbf{R}_{\widetilde{\mathbf{H}}_k} \triangleq \mathbb{E}\left[\widetilde{\mathbf{H}}_k\left(\widetilde{\mathbf{H}}_k\right)^H\right] = \mathrm{diag}\left(\beta_{k,1},\ldots,\beta_{k,K_\mathrm{u}}\right)$ as the covariance matrix of $\widetilde{\mathbf{H}}_k$, where $\mathbb{E}[\cdot]$ is the expectation operation and $\mathrm{diag}(\cdot)$ represents the diagonal matrix. Then, considering the Rician wireless fading channels, we can derive the channel estimation for our proposed CF m-MIMO schemes as detailed in the following lemma.

Lemma 1. *The minimum mean-squared error (MMSE) estimator, denoted by $\widehat{\mathbf{H}}_k$, for the NLOS component of the Rician massive MIMO based wireless fading channel $\widetilde{\mathbf{H}}_k$ between AP k and all*

mobile users is derived as follows:

$$\widehat{\mathbf{H}}_k = \frac{\sqrt{n_p \mathcal{P}_p}}{\kappa+1}\mathbf{R}_{\widetilde{\mathbf{H}}_k}\left(\frac{n_p \mathcal{P}_p}{\kappa+1}\mathbf{R}_{\widetilde{\mathbf{H}}_k}+\mathbf{I}_{N_T}\right)^{-1}\widetilde{\boldsymbol{y}}_k^{n_p}. \tag{2.7}$$

Proof. Applying the MMSE estimator of $\widetilde{\mathbf{H}}_k$ based on the observation of $\widetilde{\boldsymbol{y}}_k^{n_\mathrm{p}}$, we can obtain the following equation:

$$\widehat{\mathbf{H}}_k = \mathbb{E}\left[\widetilde{\mathbf{H}}_k|\widetilde{\boldsymbol{y}}_k^{n_\mathrm{p}}\right] = \mathbf{R}_{\widetilde{\mathbf{H}}_k,\widetilde{\boldsymbol{y}}_k^{n_\mathrm{p}}}\left(\mathbf{R}_{\widetilde{\boldsymbol{y}}_k^{n_\mathrm{p}}}\right)^{-1}\left(\widetilde{\boldsymbol{y}}_k^{n_\mathrm{p}}-\mathbb{E}\left[\widetilde{\boldsymbol{y}}_k^{n_\mathrm{p}}\right]\right)+\mathbb{E}\left[\widetilde{\mathbf{H}}_k\right] \tag{2.8}$$

where $\mathbf{R}_{\widetilde{\mathbf{H}}_k,\widetilde{\boldsymbol{y}}_k^{n_\mathrm{p}}}$and $\mathbf{R}_{\widetilde{\boldsymbol{y}}_k^{n_\mathrm{p}}}$ represent the covariance matrices given as follows:

$$\begin{cases}\mathbf{R}_{\widetilde{\mathbf{H}}_k,\widetilde{\boldsymbol{y}}_k^{n_\mathrm{p}}} = \mathbb{E}\left[\widetilde{\mathbf{H}}_k\left(\widetilde{\boldsymbol{y}}_k^{n_\mathrm{p}}\right)^H\right] = \sqrt{\frac{n_\mathrm{p}\mathcal{P}_\mathrm{p}}{\kappa+1}}\mathbf{R}_{\widetilde{\mathbf{H}}_k};\\ \mathbf{R}_{\widetilde{\boldsymbol{y}}_k^{n_\mathrm{p}}} = \mathbb{E}\left[\widetilde{\boldsymbol{y}}_k^{n_\mathrm{p}}\left(\widetilde{\boldsymbol{y}}_k^{n_\mathrm{p}}\right)^H\right] = \frac{n_\mathrm{p}\mathcal{P}_\mathrm{p}}{\kappa+1}\mathbf{R}_{\widetilde{\mathbf{H}}_k}+\mathbf{I}_{N_\mathrm{T}}.\end{cases} \tag{2.9}$$

Since $\mathbb{E}\left[\widetilde{\boldsymbol{y}}_k^{n_\mathrm{p}}\right]$ and $\mathbb{E}\left[\widetilde{\mathbf{H}}_k\right]$ are equal to zero, we have

$$\widehat{\mathbf{H}}_k = \sqrt{\frac{n_\mathrm{p}\mathcal{P}_\mathrm{p}}{\kappa+1}}\mathbf{R}_{\widetilde{\mathbf{H}}_k}\left(\frac{n_\mathrm{p}\mathcal{P}_\mathrm{p}}{\kappa+1}\mathbf{R}_{\widetilde{\mathbf{H}}_k}+\mathbf{I}_{N_\mathrm{T}}\right)^{-1}\widetilde{\boldsymbol{y}}_k^{n_\mathrm{p}} \tag{2.10}$$

which completes the proof of Lemma 1. □

As a result, the channel estimation of Rician m-MIMO based wireless fading channel model, denoted by $\widehat{\widehat{\mathbf{H}}}_k$, can be derived as follows:

$$\widehat{\widehat{\mathbf{H}}}_k = \sqrt{\frac{\kappa}{\kappa+1}}\overline{\mathbf{H}}_k+\sqrt{\frac{1}{\kappa+1}}\widehat{\mathbf{H}}_k. \tag{2.11}$$

2.2.3 Downlink Finite-Blocklength Data Transmission

We define the transmit signal matrix as $\mathbf{X}_k^{n_\mathrm{d}} \triangleq \left[\boldsymbol{x}_k^{(1)},\ldots,\boldsymbol{x}_k^{(n_\mathrm{d})}\right]$ and receive signal vector $\boldsymbol{y}_m^{n_\mathrm{d}} \triangleq \left[y_m^{(1)},\ldots,y_m^{(n_\mathrm{d})}\right]$. Based on the MMSE estimator matrix, denoted by $\widehat{\widehat{\mathbf{H}}}_k = \left[\widehat{\widehat{\boldsymbol{h}}}_{k,1},\ldots,\widehat{\widehat{\boldsymbol{h}}}_{k,K_\mathrm{u}}\right]$, ob-

tained during the uplink pilot training phase, we can derive the transmitted signal, denoted by $\boldsymbol{x}_k^{(l)}$, for transmitting data block l from AP k to mobile user m by employing conjugate beamforming [36] as follows:

$$\boldsymbol{x}_k^{(l)} = \sum_{m=1}^{K_{\mathrm{u}}} \mathbf{W}_k \left(\boldsymbol{\Sigma}_k\right)^{\frac{1}{2}} s_m^{(l)}, \quad l = 1, \ldots, n_{\mathrm{d}} \tag{2.12}$$

where $s_m^{(l)}$ represents the lth transmitted data block to mobile user m, $\boldsymbol{\Sigma}_k \triangleq \mathrm{diag}\left(\eta_{k,1}, \ldots, \eta_{k,K_{\mathrm{u}}}\right)$ is the power allocation coefficient matrix, where $\eta_{k,m}$ $(m = 1, \ldots, K_{\mathrm{u}})$ is the power allocation coefficient for transmitting finite-blocklength data block l from AP k to mobile user m, and $\mathbf{W}_k$ is the downlink precoder from AP k to all K_{u} mobile users, which is given by

$$\mathbf{W}_k \triangleq \widehat{\widehat{\mathbf{H}}}_k \left[\left(\widehat{\widehat{\mathbf{H}}}_k \right)^H \widehat{\widehat{\mathbf{H}}}_k \right]^{-1} \left(\boldsymbol{\Xi}_k\right)^{\frac{1}{2}} \tag{2.13}$$

where $\boldsymbol{\Xi}_k = \mathrm{diag}\left(\chi_1, \ldots, \chi_{K_{\mathrm{u}}}\right)$ is the normalization matrix such that the columns of $\mathbf{W}_k$ have unit norm and the normalization variable χ_k with $k \in \{1, \ldots, K_{\mathrm{u}}\}$ follows the central chi-square distribution with (2ℓ) degrees of freedom, where $\ell = K_{\mathrm{a}} - K_{\mathrm{u}} + 1$. The probability density function (PDF) of χ_k is given as follows [65]:

$$f_\ell(\chi_k) = \frac{1}{\Gamma(\ell)} \chi_k^{\ell-1} e^{-\chi_k} \tag{2.14}$$

where $\Gamma(\cdot)$ denotes the Gamma function. We have $\mathbf{W}_k = [\boldsymbol{w}_{k,1}, \ldots, \boldsymbol{w}_{k,K_{\mathrm{u}}}]$, where $\boldsymbol{w}_{k,m}$ is the downlink precoder from AP k to mobile user m $(m \in \{1, \ldots, K_{\mathrm{u}}\})$. In addition, the power control coefficients need to satisfy the following power constraint at each AP:

$$\frac{1}{n_{\mathrm{d}}} \sum_{l=1}^{n_{\mathrm{d}}} \mathbb{E}\left[\left\| \boldsymbol{x}_k^{(l)} \right\|^2 \right] \leq \overline{\mathcal{P}}_{\mathrm{d}} \tag{2.15}$$

where $\overline{\mathcal{P}}_{\mathrm{d}}$ represents the average transmit power at each AP and $\boldsymbol{x}_k^{(l)}$ is given by Eq. (2.12). Furthermore, as the number of APs K_{a} grows sufficiently large, the system will experience only small variations (relative to the average) in the achievable data transmission rate, which is known as the

channel hardening [66]. As a result, although the instantaneous CSI is not available at the mobile users, $\mathbb{E}\left[\left(\boldsymbol{h}_{k,m}\right)^T \boldsymbol{w}_{k,m}\right]$ can be used to calculate the channel gain, where $(\cdot)^T$ represents the transpose of a vector. Considering Rician wireless fading channels, we derive the received signal, denoted by $y_m^{(l)}$, from the kth AP to the mth mobile user for transmitting the lth finite-blocklength data block as follows [36]:

$$y_m^{(l)} = \underbrace{\sum_{k=1}^{K_{\mathrm{a}}} \sqrt{\overline{\mathcal{P}}_{\mathrm{d}} \eta_{k,m}}\, \mathbb{E}\left[\left(\boldsymbol{h}_{k,m}\right)^T \boldsymbol{w}_{k,m}\right] s_m^{(l)}}_{\mathrm{DS}_m} + \underbrace{\sqrt{\overline{\mathcal{P}}_{\mathrm{d}}}\Bigg\{ \sum_{k=1}^{K_{\mathrm{a}}} \sqrt{\eta_{k,m}}\left(\boldsymbol{h}_{k,m}\right)^T \boldsymbol{w}_{k,m} - \mathbb{E}\Bigg[\sum_{k=1}^{K_{\mathrm{a}}} \sqrt{\eta_{k,m}}}_{\mathrm{BU}_m}$$
$$\underbrace{\times \left(\boldsymbol{h}_{k,m}\right)^T \boldsymbol{w}_{k,m}\Bigg]\Bigg\} s_m^{(l)}}_{\mathrm{BU}_m} + \sum_{\substack{m'=1 \\ m' \neq m}}^{K_{\mathrm{u}}} \underbrace{\sum_{k=1}^{K_{\mathrm{a}}} \sqrt{\overline{\mathcal{P}}_{\mathrm{d}} \eta_{k,m'}}\left(\boldsymbol{h}_{k,m}\right)^T \boldsymbol{w}_{k,m'} s_{m'}^{(l)}}_{\mathrm{UI}_{m'}} + n_m^{(l)} \tag{2.16}$$

where $s_m^{(l)}$ and $s_{m'}^{(l)}$ are the signals sent to mobile user m and mobile user m', respectively; $\eta_{k,m}$ and $\eta_{k,m'}$ are the power allocation parameters for transmitting from AP k to mobile user m and mobile user m', respectively; $\boldsymbol{h}_{k,m} \in \mathbb{C}^{1 \times N_{\mathrm{T}}}$ represents the channel's impulse response vector from the kth AP to mobile user m; $n_m^{(l)}$ is the AWGN with zero mean and unit variance; and DS_m, BU_m, and $\mathrm{UI}_{m'}$ represent the strength of the desired signal (DS), the beamforming gain uncertainty (BU), and the interference caused by the m'th mobile user (UI), respectively. Correspondingly, we can derive the signal-to-noise-plus-interference ratio (SINR), denoted by γ_m, from the APs to mobile user m as follows:

$$\gamma_m = \frac{\left\|\mathrm{DS}_m\right\|^2}{\mathbb{E}\left[\left\|\mathrm{BU}_m\right\|^2\right] + \sum\limits_{\substack{m'=1 \\ m' \neq m}}^{K_{\mathrm{u}}} \mathbb{E}\left[\left\|\mathrm{UI}_{m'}\right\|^2\right] + 1}. \tag{2.17}$$

2.3 Statistical Delay and Error-Rate Bounded QoS Provisioning in the Finite Blocklength Regime

In this section, we derive the Mellin transform over arrival and service processes by using SNC for our proposed CF m-MIMO schemes given the non-vanishing error probability.

2.3.1 (n_d, M_m, ϵ_m)-code

Definition 1 ($(n_{\mathrm{d}}, M_m, \epsilon_m)$-code)**.** *We define a codebook consisting of M_m codewords, denoted by $(c_1, \ldots, c_M)$, with length n_d. We define a message set $\mathcal{M}_m = \{1, \ldots, M_m\}$ and a message $W_m \in \mathcal{M}_m$ which is uniformly distributed on $\mathcal{M}_m$. Denote by ϵ_m the decoding error probability. We define an (n_d, M_m, ϵ_m)-code ($\epsilon_m \in [0, 1)$) as follows:*

- *An encoder Υ: $\{1, \ldots, M_m\} \mapsto \mathbb{C}^{N_T \times n_d}$ that maps the message $W_m \in \mathcal{M}_m$ to a codeword $\mathbf{X}_m^{n_d}$ with length n_d.*
- *A decoder $\mathcal{D}$: $\mathbb{C}^{1\times N_T} \times \mathbb{C}^{N_T \times n_d} \mapsto \{1, \ldots, M_m\}$, where $\widehat{W}_m$ denotes the estimated signal received at the receiver. The decoder $\mathcal{D}$ need to satisfy the following maximum error probability constraint:*

$$Pr\left\{\widehat{W}_m \neq W_m\right\} \leq \epsilon_m. \tag{2.18}$$

In [30], the accurate approximation of the maximum achievable data rate, denoted by R_m (bits per channel use), with decoding error probability ϵ_m with $0 \leq \epsilon_m < 1$ and coding blocklength, denoted by n_{d}, for mobile user m in the finite blocklength regime can be determined as follows:

$$R_m(n_{\mathrm{d}}, \epsilon_m) \approx C(\gamma_m) - \sqrt{\frac{V(\gamma_m)}{n_{\mathrm{d}}}} Q^{-1}(\epsilon_m) \tag{2.19}$$

where $Q^{-1}(\cdot)$ is the inverse of Q-function and $C(\gamma_m)$ and $V(\gamma_m)$ are the channel capacity and channel dispersion, respectively, which are given as follows [30]:

$$\begin{cases} C(\gamma_m) = \log_2(1 + \gamma_m); \\ V(\gamma_m) = 1 - \frac{1}{(1+\gamma_m)^2}. \end{cases} \tag{2.20}$$

2.3.2 Stochastic Network Calculus

Consider that each AP is equipped with a QoS-driven first-in-first-out (FIFO) buffer. We define $a_m(l)$ as the source rate for transmitting the lth data block to mobile user m and $s_m(l)$ as the

instantaneous service rate over wireless channels for transmitting the lth data block to mobile user m. Define $A_m(l) \triangleq \sum_{j=0}^{l-1} a_m(j)$ as the accumulated source rate for transmitting l data blocks to mobile user m and $S_m(l) \triangleq \sum_{j=0}^{l-1} s_m(j)$ as the accumulated service rate over wireless channels for transmitting l data blocks to mobile user m. Define $Q_m(l)$ as the dynamics of queuing process for transmitting the lth data block to mobile user m, which is given as in the following equation:

$$Q_m(l) = \max\left\{A_m(l) - S_m(l), 0\right\}. \tag{2.21}$$

However, in practical scenarios, it is difficult to obtain the statistical characteristics of random arrival and service processes. As a result, by taking the exponential of arrival and service processes, we can transform the arrival and service processes, denoted by $A_m(l)$ and $S_m(l)$, respectively, in the bit domain into the exponential domain, i.e., *signal-to-noise ratio (SNR)-domain* [67] by using the exponential function given as follows:

$$\begin{cases} \mathcal{A}_m(l) \triangleq e^{A_m(l)}; \\ \mathcal{S}_m(l) \triangleq e^{S_m(l)}. \end{cases} \tag{2.22}$$

Define the Mellin transform, denoted by $\mathcal{M}_{\mathcal{X}}(\theta_m)$, of a non-negative random variable $\mathcal{X}$ as follows [68]:

$$\mathcal{M}_{\mathcal{X}}(\theta_m) \triangleq \mathbb{E}\left[\mathcal{X}^{(\theta_m - 1)}\right] \tag{2.23}$$

where $\theta_m > 0$ is defined as the QoS exponent. Denoting d_{th} a target delay, we can define the kernel function $\mathcal{K}(\theta_m, d_{\text{th}})$ as follows [67]:

$$\mathcal{K}(\theta_m, d_{\text{th}}) \triangleq \frac{\mathcal{M}_{\mathcal{S}_m}(1-\theta_m)^{d_{\text{th}}}}{1 - \mathcal{M}_{\mathcal{A}_m}(1+\theta_m)\mathcal{M}_{\mathcal{S}_m}(1-\theta_m)}, \tag{2.24}$$

if the following stability condition holds:

$$\mathcal{M}_{\mathcal{A}_m}(1+\theta_m)\mathcal{M}_{\mathcal{S}_m}(1-\theta_m) < 1. \tag{2.25}$$

Correspondingly, an upper bound on the delay violation probability, denoted by $p_m(d_{\text{th}})$, can be obtained using the Mellin transform over the arrival and service processes $A_m(l)$ and $S_m(l)$ in the SNR-domain as follows:

$$p_m(d_{\text{th}}) \leq \inf_{\theta_m > 0} \left\{ \mathcal{K}(\theta_m, d_{\text{th}}) \right\}. \tag{2.26}$$

2.3.3 Statistical Delay and Error-Rate Bounded QoS Provisioning for CF m-MIMO in the Finite Blocklength Regime

Statistical delay-bounded QoS guarantees [12] [69] have been extensively studied to analyze queuing behavior for time-varying arrival and service processes. The PDF of SINR γ_m over Rician wireless fading channels is given as follows [70]:

$$f_{\gamma_m}(\gamma_m) = 2(1+\kappa)\gamma_m e^{-(1+\kappa)\gamma_m - \kappa} I_0\left[2\sqrt{\kappa(1+\kappa)}\gamma_m\right] \tag{2.27}$$

where $I_0[\cdot]$ is the 0th order modified Bessel function of the first kind.

2.3.3.1 Mellin Transform Over Arrival Process

Assume that the arrivals at all time slots are independent and i.i.d. for each mobile user m, i.e., the accumulated source rate $A_m(l)$ has i.i.d. increments, denoted by $a_m(l)$, or equivalently $a_m = a_m(l)$ due to $a_m(l)$'s being i.i.d. We can derive the Mellin transform over accumulated arrival process, denoted by $\mathcal{M}_{\mathcal{A}_m}(\theta_m)$, as follows:

$$\mathcal{M}_{\mathcal{A}_m}(\theta_m) = \mathbb{E}\left[\left(\prod_{j=1}^{l} e^{a_m(j)}\right)^{\theta_m - 1}\right] = \left(\mathbb{E}\left[e^{a_m(\theta_m - 1)}\right]\right)^l = \left[\mathcal{M}_{\alpha_m}(\theta_m)\right]^l \tag{2.28}$$

where $\alpha_m = e^{a_m}$. Assume that the arrival process follows a Poisson distribution with average rate λ_m. We can derive the Mellin transform of α_m as follows:

$$\mathcal{M}_{\alpha_m}(\theta_m) = \sum_{i=1}^{\infty} e^{i(\theta_m - 1)} \frac{(\lambda_m)^i}{i!} e^{-\lambda_m} = e^{\lambda_m\left(e^{\theta_m - 1} - 1\right)}. \tag{2.29}$$

2.3.3.2 Mellin Transform Over Service Process

Equations (2.24) and (2.26) show that deriving the closed-form expression of Mellin transform over service process at mobile user m is important for analyzing the delay violation probability, which motivates the following theorem.

Theorem 1. *Given the statistical delay and error-rate bounded QoS provisioning $\{\theta_m, \epsilon_m\}$, the Mellin transform over service process, denoted by $\mathcal{M}_{\mathcal{S}_m}(1-\theta_m)$, of mobile user m over Rician wireless fading channels in the high-end SNR region can be derived as follows:*

$$\mathcal{M}_{\mathcal{S}_m}(1-\theta_m) = (1-\epsilon_m)\left[F_1(\gamma_0) + F_0(\gamma_0)\right] + \epsilon_m \tag{2.30}$$

where $\gamma_0 \triangleq e^{\sqrt{\frac{V(\gamma_m)}{n_d}}Q^{-1}(\epsilon_m)}$ *and*

$$\begin{cases} F_0(\gamma_0) \triangleq \frac{2e^{-\kappa}}{\kappa+1}\sum\limits_{i=0}^{\infty}\frac{\kappa^i}{(i!)^2}\gamma\left(i+2,(1+\kappa)\gamma_0\right); \\ F_1(\gamma_0) \triangleq 2e^{-\kappa}\left[e^{-\sqrt{n_d}}Q^{-1}(\epsilon_m)\right]^{\frac{\theta_m n_d}{(\log 2)}}\sum\limits_{i=0}^{\infty}\frac{\kappa^i(\kappa+1)^{\frac{\theta_m n_d}{(\log 2)}-1}}{(i!)^2}\Gamma\left(i+2-\frac{\theta_m n_d}{(\log 2)},(1+\kappa)\gamma_0\right), \end{cases} \tag{2.31}$$

where $\log(\cdot)$ *represents* $\log_e(\cdot)$ *and* $\gamma(a,b)$ *and* $\Gamma(a,b)$ *are the lower and upper incomplete Gamma functions, respectively.*

Proof. The proof of Theorem 1 is provided in Appendix A. □

Correspondingly, substituting Eqs. (2.28), (2.29), and (2.30) back into Eq. (2.24), we can derive the closed-form expression of the steady-state kernel $\mathcal{K}(\theta_m, d_{\text{th}})$ as follows:

$$\mathcal{K}(\theta_m, d_{\text{th}}) = \frac{\left\{(1-\epsilon_m)\left[F_1(\gamma_0)+F_0(\gamma_0)\right]+\epsilon_m\right\}^{d_{\text{th}}}}{1-e^{\lambda_m l\left(e^{\theta_m}-1\right)}(1-\epsilon_m)\left[F_1(\gamma_0)+F_0(\gamma_0)\right]+\epsilon_m}. \tag{2.32}$$

under the stability condition $\mathcal{M}_{\mathcal{A}_m}(1+\theta_m)\mathcal{M}_{\mathcal{S}_m}(1-\theta_m) < 1$.

2.4 Delay Analyses For Statistical Delay and Error-Rate Bounded QoS Provisioning in the Finite Blocklength Regime

In the previous Section 2.3, we have investigated an upper on the delay violation probability using the Mellin transform for a given decoding error probability ϵ_m. In this section, assuming the decoding error probability is a function of $\{n_{\rm d}, \gamma_m\}$, we derive the delay violation probability in terms of the average decoding error probability function over Rayleigh wireless fading channels $(\kappa = 0)$.

2.4.1 Upper-Bound On the Average Decoding Error Probability Function for CF m-MIMO in the Finite Blocklength Regime

Consider the case where $\kappa = 0$, i.e., the Rayleigh fading channel model. We define [36]

$$c_{k,m} \triangleq \frac{\sqrt{n_{\rm p}\mathcal{P}_{\rm p}}\beta_{k,m}}{\sum\limits_{m'=1}^{K_{\rm u}} n_{\rm p}\mathcal{P}_{\rm p}\beta_{k,m'}\left\|\boldsymbol{\phi}_{m'}^{n_{\rm p}}\left(\boldsymbol{\phi}_{m'}^{n_{\rm p}}\right)^H\right\|^2 + 1}. \tag{2.33}$$

Considering the massive access scenario with vary large $K_{\rm a}$, we can obtain the following equations by applying the Tchebyshev's theorem for our proposed CF m-MIMO schemes across Rayleigh fading channel model [36]:

$$\begin{cases} \frac{1}{K_{\rm a}}\sum\limits_{k=1}^{K_{\rm a}}\left(\boldsymbol{h}_{k,m}\right)^T\boldsymbol{w}_{k,m} - \frac{N_{\rm T}\sqrt{n_{\rm p}\mathcal{P}_{\rm p}\overline{\mathcal{P}}_{\rm d}}}{K_{\rm a}}\sum\limits_{k=1}^{K_{\rm a}}\eta_{k,m}\left(c_{k,m}\beta_{k,m}\chi_k\right)^2 \xrightarrow[K_{\rm a}\to\infty]{p} 0; \\ \frac{1}{K_{\rm a}}\sum\limits_{k=1}^{K_{\rm a}}\left(\boldsymbol{h}_{k,m}\right)^T\boldsymbol{w}_{k,m'} \xrightarrow[K_{\rm a}\to\infty]{p} 0, \qquad\qquad \forall m \neq m', \end{cases} \tag{2.34}$$

where the symbol $\xrightarrow[K_{\rm a}\to\infty]{p}$ represents the convergence in probability as $K_{\rm a} \to \infty$. The results given by Eq. (2.34) imply that as $K_{\rm a} \to \infty$, we only need to consider the desired parts of the received signal $y_m^{(l)}$ and ignore the noise and interference in the asymptotic analysis. As a result, we can

show that the SINR γ_m follows the following distribution:

$$\gamma_m \sim \left(N_{\mathrm{T}}\right)^2 n_{\mathrm{p}} \mathcal{P}_{\mathrm{p}} \overline{\mathcal{P}}_{\mathrm{d}} \sum_{k=1}^{K_{\mathrm{a}}} \eta_{k,m} \left(c_{k,m} \beta_{k,m} \chi_k\right)^2 \sim \sum_{k=1}^{K_{\mathrm{a}}} \mathcal{E}\left(\xi_{k,m}\right) \tag{2.35}$$

where $\mathcal{E}(\xi_{k,m})$ is the exponential distribution with its parameter equal to $\xi_{k,m}$, which is given as follows:

$$\xi_{k,m} \triangleq \frac{1}{2\left(N_{\mathrm{T}}\right)^2 n_{\mathrm{p}} \mathcal{P}_{\mathrm{p}} \overline{\mathcal{P}}_{\mathrm{d}} \eta_{k,m} \left(c_{k,m} \beta_{k,m}\right)^2} \tag{2.36}$$

where $k \in \{1, \ldots, K_{\mathrm{a}}\}$ and $m \in \{1, \ldots, K_{\mathrm{u}}\}$. We can obtain the decoding error probability function, denoted by $\epsilon_m\left(n_{\mathrm{d}}, \gamma_m\right)$, for mobile user m as follows [30]:

$$\epsilon_m\left(n_{\mathrm{d}}, \gamma_m\right) \approx Q\left(\frac{C\left(\gamma_m\right) - R_m}{\sqrt{V\left(\gamma_m\right)/n_{\mathrm{d}}}}\right) \tag{2.37}$$

where $Q(\cdot)$ is the Q-function, R_m (bits per channel use) is the achievable data rate, and $C\left(\gamma_m\right)$ and $V\left(\gamma_m\right)$ denote the channel capacity and channel dispersion, respectively, given in Eq. (2.20). Similar to Eq. (A.1), given the achievable finite-blocklength coding rate R_m and the decoding error probability function $\epsilon_m\left(n_{\mathrm{d}}, \gamma_m\right)$, we can derive the Mellin transform over service process $S_m(l)$ at mobile user m as follows:

$$\begin{aligned}
\mathcal{M}_{\mathcal{S}_m}(1-\theta_m) &= \mathbb{E}_{\gamma_m}\left[\epsilon_m\left(n_{\mathrm{d}}, \gamma_m\right) + \left[1 - \epsilon_m\left(n_{\mathrm{d}}, \gamma_m\right)\right] e^{-\theta_m n_{\mathrm{d}} R_m}\right] \\
&= \mathbb{E}_{\gamma_m}\left[\epsilon_m\left(n_{\mathrm{d}}, \gamma_m\right)\right] + \left\{1 - \mathbb{E}_{\gamma_m}\left[\epsilon_m\left(n_{\mathrm{d}}, \gamma_m\right)\right]\right\} e^{-\theta_m n_{\mathrm{d}} R_m}.
\end{aligned} \tag{2.38}$$

Equation (2.38) shows that deriving the average decoding error probability function $\mathbb{E}_{\gamma_m}\left[\epsilon_m\left(n_{\mathrm{d}}, \gamma_m\right)\right]$ is important to obtain the closed-form expression for Mellin transform over service process at mobile user m, motivating the theorem that follows.

Theorem 2. *Given the achievable finite-blocklength coding rate R_m, the average decoding error probability function $\mathbb{E}_{\gamma_m}\left[\epsilon_m\left(n_d, \gamma_m\right)\right]$ for mobile user m over 6G CF m-MIMO mobile wireless*

networks in the finite blocklength regime is determined as follows:

$$\begin{aligned}\mathbb{E}_{\gamma_m}\left[\epsilon_m\left(n_d,\gamma_m\right)\right] \approx & 1-\sum_{k=1}^{K_a}\left[1-e^{-\xi_{k,m}\left(2^{R_m-1}-\frac{1}{2\vartheta_m\sqrt{n_d}}\right)}\right]+\left[\frac{1}{2}+\vartheta_m\sqrt{n_d}\left(e^{R_m}-1\right)\right] \\ & \times\left[\sum_{k=1}^{K_a}e^{-\xi_{k,m}\left(2^{R_m-1}-\frac{1}{2\vartheta_m\sqrt{n_d}}\right)}-\sum_{k=1}^{K_a}e^{-\xi_{k,m}\left(2^{R_m-1}+\frac{1}{2\vartheta_m\sqrt{n_d}}\right)}\right]-\vartheta_m\sqrt{n_d} \\ & \times\left\{\left(2^{R_m-1}-\frac{1}{2\vartheta_m\sqrt{n_d}}\right)\left[\sum_{k=1}^{K_a}e^{-\xi_{k,m}\left(2^{R_m-1}-\frac{1}{2\vartheta_m\sqrt{n_d}}\right)}\right]-\left(2^{R_m-1}\right.\right. \\ & \left.+\frac{1}{2\vartheta_m\sqrt{n_d}}\right)\left[\sum_{k=1}^{K_a}e^{-\xi_{k,m}\left(2^{R_m-1}+\frac{1}{2\vartheta_m\sqrt{n_d}}\right)}\right]+\sum_{k=1}^{K_a}\left[Ei\left(-\xi_{k,m}\right.\right. \\ & \left.\left.\left.\times\left[2^{R_m-1}+\frac{1}{2\vartheta_m\sqrt{n_d}}\right]\right)-Ei\left(-\xi_{k,m}\left[2^{R_m-1}-\frac{1}{2\vartheta_m\sqrt{n_d}}\right]\right)\right]\right\} \quad (2.39)\end{aligned}$$

where $Ei(x)\triangleq\int_{-x}^{\infty}\frac{e^{-t}}{t}dt$ *represents the exponential integral function and* $\vartheta_m\triangleq\frac{1}{2\pi\sqrt{2^{2R_m-1}}}$.

Proof. The proof of Theorem 2 is provided in Appendix B. □

In the high-end SNR regime, we have $V\left(\gamma_m\right)=1-\left(1+\gamma_m\right)^{-2}\to 1$. Using Eq. (2.37), we define the following function:

$$\widetilde{\Phi}\left(n_{\mathrm{d}},\gamma_m\right)\triangleq\left[C\left(\gamma_m\right)-R_m\right]\sqrt{n_{\mathrm{d}}}. \quad (2.40)$$

Considering the high-end SNR regime, we can derive the average decoding error probability function as detailed in the following lemma.

Lemma 2. *The approximate average decoding error probability function* $\mathbb{E}_{\gamma_m}\left[\epsilon_m\left(n_d,\gamma_m\right)\right]$ *for mobile user* m *in the high-end SNR regime is determined as follows:*

$$\mathbb{E}_{\gamma_m}\left[\epsilon_m\left(n_d,\gamma_m\right)\right]\approx\frac{\sqrt{\pi}}{2\sqrt{2n_d}}\sum_{k=1}^{K_a}\xi_{k,m}\exp\left\{\frac{\left(\xi_{k,m}\right)^2}{2n_d}-\xi_{k,m}\nu_m\right\}\left[1-erf\left(\frac{\xi_{k,m}}{\sqrt{2n_d}}-\frac{\sqrt{n_d}}{\sqrt{2}}\nu_m\right)\right] \quad (2.41)$$

where $\nu_m\triangleq 2^{R_m}-1$.

Proof. The proof of Lemma 2 is provided in Appendix C. □

2.4.2 Performance Analyses and Rate Adaptation for Statistical Delay and Error-Rate Bounded QoS Provisioning

Substituting Eqs. (2.29), (2.30), and (2.39) back into Eq. (2.24), we can derive the closed-form expression for the kernel function $\mathcal{K}(\theta_m, d_{\text{th}})$. Correspondingly, we formulate the delay violation probability minimization problem as follows:

$$\mathbf{P_1}: R_m^{\text{opt}} = \arg\min_{R_m} \{p_m(d_{\text{th}})\} = \arg\min_{R_m} \{\mathcal{K}_m(\theta_m, d_{\text{th}})\}. \tag{2.42}$$

Using Eq. (2.24), we can convert $\mathbf{P_1}$ into an equivalent minimization problem $\mathbf{P_2}$ as in the following equation:

$$\begin{aligned}\mathbf{P_2}: R_m^{\text{opt}} &= \arg\min_{R_m} \{\mathcal{M}_{\mathcal{S}_m}(1-\theta_m)\} \\ &= \arg\min_{R_m} \left\{\mathbb{E}_{\gamma_m}\left[\epsilon_m\left(n_{\text{d}}, \gamma_m\right)\right] + \left[1 - e^{-\theta_m n_{\text{d}} R_m}\mathbb{E}_{\gamma_m}\left[\epsilon_m\left(n_{\text{d}}, \gamma_m\right)\right]\right]\right\}.\end{aligned} \tag{2.43}$$

The monotonicity of decoding error probability function $\epsilon_m\left(n_{\text{d}}, \gamma_m\right)$ plays an important role in analyzing the convexity of $\mathbf{P_2}$ given in Eq. (2.42) as detailed in the following lemma.

Lemma 3. *The decoding error probability function $\epsilon_m\left(n_d, \gamma_m\right)$ is a monotonically increasing function with respect to the achievable data rate R_m for our proposed CF m-MIMO modeling schemes.*

Proof. To prove the monotonicity of the decoding error probability function $\epsilon_m\left(n_{\text{d}}, \gamma_m\right)$, using Eq. (2.37), we can take the first-order derivative of $\epsilon_m\left(n_{\text{d}}, \gamma_m\right)$ with respect to R_m as in the following equation:

$$\frac{\partial \epsilon_m\left(n_{\text{d}}, \gamma_m\right)}{\partial R_m} = -\frac{1}{\sqrt{2\pi}} e^{-\frac{\Phi^2(n_{\text{d}}, \gamma_m)}{2}} \left[\frac{\partial \Phi\left(n_{\text{d}}, \gamma_m\right)}{\partial R_m}\right] \tag{2.44}$$

where $\Phi\left(n_{\text{d}}, \gamma_m\right) \triangleq \frac{C(\gamma_m) - R_m}{\sqrt{V(\gamma_m)/n_{\text{d}}}}$ due to Eq. (2.37) and thus its first-order derivative yields the fol-

lowing equations:

$$\frac{\partial \Phi\left(n_{\mathrm{d}}, \gamma_m\right)}{\partial R_m} = \frac{-\sqrt{n_{\mathrm{d}}}}{\sqrt{1-\frac{1}{\left(1+\gamma_m\right)^2}}} < 0. \tag{2.45}$$

Therefore, we have $\frac{\partial \epsilon_m\left(n_{\mathrm{d}}, \gamma_m\right)}{\partial R_m} > 0$, which implies that the decoding error probability function $\epsilon_m\left(n_{\mathrm{d}}, \gamma_m\right)$ is a monotonically increasing function of R_m, completing the proof of Lemma 3. □

Lemma 3 and its proof can help further investigate the convexity of $\epsilon_m\left(n_{\mathrm{d}}, \gamma_m\right)$ as shown in the following lemma.

Lemma 4. *The block error probability function $\epsilon_m\left(n_d, \gamma_m\right)$ is convex with respect to the achievable data rate R_m for each mobile user m.*

Proof. Applying Eq. (2.45), we can derive the second-order derivative of the function $\Phi\left(n_{\mathrm{d}}, \gamma_m\right)$ with respect to R_m as follows:

$$\frac{\partial^2 \Phi\left(n_{\mathrm{d}}, \gamma_m\right)}{\partial R_m^2} = 0. \tag{2.46}$$

Using Eqs. (2.37), (2.45), and (2.46) and the fact that $\Phi\left(n_{\mathrm{d}}, \gamma_m\right) > 0$ due to $C\left(\gamma_m\right) > R_m$, we obtain the following equations:

$$\frac{\partial^2 \epsilon_m\left(n_{\mathrm{d}}, \gamma_m\right)}{\partial R_m^2} = \frac{1}{\sqrt{2\pi}} e^{-\frac{\Phi^2\left(n_{\mathrm{d}}, \gamma_m\right)}{2}} \left[\Phi\left(n_{\mathrm{d}}, \gamma_m\right)\left[\frac{\partial \Phi\left(n_{\mathrm{d}}, \gamma_m\right)}{\partial R_m}\right]^2 - \frac{\partial^2 \Phi\left(n_{\mathrm{d}}, \gamma_m\right)}{\partial R_m^2}\right] > 0 \tag{2.47}$$

which implies that $\epsilon_m\left(n_{\mathrm{d}}, \gamma_m\right)$ is a convex function with respect to R_m. Therefore, we complete the proof of Lemma 4. □

Combining and extending Theorem 1, Lemma 3, and Lemma 4 yield the following theorem.

Theorem 3. *If the statistical delay and error-rate bounded QoS constraints are characterized by $\{\theta_m, \epsilon_m\left(n_d, \gamma_m\right)\}$ with $\theta_m > 0$, then the following claims hold for each mobile user m.*

Claim 1. The delay upper-bound violation probability minimization problem $\mathbf{P_2}$ is strictly convex with respect to the achievable data rate R_m for our proposed CF m-MIMO modeling schemes.

Claim 2. Our obtained Mellin transform function $\mathcal{M}_{\mathcal{S}_m}(1-\theta_m)$ over service process satisfies the following condition:

$$\frac{\partial^2 \mathcal{M}_{\mathcal{S}_m}(1-\theta_m)}{\partial R_m^2} > 0. \tag{2.48}$$

Claim 3. The unique optimal rate adaptation policy, denoted by R_m^{opt}, for each mobile user m in the high-end SNR region is given by the following equation:

$$R_m^{opt} \approx \log_2 \Bigg\{ \frac{\theta_m n_d}{(\log 2) \sum\limits_{k=1}^{K_a} \xi_{k,m}} \Bigg[\frac{(\log 2)}{\theta_m n_d} \left(\sum_{k=1}^{K_a} \xi_{k,m} \right) \left(1 - \frac{\theta_m \sqrt{2\pi n_d}}{2} \right)^{\frac{(\log 2)}{\theta_m n_d}} - \mathcal{W}\Bigg(-\frac{(\log 2) \sum\limits_{k=1}^{K_a} \xi_{k,m}}{\theta_m n_d} \times \Bigg[\frac{2\theta_m n_d}{\sum\limits_{k=1}^{K_a} \xi_{k,m} \exp\left\{ \frac{\left(\xi_{k,m}\right)^2}{2n_d} + \xi_{k,m} \right\}} \Bigg]^{\frac{(\log 2)}{\theta_m n_d}} \exp\left\{ \frac{(\log 2)}{\theta_m n_d} \left(\sum_{k=1}^{K_a} \xi_{k,m} \right) \left(1 - \frac{\theta_m \sqrt{2\pi n_d}}{2} \right)^{\frac{(\log 2)}{\theta_m n_d}} \right\} \Bigg) \Bigg] \Bigg\} \tag{2.49}$$

where $\mathcal{W}(\cdot)$ is the Lambert W function.

Proof. The proof of Theorem 3 is provided in Appendix D. □

Remarks on Theorem 3: Claim 1 guarantees the existence of the optimal solution to the optimization problem $\mathbf{P_2}$ given by Eq. (2.43) for our proposed CF m-MIMO modeling schemes when $\theta_m > 0$. Claim 2 shows that our obtained Mellin transform function over service process can characterize the convexity of $\mathbf{P_2}$. Claim 3 derives the closed-form expression of the optimal rate adaptation policy R_m^{opt} as the function of $\{\theta_m, \epsilon_m(n_{\text{d}}, \gamma_m)\}$ for each mobile user m in the high-end SNR region, which plays the important roles in the system designs and performance analyses for statistical delay and error-rate bounded QoS provisioning over 6G CF m-MIMO mobile wireless networks in the finite blocklength regime.

2.4.3 Maximizing Effective Capacity For Statistical Delay and Error-Rate Bounded QoS Constraints in the Finite Blocklength Regime

The proposed upper bound on the delay violation probability $p_m(d_{\text{th}})$ using SNC characterizes the small values of the target delay d_{th}. For analyzing fairly long delays, i.e., the tail of delay distribution, we apply the concept of *effective capacity* to proximate the delay violation probability $p_m(d_{\text{th}})$, which is defined as follows.

Definition 2. *The* effective capacity *[71], denoted by $EC_m(\theta_m)$, is defined as the maximum constant arrival rate for a given service $S_m(l)$ for mobile user m subject to statistical delay-bounded QoS constraints, which is formally expressed as follows:*

$$EC_m(\theta_m) \triangleq -\lim_{l\to\infty} \frac{1}{l\theta_m} \log\left(\mathbb{E}_\gamma\left[e^{-\theta S_m(l)}\right]\right). \tag{2.50}$$

On the other hand, considering the SNC, we can redefine the effective capacity, denoted by $EC_m(\theta_m)$, using the Mellin transform over service process in the SNR-domain as follows:

$$EC_m(\theta_m) \triangleq -\frac{1}{\theta_m} \log\left(\mathcal{M}_{\mathcal{S}_m}(1-\theta_m)\right). \tag{2.51}$$

Accordingly, we can formulate the optimization problem $\mathbf{P_3}$ for statistical delay and error-rate bounded QoS provisioning $\{\theta_m, \epsilon_m\left(n_{\text{d}}, \gamma_m\right)\}$ to maximize the downlink effective capacity $EC_m(\theta_m)$ at mobile user m for our proposed CF m-MIMO schemes in the finite blocklength regime as follows:

$$\mathbf{P_3}: \arg\max_{R_m} \left\{EC_m(\theta_m)\right\}. \tag{2.52}$$

Since $\log(\cdot)$ is monotonically increasing, the above maximization problem $\mathbf{P_3}$ can be converted

into an equivalent minimization problem $\mathbf{P_4}$ as follows:

$$\mathbf{P_4}: \arg\min_{R_m} \left\{ \mathcal{M}_{\mathcal{S}_m}(1-\theta_m) \right\}. \tag{2.53}$$

which is equivalent to the minimization problem $\mathbf{P_2}$ given in Eq. (2.43). Consequently, we can show that our derived optimal rate adaptation policy R_m^{opt} given in Eq. (2.49) also maximizes the effective capacity $EC_m(\theta_m)$ given in Eq. (2.51) for mobile user m in the finite blocklength regime considering the high-end SNR region. Therefore, using Eq. (2.38), (2.41), and (2.49), we can derive the maximum effective capacity, denoted by $EC_m^{\max}(\theta_m)$, for statistical delay and error-rate bounded QoS provisioning in supporting mURLLC over 6G CF m-MIMO and FBC mobile wireless networks in the high-end SNR region as follows:

$$\begin{aligned}
EC_m^{\max}(\theta_m) \approx & -\frac{1}{\theta_m}\log\Bigg\{\frac{\sqrt{\pi}}{2\sqrt{2n_{\text{d}}}}\sum_{k=1}^{K_{\text{a}}}\left\{\xi_{k,m}\exp\left\{\frac{\left(\xi_{k,m}\right)^2}{2n_{\text{d}}}-\xi_{k,m}\nu_m\right\}\left[1-\text{erf}\left(\frac{\xi_{k,m}}{\sqrt{2n_{\text{d}}}}-\sqrt{\frac{n_{\text{d}}}{2}}\nu_m\right)\right]\right\} \\
& +\left(1-\frac{\sqrt{\pi}}{2\sqrt{2n_{\text{d}}}}\sum_{k=1}^{K_{\text{a}}}\left\{\xi_{k,m}\exp\left\{\frac{\left(\xi_{k,m}\right)^2}{2n_{\text{d}}}-\xi_{k,m}\nu_m\right\}\left[1-\text{erf}\left(\frac{\xi_{k,m}}{\sqrt{2n_{\text{d}}}}-\sqrt{\frac{n_{\text{d}}}{2}}\nu_m\right)\right]\right\}\right) \\
& \times\Bigg\{\frac{\theta_m n_{\text{d}}}{(\log 2)\sum_{k=1}^{K_{\text{a}}}\xi_{k,m}}\Bigg[\frac{(\log 2)}{\theta_m n_{\text{d}}}\left(\sum_{k=1}^{K_{\text{a}}}\xi_{k,m}\right)\left[1-\frac{\theta_m\sqrt{2\pi n_{\text{d}}}}{2}\right]^{\frac{(\log 2)}{\theta_m n_{\text{d}}}} \\
& -\mathcal{W}\Bigg(-\frac{(\log 2)\sum_{k=1}^{K_{\text{a}}}\xi_{k,m}}{\theta_m n_{\text{d}}}\left[\frac{2\theta_m n_{\text{d}}}{\sum_{k=1}^{K_{\text{a}}}\xi_{k,m}\exp\left\{\frac{\left(\xi_{k,m}\right)^2}{2n_{\text{d}}}+\xi_{k,m}\right\}}\right]^{\frac{(\log 2)}{\theta_m n_{\text{d}}}} \\
& \times\exp\left[\frac{(\log 2)}{\theta_m n_{\text{d}}}\left(\sum_{k=1}^{K_{\text{a}}}\xi_{k,m}\right)\left(1-\frac{\theta_m\sqrt{2\pi n_{\text{d}}}}{2}\right)^{\frac{(\log 2)}{\theta_m n_{\text{d}}}}\right]\Bigg)\Bigg]\Bigg\}^{-\frac{\theta_m n_{\text{d}}}{(\log 2)}}\Bigg\}.
\end{aligned} \tag{2.54}$$

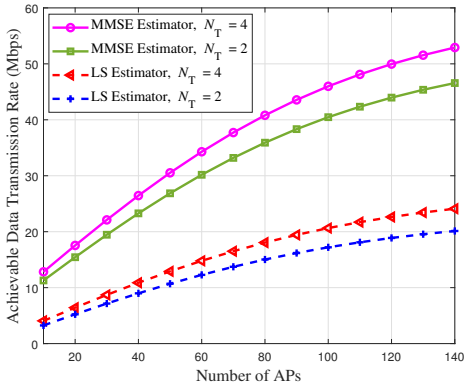

Figure 2.2: The achievable data transmission rate vs. number of APs for our proposed CF m-MIMO scheme in the finite blocklength regime.

2.5 Performance Evaluations

We use MATLAB-based simulations to validate and evaluate our proposed CF m-MIMO based schemes for statistical delay and error-rate bounded QoS provisioning in supporting mURLLC in the finite blocklength regime. Throughout our simulations, we set the number of APs $K_{\rm a} \in [50, 900]$, the number of mobile users $K_{\rm u} \in [10, 700]$, the number of transmit antennas $N_{\rm T} \in [2, 10]$, the uplink pilot transmit power $\overline{\mathcal{P}}_{\rm p}$ from $[1, 10]$ Watt for each mobile user, the average downlink transmit power $\overline{\mathcal{P}}_{\rm d}$ from $[1, 40]$ Watt for each mobile user, and the Rician factor κ from $[0, 30]$.

We set the number of Rician factor $\kappa = 4$, the number of uplink channel uses $n_{\rm p} = 100$, the number of transmit antennas $N_{\rm T} = 10$, and the decoding error probability $\epsilon_m = 10^{-6}$. Compared with the classical least-square (LS) channel estimator, Fig. 2.2 plots the achievable data transmission rate with varying numbers of APs $K_{\rm a}$ for our proposed 6G CF m-MIMO mobile wireless networks over Rician wireless fading channels in the finite blocklength regime. We can observe from Fig. 2.2 that the achievable data transmission rate increases with the number of APs. It is shown in Fig. 2.2 that the MMSE channel estimator performs better than the LS estimator over Rician wireless fading channels in terms of the achievable data transmission rate. Fig. 2.2 also shows that the gap between the MMSE estimator and LS estimator increases with $K_{\rm a}$, which is because of the channel hardening effect.

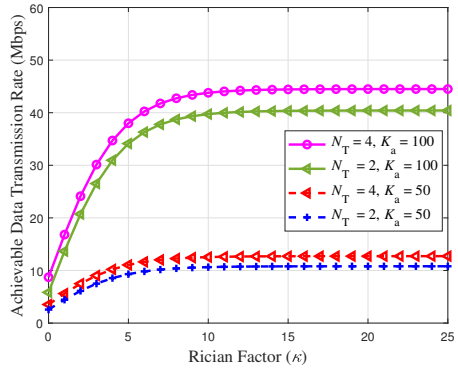

Figure 2.3: The achievable data transmission rate vs. Rician factor κ for our proposed CF m-MIMO scheme in the finite blocklength regime.

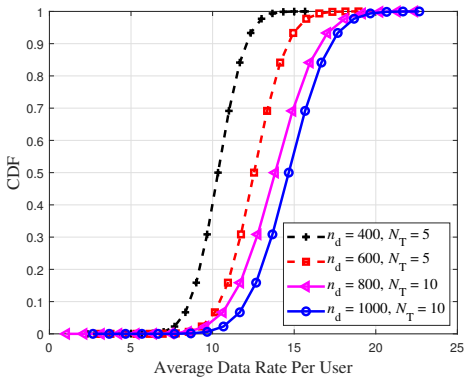

Figure 2.4: The CDFs of downlink data transmission rate per user for CF m-MIMO schemes in the finite blocklength regime.

Setting the number of transmit antennas $N_{\mathrm{T}} = 10$ and the decoding error probability $\epsilon_m = 10^{-6}$, Fig. 2.3 depicts the achievable data transmission rate with different Rician factors κ for our proposed 6G CF m-MIMO mobile wireless networks in the finite blocklength regime. We can observe from Fig. 2.3 that the achievable data rate increases as the Rician factor κ increases. Traditionally, the CSI estimation is not good enough when K_{a} is small, which leads to a low data rate. For our proposed CF m-MIMO scheme, the channel estimation quality can be significantly improved with large number of APs K_{a}.

Now we set the number of APs $K_{\mathrm{a}} = 100$, the number of downlink channel uses $n_{\mathrm{d}} = 800$, the

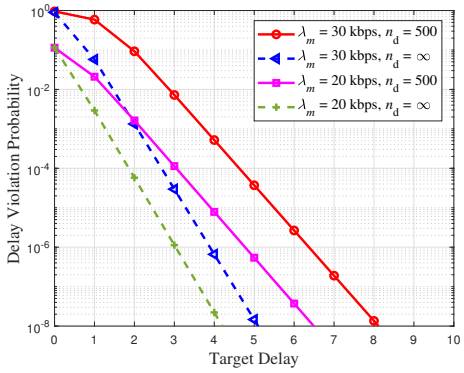

Figure 2.5: The delay violation probability $p_m(d_{\text{th}})$ vs. target delay d_{th} for our proposed CF m-MIMO scheme in the finite blocklength regime.

average downlink transmit power $\overline{\mathcal{P}}_{\text{d}} = 20$ Watt for each AP, and the Rician factor $\kappa = 2$. Fig. 2.4 plots the CDFs of the downlink data transmission rate per user for our proposed CF m-MIMO schemes in the finite blocklength regime. As shown in Fig. 2.4, the downlink data transmission rate per user increases with the number of transmit antennas N_{T}. In addition, Fig. 2.4 shows that a higher multiplexing order P_m is more beneficial for our proposed CF m-MIMO schemes with larger antenna arrays.

We set the number of APs $K_{\text{a}} = 100$, the number of transmit antennas $N_{\text{T}} = 10$, and decoding error probability $\epsilon_m = 10^{-6}$. Compared with the traditional Shannon's theorem which requires infinite blocklength, Fig. 2.5 plots the delay violation probability $p_m(d_{\text{th}})$ with different target delays d_{th} over Rician wireless fading channels for our proposed CF m-MIMO scheme in the finite blocklength regime. It is shown in Fig. 2.5 that the delay violation probability $p_m(d_{\text{th}})$ decreases as the target delay d_{th} increases. Fig. 2.5 also shows the delay violation probability increases with the increased average data arrival rate λ_m. This is because that the queues can be built up more quickly with a larger arrival rate.

We set the target delay $d_{\text{th}} = 5$ ms, Rician factor $\kappa = 10$, the number of downlink channel uses $n_{\text{d}} = 800$, the average downlink transmit power $\overline{\mathcal{P}}_{\text{d}} = 20$ Watt for AP, and decoding error probability $\epsilon_m = 10^{-6}$. Fig. 2.6 depicts the delay in millisecond (ms) with varying average arrival rates λ_m over Rician wireless fading channels for our proposed CF m-MIMO scheme in the finite

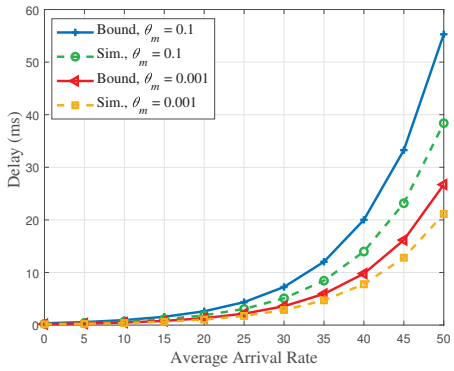

Figure 2.6: The delay (ms) vs. average arrival rate λ_m for our proposed CF m-MIMO scheme in the finite blocklength regime.

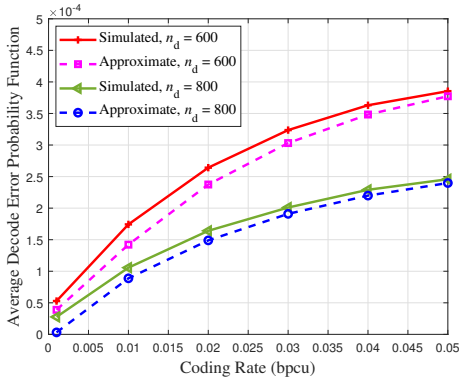

Figure 2.7: The average decoding error probability function $\epsilon_m\left(n_{\mathrm{d}}, \gamma_m\right)$ vs. achievable coding rate R_m for our proposed CF m-MIMO scheme in the finite blocklength regime.

blocklength regime, which implies the potential to support massive number of mobile users. We can observe from Fig. 2.6 that the queuing delay increases as the average arrival rate λ_m increases. Fig. 2.6 also shows that the analytical results provide a reasonable upper bound for the actual delay as obtained from simulations.

We set the number of APs $K_{\mathrm{a}} = 100$, the number of transmit antennas $N_{\mathrm{T}} = 10$, Rician factor $\kappa = 0$, and the average downlink transmit power $\overline{\mathcal{P}}_{\mathrm{d}} = 20$ Watt for each AP. Using Eq. (2.39), Fig. 2.7 depicts the average decoding error probability function $\mathbb{E}_{\gamma_m}\left[\epsilon_m\left(n_{\mathrm{d}}, \gamma_m\right)\right]$ with different achievable finite-blocklength coding rates R_m for our proposed CF m-MIMO scheme across

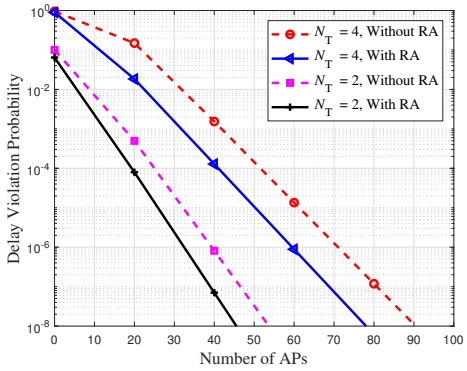

Figure 2.8: The delay violation probability $p_m(d_{\text{th}})$ vs. number of APs K_{a} for our proposed CF m-MIMO scheme in the finite blocklength regime.

Rayleigh wireless fading channels in the finite blocklength regime. We can observe from Fig. 2.7 that the average decoding error probability function $\mathbb{E}_{\gamma_m}\left[\epsilon_m\left(n_{\text{d}}, \gamma_m\right)\right]$ increases as the achievable finite-blocklength coding rate R_m increases. Fig. 2.7 also shows that the gap between the simulated average decoding error function and the approximate average decoding error function is reasonably small.

We set the number of transmit antennas $N_{\text{T}} = 10$, Rician factor $\kappa = 0$, the number of downlink channel uses $n_{\text{d}} = 800$, and the average downlink transmit power $\overline{\mathcal{P}}_{\text{d}} = 20$ Watt. Compared with the scheme without the optimal rate adaptation (RA), Fig. 2.8 depicts the delay violation probability $p_m(d_{\text{th}})$ with different numbers of APs K_{a} for our proposed CF m-MIMO scheme in the finite blocklength regime. We can observe from Fig. 2.8 that the delay violation probability $p_m(d_{\text{th}})$ decreases as the numbers of AP K_{a} increases. Fig. 2.8 also shows that our proposed schemes with optimal RA outperform the schemes without applying the optimal RA in terms of the delay violation probability over 6G CF m-MIMO mobile wireless networks in the finite blocklength regime.

Given different numbers of mobile users K_{u}, Fig. 2.9 depicts the block error probability function $\epsilon_m\left(n_{\text{d}}, \gamma_m\right)$ with varying blocklengths n_{d} for our proposed CF m-MIMO scheme in the finite blocklength regime. We can observe from Fig. 2.9 that the performance degradation in terms of block error probability function $\epsilon_m\left(n_{\text{d}}, \gamma_m\right)$ with the increasing number of mobile users K_{u} is mild,

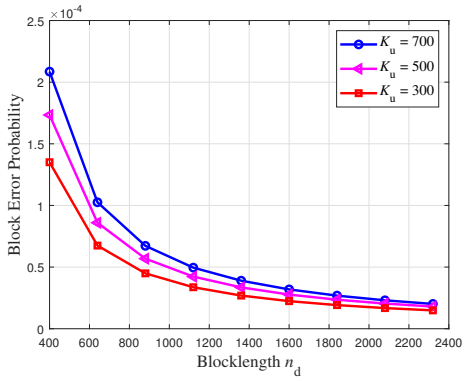

Figure 2.9: The block error probability function $\epsilon_m\left(n_{\mathrm{d}}, \gamma_m\right)$ vs. blocklength n_{d} for our proposed CF m-MIMO scheme in the finite blocklength regime.

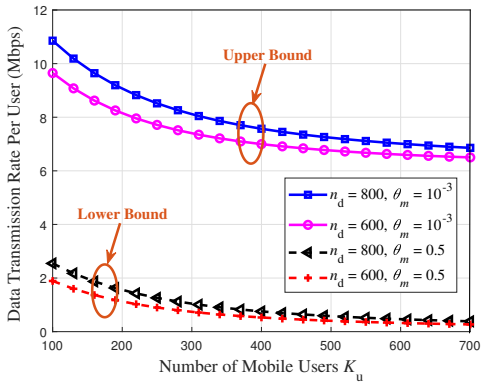

Figure 2.10: The data transmission rate per user vs. number of mobile users K_{u} for our proposed CF m-MIMO scheme in the finite blocklength regime.

implying the remarkable potential as well as the strong and robust scalability in supporting massive access by vast mobile devices over our proposed 6G CF m-MIMO mobile wireless networks.

Setting the number of transmit antennas $N_{\mathrm{T}} = 2$, Rician factor $\kappa = 0$, and the average downlink transmit power $\overline{\mathcal{P}}_{\mathrm{d}} = 20$ Watt, Fig. 2.10 plots the data transmission rate per user with different numbers of mobile users K_{u} for our proposed CF m-MIMO scheme in the finite blocklength regime. We can observe from Fig. 2.10 that the data transmission rate per user decreases as the number of mobile users K_{u} increases and will finally converge to a certain value, which implies the potential to support massive number of mobile users. Fig. 2.10 also shows that loose QoS con-

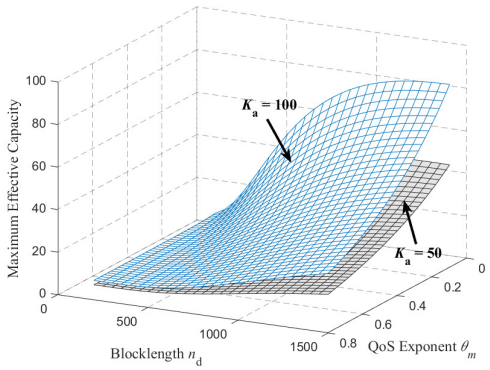

Figure 2.11: The maximum effective capacity $EC_m^{\max}(\theta_m)$ vs. blocklength $n_{\rm d}$ and QoS exponent θ_m for our proposed CF m-MIMO scheme in the finite blocklength regime.

straint ($\theta_m = 10^{-3}$) and stringent QoS constraint ($\theta_m = 0.5$) set the upper bound and lower bound on the data transmission rate per user, receptively.

Figure 2.11 plots the maximum effective capacity $EC_m^{\max}(\theta_m)$ with different blocklengths $n_{\rm d}$ and QoS exponents θ_m for our proposed CF m-MIMO scheme in the finite blocklength regime. We can observe from Fig. 2.11 that the maximum effective capacity $EC_m^{\max}(\theta_m)$ decreases as the QoS exponent θ_m increases. Fig. 2.11 also shows that the maximum effective capacity $EC_m^{\max}(\theta_m)$ is an increasing function of the blocklength $n_{\rm d}$ over 6G CF m-MIMO mobile wireless networks in the finite blocklength regime.

2.6 Summary

We have developed an analytical model to quantitatively characterize the performance for statistical delay and error-rate bounded QoS provisioning in supporting mURLLC over 6G CF m-MIMO mobile wireless networks in the finite blocklength regime. In particular, we have developed CF m-MIMO based system models. Then, we have applied the Mellin transform to model and characterize both arrival and service processes, derived the closed-form expressions of the delay violation probability function, and formulated and solved the delay violation probability minimization problem for our proposed CF m-MIMO modeling schemes in the finite blocklength regime. Furthermore, applying our developed system modeling techniques, we have derived the

closed-form solution for the optimal rate adaptation policy, which plays an important role in the system design and performance analyses for statistical delay and error-rate bounded QoS provisioning over 6G CF m-MIMO mobile wireless networks in the finite blocklength regime. We also have conducted a set of simulations to validate and evaluate our proposed CF m-MIMO schemes and show that our proposed schemes outperform the other existing schemes for statistical delay and error-rate bounded QoS provisioning in the finite blocklength regime.

3. STATISTICAL DELAY AND ERROR-RATE BOUNDED QOS PROVISIONING OVER MMWAVE CELL-FREE M-MIMO AND FBC-HARQ-IR BASED 6G MOBILE NETWORKS*

3.1 Introduction

Due to the ultra-low latency and high reliable guarantees of mURLLC, traditional automatic repeat and request (ARQ) scheme, which requires acknowledgement (ACK) or non-ACK(NACK) feedbacks, is no longer efficient for supporting delay-sensitive wireless multimedia applications. Towards this end, researchers have developed hybrid automatic repeat request (HARQ) [72] protocols, including HARQ with incremental redundancy (HARQ-IR) [73] and HARQ chase combining (HARQ-CC) [74], to adaptively control the transmission rate based on decoding feedbacks. There has been a great deal of research focusing on the performance analyses of HARQ protocols while being integrated with FBC. The authors of [75] have compared the link-level system performance with HARQ-IR and HARQ-CC, and shown that HARQ-IR can significantly improve channel coding rate as compared with HARQ-CC. The authors of [73] have studied power allocation policies using HARQ-IR protocol when analyzing reliable downlink data transmissions under QoS constraints. The impact of fixed transmission rate, queuing constraints, and hard-deadline limitations on the throughput has been studied in [76] while applying HARQ-IR protocol.

In addition, for the traditional m-MIMO systems, the cell-center mobile users can achieve higher data rates compared with cell-edge users, which implies that the latter suffers from a longer data transmission delay. Thus, at a given time instance, most of the active mobile users are likely at the cell edge. The fact that “cell-free" networks provide the largest performance gain to these mobile users demonstrate how effectively it can alleviate inter-cell interference. To reduce the backhaul overhead, a “user-centric" approach has been proposed for cell-free m-MIMO systems,

where each mobile user is served by a selected subset of APs which are within the user-centric cluster, which is also known as “user-specific dynamic clustering" developed for cooperative MIMO based mobile wireless networks. Only the APs that are geographically close to a given mobile user will be selected and each AP only coordinates its resource allocation policies with the APs that are in the same user-centric cluster. Two AP selection methods for user-centric cell-free m-MIMO systems are proposed in [77], including the received-power-based selection and largest-large-scale-fading-based selection. The authors of [78] have shown that such user-centric cell-free m-MIMO approach outperforms the pure cell-free m-MIMO approach in terms of achievable rate per-user for the vast majority of the mobile users in the network. The authors of [79] have studied the downlink performance of cell-free m-MIMO systems in terms of the minimum rate among all users.

When integrating m-MIMO with mmWave technique, the major design issues, such as accurate channel estimations, have been investigated to reduce the hardware complexity as well as power consumption over the mmWave m-MIMO based wireless fading channels. To resolve such problems, the authors of [80] have developed the low-complexity multiuser hybrid analog/digital precoding algorithms with limited feedbacks. Although the traditional suboptimal approaches for selecting analog precoder and combiner can avoid exhaustive search, it still suffers from some high-complexity operations. Due to the sparsity characteristics of mmWave wireless fading channels, researchers have developed dictionary learning method [81] to solve the hybrid beamforming optimization problem in a low-complexity way. The authors of [82] have proposed an algorithm for adapting dictionaries in order to achieve sparse signal representations. Furthermore, when being integrated with the mmWave technique, the assumptions and analytical results in [36, 79, 83] for the cell-free m-MIMO systems cannot be directly applied at mmWave frequency bands. The authors of [84] have introduced and analyzed the user-centric and cell-free system architectures at millimeter wave frequencies. The authors of [85] have proposed downlink power control algorithms to maximize the global energy efficiency in mmWave user-centric and cell-free m-MIMO architectures. However, how to efficiently integrate mmWave with cell-free m-MIMO architecture models in the finite blocklength regime under statistical delay/error-rate bounded constraints is still

an open problem.

To effectively overcome the above-mentioned challenges, in this chapter we integrate the mmWave user-centric cell-free m-MIMO system with FBC-HARQ technique over 6G wireless networks. In particular, we establish mmWave user-centric cell-free m-MIMO based system models. Then, we apply the dictionary learning method to design a low-complexity beam-training algorithm for solving the beam-training optimization problem. We also apply FBC-HARQ protocol to determine the channel capacity as well as error probability using FBC. Based on the information theoretic results in QoS theory, we characterize QoS metrics in terms of error probability and derive the corresponding effective capacity function for our proposed FBC-HARQ based mmWave cell-free m-MIMO schemes. We also conduct a set of simulations to validate and evaluate our proposed mmWave user-centric cell-free m-MIMO schemes by implementing statistical delay/error-rate bounded QoS provisioning in the finite blocklength regime.

The rest of this chapter is organized as follows: Section 3.2 establishes mmWave user-centric cell-free m-MIMO based system models. Section 3.3 designs the dictionary learning based beam-training algorithm. Section 3.4 derives the channel capacity and error probability using FBC-HARQ protocol. Section 3.5 derives and analyzes statistical delay/error-rate bounded QoS metrics and effective capacity function in the finite blocklength regime. Section 3.6 evaluates and analyzes the system performance for our proposed FBC-HARQ based mmWave user-centric cell-free m-MIMO schemes. The chapter concludes with Section 3.7.

3.2 The Network Architecture and System Models

3.2.1 The MmWave User-Centric Cell-Free m-MIMO System Architecture

Consider an mmWave user-centric cell-free m-MIMO network model, where each mobile user is served by coherent joint transmissions from a selected subset of APs which are within the user-centric cluster. Fig. 3.1 shows the system modeling for our proposed mmWave cell-free m-MIMO and FBC-HARQ based 6G multimedia mobile wireless networks. We assume that each AP is equipped with N_{T} antennas and L_{T} RF chains ($N_{\mathrm{T}} > K_{\mathrm{u}}, N_{\mathrm{T}} \geq L_{\mathrm{T}}$, and $L_{\mathrm{T}} < K_{\mathrm{u}}$). Define $\mathcal{G}(k)$

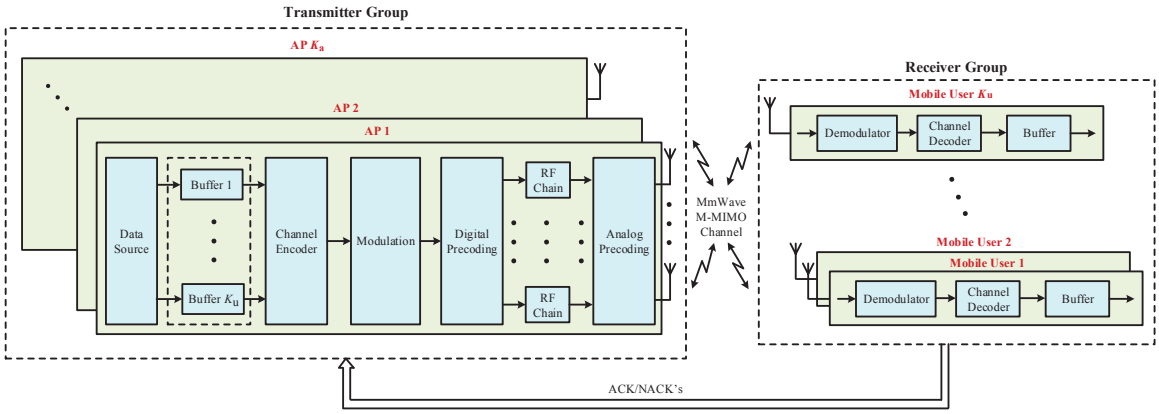

Figure 3.1: The system modeling for our proposed mmWave cell-free m-MIMO and FBC-HARQ based 6G multimedia mobile wireless networks.

as the group of mobile users served by the kth AP, where $|\mathcal{G}(k)| = L_{\mathrm{T}} < K_{\mathrm{u}}$. Define $\mathcal{K}(m)$ as the cluster APs that serve mobile user m.

3.2.2 The MmWave User-Centric Cell-Free m-MIMO Based System Models

As shown in Fig. 3.2, each time interval is divided into the following three phases:

1. *Large-scale beam-training phase:* Each AP chooses an optimal RF precoder and selects a group of mobile users $\mathcal{G}(k)$ with the best channel quality;

2. *Small-scale uplink training phase:* Mobile users send uplink pilot symbols to the APs, then each AP estimates the wireless channels to all mobile users based on the received pilot symbols;

3. *Downlink finite-blocklength data transmission phase:* The APs use the knowledge of channel estimation obtained in the previous small-scale uplink training phase, precode, and transmit the finite-blocklength data to mobile users under HARQ-IR protocol, as shown in Fig. 3.2. HARQ-IR protocol will be discussed in detail in Section 3.4.

Define n_{d} as the number of channel uses reserved for transmitting L equal-length downlink-data blocks with $\widehat{n}$ symbols each for implementing HARQ-IR protocol, i.e., $n_{\mathrm{d}} = L\widehat{n}$.

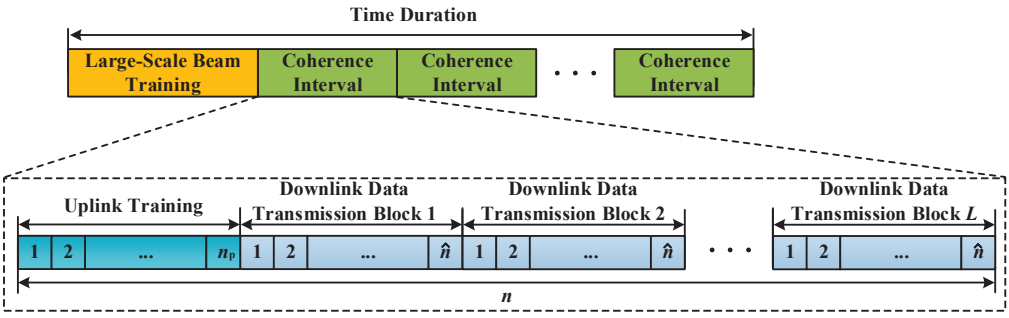

Figure 3.2: Frame structure with large-scale beam-training, small-scale uplink training, and finite-blocklength downlink data transmission phases using HARQ-IR protocol in mmWave user-centric cell-free m-MIMO scheme, where L is the number of finite-blocklength data blocks for the downlink data transmission using HARQ-IR protocol and $\widehat{n}$ is the blocklength of each data block using HARQ-IR protocol.

B.1 Large-Scale Beam-Training Phase

The goal of large-scale beam-training phase is to develop an efficient algorithm to design an optimal RF precoder $\mathbf{F}_{k,m}^{\mathrm{R,opt}} \in \mathbb{C}^{N_{\mathrm{T}} \times L_{\mathrm{T}}}$ and user selection group $\mathcal{G}(k)$. Define an equivalent channel's impulse response vector, denoted by $\widetilde{\boldsymbol{h}}_{k,m}$, between the kth AP and mobile user m as in the following equation:

$$\widetilde{\boldsymbol{h}}_{k,m} = \boldsymbol{h}_{k,m} \mathbf{F}_{k,m}^{\mathrm{R}} \tag{3.1}$$

where $\boldsymbol{h}_{k,m} \in \mathbb{C}^{1 \times N_{\mathrm{T}}}$ represents the channel's impulse response vector from the kth AP to mobile user m and $\mathbf{F}_{k,m}^{\mathrm{R}} \in \mathbb{C}^{N_{\mathrm{T}} \times L_{\mathrm{T}}}$ is the analog precoder from AP k to mobile user m. Correspondingly, we can formulate the maximization problem $\mathbf{P_5}$ which selects the best mobile user and the optimal precoding matrix $\left\{m^{\mathrm{opt}}, \mathbf{F}_{k,m}^{\mathrm{R,opt}}\right\}$ as follows:

$$\mathbf{P_5}: \left\{m^{\mathrm{opt}}, \mathbf{F}_{k,m}^{\mathrm{R,opt}}\right\} = \arg \max_{\left\{m, \mathbf{F}_{k,m}^{\mathrm{R}}\right\}} \left\{ \left\| \boldsymbol{h}_{k,m} \mathbf{F}_{k,m}^{\mathrm{R}} \right\|_F^2 \right\} \tag{3.2}$$

$$\text{s.t. C1: } \mathbf{F}^{\mathrm{R}}_{k,m} \in \boldsymbol{\mathcal{F}}_c, \quad \forall m;$$
$$\text{C2: } \left\|\mathbf{F}^{\mathrm{R}}_{k,m}\mathbf{F}^{\mathrm{B}}_{k,m}\right\|^2_F = 1, \quad \forall m, \tag{3.3}$$

where $\|\mathbf{M}\|^2_F$ is the Frobenius norm of matrix $\mathbf{M}$, which is defined as $\sqrt{\mathrm{Tr}\left((\mathbf{M}^{\dagger})\mathbf{M}\right)}$, $(\cdot)^{\dagger}$ denotes the Hermitian transpose of a matrix, Tr$(\cdot)$ denotes the trace of a matrix, $\mathbf{F}^{\mathrm{B}}_{k,m}$ is the digital precoder from AP k to mobile user m, and $\boldsymbol{\mathcal{F}}_c = \{\boldsymbol{f}_c(1), \ldots, \boldsymbol{f}_c(N_{\mathrm{T}})\}$ is the beam steering codebook stored at the APs, given by

$$\boldsymbol{f}_c(i) = \frac{1}{\sqrt{N_{\mathrm{T}}}}\left[1, e^{\jmath\pi\left(-1+\frac{(2i-1)}{N_{\mathrm{T}}}\right)}, \ldots, e^{\jmath\pi(N_{\mathrm{T}}-1)\left(-1+\frac{2i-1}{N_{\mathrm{T}}}\right)}\right]^T \tag{3.4}$$

for $i = 1, \ldots, N_{\mathrm{T}}$ where $\jmath = \sqrt{-1}$. Note that the vector $\boldsymbol{f}_c(i)$ has the same structure as the antenna array's response vector. To solve the above optimization problem $\mathbf{P_5}$, we can apply the exhaustive search method. However, the complexity of such exhaustive search method is too high, especially for m-MIMO scenario. Accordingly, we design low-complexity suboptimal beam-training algorithm to solve $\mathbf{P_5}$ and the corresponding user selection method in Section 3.3.

B.2 Small-Scale Uplink Training Phase

Define the pilot training sequence from all K_{u} mobile users as $\boldsymbol{s}_m \triangleq \left[s^{(1)}_m, \ldots, s^{(n_{\mathrm{p}})}_m\right]$ and $\|\boldsymbol{s}_m\|^2_F = 1$. During the small-scale uplink training phase, we can derive the received signal, denoted by $\boldsymbol{y}^{(l)}_k$, at the kth AP for transmitting the lth training data block as in the following equation:

$$\boldsymbol{y}^{(l)}_k = \sum_{m=1}^{K_{\mathrm{u}}} \sqrt{\mathcal{P}_{\mathrm{p}}}\widetilde{\boldsymbol{h}}_{k,m}s^{(l)}_m + \boldsymbol{n}^{(l)}_k, \quad l = 1, \ldots, n_{\mathrm{p}} \tag{3.5}$$

where $\mathcal{P}_{\mathrm{p}}$ is the uplink pilot transmit power from each mobile user to the AP; $s^{(l)}_m$ denotes the pilot training signal sent from mobile user m to the kth AP; $\widetilde{\boldsymbol{h}}_{k,m}$ represents the equivalent channel's impulse response vector between mobile user m and the kth AP, given in Eq. (3.1); and $\boldsymbol{n}^{(l)}_k$ is the AWGN with zero mean and variance σ^2. Then, we can derive the MMSE channel estimation as

follows:

$$\widehat{\boldsymbol{h}}_{k,m} = \frac{\mathbb{E}_{\widetilde{\boldsymbol{h}}_{k,m}}\left[\widetilde{\boldsymbol{h}}_{k,m}\left(\widetilde{\boldsymbol{h}}_{k,m}\right)^{\dagger}\right]}{\sum\limits_{m=1}^{K_{\mathrm{u}}}\left(\mathbf{F}_{k,m}^{\mathrm{R}}\right)^{\dagger}\mathbb{E}_{\boldsymbol{h}_{k,m}}\left[\boldsymbol{h}_{k,m}\left(\boldsymbol{h}_{k,m}\right)^{\dagger}\right]\mathbf{F}_{k,m}^{\mathrm{R}}+\sigma^{2}\mathbf{I}_{K_{\mathrm{u}}}} = \frac{\left\|\left(\mathbf{F}_{k,m}^{\mathrm{R}}\right)^{\dagger}\mathbb{E}_{\boldsymbol{h}_{k,m}}\left[\boldsymbol{h}_{k,m}\left(\boldsymbol{h}_{k,m}\right)^{\dagger}\right]\mathbf{F}_{k,m}^{\mathrm{R}}\right\|^{2}}{\sum\limits_{m=1}^{K_{\mathrm{u}}}\left(\mathbf{F}_{k,m}^{\mathrm{R}}\right)^{\dagger}\mathbb{E}_{\boldsymbol{h}_{k,m}}\left[\boldsymbol{h}_{k,m}\left(\boldsymbol{h}_{k,m}\right)^{\dagger}\right]\mathbf{F}_{k,m}^{\mathrm{R}}+\sigma^{2}\mathbf{I}_{K_{\mathrm{u}}}} \tag{3.6}$$

where $\|\cdot\|$ is the norm of a matrix, $\mathbb{E}_{\widetilde{\boldsymbol{h}}_{k,m}}[\cdot]$ is the expectation over $\widetilde{\boldsymbol{h}}_{k,m}$, and $\mathbf{I}_{K_{\mathrm{u}}}$ is the identity matrix of size K_{u}.

B.3 User-Centric Downlink Finite-Blocklength Data Transmission Phase

We define the transmit signal matrix as $\mathbf{X}_{m}^{n_{\mathrm{d}}} \triangleq \left[\boldsymbol{x}_{m}^{(1)},\ldots,\boldsymbol{x}_{m}^{(n_{\mathrm{d}})}\right]$ and receive signal vector as $\boldsymbol{y}_{m}^{n_{\mathrm{d}}} \triangleq \left[y_{m}^{(1)},\ldots,y_{m}^{(n_{\mathrm{d}})}\right]$, respectively. Considering Rayleigh block-fading channel, we can derive the received signal, denoted by $\boldsymbol{y}_{m}^{n_{\mathrm{d}}} \in \mathbb{C}^{1\times n_{\mathrm{d}}}$, from the kth AP to the mth mobile user for transmitting n_{d} finite-blocklength data blocks as follows:

$$\boldsymbol{y}_{m}^{n_{\mathrm{d}}} = \sum_{k\in K(m)}\boldsymbol{h}_{k,m}\mathbf{F}_{k,m}^{\mathrm{R}}\mathbf{F}_{k,m}^{\mathrm{B}}\left(\boldsymbol{\Omega}_{k,m}\right)^{\frac{1}{2}}\mathbf{X}_{m}^{n_{\mathrm{d}}} + \sum_{\substack{m'=1\\ m'\neq m}}^{K_{\mathrm{u}}}\sum_{k\in\mathcal{K}(m')}\boldsymbol{h}_{k,m}\mathbf{F}_{k,m'}^{\mathrm{R}}\mathbf{F}_{k,m'}^{\mathrm{B}}\left(\boldsymbol{\Omega}_{k,m'}\right)^{\frac{1}{2}}\mathbf{X}_{m'}^{n_{\mathrm{d}}} + \boldsymbol{n}_{m} \tag{3.7}$$

where $\mathbf{X}_{m}^{n_{\mathrm{d}}}$ and $\mathbf{X}_{m'}^{n_{\mathrm{d}}}$ are the signals sent to mobile user m and mobile user m', respectively; $\mathbf{F}_{k,m}^{\mathrm{R}} \in \mathbb{C}^{N_{\mathrm{T}}\times L_{\mathrm{T}}}$ and $\mathbf{F}_{k,m'}^{\mathrm{R}} \in \mathbb{C}^{N_{\mathrm{T}}\times L_{\mathrm{T}}}$ are the analog precoders for mobile user m and mobile user m', respectively; $\mathbf{F}_{k,m}^{\mathrm{B}} \in \mathbb{C}^{L_{\mathrm{T}}\times N_{\mathrm{T}}}$ and $\mathbf{F}_{k,m'}^{\mathrm{B}} \in \mathbb{C}^{L_{\mathrm{T}}\times N_{\mathrm{T}}}$ represent the digital precoders for mobile user m and mobile user m', respectively; $\boldsymbol{\Omega}_{k,m} \in \mathbb{C}^{N_{\mathrm{T}}\times N_{\mathrm{T}}}$ and $\boldsymbol{\Omega}_{k,m'} \in \mathbb{C}^{N_{\mathrm{T}}\times N_{\mathrm{T}}}$ denote the power allocation matrices which allocate total transmit power among N_{T} streams at the kth AP to mobile user m and mobile user m', respectively; and $\boldsymbol{n}_{m}$ is the AWGN with zero mean and covariance $\mathbf{I}_{n_{\mathrm{d}}}\sigma^{2}$. Define $\boldsymbol{\Omega}_{k,m} \triangleq \mathrm{diag}\left\{\omega_{k,m}^{(1)},\ldots,\omega_{k,m}^{(N_{\mathrm{T}})}\right\}$ as the power allocation matrix, where $\mathrm{diag}\{\cdot\}$ represents the diagonal matrix. In addition, we normalize the precoding matrices

as $\left\|\mathbf{F}_{k,m}^{\mathrm{R}}\mathbf{F}_{k,m}^{\mathrm{B}}\right\|_F^2 = 1$. As a result, the received signal at mobile user m can be rewritten as in the following equation:

$$\boldsymbol{y}_m^{n_\mathrm{d}} = \sum_{k\in\mathcal{K}(m)} \widetilde{\boldsymbol{h}}_{k,m}\mathbf{F}_{k,m}^{\mathrm{B}}\left(\boldsymbol{\Omega}_{k,m}\right)^{\frac{1}{2}}\mathbf{X}_m^{n_\mathrm{d}} + \sum_{\substack{m'=1\\m'\neq m}}^{K_\mathrm{u}}\sum_{k\in\mathcal{K}(m')} \widetilde{\boldsymbol{h}}_{k,m}\mathbf{F}_{k,m'}^{\mathrm{B}}\left(\boldsymbol{\Omega}_{k,m'}\right)^{\frac{1}{2}}\mathbf{X}_{m'}^{n_\mathrm{d}} + \boldsymbol{n}_m. \tag{3.8}$$

In addition, we can determine the SINR, denoted by γ_m, for mobile user m as follows:

$$\gamma_m = \frac{\sum\limits_{k\in\mathcal{K}(m)}\left\|\widetilde{\boldsymbol{h}}_{k,m}\mathbf{F}_{k,m}^{\mathrm{B}}\left(\boldsymbol{\Omega}_{k,m}\right)^{\frac{1}{2}}\right\|^2}{\left\|\sum\limits_{\substack{m'=1\\m'\neq m}}^{K_\mathrm{u}}\sum\limits_{k\in\mathcal{K}(m')}\widetilde{\boldsymbol{h}}_{k,m}\mathbf{F}_{k,m'}^{\mathrm{B}}\left(\boldsymbol{\Omega}_{k,m'}\right)^{\frac{1}{2}}\right\|^2 + \sigma^2}. \tag{3.9}$$

3.3 Dictionary Learning Based Low-Complexity Hybrid Precoder Design

Although the traditional suboptimal methods for selecting analog precoder and combiner can avoid exhaustive search, it still involves some high-complexity matrix operations. Due to the sparsity characteristics of mmWave wireless fading channels, we apply the dictionary learning method [81] to solve the optimization problem in a low-complexity way. During the dictionary learning based beam-training phase, using Eq. (3.4), we can define the following over-complete beam steering codebook for the RF precoder to achieve the sparse representation for solving the optimization problem $\mathbf{P_5}$:

$$\widetilde{\boldsymbol{f}}_c(i) = \frac{1}{\sqrt{N_\mathrm{T}}}\left[1, e^{\jmath\pi\left(-1+\frac{(2i-1)}{M_\mathrm{T}}\right)}, \ldots, e^{\jmath\pi(N_\mathrm{T}-1)\left(-1+\frac{2i-1}{M_\mathrm{T}}\right)}\right]^T \tag{3.10}$$

for $i = 1, \ldots, M_\mathrm{T}$ where $M_\mathrm{T} > N_\mathrm{T}$. Thus, we can rewrite the beam-training codebook at the APs as $\widetilde{\boldsymbol{\mathcal{F}}}_c = \left\{\widetilde{\boldsymbol{f}}_c(1), \ldots, \widetilde{\boldsymbol{f}}_c(M_\mathrm{T})\right\}$. Such an over-complete matrix introduces redundancy to the original beamforming codebook matrix, improving both flexibility and capability of sparse representation. Using the singular value decomposition (SVD), the channel's impulse response vector $\boldsymbol{h}_{k,m}$ can be

decomposed as follows:

$$\boldsymbol{h}_{k,m} = \mathbf{U}_{k,m}\boldsymbol{\Sigma}_{k,m}\left(\mathbf{V}_{k,m}\right)^{\dagger} \tag{3.11}$$

where the columns of $\mathbf{U}_{k,m}$ is the left singular vector of $\boldsymbol{h}_{k,m}$; $\boldsymbol{\Sigma}_{k,m}$ denotes the diagonal matrix containing the singular values of $\boldsymbol{h}_{k,m}$; and the rows of $(\mathbf{V}_{k,m})^{\dagger}$ represent the right singular vectors of $\boldsymbol{h}_{k,m}$. Define an optimal precoder matrix as $\mathbf{F}_{k,m}^{\text{opt}} \triangleq \mathbf{V}_{k,m}$. Then, we define $\mathbf{D}_{k,m} \triangleq [\mathbf{D}_{k,1}, \ldots, \mathbf{D}_{k,K_{\text{u}}}]$ as the dictionary of beamforming codewords learned from large-scale beam-training phase at AP k for mobile user m. Motivated by $\mathbf{P_5}$, we need to minimize the "distance" between the layered precoder $\left\{\mathbf{F}_{k,m}^{\text{R}}, \mathbf{F}_{k,m}^{\text{B}}\right\}$ and an optimal precoder $\mathbf{F}_{k,m}^{\text{opt}}$. As a result, converting $\mathbf{P_5}$, we can formulate the following maximization problem $\mathbf{P_6}$ by using the concept of the Fubini-Study distance [86]:

$$\mathbf{P_6}: \arg \max_{\left\{m, \mathbf{F}_{k,m}^{\text{R}}, \mathbf{F}_{k,m}^{\text{B}}\right\}} \left\{ \left\| \left(\mathbf{F}_{k,m}^{\text{opt}}\right)^{\dagger} \mathbf{F}_{k,m}^{\text{R}} \mathbf{F}_{k,m}^{\text{B}} \right\| \right\} \tag{3.12}$$

subject to constraints C1 and C2 given in Eq. (3.3), where $\|\cdot\|$ denotes the Euclidean norm. To solve the maximization problem $\mathbf{P_6}$, we can formulate an equivalent optimization problem to minimize the Frobenius norm of the error between the two precoders. Accordingly, the maximization problem $\mathbf{P_6}$ can be reconstructed as the following overall error minimization problem $\mathbf{P_7}$ for designing an optimal beam-training codebook for our proposed cell-free mmWave m-MIMO schemes:

$$\mathbf{P_7}: \arg \min_{\left\{m, \mathbf{F}_{k,m}^{\text{R}}, \mathbf{F}_{k,m}^{\text{B}}\right\}} \left\{ \left\| \mathbf{F}_{k,m}^{\text{opt}} - \mathbf{F}_{k,m}^{\text{R}} \mathbf{F}_{k,m}^{\text{B}} \right\|_F \right\} \tag{3.13}$$

subject to constraints C1 and C2 given in Eq. (3.3). Correspondingly, using the dictionary learning approach, we can reformulate problem $\mathbf{P_7}$ into an equivalent minimization problem $\mathbf{P_8}$ as follows:

$$\mathbf{P_8}: \arg \min_{\left\{m, \mathbf{D}_{k,m}, \mathbf{F}_{k,m}^{\text{B}}\right\}} \left\{ \left\| \mathbf{F}_{k,m}^{\text{opt}} - \mathbf{D}_{k,m} \mathbf{F}_{k,m}^{\text{B}} \right\|_F \right\} \tag{3.14}$$

$$\text{s.t. C3: } \left\| \mathbf{F}_{k,m}^{\mathrm{B}} \left(\mathbf{F}_{k,m}^{\mathrm{B}} \right)^{\dagger} \right\|_0 = L_{\mathrm{T}}, \quad \forall m;$$
$$\text{C4: } \left\| \mathbf{D}_{k,m} \mathbf{F}_{k,m}^{\mathrm{B}} \right\|_F^2 = 1, \quad \forall m, \tag{3.15}$$

where $\|\mathbf{M}\|_0$ represents the ℓ_0-pseudo-norm that counts the number of non-zero entries in matrix $\mathbf{M}$. For our dictionary learning based beam-training algorithm, our goal is to minimize the object function given in Eq. (3.14) iteratively. To solve the minimization problem $\mathbf{P_8}$, we need to proceed with the following stages. 1) Sparse coding stage: We fix the dictionary $\mathbf{D}_{k,m}$ and find the best matrix $\mathbf{F}_{k,m}^{\mathrm{B}}$ by applying any suitable approximation pursuit method. In this chapter, we apply the orthogonal matching pursuit (OMP) algorithm [87]. 2) Dictionary update stage: In the dictionary update stage, the algorithm searches for a better dictionary by updating one column at a time. During each iteration, all columns in $\mathbf{D}_{k,m}$ is fixed except $[\mathbf{D}_{k,m}]_{:,i}$, where $[\mathbf{D}_{k,m}]_{:,i}$ represents the ith column of matrix $\mathbf{D}_{k,m}$. Also, $[\mathbf{D}_{k,m}]_{:,i}$ and the corresponding matrix $\mathbf{F}_{k,m}^{\mathrm{B}}$ are updated for achieving the minimum overall representation error in the optimization problem $\mathbf{P_8}$ at the end of each iteration. We define $\mathbf{D}_{k,m}^{(\ell)}$ and $\mathbf{F}_{k,m}^{(\ell,\mathrm{B})}$ as the updated dictionary and the sparse representation matrix after ℓth iteration, respectively. **Algorithm 1** is the pseudo-code outlining our proposed dictionary learning based beam-training algorithm.

Assume that the sparse coding stage is perfectly conducted, we can retrieve the best approximations to $\mathbf{F}_{k,m}^{\mathrm{R}}$ that contains no more than e_0 non-zero entries. In this case, when fixing the dictionary $\mathbf{D}_{k,m}$, the overall representation error given in Eq. (3.14) will be decreased after each iteration. In addition, during the dictionary update stage, an additional reduction or no change in the overall representation error is guaranteed, while not violating the constraints. As a result, such series of iterations ensures a monotonic overall representation error reduction, which indicates that the convergence to a local minimum is guaranteed.

3.4 The HARQ-IR Protocol in the Finite Blocklength Regime

Unlike the traditional ARQ protocol, HARQ protocol enables receiver to exploit the received information from previous HARQ transmission rounds to increase the successful decoding prob-

Algorithm 1 Dictionary Learning Based Beam-Training Algorithm

Input: K_{u}, L_{T}, and N_{T}
Initialization: Set the initial dictionary $\mathbf{D}_{k,m}^{(0)} = \widetilde{\boldsymbol{\mathcal{F}}}_c \in \mathbb{R}^{N_{\mathrm{T}} \times M_{\mathrm{T}}}$, $\mathbf{F}_{k,m}^{\mathrm{R}} = \emptyset$, $\mathcal{G}_{\mathrm{k}} = \emptyset$, and $\ell = 1$
Dictionary Learning:
repeat
  Sparse coding stage:
  for $m = 1 : K_{\mathrm{u}}$ **do**
    Use OMP method to determine $\mathbf{F}_{k,m}^{(\ell,\mathrm{B})}$ for each example $[\mathbf{D}_{k,m}]_{:,i}$
    Select the best matrix $\mathbf{F}_{k,m}^{(\ell,\mathrm{B})}$ and the strongest user with the corresponding best precoder $\mathbf{F}_{k,m}^{(\ell,\mathrm{B})}$ by solving $\arg \min_{\left\{m, \mathbf{F}_{k,m}^{\mathrm{B}}\right\}} \left\{ \left\| \mathbf{F}_{k,m}^{\mathrm{opt}} - \mathbf{D}_{k,m} \mathbf{F}_{k,m}^{\mathrm{B}} \right\|_F \right\}$
    $\mathcal{G}_{\mathrm{k}} = \mathcal{G}_{\mathrm{k}} \bigcup \{m^{\mathrm{opt}}\}$
  end for
  Dictionary update stage:
  for $i = 1 : M_{\mathrm{T}}$ **do**
    Update $\mathbf{F}_{k,m}^{(\ell,\mathrm{B})}$ and $\mathbf{D}_{:,i}^{(\ell)}$ using Eq. (3.14)
  end for
  Set $\ell \leftarrow \ell + 1$
until convergence

ability of a data packet. Define M_m as the total bits of data packet that is intended to be transmitted for mobile user m. Each downlink finite-blocklength codeword with length n_{d} is divided into L blocks of $\widehat{n}$ symbols for implementing HARQ-IR protocol, i.e., $n_{\mathrm{d}} = L\widehat{n}$ (see Fig. 3), and will be transmitted consecutively in the following time slots. Accordingly, we define the codeword with length L finite-blocklength data blocks as $\mathbf{X}_m^{n_{\mathrm{d}}} \triangleq \left[\mathbf{X}_m^{(1)}, \ldots, \mathbf{X}_m^{(L)}\right]$, where $\mathbf{X}_m^{(l)} \triangleq \left[\boldsymbol{x}_m^{(\widehat{n}(l-1)+1)}, \ldots, \boldsymbol{x}_m^{(\widehat{n}l)}\right]$ for $l = 1, \ldots, L$. Under HARQ-IR protocol, if the received data packet can be successfully decoded at the receiver, an ACK will be sent back to the transmitter, and the corresponding data packet will be removed from buffer. Otherwise, a NACK is sent back to the transmitter and another data block will be transmitted until the codeword is successfully decoded at the receiver or the maximum number of transmissions for the packet is reached. By using the dictionary learning based beam-training precoder design given by **Algorithm 1**, we can characterize the channel capacity as well as the error probability using our proposed HARQ-IR based mmWave user-centric cell-free m-MIMO system models.

We apply the *threshold decoding rule* [88], i.e., $\boldsymbol{i}\left(\mathbf{X}_m^{\widehat{n}l};\boldsymbol{y}_m^{\widehat{n}l},\widetilde{\boldsymbol{h}}_{k,m}\right)>\beta_m$, where $\beta_m \triangleq \log\frac{M_m-1}{2}$ denotes the decoding threshold and $\boldsymbol{i}\left(\mathbf{X}_m^{\widehat{n}l};\boldsymbol{y}_m^{\widehat{n}l},\widetilde{\boldsymbol{h}}_{k,m}\right)$ is defined as the *information density* for the codeword of finite blocklength $\widehat{n}l$, which can be expressed as follows:

$$\boldsymbol{i}\left(\mathbf{X}_m^{\widehat{n}l};\boldsymbol{y}_m^{\widehat{n}l},\widetilde{\boldsymbol{h}}_{k,m}\right)=\frac{1}{\widehat{n}lN_{\mathrm{T}}}\sum_{j=1}^{\widehat{n}l}\boldsymbol{i}_{m,j}\triangleq\frac{1}{\widehat{n}lN_{\mathrm{T}}}\sum_{j=1}^{\widehat{n}l}\log\frac{P_{y_m^{(j)}|\widetilde{\boldsymbol{h}}_{k,m},\boldsymbol{x}_m^{(j)}}\left(y_m^{(j)}|\widetilde{\boldsymbol{h}}_{k,m},\boldsymbol{x}_m^{(j)}\right)}{P_{y_m^{(j)}|\widetilde{\boldsymbol{h}}_{k,m}}\left(y_m^{(j)}|\widetilde{\boldsymbol{h}}_{k,m}\right)} \tag{3.16}$$

where $\log(\cdot)$ represents $\log_e(\cdot)$, $\boldsymbol{y}_m^{\widehat{n}N_l}$ is the received signal with length $\widehat{n}l$, $P_{y_m^{(j)}|\widetilde{\boldsymbol{h}}_{k,m},\boldsymbol{x}_m^{(j)}}$ and $P_{y_m^{(j)}|\widetilde{\boldsymbol{h}}_{k,m}}$ denote the conditional probabilities, and $\boldsymbol{i}_{m,j}$ denotes the random variable with the same distribution of the information density $\boldsymbol{i}\left(\mathbf{X}_m^{\widehat{n}l};\boldsymbol{y}_m^{\widehat{n}l},\widetilde{\boldsymbol{h}}_{k,m}\right)$. In addition, using HARQ-IR protocol, we can define the initial transmission rate, denoted by $R_{m,\text{in}}$, for mobile user m as follows:

$$R_{m,\text{in}}\triangleq\frac{\log M_m}{\widehat{n}}\ \text{bits/channel use.} \tag{3.17}$$

Accordingly, the data transmission rate, denoted by $R_{m,l}$, for transmitting data block l to mobile user m can be defined as follows:

$$R_{m,l}\triangleq\frac{\log M_m}{\widehat{n}l}=\frac{R_{m,\text{in}}}{l}\ \text{bits/channel use.} \tag{3.18}$$

Under the dependence testing (DT) bound, previous results [30] have shown that there exists an $(\widehat{n}l,M_m,\epsilon_{m,l})$-code and average error probability, denoted by $\epsilon_{m,l}$, not exceeding the following constraint:

$$\begin{aligned}\epsilon_{m,l}\leq&\mathbb{E}_{\widetilde{\boldsymbol{h}}_{k,m}}\Bigg[\Pr\left\{\boldsymbol{i}\left(\mathbf{X}_m^{\widehat{n}l};\boldsymbol{y}_m^{\widehat{n}l},\widetilde{\boldsymbol{h}}_{k,m}\right)<\log\left(\frac{M_m-1}{2}\right)\right\}\\&+\frac{M_m-1}{2}\Pr P_{\overline{Y}_m^{\widehat{n}l}|\widetilde{\boldsymbol{h}}_{k,m}}\left(\boldsymbol{i}\left(\mathbf{X}_m^{\widehat{n}l};\overline{\boldsymbol{y}}_m^{\widehat{n}l},\widetilde{\boldsymbol{h}}_{k,m}\right)>\log\left(\frac{M_m-1}{2}\right)\right)\Bigg]\end{aligned} \tag{3.19}$$

where $\overline{\boldsymbol{y}}_m^{\widehat{n}l}$ follows the same distribution as the output signal $\boldsymbol{y}_m^{\widehat{n}l}$ and is independent of the input signal $\mathbf{X}_m^{\widehat{n}l}$. When calculating the average decoding error probability, we consider two different

error events, i.e., miss-detection error and confusion error. Using the Berry-Esseen Theorem [89], we can derive the miss-detection error probability which is given in the first term on the right-hand side in Eq. (3.19) as follows:

$$\Pr\left\{\boldsymbol{i}\left(\mathbf{X}_m^{\widehat{n}l};\boldsymbol{y}_m^{\widehat{n}l},\widetilde{\boldsymbol{h}}_{k,m}\right)<\log\left(\frac{M_m-1}{2}\right)\right\}=Q\left(\frac{\widehat{n}lC_m\left(\widetilde{\boldsymbol{h}}_{k,m}\right)-\log\left(\frac{M_m-1}{2}\right)}{\sqrt{\widehat{n}lV_m\left(\widetilde{\boldsymbol{h}}_{k,m}\right)}}\right)$$
$$-2\left(\frac{\log 2}{\sqrt{2\pi}}+B_1\right)\frac{1}{\sqrt{\widehat{n}l}} \tag{3.20}$$

where $Q(\cdot)$ is the Q-function, $C_m\left(\widetilde{\boldsymbol{h}}_{k,m}\right)$ denotes the channel capacity, $V_m\left(\widetilde{\boldsymbol{h}}_{k,m}\right)$ is the channel dispersion, and

$$B_1=\frac{6\mathcal{S}\left[\boldsymbol{i}\left(\mathbf{X}_m^{\widehat{n}l};\boldsymbol{y}_m^{\widehat{n}l},\widetilde{\boldsymbol{h}}_{k,m}\right)\right]}{\left[V_m\left(\widetilde{\boldsymbol{h}}_{k,m}\right)\right]^{\frac{3}{2}}} \tag{3.21}$$

where $\mathcal{S}[\cdot]$ is the third moment operator. Furthermore, according to [30], we can obtain the following confusion error probability which is given in the second term on the right-hand side in Eq. (3.19):

$$\frac{M_m-1}{2}\Pr\left\{\boldsymbol{i}\left(\mathbf{X}_m^{\widehat{n}l};\boldsymbol{y}_m^{\widehat{n}l},\widetilde{\boldsymbol{h}}_{k,m}\right)\geq\log\left(\frac{M_m-1}{2}\right)\right\}$$
$$=\mathbb{E}_{\widetilde{\boldsymbol{h}}_{k,m}}\left[\exp\left\{-\sum_{j=1}^{\widehat{n}l}\boldsymbol{i}_{m,j}\right\}1_{\left\{\sum_{j=1}^{\widehat{n}l}\boldsymbol{i}_{m,j}>\log\left(\frac{M_m-1}{2}\right)\right\}}\right]\leq 2\left(\frac{\log 2}{\sqrt{2\pi}}+B_2\right)\frac{1}{\sqrt{\widehat{n}l}} \tag{3.22}$$

where

$$B_2=\frac{1}{V_m\left(\widetilde{\boldsymbol{h}}_{k,m}\right)}\left(12\mathcal{S}\left[\left|\boldsymbol{i}\left(\mathbf{X}_m^{\widehat{n}l};\boldsymbol{y}_m^{\widehat{n}l},\widetilde{\boldsymbol{h}}_{k,m}\right)-\mathbb{E}_{\widetilde{\boldsymbol{h}}_{k,m}}\left[\boldsymbol{i}\left(\mathbf{X}_m^{\widehat{n}l};\boldsymbol{y}_m^{\widehat{n}l},\widetilde{\boldsymbol{h}}_{k,m}\right)\right]\right|\right]\right). \tag{3.23}$$

Correspondingly, we can obtain the average decoding error probability, denoted by $\epsilon_{m,l}$, for data packets with length $\widehat{n}l$ under HARQ-IR protocol over mmWave cell-free m-MIMO based 6G mul-

timedia mobile wireless networks as follows:

$$\epsilon_{m,l} \leq Q\left(\frac{\widehat{n}lC_m\left(\widetilde{\boldsymbol{h}}_{k,m}\right) - \log\left(\frac{M_m-1}{2}\right)}{\sqrt{\widehat{n}lV_m\left(\widetilde{\boldsymbol{h}}_{k,m}\right)}}\right) + \frac{B_1+B_2}{\sqrt{\widehat{n}l}}$$
$$\approx Q\left(\frac{\widehat{n}lC_m\left(\widetilde{\boldsymbol{h}}_{k,m}\right) - \log\left(\frac{M_m-1}{2}\right)}{\sqrt{nK/N_{\mathrm{T}}}}\right) + \frac{B_1+B_2}{\sqrt{\widehat{n}l}}. \tag{3.24}$$

Using Taylor's expansion for inverse Q function, we can derive an upper bound on the finite block-length coding rate for our proposed mmWave cell-free m-MIMO schemes as in the following equations:

$$\frac{\log M_m}{\widehat{n}l} \leq C_m\left(\widetilde{\boldsymbol{h}}_{k,m}\right) - \sqrt{\frac{V_m\left(\widetilde{\boldsymbol{h}}_{k,m}\right)}{\widehat{n}l}}Q^{-1}\left(\epsilon_{m,l} - \frac{B_1+B_2}{\widehat{n}l}\right)$$
$$\approx C_m\left(\widetilde{\boldsymbol{h}}_{k,m}\right) - \sqrt{\frac{V_m\left(\widetilde{\boldsymbol{h}}_{k,m}\right)}{\widehat{n}l}}Q^{-1}\left(\epsilon_{m,l}\right) + O\left(\frac{1}{\sqrt{\widehat{n}l}}\right) \tag{3.25}$$

where $f(x) = O(g(x))$ if and only if there exists a positive real number M and a real number x_0 such that $|f(x)| \leq Mg(x)$ for all $x \geq x_0$. As a result, for our proposed $(\widehat{n}l, M_m, \epsilon_{m,l})$-code, we can derive the approximate decoding error probability for transmitting data packet of length $\widehat{n}l$ to mobile user m under perfect CSI as follows:

$$\epsilon_{m,l} \approx Q\left(\sqrt{\frac{\widehat{n}}{lV_m\left(\widetilde{\boldsymbol{h}}_{k,m}\right)}}\left(lC_m\left(\widetilde{\boldsymbol{h}}_{k,m}\right) - R_{m,\text{in}}\right)\right) \tag{3.26}$$

where $R_{m,\text{in}}$ is the initial data transmission rate for mobile user m, specified by Eq. (3.17).

Considering the non-vanishing error probability, it is challenging to derive the closed-form expression of the channel capacity for our proposed mmWave user-centric cell-free m-MIMO schemes compared with the traditional m-MIMO schemes. In the following Lemma 5, we give the concrete expression to derive an lower bound on the channel capacity $C_m\left(\widetilde{\boldsymbol{h}}_{k,m}\right)$ for our pro-

posed mmWave user-centric cell-free m-MIMO schemes in the finite blocklength regime.

Lemma 5. *A lower bound on the channel capacity $C_m\left(\widetilde{\boldsymbol{h}}_{k,m}\right)$ for our proposed mmWave user-centric cell-free m-MIMO and FBC-HARQ based 6G mobile wireless networks can be derived as follows:*

$$C_m\left(\widetilde{\boldsymbol{h}}_{k,m}\right) \geq \mathbb{E}_{\widetilde{\boldsymbol{h}}_{k,m}}\left[\log_2\left(det\left(\left((\boldsymbol{\Xi}_{k,m})^{-1}-\widetilde{\boldsymbol{h}}_{k,m}\left(\widetilde{\boldsymbol{h}}_{k,m}\right)^{\dagger}\right)+\left(\widetilde{\boldsymbol{h}}_{k,m}\right)^{\dagger}\widetilde{\boldsymbol{h}}_{k,m}\right)\right)\right] - \mathbb{E}_{\widetilde{\boldsymbol{h}}_{k,m}}\left[\log_2 det\left(\left((\boldsymbol{\Xi}_{k,m})^{-1}-\widetilde{\boldsymbol{h}}_{k,m}\left(\widetilde{\boldsymbol{h}}_{k,m}\right)^{\dagger}\right)\right)\right] \tag{3.27}$$

where det$(\cdot)$ is the determinant of a matrix and

$$\boldsymbol{\Xi}_{k,m} \triangleq \left(\mathbb{E}_{\widetilde{\boldsymbol{h}}_{k,m}}\left[\boldsymbol{h}_{k,m}\sum_{m'=1}^{K_u}\sum_{k\in\mathcal{K}(m')}\mathbf{F}^{R}_{k,m'}\mathbf{F}^{B}_{k,m'}\boldsymbol{\Omega}_{k,m'}\left(\mathbf{F}^{R}_{k,m'}\mathbf{F}^{B}_{k,m'}\right)^{\dagger}(\boldsymbol{h}_{k,m})^{\dagger}\right]+\sigma^2\right)^{-1}. \tag{3.28}$$

Proof. The proof is provided in Appendix E. □

Traditionally, it is challenging to derive the closed-form expression of the channel dispersion for mmWave cell-free m-MIMO schemes in the finite blocklength regime. We can derive an upper bound on the channel dispersion $V_m\left(\widetilde{\boldsymbol{h}}_{k,m}\right)$ for our proposed FBC-HARQ based mmWave user-centric cell-free m-MIMO scheme as summarized in Theorem 1.

Theorem 4. *An upper bound on the channel dispersion $V_m\left(\widetilde{\boldsymbol{h}}_{k,m}\right)$ for our proposed mmWave user-centric cell-free m-MIMO and FBC-HARQ based 6G mobile wireless networks can be specified as follows:*

$$V_m\left(\widetilde{\boldsymbol{h}}_{k,m}\right) \leq 8\widehat{n}l\left(\frac{3\overline{\mathcal{P}}_m}{\sigma^4}\mathbb{E}_{\widetilde{\boldsymbol{h}}_{k,m}}\left[\left\|\sum_{m'=1}^{K_u}\sum_{k\in\mathcal{K}(m')}\widetilde{\boldsymbol{h}}_{k,m}\mathbf{F}^{B}_{k,m'}\left(\boldsymbol{\Omega}_{k,m'}\right)^{\frac{1}{2}}\right\|^2\right]+2\right). \tag{3.29}$$

Proof. The proof is provided in Appendix F. □

3.5 Statistical Delay/Error-Rate Bounded QoS Guarantees Through Effective Capacity in the Finite Blocklength Regime

In this section, by using the decode error probability function given in Eq. (3.26) in the previous section, we can then characterize the analytical relationship between the statistical delay/error-rate bounded QoS metrics/schemes and decode error probability function. In addition, we derive the corresponding effective capacity function under HARQ-IR protocol for our proposed mmWave user-centric cell-free m-MIMO schemes in the finite blocklength regime.

3.5.1 Statistical Delay/Error-Rate Bounded QoS Metrics Under Constant Arrival Rate in the Finite Blocklength Regime

Denote by N_l the number of HARQ-IR retransmissions, where $1 \leq N_l \leq L$. For our proposed HARQ-IR protocol, we define $a_{k,m}(l)$ as the source rate for transmitting the lth data block from the kth AP to mobile user m and $s_{k,m}(l)$ as the instantaneous data transmission rate over wireless channels for transmitting the lth data block from the k AP to mobile user m. Define $A_m(N_\kappa) = \sum\limits_{k\in\mathcal{K}(m)} \sum\limits_{l=0}^{N_\kappa-1} a_{k,m}(l)$ as the accumulated source rate for transmitting the κth message to mobile user m and $S_m(N_\kappa) = \sum\limits_{k\in\mathcal{K}(m)} \sum\limits_{l=0}^{N_\kappa-1} s_{k,m}(l)$ as the accumulated data transmission rate over wireless channels for transmitting the κth message to mobile user m. Define $Q_m(N_\kappa)$ as the dynamics of queuing process for transmitting the κth message to mobile user m, which is given as in the following equation:

$$Q_m(N_\kappa) = \max\left\{A_m(N_\kappa) - S_m(N_\kappa), 0\right\}. \tag{3.30}$$

Define $U_m(N_\kappa) \triangleq A_m(N_\kappa) - S_m(N_\kappa)$. We can rewrite the queuing process for transmitting the κth message to mobile user m as in the following equation:

$$Q_m(N_\kappa) = \max\left\{0, U_m(N_\kappa), U_m(N_\kappa) + U_m(N_\kappa - 1), \dots\right\}. \tag{3.31}$$

Assume that the average data arrival rate, denoted by $\overline{\mu}_{k,m}$, is a constant. Then, given the decode error probability function ϵ_{m,N_κ} for N_κ number of HARQ-IR retransmissions in Eq. (3.26), the

delay-bounded QoS constraint of mobile user m for transmitting N_κ data blocks can be derived as follows:

$$\Pr\left(\bigcup_{N_\kappa}\{Q_m(N_\kappa) > Q_{m,\text{th}}\}\right) = \Pr\left(\bigcup_{N_\kappa}\left\{\sum_{l=1}^{N_\kappa} U_m(l) > Q_{m,\text{th}}\right\}\right)$$
$$\approx \eta_m\left(\mu_{k,m}, \epsilon_{m,N_\kappa}\right) e^{-\theta_m^{\text{con}}\left(\mu_{k,m},\epsilon_{m,N_\kappa}\right)Q_{m,\text{th}}} \tag{3.32}$$

where $\bigcup$ is the *or* operation, $\theta_m^{\text{con}}\left(\mu_{k,m}, \epsilon_{m,N_\kappa}\right)$ is defined as the QoS exponent function considering the constant average arrival rate scenario, and $\eta_m\left(\mu_{k,m}, \epsilon_{m,N_\kappa}\right)$ is the probability that queue is non-empty. Note that the pair of functions $\left\{\eta_m\left(\mu_{k,m}, \epsilon_{m,N_\kappa}\right), \theta_m^{\text{con}}\left(\mu_{k,m}, \epsilon_{m,N_\kappa}\right)\right\}$ are functions of the source rate $\mu_{k,m}$ and the decoding error probability ϵ_{m,N_κ}, which depend on the channel condition and decoding process.

On the other hand, we can characterize the queuing delay of the buffer for the κth message as $D_m(N_\kappa)$. First, using Eq. (3.32), we can derive the bound for the steady-state delay distribution in terms of the delay violation probability, denoted by $\epsilon_{\text{q},m}$, given the decode error probability function ϵ_{m,N_κ} in Eq. (3.26) as follows:

$$\epsilon_{\text{q},m} = \Pr\left(\bigcup_{N_\kappa}\{D_m(N_\kappa) > D_{m,\text{th}}\}\right) \approx \eta_m\left(\mu_{k,m}, \epsilon_{m,N_\kappa}\right) e^{-\theta_m^{\text{con}}\left(\mu_{k,m},\epsilon_{m,N_\kappa}\right)R_{m,N_\kappa}D_{m,\text{th}}} \tag{3.33}$$

where $D_{m,\text{th}}$ is the delay bound for mobile user m and R_{m,N_κ} denotes data transmission rate for transmitting the κth message for mobile user m, specified by Eq. (3.18). **Remarks:** *Comparing Eq.* (3.32) *with its equivalent Eq.* (3.33)*, we obtain the following relationships:* $Q_{m,\text{th}} = R_{m,N_l}D_{m,\text{th}}$. Then, based on the derivations in [90], we can characterize the estimated analytical relationship between the functions $\left\{\eta_m\left(\mu_{k,m}, \epsilon_{m,N_\kappa}\right), \theta_m^{\text{con}}\left(\mu_{k,m}, \epsilon_{m,N_\kappa}\right)\right\}$ as follows:

$$\begin{cases} \frac{\eta_m\left(\mu_{k,m},\epsilon_{m,N_\kappa}\right)}{\theta_m^{\text{con}}\left(\mu_{k,m},\epsilon_{m,N_\kappa}\right)} = \mathbb{E}\left[D_m(N_\kappa)\right]; \\ \eta_m\left(\mu_{k,m}, \epsilon_{m,N_\kappa}\right) = \Pr\left\{Q_m(N_\kappa) > 0\right\}. \end{cases} \tag{3.34}$$

Accordingly, the expectation of the delay process can be derived as in the following equation:

$$\mathbb{E}\left[D_m(N_\kappa)\right] = \mathbb{E}\left[\frac{A_m(N_\kappa) - S_m(N_\kappa)}{\sum\limits_{k\in\mathcal{K}(m)} \overline{\mu}_{k,m}}\right]. \tag{3.35}$$

Since $A_m(N_\kappa)$ and $S_m(N_\kappa)$ are independent of each other, we can determine the value of $\mathbb{E}\left[A_m(N_\kappa)\right]$ when $N_\kappa \to \infty$. Using the Central Limit Theorem, we get

$$\mathbb{E}\left[A_m(N_\kappa)\right] = \sum_{k\in\mathcal{K}(m)} \overline{\mu}_{k,m}. \tag{3.36}$$

In order to derive the expected value of the accumulated process $S_m(N_\kappa)$, using Eqs. (3.17) and (3.18), we have

$$\mathbb{E}\left[S_m(N_\kappa)\right] = \widehat{n}\mathbb{E}\left[R_{m,N_\kappa}\right] = \widehat{n}\mathbb{E}\left[\frac{R_{m,\text{in}}}{N_\kappa}\right]. \tag{3.37}$$

To derive the average number of HARQ-IR retransmissions $\mathbb{E}\left[N_\kappa\right]$, we derive the probability that the number of HARQ retransmission rounds when $N_\kappa = l$ as in the following equation:

$$\Pr\left\{N_\kappa = l\right\} = \begin{cases} \Pr\left\{\overline{\mathcal{A}}_0\right\} - \Pr\left\{\overline{\mathcal{A}}_1\right\}, & \text{for } l = 1; \\ \Pr\left\{\bigcap\limits_{\iota=1}^{l-1}\left\{\overline{\mathcal{A}}_\iota\right\}\right\} - \Pr\left\{\bigcap\limits_{\iota=1}^{l}\left\{\overline{\mathcal{A}}_\iota\right\}\right\}, & \text{for } 1 < l < L; \\ \Pr\left\{\bigcap\limits_{l=1}^{L-1}\left\{\overline{\mathcal{A}}_l\right\}\right\}, & \text{for } l = L, \end{cases} \tag{3.38}$$

where $\bigcap$ is the *and* operation and $\overline{\mathcal{A}}_l$ $(l = 1, \ldots, L)$ denotes the event that the received data packet cannot be decoded correctly at the end of lth HARQ retransmission round. Correspondingly, the average number of HARQ-IR retransmissions $\mathbb{E}\left[N_\kappa\right]$ can be upper-bounded as follows:

$$\begin{aligned} \mathbb{E}[N_\kappa] &= \sum_{l=1}^{L} l\Pr\left\{N_\kappa = l\right\} = \Pr\left\{\overline{\mathcal{A}}_0\right\} + \sum_{l=1}^{L-1}\Pr\left\{\bigcap_{l=1}^{L-1}\left\{\overline{\mathcal{A}}_l\right\}\right\} \\ &\leq 1 + \sum_{l=1}^{L-1}\Pr\left\{\overline{\mathcal{A}}_l\right\} \approx 1 + \sum_{l=1}^{L-1}\epsilon_{m,l} \end{aligned} \tag{3.39}$$

where $\Pr\left\{\overline{\mathcal{A}}_0\right\} = 1$ and $\epsilon_{m,l} \approx \Pr\left\{\overline{\mathcal{A}}_l\right\}$ is the approximate decoding error probability after lth HARQ retransmission round for mobile user m given by Eq. (3.26).

The probability that buffer is non-empty is similar to the probability that the received SINR falls below a certain specified threshold, i.e., the decoding error probability at the receiver [91]. Due to the fact that the non-empty buffer probability also considers the effect of packet accumulation in the queue, the non-empty buffer probability is larger than the decoding error probability, i.e.,

$$\eta_m\left(\mu_{k,m}, \epsilon_{m,N_\kappa}\right) \geq \epsilon_{m,L} \tag{3.40}$$

where $\epsilon_{m,L}$ is the decoding error probability after L HARQ retransmission rounds for mobile user m, specified by Eq. (3.26) when $N_\kappa = L$. Using Eqs. (3.34), (3.35), (3.39) and (3.40), we can obtain the following equation that characterizes the analytical relationship between the decoding error probability and the QoS exponent function considering the constant average data arrival rate scenario:

$$\theta_m^{\text{con}}\left(\mu_{k,m}, \epsilon_{m,N_\kappa}\right) \approx \frac{\epsilon_{m,L}}{1 - R_{m,\text{in}}\left[\sum\limits_{k\in\mathcal{K}(m)} \overline{\mu}_{k,m}\left(1 + \sum\limits_{l=1}^{L-1} \epsilon_{m,l}\right)\right]^{-1}} \tag{3.41}$$

where $R_{m,\text{in}}$ is the initial transmission rate for mobile user m given by Eq. (3.17). Note that the above Eq. (3.41) implies that there exists an analytical relationship between the decoding error probability function and the QoS exponent function using FBC-HARQ protocol in the finite blocklength, i.e., given the error-rate constraints, we can them characterize the delay-bounded QoS exponent function $\theta_m^{\text{con}}\left(\mu_{k,m}, \epsilon_{m,N_\kappa}\right)$ for our proposed mmWave user-centric cell-free m-MIMO schemes in the finite blocklength regime.

3.5.2 Statistical Delay/Error-Rate Bounded QoS Metrics Under Random Arrival Rate in the Finite Blocklength Regime

3.5.2.1 Discrete-Time Markov Model

Consider a two-state discrete-time Markov model for which the transition probability matrix, denoted by $\mathbf{J}_m$, is given as in the following equation:

$$\mathbf{J}_m = \begin{bmatrix} p_{m,11} & p_{m,12} \\ p_{m,21} & p_{m,22} \end{bmatrix} \tag{3.42}$$

where $p_{m,11}$ and $p_{m,22}$ represent the probabilities that data source remains in the ON state and OFF state, respectively, in the next time slot and $p_{m,12}$ and $p_{m,21}$ are the probabilities of transitioning to a different state in the next time slot. In the OFF state of the discrete-time Markov model, no data arrives from the source, while in the ON state, data arrives at rate $\mu_{k,m}$ for mobile user m. Using the transition probability matrix $\mathbf{J}_m$, we can derive the steady state probability of ON state, denoted by $p_{m,\text{ON}}$, as follows [92]:

$$p_{m,\text{ON}} = \frac{1 - p_{m,11}}{2 - p_{m,11} - p_{m,22}}. \tag{3.43}$$

Accordingly, we can characterize the average source rate as follows:

$$\mathbb{E}\left[A_m(N_\kappa)\right] = \frac{\sum\limits_{k \in \mathcal{K}(m)} \overline{\mu}_{k,m}(1 - p_{m,11})}{2 - p_{m,11} - p_{m,22}}. \tag{3.44}$$

Similar to Eq. (3.41), we can derive the QoS exponent function, denoted by $\theta_m^{\text{DM}}\left(\mu_{k,m}, \epsilon_{m,N_\kappa}\right)$, for discrete-time Markov model as follows:

$$\theta_m^{\text{DM}}\left(\mu_{k,m}, \epsilon_{m,N_\kappa}\right) \approx \frac{\epsilon_{m,L}}{1 - \frac{R_{m,\text{in}}(2 - p_{m,11} - p_{m,22})}{\sum\limits_{k \in \mathcal{K}(m)} \overline{\mu}_{k,m}(1 - p_{m,11})\left(1 + \sum\limits_{l=1}^{L-1} \epsilon_{m,l}\right)}}. \tag{3.45}$$

3.5.2.2 *Markov Fluid Model*

Consider data arrival as a continuous-time Markov process. We can derive the transition rate matrix, denoted by $\mathbf{G}_m$, of data arrival process as follows:

$$\mathbf{G}_m = \begin{bmatrix} -\upsilon_{m,1} & \upsilon_{m,1} \\ \upsilon_{m,2} & -\upsilon_{m,2} \end{bmatrix} \tag{3.46}$$

where $\upsilon_{m,1} > 0$ and $\upsilon_{m,2} > 0$ are the transition rates between ON state and OFF state. Then, we can derive the steady state probability of ON state as follows:

$$p_{m,\text{ON}} = \frac{\upsilon_{m,1}}{\upsilon_{m,1} + \upsilon_{m,2}}. \tag{3.47}$$

Accordingly, we can characterize the average source rate as follows:

$$\mathbb{E}\left[A_m(N_\kappa)\right] = \frac{\sum\limits_{k\in\mathcal{K}(m)} \overline{\mu}_{k,m}\upsilon_{m,1}}{\upsilon_{m,1} + \upsilon_{m,2}}. \tag{3.48}$$

Similarly, we can derive the QoS exponent function, denoted by $\theta_m^{\text{MF}}\left(\mu_{k,m}, \epsilon_{m,N_\kappa}\right)$, for Markov Fluid model as follows:

$$\theta_m^{\text{MF}}\left(\mu_{k,m}, \epsilon_{m,N_\kappa}\right) \approx \frac{\epsilon_{m,L}}{1 - \frac{R_{m,\text{in}}(\upsilon_{m,1}+\upsilon_{m,2})}{\sum\limits_{k\in\mathcal{K}(m)} \overline{\mu}_{k,m}\upsilon_{m,1}\left(1+\sum\limits_{l=1}^{L-1}\epsilon_{m,l}\right)}}. \tag{3.49}$$

3.5.3 Effective Capacity Under HARQ-IR Protocol in the Finite Blocklength Regime

We define the asymptotic log-moment generating function [93], denoted by $\Lambda_{U_m}(\theta_m)$, of $U_m(N_\kappa)$ as follows:

$$\Lambda_{U_m}(\theta_m) \triangleq \lim_{N_\kappa\to\infty} \frac{1}{N_\kappa} \log\left\{\mathbb{E}\left[e^{\theta_m U_m(N_\kappa)}\right]\right\}. \tag{3.50}$$

Since $a_{k,m}(l)$ and $s_{k,m}(l)$ are independent of each other, we have $\Lambda_{U_m}(\theta_m) = \Lambda_{A_m}(\theta_m)+\Lambda_{S_m}(-\theta_m)$, where $\Lambda_{A_m}(\theta_m)$ and $\Lambda_{S_m}(\theta_m)$ are the asymptotic log-moment generating functions of the accumulated source process $A_m(N_\kappa)$ and the accumulated channel process $S_m(N_\kappa)$, respectively. For a given QoS exponent θ_m, the processes $S_m(N_\kappa)$ and $A_m(N_\kappa)$ need to satisfy the following equation:

$$\Lambda_{A_m}(\theta_m) = -\Lambda_{S_m}(-\theta_m). \tag{3.51}$$

The effective capacity [3] is defined as the maximum constant arrival rate that a given service process can support in order to guarantee a QoS requirement specified by θ_m. Considering the non-vanishing error probability, it is challenging to derive the closed-form expression of the effective capacity for our proposed mmWave user-centric cell-free m-MIMO schemes using the HARQ-IR protocol. In the following Theorem 5, we give the concrete expression to derive a closed-form expression on the effective capacity $EC_m(\theta_m)$ for our proposed mmWave user-centric cell-free m-MIMO schemes under statistical delay/error-rate bounded QoS constraints in the finite blocklength regime.

Theorem 5. *If the statistical delay/error-rate bounded QoS constraints are specified by Eqs. (3.50)-(3.51), then the effective capacity $EC_m(\theta_m)$ for our proposed mmWave user-centric cell-free m-MIMO and FBC-HARQ based 6G mobile wireless networks is given by the following equation:*

$$EC_m(\theta_m) = \frac{R_{m,in}}{2\left(1+\sum\limits_{l=1}^{L-1}\epsilon_{m,l}\right)} + \frac{R_{m,in}}{2}\sqrt{\frac{1}{\left(1+\sum\limits_{l=1}^{L-1}\epsilon_{m,l}\right)^2} + \frac{2\widehat{n}\log\left(\epsilon_{q,m}\right)}{D_{m,th}\left(\sum\limits_{l=1}^{L-1}(2l-1)\epsilon_{m,l} - \left(\sum\limits_{l=1}^{L-1}\epsilon_{m,l}\right)^2\right)}} \tag{3.52}$$

where $R_{m,in}$ is the initial transmission rate specified by Eq. (3.17), $\epsilon_{q,m}$ represents the delay violation probability given by Eq. (3.33), $\epsilon_{m,l}$ is the probability that the received data packet cannot be decoded at the end of lth HARQ retransmission round for mobile user m, which is given in Eq. (3.39), and $D_{m,th}$ is the delay bound for mobile user m.

Proof. Given statistical delay and error-rate bounded QoS constraints, we can exploit the definition of the effective capacity and obtain the following equation:

$$EC_m(\theta_m) = -\frac{\Lambda_{S_m}(-\theta_m)}{\theta_m} = -\lim_{N_\kappa \to \infty} \frac{1}{\theta_m N_\kappa} \log \left\{ \mathbb{E}\left[e^{-\theta_m \sum\limits_{k \in \mathcal{K}(m)} \sum\limits_{l=0}^{N_\kappa - 1} s_{k,m}(l)} \right] \right\}. \tag{3.53}$$

Then, using the Central Limit Theorem, we can rewrite the effective capacity $EC_m(\theta_m)$ when $N_\kappa \to \infty$ as in the following equation [94]:

$$EC_m(\theta_m) = \frac{\mathbb{E}\left[S_m(N_\kappa)\right]}{2\widehat{n}} + \frac{1}{2\widehat{n}} \sqrt{\left(\mathbb{E}\left[S_m(N_\kappa)\right]\right)^2 - \frac{2\widehat{n}\left(-\log\left(\epsilon_{\text{q},m}\right)\right)}{D_{m,\text{th}}} \text{Var}\left[S_m(N_\kappa)\right]} \tag{3.54}$$

where

$$\text{Var}\left[S_m(N_\kappa)\right] = \frac{\left(\widehat{n} R_{m,\text{in}}\right)^2}{\text{Var}\left[N_\kappa\right]}. \tag{3.55}$$

Accordingly, we can derive the variance of N_κ as follows:

$$\begin{aligned}
\text{Var}[N_\kappa] &= \mathbb{E}\left[N_\kappa^2\right] - \left(\mathbb{E}\left[N_\kappa\right]\right)^2 \approx \sum_{l=1}^{N_\kappa} l^2 \text{Pr}\left\{N_\kappa = l\right\} - \left(1 + \sum_{l=1}^{N_\kappa - 1} \epsilon_{m,l}\right)^2 \\
&= 1 + \sum_{l=1}^{N_\kappa - 1} (2l+1) \text{Pr}\left\{ \bigcap_{\iota=1}^{l} \left\{\overline{\mathcal{A}}_\iota\right\} \right\} - \left(1 + \sum_{l=1}^{N_\kappa - 1} \epsilon_{m,l}\right)^2 \\
&\leq 1 + \sum_{l=1}^{N_\kappa - 1} (2l+1) \text{Pr}\left\{ \overline{\mathcal{A}}_l \right\} - \left(1 + \sum_{l=1}^{N_\kappa - 1} \epsilon_{m,l}\right)^2 \\
&\approx 1 + \sum_{l=1}^{N_\kappa - 1} (2l+1) \epsilon_{m,l} - \left(1 + \sum_{l=1}^{N_\kappa - 1} \epsilon_{m,l}\right)^2 = \sum_{l=1}^{N_\kappa - 1} (2l-1) \epsilon_{m,l} - \left(\sum_{l=1}^{N_\kappa - 1} \epsilon_{m,l}\right)^2.
\end{aligned} \tag{3.56}$$

Using Eqs. (3.54) and (3.56), we can obtain the expression for effective capacity $EC_m(\theta_m)$ as given by Eq. (3.52), which completes the proof of Theorem 5. □

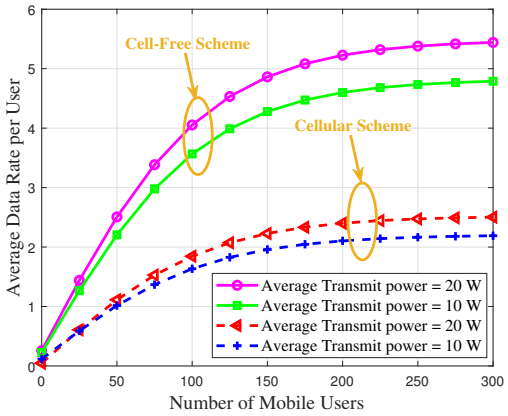

Figure 3.3: The average data transmission rate per user vs. number of mobile users K_{u} in the finite blocklength regime.

3.6 Performance Evaluations

We use simulations to validate and evaluate our proposed mmWave user-centric cell-free m-MIMO based schemes in the finite blocklength regime under HARQ-IR protocol. Throughout our simulations, we set the total bits of the required data packet $M_m = 10^8$ bits, the average transmit power $\overline{\mathcal{P}}_m$ can be choose from $[1, 30]$ Watt for each mobile user, the number of APs $K_{\mathrm{a}} = 1000$, the number of mobile users $K_{\mathrm{u}} \in [10, 300]$, the pilot signal transmit power $\mathcal{P}_{\mathrm{p}}$ can be choose from $[1, 5]$ Watt for each mobile user, the number of transmit antennas $N_{\mathrm{T}} \in [100, 800]$, the number of RF chains $L_{\mathrm{T}} \in [5, 40]$, the number of entries of the over-complete beam steering codebook $M_{\mathrm{T}} \in [200, 1000]$, and the maximum number of HARQ retransmission rounds $L \in [5, 20]$.

We set the number of transmit antennas $N_{\mathrm{T}} = 400$, the number of RF chains $L_{\mathrm{T}} = 10$, and the number of entries of the over-complete beam steering codebook $M_{\mathrm{T}} = 600$, the maximum number of HARQ retransmission rounds $L = 10$, the blocklength $\widehat{n} = 600$. Compared with the mmWave m-MIMO based cellular schemes, Fig. 3.3 depicts the average data transmission rate per user with different numbers of mobile users K_{u} for our proposed mmWave cell-free m-MIMO schemes. We can observe from Fig. 3.3 that the average data transmission rate per user increases with the number of mobile users for both cellular and cell-free schemes. Fig. 3.3 also shows that with a higher average transmit power at the APs, a better average data transmission rate per user

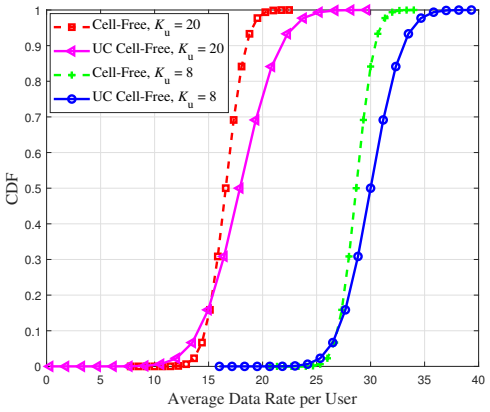

Figure 3.4: The CDFs of downlink data transmission rate per user in the finite blocklength regime.

can be achieved. It is shown in Fig. 3.3 that our proposed mmWave cell-free m-MIMO schemes outperform the traditional mmWave m-MIMO based cellular schemes in terms of the average data transmission rate per user.

Using the same settings as in Fig. 3.3, Fig. 3.4 plots the cumulative distribution functions (CDFs) of the downlink data transmission rates per user for our proposed mmWave user-centric cell-free m-MIMO schemes compared with the traditional cell-free m-MIMO schemes. We can observe from Fig. 3.4 that there is always a crossing point between the CDF curves corresponding to the user-centric (UC) cell-free approach and the traditional cell-free approach. As shown in Fig. 3.4, the Y-coordinate of the crossing point is far below 0.5 in both $K_{\mathrm{u}} = 20$ and $K_{\mathrm{u}} = 8$ scenarios. This indicates that for the majority of mobile users, our proposed mmWave user-centric cell-free m-MIMO schemes outperform the traditional mmWave m-MIMO based cellular schemes in terms of the CDFs.

We set the number of mobile users $K_{\mathrm{u}} = 20$, the number of RF chains $L_{\mathrm{T}} = 10$, and the number of entries of the over-complete beam steering codebook $M_{\mathrm{T}} = 600$. Compared with the discrete Fourier transform (DFT) based processing scheme [95], Fig. 3.5 depicts the MMSE performance with respect to the beam-training duration for our proposed mmWave user-centric cell-free m-MIMO scheme. As shown in Fig. 3.5, the DFT based processing scheme requires much more training time compared with our proposed dictionary learning based beam-training algorithm for

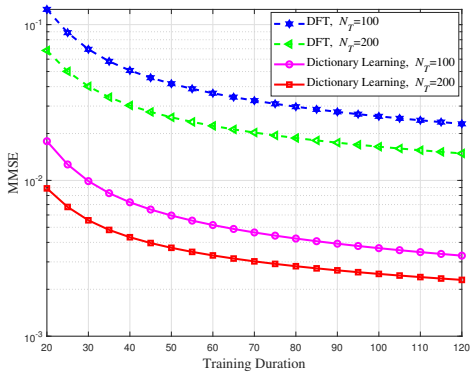

Figure 3.5: The MMSE performance vs. beam-training duration for our proposed mmWave user-centric cell-free m-MIMO schemes.

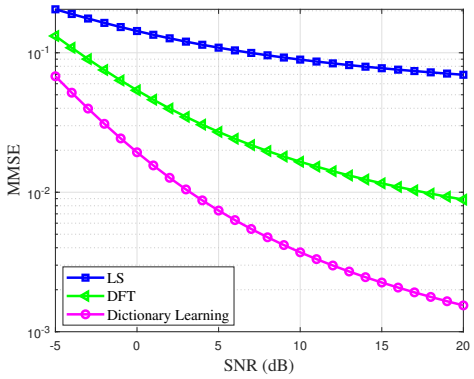

Figure 3.6: The MMSE performance vs. SINR (dB) for our proposed schemes.

achieving the same MMSE performance. We can observe from Fig. 3.5 that for our proposed dictionary learning based beam-training algorithm and DFT based processing scheme, we can achieve better MMSE performance with more transmit antennas N_{T} over mmWave user-centric cell-free m-MIMO based 6G mobile wireless networks.

Setting the number of mobile users $K_{\mathrm{u}} = 20$, the number of transmit antennas $N_{\mathrm{T}} = 100$, the number of RF chains $L_{\mathrm{T}} = 10$, and the number of entries of the over-complete beam steering codebook $M_{\mathrm{T}} = 600$, Fig. 3.6 plots the MMSE performance with different values of SINR for our proposed mmWave user-centric cell-free m-MIMO schemes in comparison with the Least Square (LS) based channel estimation scheme and DFT based processing scheme. As shown in Fig. 3.6,

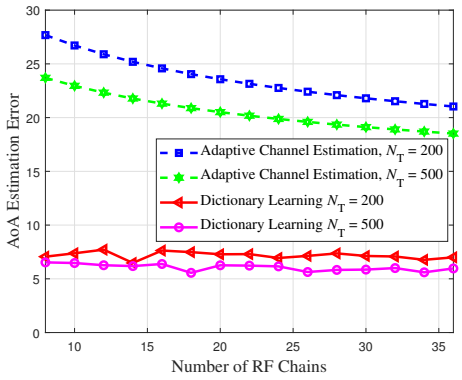

Figure 3.7: The AoA estimation error vs. number of RF chains at the AP L_{T} for our proposed mmWave user-centric cell-free m-MIMO schemes.

our proposed dictionary learning based beam-training algorithm outperforms the LS based channel estimation scheme and DFT based processing scheme in terms of the MMSE performance even in very noisy environment (small SINR environment). Fig. 3.6 also shows that when the value of SINR is small, i.e., the noise is large, the gaps among different curves are relatively small compared with large SINR environment. This indicates that since the accuracy of channel estimation is limited mostly by noise in low SINR environment, different channel estimation methods only has a small influence on the MMSE performance.

We set the number of mobile users $K_{\mathrm{u}} = 20$ and the number of entries of the over-complete beam steering codebook $M_{\mathrm{T}} = 600$. Fig. 3.7 depicts the average AoA estimation error with varying numbers of RF chains at the AP L_{T} for our proposed mmWave user-centric cell-free m-MIMO schemes in comparison with the hybrid design based adaptive channel estimation scheme proposed in [96]. As shown in Fig. 3.7, the average AoA estimation error for our proposed dictionary learning based beam-training algorithm is always less than 10°, which is independent from the number of RF chains at the AP L_{T} and mobile users L_{R}. Fig. 3.7 also shows that our proposed dictionary learning based beam-training algorithm outperforms the hybrid design based adaptive channel estimation scheme in terms of the average AoA estimation error.

We set the number of mobile users $K_{\mathrm{u}} = 20$, the number of entries of the over-complete beam steering codebook $M_{\mathrm{T}} = 1000$, the blocklength $\widehat{n} = 600$, the number of transmit anten-

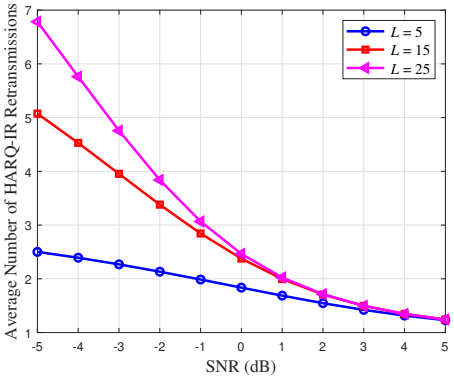

Figure 3.8: The average number of HARQ-IR retransmissions $\mathbb{E}[N_\kappa]$ vs. SINR (dB) under HARQ-IR protocol in the finite blocklength regime.

nas $N_{\mathrm{T}} = 800$, and the number of RF chains $L_{\mathrm{T}} = 20$. Using the function of $\mathbb{E}[N_\kappa]$ derived in Eq. (3.39), Fig. 3.8 plots the average number of HARQ-IR retransmissions $\mathbb{E}[N_\kappa]$ with different values of SINR under HARQ-IR protocol for our proposed mmWave user-centric cell-free m-MIMO schemes in the finite blocklength regime. We can observe from Fig. 3.8 that for a given maximum number of HARQ retransmission rounds L, $\mathbb{E}[N_\kappa]$ is a decreasing function of the SINR. This implies that as SINR increases, the average decoding error probability decreases, which results in the decreased value of $\mathbb{E}[N_\kappa]$. Also, as shown in Fig. 3.8, we can achieve a higher value of $\mathbb{E}[N_\kappa]$ with a larger number of the maximum HARQ retransmission rounds L, which validates the analytical results specified in Eq. (3.39).

Setting the number of mobile users $K_{\mathrm{u}} = 20$, the number of RF chains $L_{\mathrm{T}} = 20$, the maximum number of HARQ retransmission rounds $L = 25$ and SINR to be 5 dB, Fig. 3.9 depicts the average number of HARQ-IR retransmissions $\mathbb{E}[N_\kappa]$ with varying values of the blocklengths $\widehat{n}$ under HARQ-IR protocol for our proposed mmWave user-centric cell-free m-MIMO schemes in the finite blocklength regime. We can observe from Fig. 3.9 that for a given number of transmit antennas N_{T}, $\mathbb{E}[N_\kappa]$ decreases as the blocklength $\widehat{n}$ increases, and will finally converge to one as $\widehat{n} \to \infty$, which means that as $\widehat{n} \to \infty$, we only need one HARQ retransmission round for a successful decoded message at the receiver. This observation obtained from Fig. 3.9 implies that as the codeword of length $\widehat{n}$ gets larger, the average decoding error probability decreases, which

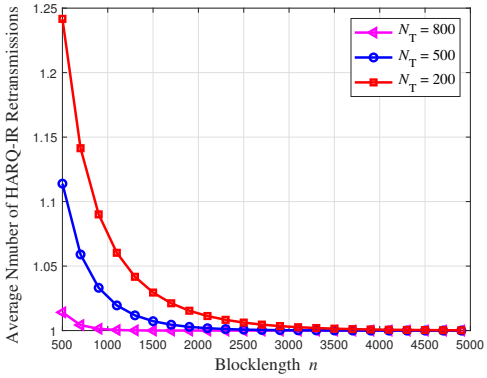

Figure 3.9: The average number of HARQ-IR retransmissions $\mathbb{E}[N_\kappa]$ vs. blocklength $\widehat{n}$ under HARQ-IR protocol for mmWave user-centric cell-free m-MIMO schemes.

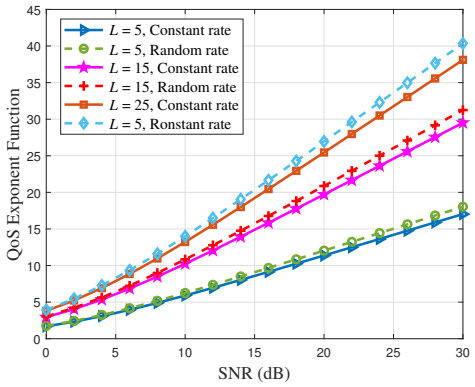

Figure 3.10: The QoS exponent function vs. SINR (dB) under HARQ-IR protocol in the finite blocklength regime.

results in the decreased value of $\mathbb{E}[N_\kappa]$, verifying the analytical results specified in Eqs. (3.26) and (3.39).

Then, we set the number of mobile users $K_{\text{u}} = 20$, the blocklength $\widehat{n} = 600$, and the number of transmit antennas $N_{\text{T}} = 500$. Compared with the discrete-time Markov arrival rate model, Fig. 3.10 plots the QoS exponent function with different values of SINR under HARQ-IR protocol using the average constant arrival rate model and the random arrival rate model in the finite blocklength regime. Fig. 3.10 shows that the QoS exponent function increases with higher value of the SINR. We can observe from Fig. 3.10 that we can achieve a higher value of the QoS exponent function

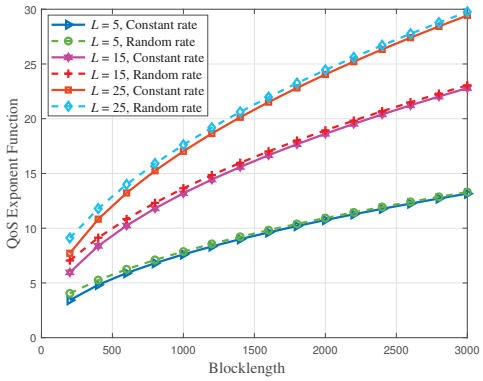

Figure 3.11: The QoS exponent function vs. blocklength $\widehat{n}$ under HARQ-IR protocol in the finite blocklength regime.

by setting a larger number of the maximum HARQ retransmission rounds L, which validates the analytical results specified in Eq. (3.41).

Now we set the number of mobile users $K_{\mathrm{u}} = 20$, the number of entries of the over-complete beam steering codebook $M_{\mathrm{T}} = 700$, the maximum number of HARQ retransmission rounds $L \in \{5, 15, 20\}$, SINR to be 10 dB, and the number of transmit antennas $N_{\mathrm{T}} = 500$. Using the QoS exponent function derived in Eqs. (3.41) and (3.45), Fig. 3.11 depicts the QoS exponent function with varying values of the blocklengths $\widehat{n}$ under HARQ-IR protocol for our proposed mmWave cell-free m-MIMO schemes in the finite blocklength regime. Fig. 3.11 shows that for a given value of L, the QoS exponent function is an increasing function of the blocklength $\widehat{n}$, which is consistent with the analytical results specified in Eq. (3.41).

We set the number of mobile users $K_{\mathrm{u}} = 20$, the number of entries of the over-complete beam steering codebook $M_{\mathrm{T}} = 800$, the blocklength $\widehat{n} = 600$, the number of transmit antennas $N_{\mathrm{T}} = 600$, and the number of RF chains $L_{\mathrm{T}} = 20$. Fig. 3.12 plots the effective capacity $EC_m(\theta_m)$ with different numbers of the maximum HARQ retransmission rounds L under HARQ-IR protocol for our proposed mmWave user-centric cell-free m-MIMO schemes in the finite blocklength regime. We can observe from Fig. 3.12 that as the number of the maximum HARQ retransmission rounds L increases, the effective capacity $EC_m(\theta_m)$ decreases and will finally converge to a cer-

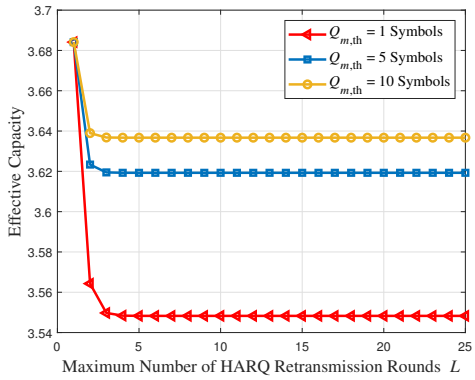

Figure 3.12: The effective capacity $EC_m(\theta_m)$ vs. number of the maximum HARQ retransmission rounds L under HARQ-IR protocol for mmWave user-centric cell-free m-MIMO schemes in the finite blocklength regime.

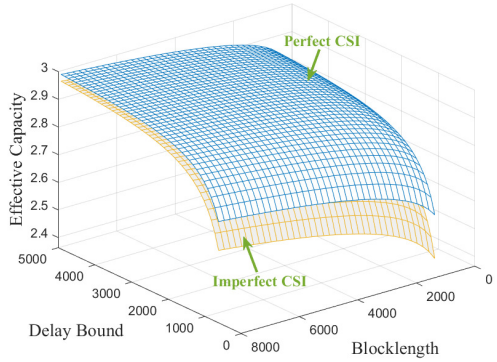

Figure 3.13: The effective capacity $EC_m(\theta_m)$ vs. delay bound $D_{m,\text{th}}$ and blocklength $\widehat{n}$ under HARQ-IR protocol for our proposed mmWave user-centric cell-free schemes in the finite blocklength regime.

tain value. In addition, Fig. 3.12 shows that with a large/loose delay bound $D_{m,\text{th}}$, or equivalently a large/loose buffer-size overflow threshold $Q_{m,\text{th}}$, we can achieve a larger value of the effective capacity $EC_m(\theta_m)$, which verifies the analytical results specified in Eq. (3.52).

Setting the number of mobile users $K_{\text{u}} = 20$, the number of entries of the over-complete beam steering codebook $M_{\text{T}} = 800$, the number of transmit antennas $N_{\text{T}} = 600$, the number of RF chains $L_{\text{T}} = 20$, the maximum HARQ retransmission rounds $L = 10$, and SINR to be 15 dB, Fig. 3.13 depicts the effective capacity $EC_m(\theta_m)$ with varying delay bounds $D_{m,\text{th}}$ and

blocklengths $\widehat{n}$ under HARQ-IR protocol for our proposed mmWave cell-free m-MIMO schemes in the finite blocklength regime considering both perfect CSI and imperfect CSI scenarios. We can observe from Fig. 3.13 that the effective capacity $EC_m(\theta_m)$ increases as the blocklength $\widehat{n}$ gets larger and will eventually converge to a certain value, which is consistent with the analytical results specified in Eq. (3.52) in Theorem 5.

3.7 Summary

We have proposed the system models which efficiently integrate HARQ-IR protocol with FBC over mmWave user-centric cell-free m-MIMO based 6G mobile wireless networks. In particular, we have established mmWave user-centric cell-free m-MIMO-based system models. Then, we have designed dictionary learning based beam-training algorithm for solving the low-complex beamforming optimization problem. We also have characterized channel capacity, channel dispersion, and block error probability under HARQ-IR protocol using FBC. Based on the information theoretic results in QoS theory, we have derived QoS metrics in terms of error probability and corresponding effective capacity function for our proposed FBC-HARQ based mmWave cell-free m-MIMO schemes. We also have conducted a set of simulations to validate and evaluate our proposed mmWave user-centric cell-free m-MIMO schemes by implementing statistical delay/error-rate bounded QoS provisioning in the finite blocklength regime.

4. STATISTICAL DELAY AND ERROR-RATE BOUNDED QOS FOR SWIPT OVER CF M-MIMO 6G NETWORKS Using FBC *

4.1 Introduction

Taking advantage of the broadcast nature of RF wave propagation, researchers have developed the concept of SWIPT [40, 97] for prolonging the battery-life or to serve as an alternative power source of energy-constrained, low-power wireless devices. There have been a number of works focusing on investigating the SWIPT technique to support mURLLC. In particular, the authors of [98] have analyzed the performance of a non-orthogonal SWIPT-enabled system using FBC and derived novel analytical expressions for the end-to-end average block error probability. The authors of [99] have analyzed a WPT system with finite blocklength and finite power/battery supply under Nakagami-m wireless fading channels. The authors of [100] have characterized the fundamental limits of SWIPT in terms of the information-energy capacity region in the non-asymptotic regime. The authors of [101] have investigated the rate-energy tradeoff and the decoding error probability-energy tradeoff for SWIPT systems in the finite blocklength realm.

In addition, CF m-MIMO system use advanced backhaul to achieve coherent processing across geographically distributed APs, in order to provide uniformly high-quality service for all mobile users in the network. Due to the closer distance between the APs and mobile devices, integrating CF m-MIMO with SWIPT can significantly improve the coverage probability while minimizing the throughput as well as energy outage probabilities as compared with the traditional co-located m-MIMO systems.

Since CF m-MIMO has been shown to be much more robust to shadow against the correlated small/large-scale fading as compared with the co-located m-MIMO systems [36], the CF m-MIMO can significantly boost the performance gains of SWIPT. Although there has been a

sizeable volume of research works on integrating SWIPT with co-located massive MIMO, only a limited number of research works have focused on investigating SWIPT-driven CF m-MIMO based system models. In particular, the performance of SWIPT-driven CF m-MIMO schemes has been characterized in [102]. The authors of [103] have shown that the achievable energy-rate tradeoff of SWIPT can be significantly enhanced by employing the CF m-MIMO technique. A secure SWIPT-enabled CF m-MIMO system is presented in [104]. However, how to efficiently integrate SWIPT with CF m-MIMO architecture models while supporting mURLLC traffics in the finite blocklength regime is still an open problem over 6G wireless networks.

To effectively overcome the above-mentioned challenges, in this chapter we propose and develop statistical delay and error-rate bounded QoS provisioning schemes over SWIPT-enabled CF m-MIMO 6G wireless networks in the finite blocklength regime. In particular, we establish the SWIPT-enabled CF m-MIMO based system models through employing FBC. We also quantitatively characterize the fundamental tradeoff between harvested energy and ϵ-effective capacity for statistical delay and error-rate bounded QoS provisioning. Furthermore, we formulate and solve the optimization problems for the tradeoff between the ϵ-effective capacity and harvested energy under both TS and PS protocols by developing the joint optimization algorithms in supporting 6G mURLLC. Also conducted is a set of simulations to validate and evaluate our proposed schemes over SWIPT-enabled CF m-MIMO based 6G wireless networks.

The rest of this chapter is organized as follows: Section 4.2 establishes SWIPT-enabled CF m-MIMO based system models. Section 4.3 formulates and solves the optimization problems for the tradeoff between downlink ϵ-effective capacity and harvested energy. Section 4.4 formulates and solves the joint optimization problems for the tradeoff between uplink ϵ-effective capacity and harvested energy. Section 4.5 evaluates and analyzes the system performances for our proposed SWIPT-enabled CF m-MIMO schemes. The chapter concludes with Section 4.6.

4.2 The System Models

Figure 4.1 shows the system architecture model for our proposed SWIPT-enabled CF m-MIMO 6G wireless networks, where each mobile device is served by coherent joint transmissions from all

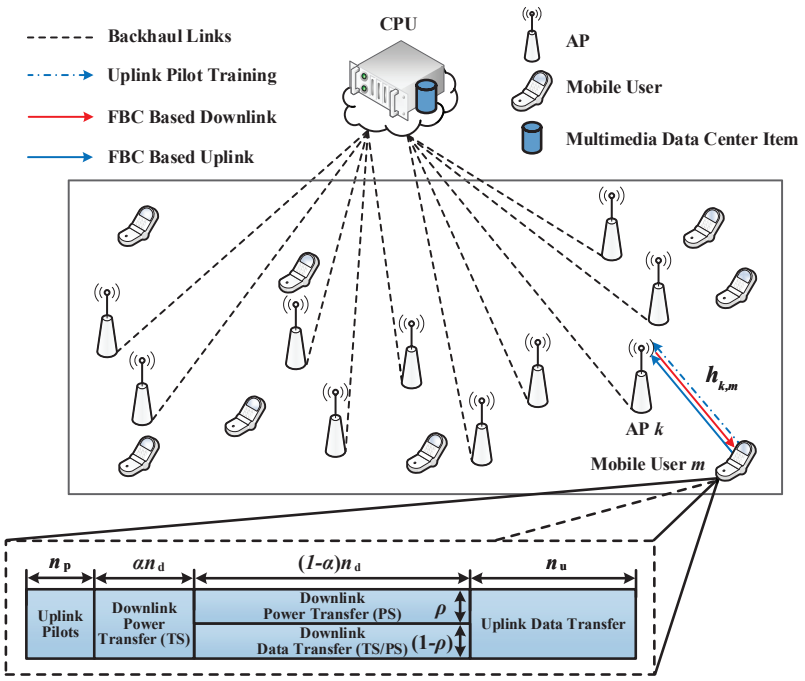

Figure 4.1: The system architecture model for our proposed SWIPT-enabled CF m-MIMO based 6G wireless networks in the finite blocklength regime, where n_{u} is the number of channel uses for the uplink data transmission phase and α and ρ are the TS and PS factors, respectively.

APs. We adopt the TS and PS receivers at the mobile devices.We assume that the system operates in a time-slotted fashion, where time is divided into frames. Each frame is divided into three main orthogonal phases, i.e., uplink pilot training, downlink SWIPT transmission, and uplink data transmission, as follows.

1. *Uplink pilot training phase:* The mobile devices send pilot signals to the APs for channel estimation during the uplink pilot training phase over n_{p} channel uses;

2. *Downlink SWIPT phase:* By adopting the TS and PS receivers, the downlink SWIPT phase is divided into two sub-phases based on the TS factor, denoted by α, and PS factor, denoted by ρ. As shown in Fig. 4.1, in the first downlink power transfer sub-phase, the mobile devices harvest energy from the APs over αn_{d} channel uses by using TS protocol. Each mobile device performs as a pure EH receiver and harvests energy from the APs. In the second downlink information transfer sub-phase, the remaining $(1-\alpha)n_{\mathrm{d}}$ channel uses are

allocated for simultaneous downlink information transfer by using PS protocol with the PS factor ρ.

3. *Uplink data transmission phase:* Define n_{u} as the number of channel uses for the uplink data transmission from the mobile devices to the APs. During the uplink data transmission phase, each mobile device transmits the finite-blocklength data to the APs using the energy harvested in the previous downlink SWIPT phase.

4.2.1 Uplink Pilot Training

We consider the small-scale Rayleigh fading vector $\boldsymbol{g}_{k,m} \sim \mathcal{CN}(\mathbf{0}, \mathbf{I}_{N_{\mathrm{T}}})$. The uplink pilot training phase is similar to Section 2.2.2 in Chapter 2. Denote by $\mathbf{H}_k \triangleq \left[(\boldsymbol{h}_{k,1})^T, \ldots, (\boldsymbol{h}_{k,K_{\mathrm{u}}})^T\right]^T \in \mathbb{C}^{\widetilde{N}_{\mathrm{T}} \times 1}$ the channel's impulse response vector between AP k and all mobile users. Define $\mathbf{R}_{\mathbf{h}_{k,m}} \triangleq \mathbb{E}\left[\mathbf{h}_{k,m} \left(\mathbf{h}_{k,m}\right)^H\right]$ as the covariance matrix of $\mathbf{h}_{k,m}$. Applying the MMSE estimator of $\mathbf{h}_{k,m}$ based on the observation of the received signal $\widetilde{\boldsymbol{y}}_k^{n_{\mathrm{p}}}$, we can obtain the estimated channel's impulse response matrix, denoted by $\widehat{\boldsymbol{h}}_{k,m}$, between AP k and mobile user m as follows:

$$\widehat{\boldsymbol{h}}_{k,m} = \mathbb{E}\left[\mathbf{h}_{k,m} | \widetilde{\boldsymbol{y}}_k^{n_{\mathrm{p}}}\right] = \mathbf{R}_{\mathbf{h}_{k,m}, \widetilde{\boldsymbol{y}}_k^{n_{\mathrm{p}}}} \left(\mathbf{R}_{\widetilde{\boldsymbol{y}}_k^{n_{\mathrm{p}}}}\right)^{-1} \left(\widetilde{\boldsymbol{y}}_k^{n_{\mathrm{p}}} - \mathbb{E}\left[\widetilde{\boldsymbol{y}}_k^{n_{\mathrm{p}}}\right]\right) + \mathbb{E}\left[\mathbf{h}_{k,m}\right] \tag{4.1}$$

where $\mathbf{R}_{\mathbf{h}_{k,m}, \widetilde{\boldsymbol{y}}_k^{n_{\mathrm{p}}}}$ and $\mathbf{R}_{\widetilde{\boldsymbol{y}}_k^{n_{\mathrm{p}}}}$ represent the covariance matrices given as follows:

$$\begin{cases} \mathbf{R}_{\mathbf{h}_{k,m}, \widetilde{\boldsymbol{y}}_k^{n_{\mathrm{p}}}} = \mathbb{E}\left[\mathbf{h}_{k,m} \left(\widetilde{\boldsymbol{y}}_k^{n_{\mathrm{p}}}\right)^H\right] = \sqrt{n_{\mathrm{p}} \mathcal{P}_{\mathrm{p}}} \mathbf{R}_{\mathbf{h}_{k,m}}; \\ \mathbf{R}_{\widetilde{\boldsymbol{y}}_k^{n_{\mathrm{p}}}} = \mathbb{E}\left[\widetilde{\boldsymbol{y}}_k^{n_{\mathrm{p}}} \left(\widetilde{\boldsymbol{y}}_k^{n_{\mathrm{p}}}\right)^H\right] = n_{\mathrm{p}} \mathcal{P}_{\mathrm{p}} \mathbf{R}_{\mathbf{h}_{k,m}} + \mathbf{I}_{N_{\mathrm{T}}}. \end{cases} \tag{4.2}$$

Since $\mathbb{E}\left[\widetilde{\boldsymbol{y}}_k^{n_{\mathrm{p}}}\right]$ and $\mathbb{E}\left[\mathbf{h}_{k,m}\right]$ are equal to zero, we have

$$\widehat{\boldsymbol{h}}_{k,m} = \sqrt{n_{\mathrm{p}} \mathcal{P}_{\mathrm{p}}} \mathbf{R}_{\mathbf{h}_{k,m}} \left(n_{\mathrm{p}} \mathcal{P}_{\mathrm{p}} \mathbf{R}_{\mathbf{h}_{k,m}} + \mathbf{I}_{N_{\mathrm{T}}}\right)^{-1} \widetilde{\boldsymbol{y}}_k^{n_{\mathrm{p}}}. \tag{4.3}$$

4.2.2 Downlink Energy Harvesting Model in the Finite Blocklength Regime

We can derive the harvested energies, denoted by E_m^{TS} and E_m^{PS}, for TS and PS receivers at mobile device m, respectively, during the downlink SWIPT phase as follows:

$$\begin{cases} E_m^{\text{TS}} = \alpha n_{\text{d}} T_s \mathcal{P}_{\text{d}} \zeta \left| \sum\limits_{k=1}^{K_{\text{a}}} \sum\limits_{m'=1}^{K_{\text{u}}} \sqrt{\eta_{k,m'}} \left(\widehat{\boldsymbol{h}}_{k,m'} \right)^H \boldsymbol{h}_{k,m} \right|; \\ E_m^{\text{PS}} = n_{\text{d}} T_s \mathcal{P}_{\text{d}} \rho \zeta \left| \sum\limits_{k=1}^{K_{\text{a}}} \sum\limits_{m'=1}^{K_{\text{u}}} \sqrt{\eta_{k,m'}} \left(\widehat{\boldsymbol{h}}_{k,m'} \right)^H \boldsymbol{h}_{k,m} \right|, \end{cases} \tag{4.4}$$

where $\zeta \in (0, 1)$ is the energy conversion efficiency, T_s is the duration of each channel use, and $\mathcal{P}_{\text{d}}$ is the power for downlink transmission at the APs. Observing from Eq. (4.4), in addition to the channel gain, the amount of harvested energy depends on the PS and TS factors ρ and α. Then, we can derive the total harvested energy, denoted by E_m, for the joint TS-PS protocol at mobile device m during the downlink SWIPT phase as follows:

$$E_m = E_m^{\text{TS}} + (1 - \alpha) E_m^{\text{PS}}. \tag{4.5}$$

The charging state of battery,denoted by B_m, at mobile device m before the next uplink information transmission phase is given by

$$B_m = \min \left\{ B_{\max}, E_m \right\} \tag{4.6}$$

where $B_{\max}$ is the pre-defined maximum storable energy at the mobile device. Then, the remaining energy, denoted by $E_{\text{r},m}$, at mobile device m for the next uplink data transmission phase is derived as follows:

$$E_{\text{r},m} = B_m - (1 - \alpha) n_{\text{d}} T_s \mathcal{P}_c \tag{4.7}$$

where $\mathcal{P}_c$ is the circuit and baseband processing power consumption. Without loss of generality, we assume that $\mathcal{P}_c$ is a constant. If the harvested energy during the downlink SWIPT phase is insufficient for the next uplink data transmission, there will be an outage, resulting in data transmission failure. Otherwise, all the remaining energy will be used for data transmissions in the next

phase.

4.2.3 Downlink Data Transmission in the Finite Blocklength Regime

4.2.3.1 Wireless Downlink Data Transmission Model

Denote by $\widetilde{n}_{\mathrm{d}} = (1-\alpha)n_{\mathrm{d}}$ the downlink data blocklength during the downlink information transfer sub-phase. We define the transmit signal matrix as $\boldsymbol{X}_k^{\widetilde{n}_{\mathrm{d}}} \triangleq \left[\boldsymbol{x}_k^{(1)}, \ldots, \boldsymbol{x}_k^{(\widetilde{n}_{\mathrm{d}})}\right]$ at AP k for transmitting $\widetilde{n}_{\mathrm{d}}$ data blocks where $\boldsymbol{x}_k^{(l)}$ ($l = 1, \ldots, \widetilde{n}_{\mathrm{d}}$) is the transmit signal vector for the lth data block. Define receive signal vector as $\boldsymbol{y}_{\mathrm{d},m}^{\widetilde{n}_{\mathrm{d}}} \triangleq \left[y_{\mathrm{d},m}^{(1)}, \ldots, y_{\mathrm{d},m}^{(\widetilde{n}_{\mathrm{d}})}\right]$ at mobile device m. Based on the MMSE estimator $\widehat{\boldsymbol{h}}_{k,m}$, we can derive the transmitted signal with length $\widetilde{n}_{\mathrm{d}}$ at AP k by employing conjugate beamforming [36] as follows:

$$\boldsymbol{X}_k^{\widetilde{n}_{\mathrm{d}}} = \sqrt{(1-\rho)\mathcal{P}_{\mathrm{d}}} \sum_{m=1}^{K_{\mathrm{u}}} \sqrt{\eta_{k,m}} \boldsymbol{b}_{k,m} \boldsymbol{s}_m^{\widetilde{n}_{\mathrm{d}}} \tag{4.8}$$

where $\boldsymbol{s}_m^{\widetilde{n}_{\mathrm{d}}}$ represents the transmitted signal vector for mobile device m, $\boldsymbol{b}_{k,m} \in \mathbb{C}^{N_{\mathrm{T}} \times 1}$ is the precoder vector that AP k assigns to mobile users m, which is given as follows:

$$\boldsymbol{b}_{k,m} = \frac{\widehat{\boldsymbol{h}}_{k,m}}{\sqrt{\mathbb{E}\left[\left\|\widehat{\boldsymbol{h}}_{k,m}\right\|^2\right]}} \tag{4.9}$$

and $\eta_{k,m}$ is the downlink power allocation coefficient for transmitting from AP k to mobile device m, which is chosen to satisfy the following power constraint at each AP:

$$\sum_{m=1}^{K_{\mathrm{u}}} \eta_{k,m} \nu_{k,m} \leq 1 \tag{4.10}$$

where

$$\nu_{k,m} \triangleq \mathbb{E}\left[\left|\widehat{\boldsymbol{h}}_{k,m}\right|^2\right]. \tag{4.11}$$

Then, we can derive the received downlink signal, denoted by $\boldsymbol{y}_{\mathrm{d},m}^{\widetilde{n}_{\mathrm{d}}}$, at the mth mobile device as follows:

$$\begin{aligned}\boldsymbol{y}_{\mathrm{d},m}^{\widetilde{n}_{\mathrm{d}}} &= \sum_{k=1}^{K_{\mathrm{a}}} (\boldsymbol{h}_{k,m})^H \boldsymbol{X}_k^{\widetilde{n}_{\mathrm{d}}} + \boldsymbol{w}_{\mathrm{d},m}^{\widetilde{n}_{\mathrm{d}}} \\ &= \sqrt{(1-\rho)\mathcal{P}_{\mathrm{d}}} \sum_{k=1}^{K_{\mathrm{a}}} \sqrt{\eta_{k,m}} (\boldsymbol{h}_{k,m})^H \boldsymbol{h}_{k,m} \boldsymbol{s}_m^{\widetilde{n}_{\mathrm{d}}} + \sqrt{(1-\rho)\mathcal{P}_{\mathrm{d}}} \\ &\quad \times \sum_{k=1}^{K_{\mathrm{a}}} \left[\sum_{\substack{m'=1 \\ m' \neq m}}^{K_{\mathrm{u}}} \sqrt{\eta_{k,m'}} (\boldsymbol{h}_{k,m'})^H \boldsymbol{h}_{k,m} \boldsymbol{s}_{m'}^{\widetilde{n}_{\mathrm{d}}} \right] + \boldsymbol{w}_{\mathrm{d},m}^{\widetilde{n}_{\mathrm{d}}} \end{aligned} \tag{4.12}$$

where $\boldsymbol{s}_m^{\widetilde{n}_{\mathrm{d}}}$ and $\boldsymbol{s}_{m'}^{\widetilde{n}_{\mathrm{d}}}$ are the signals sent to mobile device m and mobile device m', respectively; $\eta_{k,m}$ and $\eta_{k,m'}$ are the downlink power allocation coefficients for transmitting from AP k to mobile device m and mobile device m', respectively; and $\boldsymbol{w}_{\mathrm{d},m}^{\widetilde{n}_{\mathrm{d}}}$ is the AWGN with zero mean and unit variance at mobile device m. Correspondingly, we can derive the downlink SNR, denoted by $\gamma_{\mathrm{d},m}$, at mobile device m as follows:

$$\begin{aligned}\gamma_{\mathrm{d},m} = (1-\rho)\mathcal{P}_{\mathrm{d}} \left| \mathbb{E}\left[\sum_{k=1}^{K_{\mathrm{a}}} \sqrt{\eta_{k,m}} (\boldsymbol{h}_{k,m})^H \boldsymbol{b}_{k,m} \right] \right|^2 \left\{ (1-\rho)\mathcal{P}_{\mathrm{d}} \sum_{m'=1}^{K_{\mathrm{u}}} \mathbb{E}\left[\left| \sum_{k=1}^{K_{\mathrm{a}}} \sqrt{\eta_{k,m'}} (\boldsymbol{h}_{k,m'})^H \boldsymbol{b}_{k,m} \right|^2 \right] \right. \\ \left. - (1-\rho)\mathcal{P}_{\mathrm{d}} \left| \mathbb{E}\left[\sum_{k=1}^{K_{\mathrm{a}}} \sqrt{\eta_{k,m}} (\boldsymbol{h}_{k,m})^H \boldsymbol{b}_{k,m} \right] \right|^2 + 1 \right\}^{-1}. \end{aligned} \tag{4.13}$$

Note that the SNR function given in Eq. (4.13) can be used to investigate the system performance for both TS and PS protocols. By setting $\alpha \neq 0$ and $\rho = 0$, we can derive the SNR function for the TS protocol. On the other hand, setting $\alpha = 0$ and $\rho \neq 0$, we can derive the SNR function for the PS protocol. When $\alpha \neq 0$ and $\rho \neq 0$, Eq. (4.13) can be used to characterize the SNR for a joint TS-PS protocol.

4.3 Downlink ϵ-Effective Capacity and Harvested Energy Tradeoff Optimization for Statistical Delay/Error-Rate Bounded QoS Using FBC

The effective capacity function only guarantees statistical delay-bounded QoS constraints without considering reliability requirements due to finite-blocklength data transmissions. Therefore, the traditional queuing behavior and effective capacity measurement approaches are no longer appropriate for our proposed performances modeling schemes. Correspondingly, we need to derive a new analytical model for characterizing statistical QoS metrics for upper-bounding both delay and error-rate to support mURLLC services. Integrating the statistical delay-bounded QoS provisioning theory and the FBC theory, we propose a novel definition of the *ϵ-effective capacity* as follows.

Definition 3. *For an $(n_d, M_m, \epsilon_{d,m})$-code, the downlink ϵ-effective capacity, denoted by $EC_{d,m}^{\epsilon,TS}$, for mobile user m under TS protocol is defined as the maximum constant arrival rate for a given service process considering the non-vanishing decoding error-probability ϵ subject to statistical delay and error-rate bounded QoS constraints, which is formally expressed as follows:*

$$EC_{d,m}^{\epsilon,TS} \triangleq -\frac{1}{\theta_m} \log \left\{ \mathbb{E}_{\gamma_{d,m}} \left[\epsilon_{d,m} + (1 - \epsilon_{d,m})\, e^{-\theta_m (1-\alpha) n_d T_s R_{d,m}} \right] \right\}. \tag{4.14}$$

The goal of this section is to formulate and solve the ϵ-effective capacity maximization problems for statistical delay and error-rate bounded QoS provisioning over our proposed SWIPT-enabled CF m-MIMO based 6G mobile wireless networks to obtain the boundaries of ϵ-effective capacity-energy region under both TS and PS protocols in the finite blocklength regime.

4.3.1 TS Protocol

Previous works have shown the optimal transmission strategies for the maximum power transfer and information transfer are in general different [105, 106]. The rate-energy (R-E) tradeoff is a very effective way to fundamentally characterize the performance of SWIPT-enabled schemes. Towards this end, the R-E tradeoff has been extensively studied in the previous literatures consid-

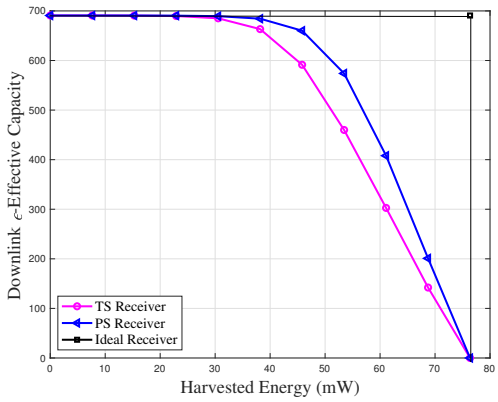

Figure 4.2: The downlink ϵ-effective capacity-energy region of different SWIPT receivers for the case of no power adaptation using FBC.

ering infinite blocklength using Shannon's second theorem. For our proposed SWIPT-enabled CF m-MIMO based schemes, we apply the FBC technique and characterize the downlink ϵ-effective capacity-energy tradeoff for statistical delay and error-rate bounded QoS provisioning in supporting mURLLC with non-vanishing decoding error probability. There have been a number of works focusing on investigating the rate-energy tradeoff curves for implementing SWIPT technique in the finite blocklength regime to support mURLLC. In particular, the authors of [100] have characterized the fundamental limits of SWIPT in terms of the information-energy capacity region in the non-asymptotic regime. The authors of [101] have investigated the rate-energy tradeoff and the decoding error probability-energy tradeoff for SWIPT systems in the finite blocklength realm. However, the previous research works have not analyzed the information-energy tradeoff by taking into account the statistical delay and error-rate QoS provisioning, which is an importing issue for supporting the mURLLC services. Therefore, we focus on investigating the optimal ϵ-effective capacity-energy tradeoff problems for SWIPT-enabled schemes for statistical delay and error-rate bounded QoS provisioning to support mURLLC with non-vanishing decoding error probability. Considering the case of no power adaptation, Fig. 4.2 plots the downlink ϵ-effective capacity-energy region for both TS and PS receivers compared with the ideal receiver, which is assumed to be able to decode information and harvest energy from the same signal simultaneously [107, 108].

As shown in Fig. 4.2, the downlink ϵ-effective capacity-energy region for TS and PS receivers is a concave-shape region. We can observe from Fig. 4.2 that a PS receiver outperforms a TS receiver in terms of the downlink ϵ-effective capacity-energy tradeoff.

In this chapter, we focus on investigating the optimal ϵ-effective capacity-energy tradeoff problems for SWIPT-enabled schemes with power allocation. Thus, taking into account both TS factor and power allocation coefficient, we define the downlink ϵ-effective capacity-energy region, denoted by $\mathcal{C}_{\mathrm{EC}_{\mathrm{d},m}^{\epsilon,\mathrm{TS}}-\mathrm{E}_m^{\mathrm{TS}}}$, under TS protocol for statistical delay and error-rate bounded QoS provisioning in the finite blocklength as follows:

$$\mathcal{C}_{\mathrm{EC}_{\mathrm{d},m}^{\epsilon,\mathrm{TS}}-\mathrm{E}_m^{\mathrm{TS}}} \triangleq \bigcup_{\substack{0\leq\eta_{k,m}\leq 1,\forall k \\ 0\leq\alpha\leq 1}} \Bigg\{ \left(EC_{\mathrm{d},m}^{\epsilon,\mathrm{TS}}, E_m^{\mathrm{TS}}\right) \Big| EC_{\mathrm{d},m}^{\epsilon,\mathrm{TS}} \leq -\frac{1}{\theta_m} \times \log\left\{\mathbb{E}_{\gamma_{\mathrm{d},m}}\left[\epsilon_{\mathrm{d},m} + (1-\epsilon_{\mathrm{d},m})\, e^{-\theta_m(1-\alpha)n_{\mathrm{d}}T_s R_{\mathrm{d},m}}\right]\right\}, E_m^{\mathrm{TS}} \leq \alpha n_{\mathrm{d}} T_s \mathcal{P}_{\mathrm{d}} \zeta \left| \sum_{k=1}^{K_{\mathrm{a}}} \sum_{m'=1}^{K_{\mathrm{u}}} \sqrt{\eta_{k,m'}} \left(\widehat{\boldsymbol{h}}_{k,m'}\right)^H \boldsymbol{h}_{k,m} \right| \Bigg\}. \tag{4.15}$$

Since the optimal tradeoff between the maximum downlink ϵ-effective capacity and harvested energy is characterized by the boundary of the downlink ϵ-effective capacity-energy region, it is important to characterize all the boundary pairs of downlink ϵ-effective capacity and harvested energy. We can formulate the following optimization problem for our proposed SWIPT-enabled CF m-MIMO based schemes to obtain the boundaries of downlink ϵ-effective capacity-energy region under TS protocol in the finite blocklength regime:

$$\mathbf{P_9} : \arg \max_{\left\{\alpha, n_{\mathrm{d}}, \eta_{k,m}, \forall m,k\right\}} \left\{ \sum_{m=1}^{K_u} EC_{\mathrm{d},m}^{\epsilon,\mathrm{TS}}(\theta_m) \right\} \tag{4.16}$$

$$\text{s.t. } C5: E_m^{\text{TS}} \geq \overline{E}_{\min}; \tag{4.17}$$

$$C6: \sum_{m=1}^{K_{\text{u}}} \eta_{k,m}\nu_{k,m} \leq 1; \tag{4.18}$$

$$C7: 0 < \alpha < 1, \tag{4.19}$$

where $\overline{E}_{\min}$ is the minimum required harvested energy. Then, we can convert $\mathbf{P_9}$ into the following equivalent minimization problem:

$$\mathbf{P_{10}}: \arg \min_{\left\{\alpha, n_{\text{d}}, \eta_{k,m}, \forall m,k\right\}} \left\{ \sum_{m=1}^{K_u} \mathbb{E}_{\gamma_{\text{d},m}} \left[\epsilon_{\text{d},m} + (1-\epsilon_{\text{d},m}) \exp\left\{ -\theta_m (1-\alpha) n_{\text{d}} T_s R_{\text{d},m} \right\} \right] \right\} \tag{4.20}$$

subject to the same constraints C5, C6, and C7 given by Eqs. (4.17), (4.18), and (4.19), respectively. The optimization problem $\mathbf{P_{10}}$ given by Eq. (4.20) is challenging in terms of finding the global optimal solution due to highly-coupling among variables. To overcome such issue, an alternative optimization technique can be developed in an efficient manner where an improved solution is obtained at each step of iteration with guaranteed convergence by applying the successive convex approximation (SCA) techniques. By using the SCA techniques, we do not need to characterize the joint convexity across all variables, and instead, we can only characterize the convexity for each given individual variable when fixing the other variables in our proposed optimization problems to make the complexity-analysis problem feasible. Therefore, to solve the optimization problem $\mathbf{P_{10}}$, we characterize the convexity of the objective function in $\mathbf{P_{10}}$ as detailed in the following theorem.

Theorem 6. ***If*** *the harvested energy E_m^{TS} is characterized by Eq. (4.4),* ***then*** *the following claims hold for our proposed SWIPT-enabled CF m-MIMO based schemes in supporting statistical delay and error-rate bounded QoS provisioning under TS protocol in the finite blocklength regime.*

Claim 1. Given fixed downlink power allocation coefficient $\eta_{k,m}$ and downlink data blocklength

Algorithm 2 : Joint Optimization Algorithm Under TS Protocol for solving $\mathbf{P_{10}}$ in Eq. (4.20)

Input: $K_{\rm a}, K_{\rm u}, M, n_{\rm p}, \beta_{k,m}, \mathcal{P}_{\rm p}, \mathcal{P}_{\rm d}, \theta_m, T_s, \overline{E}_{\min}$

Initialization: $\ell = 0$ and $\left\{\alpha^{(0)}, n_{\rm d}^{(0)}, \eta_{k,m}^{(0)}\right\}$

Repeat

Step 1:

Solve $\arg\min_{n_{\rm d}} \left\{ \sum_{m=1}^{K_u} F\left(\gamma_{{\rm d},m}\right) \right\}$ in Eq. (4.20), denote the solution by $n_{\rm d}^{(\ell+1)}$

if $n_{\rm d}^{(\ell+1)}$ is an integer **then**

$n_{\rm d}^{(\ell+1)} \rightarrow n_{\rm d}^{\rm opt}$

else

$n_{\rm d}^{(\ell+1)} = \arg \min_{n_{\rm d} \in \left\{n_{\rm d}^{\rm floor}, n_{\rm d}^{\rm cell}\right\}} \left\{ \sum_{m=1}^{K_u} F\left(\gamma_{{\rm d},m}\right) \right\}$, where $n_{\rm d}^{\rm floor} = \lfloor n_{\rm d}^{\rm opt} \rfloor$ and $n_{\rm d}^{\rm cell} = \lceil n_{\rm d}^{\rm opt} \rceil$

end if

Step 2:

Solve $\arg\min_{\alpha} \left\{ \sum_{m=1}^{K_u} F\left(\gamma_{{\rm d},m}\right) \right\}$ in Eq. (4.20), denote the solution by $\alpha^{(\ell+2)}$

Step 3:

Solve $\arg \min_{\eta_{k,m}, \forall m,k} \left\{ \sum_{m=1}^{K_u} F\left(\gamma_{{\rm d},m}\right) \right\}$ in Eq. (4.20), denote the solution by $\eta_{k,m}^{(\ell+3)}$

$\ell \leftarrow (\ell + 1)$

Repeat Step 1–Step 3 until the solution converges

n_d, the objective function in $\mathbf{P_{10}}$ is convex in α when $\epsilon_{d,m} \in (0, 0.5)$ and $n_d > n_{d,th}^{TS}$, where

$$n_{d,th}^{TS} \triangleq \frac{1}{(1-\alpha)} \left[\frac{Q^{-1}(\epsilon_{d,m})}{C\left(\gamma_{d,m}\right) - \frac{C\left(\gamma_{d,m}\right)}{4(1-\alpha)\theta_m n_d T_s C\left(\gamma_{d,m}\right)+1}} \right]^2 . \tag{4.21}$$

Claim 2. Given fixed TS factor α and downlink power allocation coefficient $\eta_{k,m}$, the objective function in $\mathbf{P_{10}}$ is convex in n_d when $\epsilon_{d,m} \in (0, 0.5)$.

Claim 3. Given fixed TS factor α and downlink data blocklength n_d, the objective function in $\mathbf{P_{10}}$ is convex in $\eta_{k,m}$ when $\epsilon_{d,m} \in (0, 0.5)$.

Proof. The proof is provided in Appendix G. □

Remarks on Theorem 6: Theorem 6 implies that there exists a local optimal solution to the minimization problem $\mathbf{P_{10}}$ when the other two variables are fixed. Therefore, the minimization

problem $\mathbf{P_{10}}$ can be efficiently solved by applying the SCA techniques with an iterative search method. In particular, we start with the initialized values of the TS factor, denoted by $\alpha^{(0)}$, downlink data blocklength, denoted by $n_{\mathrm{d}}^{(0)}$, and downlink power allocation coefficient, denoted by $\eta_{k,m}^{(0)}$. In Step 1, we formulate a local problem aiming at minimizing the objective function in $\mathbf{P_{10}}$ over n_{d}. We solve this local minimization problem and determine the optimal downlink data blocklength, denoted by $n_{\mathrm{d}}^{\mathrm{opt}}$, to $\mathbf{P_{10}}$. In Step 2, based on $n_{\mathrm{d}}^{\mathrm{opt}}$, we repeat the same process for new local problem to minimize the objective function in $\mathbf{P_{10}}$ over the TS factor α. In Step 3, based on $n_{\mathrm{d}}^{\mathrm{opt}}$ and α derived in the previous Step 1 and Step 2, we repeat the same process to solve the local problem to minimize the objective function in $\mathbf{P_{10}}$ over $\eta_{k,m}$. We repeat Step 1–Step 3 until the solution converges. We define $n_{\mathrm{d}}^{(\ell)}$, $\alpha^{(\ell)}$, and $\eta_{k,m}^{(\ell)}$ as the downlink blocklength, TS factor, and downlink power allocation coefficient in the ℓth iteration ($\ell = 0, 1, 2, \dots$), respectively. We develop an iterative algorithm as shown in **Algorithm 2** to solve the optimization problem $\mathbf{P_{10}}$ for our proposed SWIPT-enabled CF m-MIMO based schemes under TS protocol in the finite blocklength regime. To analyze the convergence of the above **Algorithm 2**, it is easy to show that the optimal value of each local problem is definitely not lower than the optimal value of the original problem given by Eq. (4.20). According to [102], the convergence of **Algorithm 2** is therefore guaranteed, i.e., at least a local optimal solution can be achieved. Note that according to Theorem 6, the objective function in $\mathbf{P_{10}}$ is smooth and differentiable in $\{\alpha, n_{\mathrm{d}}, \eta_{k,m}\}$ in the feasible set, and the objective function in $\mathbf{P_{10}}$ is convex in α, n_{d}, and $\eta_{k,m}$, respectively, when the other two variables are fixed. Therefore, it is easy to show that the local optimal solution is unique, thus, it is also the global optimal solution.

4.3.2 PS Protocol

Considering the PS protocol, we define the downlink ϵ-effective capacity-energy region, denoted by $\mathcal{C}_{\mathrm{EC}_{\mathrm{d},m}^{\epsilon,\mathrm{PS}}-\mathrm{E}_m^{\mathrm{PS}}}$, as follows:

$$\mathcal{C}_{\mathrm{EC}_{\mathrm{d},m}^{\epsilon,\mathrm{PS}}-\mathrm{E}_m^{\mathrm{PS}}} \triangleq \bigcup_{\substack{0\leq\eta_{k,m}\leq 1,\forall k \\ 0\leq\rho\leq 1}} \Bigg\{ \Big(EC_{\mathrm{d},m}^{\epsilon,\mathrm{PS}}, E_m^{\mathrm{PS}}\Big) \Big| EC_{\mathrm{d},m}^{\epsilon,\mathrm{PS}} \leq -\frac{1}{\theta_m} \log\left\{\mathbb{E}_{\gamma_{\mathrm{d},m}}\left[\epsilon_{\mathrm{d},m}+(1-\epsilon_{\mathrm{d},m})\, e^{-\theta_m n_{\mathrm{d}} T_s R_{\mathrm{d},m}}\right]\right\}, \\ E_m^{\mathrm{PS}} \leq n_{\mathrm{d}} T_s \mathcal{P}_{\mathrm{d}} \rho \zeta \left| \sum_{k=1}^{K_{\mathrm{a}}} \sum_{m'=1}^{K_{\mathrm{u}}} \sqrt{\eta_{k,m'}} \Big(\widehat{\boldsymbol{h}}_{k,m'}\Big)^H \boldsymbol{h}_{k,m} \right| \Bigg\} \tag{4.22}$$

where $EC_{\mathrm{d},m}^{\epsilon,\mathrm{PS}}$ is the downlink ϵ-effective capacity under PS protocol. As a result, we can formulate the following optimization problem for our proposed SWIPT-enabled CF m-MIMO based schemes under PS protocol in the finite blocklength regime:

$$\mathbf{P_{11}} : \arg \max_{\left\{\rho, n_{\mathrm{d}}, \eta_{k,m}, \forall m,k\right\}} \left\{ \sum_{m=1}^{K_u} EC_{\mathrm{d},m}^{\epsilon,\mathrm{PS}}(\theta_m) \right\} \tag{4.23}$$

$$\text{s.t. } C5, C6; \\ C8 : 0 < \rho < 1. \tag{4.24}$$

Then, we can convert $\mathbf{P_{11}}$ into the following equivalent minimization problem:

$$\mathbf{P_{12}} : \arg \min_{\left\{\rho, n_{\mathrm{d}}, \eta_{k,m}, \forall m,k\right\}} \left\{ \sum_{m=1}^{K_u} \mathbb{E}_{\gamma_{\mathrm{d},m}} \left[\epsilon_{\mathrm{d},m} + (1-\epsilon_{\mathrm{d},m})\, e^{-\theta_m n_{\mathrm{d}} T_s R_{\mathrm{d},m}} \right] \right\} \tag{4.25}$$

subject to the same constraints C5, C6, and C8 given by Eqs. (4.17), (4.18) and (4.24), respectively. Similar to Theorem 6, the optimization problem $\mathbf{P_{12}}$ given by Eq. (4.25) is challenging in terms of finding the global optimal solution due to highly-coupling among variables. We apply an alternative optimization technique in an efficient manner where an improved solution is obtained at each step of iteration with guaranteed convergence by applying the SCA techniques. Therefore, to solve

the optimization problem $\mathbf{P_{12}}$, we need to characterize the convexity of the objective function in $\mathbf{P_{12}}$ as detailed in the following theorem.

Theorem 7. *Given fixed power allocation coefficient $\eta_{k,m}$ and downlink blocklength n_d, the objective function in $\mathbf{P_{12}}$ specified by Eq. (4.25) is convex in the PS factor ρ for our proposed SWIPT-enabled CF m-MIMO based schemes under PS protocol in the finite blocklength regime when $\epsilon_{d,m} \in (0, 0.5)$ and $n_d > n_{d,th}^{PS}$, where*

$$n_{d,th}^{PS} \triangleq \frac{9}{V\left(\gamma_{d,m}\right)} \left[\frac{Q^{-1}(\epsilon_{d,m})(\log 2)}{\left(1+\gamma_{d,m}\right)^2}\right]^2. \tag{4.26}$$

Proof. The proof is provided in Appendix H. □

Remarks on Theorem 7: Similar to Theorem 6, Theorem 7 implies that there exists a local optimal solution to the minimization problem $\mathbf{P_{12}}$ when the other two variables are fixed. It is easy to show that the local optimal solution is unique, thus, it is also the global optimal solution. Therefore, $\mathbf{P_{12}}$ can be efficiently solved by using the similar approach as described in **Algorithm 2**.

4.4 Joint Uplink ϵ-Effective Capacity and Harvested Energy Tradeoff for Statistical Delay/Error-Rate Bounded QoS Using FBC

4.4.1 Uplink Data Transmission in the Finite Blocklength Regime

During the uplink data transmission phase, all K_{u} mobile devices simultaneously transmit their data to the APs using the energy harvested from the previous downlink SWIPT phase. We can derive the uplink transmit power, denoted by $\mathcal{P}_m$, from mobile device m to the APs as follows:

$$\mathcal{P}_m = \frac{E_{\mathrm{r},m}}{n_{\mathrm{u}} T_s}. \tag{4.27}$$

We can derive the received signal, denoted by $\boldsymbol{Y}_{\mathrm{u},k}^{n_{\mathrm{u}}}$, from all mobile devices to AP k as follows:

$$\boldsymbol{Y}_{\mathrm{u},k}^{n_{\mathrm{u}}} = \sum_{m=1}^{K_{\mathrm{u}}} \sqrt{\eta_{\mathrm{u},m}\mathcal{P}_m}\boldsymbol{h}_{k,m}\boldsymbol{q}_m^{n_{\mathrm{u}}} + \boldsymbol{W}_{\mathrm{u},k}^{n_{\mathrm{u}}} \tag{4.28}$$

where $\eta_{\mathrm{u},m}$ is the uplink power allocation coefficient for mobile device m, $\boldsymbol{W}_{\mathrm{u},k}^{n_{\mathrm{u}}} \in \mathbb{C}^{N_{\mathrm{T}} \times n_{\mathrm{u}}}$ is the AWGN matrix with zero mean and covariance $\mathbf{I}_{N_{\mathrm{T}} \times n_{\mathrm{u}}}$ at AP k, and $\boldsymbol{q}_m^{n_{\mathrm{u}}}$ is the signal transmitted by mobile device m, which need to satisfy the following constraint:

$$\mathbb{E}\left[\|\boldsymbol{q}_m^{n_{\mathrm{u}}}\|^2\right] = 1. \tag{4.29}$$

Then, after the conjugate precoder at the AP, the processed uplink signal, denoted by $\boldsymbol{r}_{\mathrm{u},m}$, at the CPU from mobile device m can be derived as follows:

$$\boldsymbol{r}_{\mathrm{u},m} = \sum_{k=1}^{K_{\mathrm{a}}} \left(\widehat{\boldsymbol{h}}_{k,m}\right)^H \boldsymbol{Y}_k^{n_{\mathrm{u}}} = \sum_{m'=1}^{K_{\mathrm{u}}} \sum_{k=1}^{K_{\mathrm{a}}} \sqrt{\eta_{\mathrm{u},m'} \mathcal{P}_{m'}} \left(\widehat{\boldsymbol{h}}_{k,m}\right)^H \boldsymbol{h}_{k,m'} \boldsymbol{q}_{m'}^{n_{\mathrm{u}}} + \sum_{k=1}^{K_{\mathrm{a}}} \left(\widehat{\boldsymbol{h}}_{k,m}\right)^H \boldsymbol{w}_{\mathrm{u},k}^{n_{\mathrm{u}}}. \tag{4.30}$$

Correspondingly, we can derive the uplink SNR, denoted by $\gamma_{\mathrm{u},m}$, at AP k as follows:

$$\begin{aligned}\gamma_{\mathrm{u},m} = & \eta_{\mathrm{u},m} \mathcal{P}_m \left| \mathbb{E}\left[\sum_{k=1}^{K_{\mathrm{a}}} (\widehat{\boldsymbol{h}}_{k,m})^H \boldsymbol{h}_{k,m}\right] \right|^2 \left\{ \sum_{m'=1}^{K_{\mathrm{u}}} \eta_{\mathrm{u},m'} \mathcal{P}_{m'} \mathbb{E}\left[\left| \sum_{k=1}^{K_{\mathrm{a}}} (\widehat{\boldsymbol{h}}_{k,m'})^H \boldsymbol{h}_{k,m} \right|^2 \right] \right. \\ & \left. - \left| \mathbb{E}\left[\sum_{k=1}^{K_{\mathrm{a}}} (\widehat{\boldsymbol{h}}_{k,m})^H \boldsymbol{h}_{k,m}\right] \right|^2 \eta_{\mathrm{u},m} \mathcal{P}_m + \mathbb{E}\left[\left\| \sum_{k=1}^{K_{\mathrm{a}}} \widehat{\boldsymbol{h}}_{k,m} \right\|^2 \right] \right\}^{-1}. \end{aligned} \tag{4.31}$$

4.4.2 Joint Uplink Resource Allocation Optimization for Statistical Delay and Error-Rate Bounded QoS Provisioning Using FBC

Define the uplink ϵ-effective capacity, denoted by $EC_{\mathrm{u},m}^{\epsilon,\text{TS-PS}}(\theta_m)$, under joint TS-PS protocol for mobile device m as follows:

$$EC_{\mathrm{u},m}^{\epsilon,\text{TS-PS}}(\theta_m) = -\frac{1}{\theta_m} \log\left\{ \mathbb{E}_{\gamma_{\mathrm{u},m}}\left[\epsilon_{\mathrm{u},m} + (1 - \epsilon_{\mathrm{u},m})\, e^{-\theta_m n_{\mathrm{u}} T_s R_{\mathrm{u},m}} \right] \right\} \tag{4.32}$$

where $\epsilon_{\mathrm{u},m}$ is the uplink decoding error probability for mobile device m and $R_{\mathrm{u},m}$ is the uplink coding rate, which is given as follows:

$$R_{\mathrm{u},m} = C\left(\gamma_{\mathrm{u},m}\right) - \sqrt{\frac{V\left(\gamma_{\mathrm{u},m}\right)}{n_{\mathrm{u}}}} Q^{-1}(\epsilon_{\mathrm{u},m}) \tag{4.33}$$

where $C\left(\gamma_{\mathrm{u},m}\right)$ and $V\left(\gamma_{\mathrm{u},m}\right)$ are the uplink channel capacity and channel dispersion, respectively. Considering the joint TS-PS protocol, we define the uplink ϵ-effective capacity-energy region, denoted by $\mathcal{C}_{\mathrm{EC}_{\mathrm{u},m}^{\epsilon,\text{TS-PS}}-\mathrm{E}_m^{\text{TS-PS}}}$, as follows:

$$\begin{aligned}\mathcal{C}_{\mathrm{EC}_{\mathrm{u},m}^{\epsilon,\text{TS-PS}}-\mathrm{E}_m^{\text{TS-PS}}} \triangleq \bigcup_{\substack{0\le\eta_{k,m}\le 1,\forall k\\ 0\le\alpha\le 1\\ 0\le\rho\le 1}} \Bigg\{ & \left(EC_{\mathrm{u},m}^{\epsilon,\text{TS-PS}}, E_m^{\text{TS-PS}}\right) : \\ & EC_{\mathrm{u},m}^{\epsilon,\text{TS-PS}} \le -\frac{1}{\theta_m}\log\left\{\mathbb{E}_{\gamma_{\mathrm{u},m}}\left[\epsilon_{\mathrm{u},m}+(1-\epsilon_{\mathrm{u},m})\, e^{-\theta_m n_{\mathrm{u}} T_s R_{\mathrm{u},m}}\right]\right\}, \\ & E_m \le \alpha n_{\mathrm{d}} T_s \mathcal{P}_{\mathrm{d}} \zeta \left| \sum_{k=1}^{K_{\mathrm{a}}} \sum_{m'=1}^{K_{\mathrm{u}}} \sqrt{\eta_{k,m'}} \left(\widehat{\boldsymbol{h}}_{k,m'}\right)^H \boldsymbol{h}_{k,m} \right| \\ & \quad + (1-\alpha) n_{\mathrm{d}} T_s \mathcal{P}_{\mathrm{d}} \rho \zeta \left| \sum_{k=1}^{K_{\mathrm{a}}} \sum_{m'=1}^{K_{\mathrm{u}}} \sqrt{\eta_{k,m'}} \left(\widehat{\boldsymbol{h}}_{k,m'}\right)^H \boldsymbol{h}_{k,m} \right| \Bigg\}.\end{aligned} \tag{4.34}$$

The max-min power control optimization is a centralized algorithm for guaranteeing a uniform SINR for all mobile devices. However, if an mobile device suffers from a bad channel gain and experiences poor SINR, the ϵ-effective capacity for all the other mobile devices will be compromised. Therefore, taking into account both the downlink harvested energy and uplink transmit power constraints, we formulate a distributed joint uplink resource allocation optimization problem for our proposed SWIPT-enabled CF m-MIMO based schemes under a joint TS-PS protocol in the finite blocklength regime as follows:

$$\mathbf{P_{13}} : \arg \max_{\substack{\alpha,\rho,n_{\mathrm{d}},n_{\mathrm{u}},\\ \eta_{k,m},\eta_{\mathrm{u},m},\forall m,k}} \left\{ \sum_{m=1}^{K_u} EC_{\mathrm{u},m}^{\epsilon,\text{TS-PS}}(\theta_m) \right\} \tag{4.35}$$

$$\text{s.t. } C5 - C8;$$

$$C9 : \gamma_{\text{u},m} \geq \gamma_{\text{th}}, \quad \forall m; \tag{4.36}$$

$$C10 : 0 \leq \eta_{\text{u},m} \leq 1, \quad \forall m, k, \tag{4.37}$$

where γ_{th} is the SNR threshold for all mobile devices. Then, the above optimization problem can be reformulated into the following equivalent minimization problem:

$$\mathbf{P_{14}} : \arg \min_{\substack{\alpha,\rho,n_{\text{d}},n_{\text{u}},\\ \eta_{k,m},\eta_{\text{u},m},\forall m,k}} \left\{ \sum_{m=1}^{K_u} \mathbb{E}_{\gamma_{\text{u},m}} \left[\epsilon_{\text{u},m} + (1 - \epsilon_{\text{u},m})\, e^{-\theta_m n_{\text{u}} T_s R_{\text{u},m}} \right] \right\} \tag{4.38}$$

subject to the same constraints C5-C10 given by Eqs. (4.17) (4.18), (4.19), (4.19), (4.24), and (4.37), respectively. Since Theorem 6 and Theorem 7 have shown that $F\left(\gamma_{\text{d},m}\right)$ is convex in α, ρ, and n_{d}, $\eta_{k,m}$ respectively, we can easily obtain that the objective function in problem $\mathbf{P_{14}}$ is convex with respect to n_{d} and $\eta_{\text{u},m}$, respectively, when the other parameters are fixed. Therefore, the optimization problem $\mathbf{P_{14}}$ specified by Eq. (4.38) is a convex optimization problem and thus can be efficiently solved by applying the SCA techniques with an iterative search method, which is similar to **Algorithm 2**.

4.5 Performance Evaluations

We use simulations to validate and evaluate our proposed SWIPT-enabled CF m-MIMO based schemes in the finite blocklength regime. Throughout our simulations, we set the number of APs $K_{\text{a}} = 100$, the number of mobile devices $K_{\text{u}} = 50$, the duration of each channel use $T_s = 10$ μs, the energy conversion efficiency $\zeta = 0.5$, the uplink pilot transmit power $\mathcal{P}_{\text{p}} = 20$ dBm, and the downlink transmit power $\mathcal{P}_{\text{d}} = 80$ dBm.

We set the downlink blocklength error probability $\epsilon_{\text{d},m} = 1 \times 10^{-6}$. Using Eq. (G.9), Fig. 4.3 plots the second-order derivative $\partial^2 F\left(\gamma_{\text{d},m}\right)/\partial\alpha^2$ as a function of the downlink SNR $\gamma_{\text{d},m}$ for our proposed SWIPT-enabled CF m-MIMO scheme using FBC. Fig. 4.3 shows that the second-order derivative $\partial^2 F\left(\gamma_{\text{d},m}\right)/\partial\alpha^2$ increases as the SNR $\gamma_{\text{d},m}$ increases. In the high SNR region, we observe from Fig. 4.3 that $\partial^2 F\left(\gamma_{\text{d},m}\right)/\partial\alpha^2 > 0$, which implies that the objective function in $\mathbf{P_{10}}$

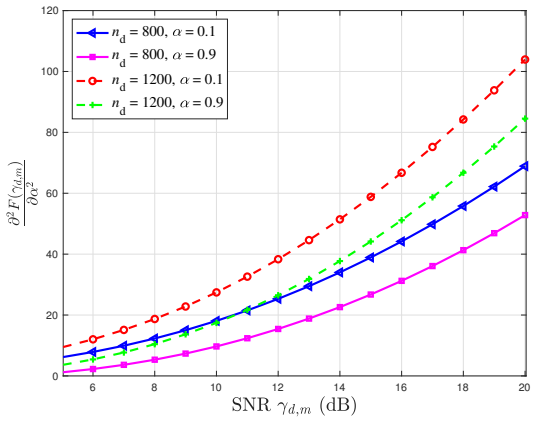

Figure 4.3: The second-order derivative $\partial^2 F\left(\gamma_{\mathrm{d},m}\right)/\partial\alpha^2$ vs. SNR $\gamma_{\mathrm{d},m}$ for our proposed SWIPT-enabled CF m-MIMO scheme using FBC with the TS factor $\alpha = 0.9$.

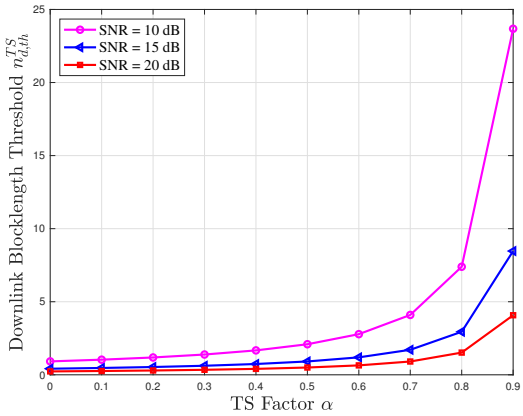

Figure 4.4: The downlink blocklength threshold $n_{\mathrm{d,th}}^{\mathrm{TS}}$ vs. TS factor α for our proposed SWIPT-enabled CF m-MIMO scheme under TS protocol using FBC.

specified by Eq. (4.20) is convex with respect to the TS factor α. Thus, Theorem 6 holds in the high SNR scenario. Fig. 4.3 also shows that $\partial^2 F\left(\gamma_{\mathrm{d},m}\right)/\partial\alpha^2$ is an increasing function of the downlink blocklength n_{d}. This implies that a smaller value of n_{d} and a larger value of n_{d} set an lower bound and upper bound on the second-order derivative of the auxiliary function $\partial^2 F\left(\gamma_{\mathrm{d},m}\right)/\partial\alpha^2$, respectively.

Using the downlink data blocklength threshold in Eq. (4.21), Fig. 4.4 depicts the threshold on

downlink blocklength $n_{\text{d,th}}^{\text{TS}}$ as a function of TS factor α for our proposed SWIPT-enabled CF m-MIMO scheme under TS protocol in the finite blocklength regime. Fig. 4.4 shows that the threshold on downlink blocklength $n_{\text{d,th}}^{\text{TS}}$ increases as the TS factor α increases. Fig. 4.4 also shows that the threshold on downlink blocklength $n_{\text{d,th}}^{\text{TS}}$ is a decreasing function of SNR $\gamma_{\text{d},m}$. We can observe from Fig. 4.4 that the value of $n_{\text{d,th}}^{\text{TS}}$ increases from 0.92 to 23.68 as the value of TS factor increases from 0 to 0.9 when the SNR is 10 dB. Since the authors in [30] have shown that the data transmission rate is quite accurate when the blocklength is as short as 100, the downlink blocklength threshold $n_{\text{d,th}}^{\text{TS}} \ll 100$ would automatically hold for $n > n_{\text{d,th}}^{\text{TS}}$, especially in the high SNR scenario, which validates Theorem 6.

In addition, using the downlink data blocklength threshold in Eq. (4.26), Fig. 4.5 plots the threshold on downlink blocklength $n_{\text{d,th}}^{\text{PS}}$ as a function of the SNR $\gamma_{\text{d},m}$ for our proposed SWIPT-enabled CF m-MIMO scheme under PS protocol in the finite blocklength regime. Fig. 4.5 shows that the threshold on downlink blocklength $n_{\text{d,th}}^{\text{PS}}$ decreases as the SNR $\gamma_{\text{d},m}$ increases. Fig. 4.5 also shows that the threshold on downlink blocklength $n_{\text{d,th}}^{\text{PS}}$ is a decreasing function of the decoding error probability $\epsilon_{\text{d},m}$. We can observe from Fig. 4.5 that the value of $n_{\text{d,th}}^{\text{PS}}$ decreases from 4.67 to 0 as the value of SNR $\gamma_{\text{d},m}$ increases from 0 to 15 dB when the decoding error probability $\epsilon_{\text{d},m} = 1 \times 10^{-6}$. Since the data transmission rate is quite accurate when the blocklength is as short as 100 [30], the downlink blocklength threshold $n_{\text{d,th}}^{\text{PS}}$ would automatically hold for $n > n_{\text{d,th}}^{\text{PS}}$, which validates Theorem 7.

Setting the blocklength error probability $\epsilon_{\text{d},m} = 1 \times 10^{-6}$, Fig. 4.6 plots the downlink ϵ-effective capacity as a function of TS factor α for our proposed SWIPT-enabled CF m-MIMO scheme using FBC. We can observe from Fig. 4.6 that the downlink ϵ-effective capacity is a decreasing function of TS factor α. In addition, Fig. 4.7 depicts the downlink ϵ-effective capacity as a function of both the TS factor α and QoS exponent θ_m for our proposed SWIPT-enabled CF m-MIMO scheme using FBC. We can observe from Fig. 4.7 that the downlink ϵ-effective capacity decreases as the decoding error probability $\epsilon_{\text{d},m}$ increases. Fig. 4.7 also shows that the downlink ϵ-effective capacity is a decreasing function of QoS exponent θ_m, which implies that a smaller θ_m ($\theta_m \to 0$) and

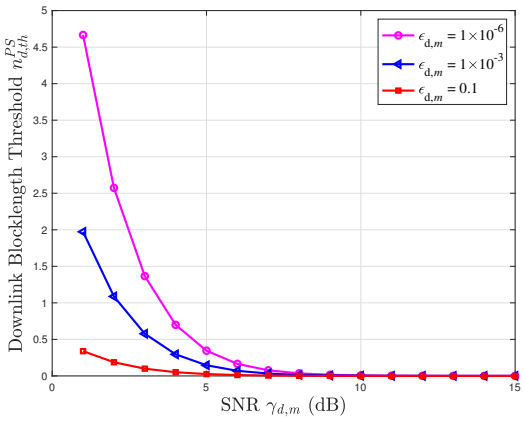

Figure 4.5: The downlink blocklength threshold $n_{\text{d,th}}^{\text{PS}}$ vs. SNR $\gamma_{\text{d},m}$ for our proposed SWIPT-enabled CF m-MIMO scheme under PS protocol using FBC.

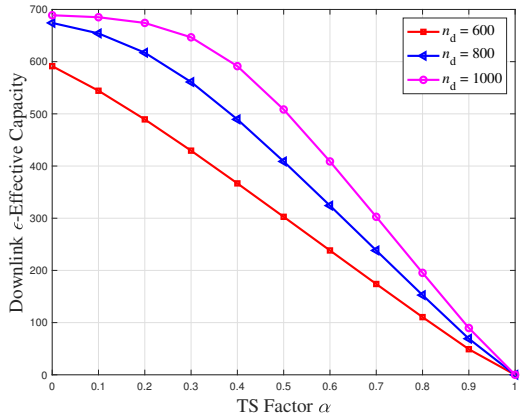

Figure 4.6: The downlink ϵ-effective capacity vs. TS factor α for our proposed SWIPT-enabled CF m-MIMO scheme using FBC.

a larger θ_m ($\theta_m \rightarrow \infty$) lead to an upper bound and lower bound on the downlink ϵ-effective capacity, respectively.

Setting the blocklength error probability $\epsilon_{\text{d},m} = 1\times10^{-6}$, Fig. 4.8 plots the downlink ϵ-effective capacity as a function of PS factor ρ for our proposed SWIPT-enabled CF m-MIMO scheme in the finite blocklength regime. We can observe from Fig. 4.8 that the downlink ϵ-effective capacity is a decreasing function of PS factor ρ and is an increasing function of downlink data blocklength n_{d}.

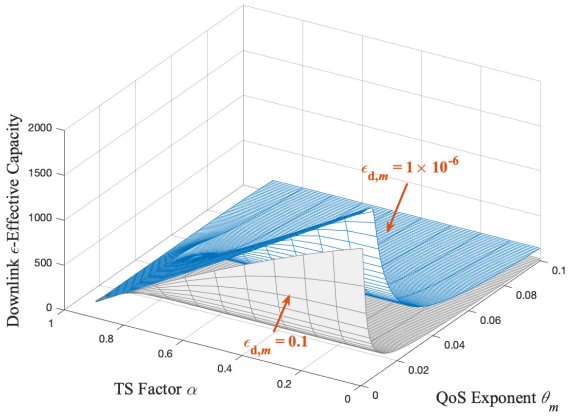

Figure 4.7: The downlink ϵ-effective capacity vs. TS factor α and QoS exponent θ_m for our proposed SWIPT-enabled CF m-MIMO scheme using FBC.

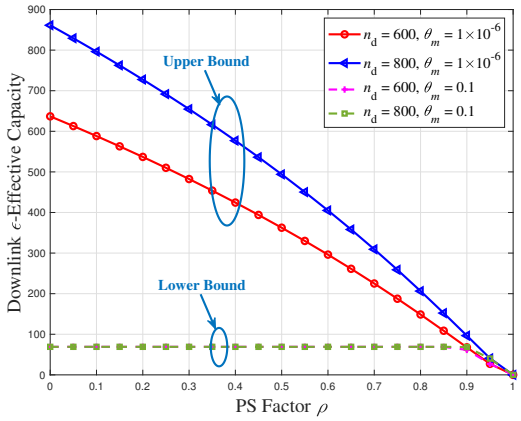

Figure 4.8: The downlink ϵ-effective capacity vs. PS factor ρ for our proposed SWIPT-enabled CF m-MIMO scheme using FBC.

Fig. 4.8 also shows that the gap between the curves when $n_{\mathrm{d}} = 600$ and $n_{\mathrm{d}} = 800$ is negligible for large θ_m. This is because the downlink ϵ-effective capacity goes to zero when the delay-bounded QoS constraint is very stringent, i.e., $\theta_m \to \infty$.

Setting the downlink blocklength $n_{\mathrm{d}} = 1000$, downlink blocklength error probability $\epsilon_{\mathrm{d},m} = 1 \times 10^{-6}$, and uplink blocklength error probability $\epsilon_{\mathrm{u},m} = 1 \times 10^{-3}$, Fig. 4.9 depicts the uplink ϵ-effective capacity as a function of harvested energy for our proposed SWIPT-enabled CF m-

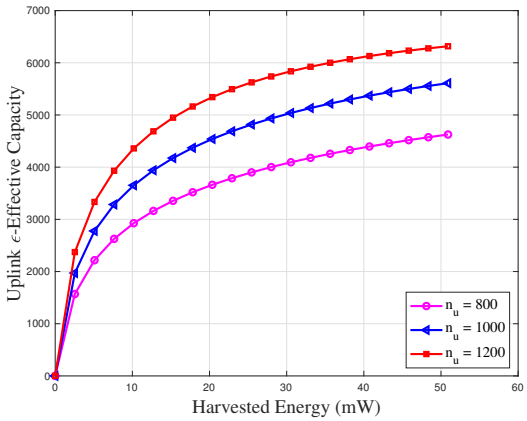

Figure 4.9: The uplink ϵ-effective capacity vs. harvested energy for our proposed SWIPT-enabled CF m-MIMO scheme using FBC.

MIMO scheme using FBC. We can observe from Fig. 4.9 that the uplink ϵ-effective capacity is an increasing function of uplink data blocklength n_{u}. Fig. 9 shows that the uplink ϵ-effective capacity becomes negligible at the same operating point when $\alpha = 0$, $\rho = 0$, and $n_{\mathrm{u}} \in \{800, 1000, 1200\}$. This is due to the fact that when $\alpha = 0$ and $\rho = 0$, the entire downlink SWIPT phase are allocated for downlink information transfer, thus the mobile devices cannot harvest energy. On the other hand, when $\alpha, \rho \to 1$, the harvested energy becomes a maximum since the mobile devices perform energy harvesting for the entire downlink SWIPT phase. As a result, the uplink ϵ-effective capacity is an increasing function of the harvested energy.

4.6 Summary

We have proposed and developed statistical delay and error-rate bounded QoS provisioning schemes over SWIPT-enabled CF m-MIMO 6G wireless networks in the finite blocklength regime. In particular, we have developed SWIPT-enabled CF m-MIMO based system models using FBC. Taking into account both the harvested energy and transmit power constraints, we have formulated and solved the optimization problems for the tradeoff between the ϵ-effective capacity and harvested energy for both downlink SWIPT and uplink data transfer phases under statistical delay and error rate bounded QoS provisioning in supporting mURLLC. We have conducted a set of

simulations to validate and evaluate our proposed SWIPT-enabled CF m-MIMO schemes subject to statistical delay and error-rate bounded QoS constraints in the finite blocklength regime.

5. OPTIMAL RESOURCE ALLOCATIONS FOR STATISTICAL QOS TO SUPPORT MURLLC OVER FBC-EH BASED 6G THZ WIRELESS NANO-NETWORKS *

5.1 Introduction

Over the last decades, the limited available bandwidth for communication systems in the microwave frequency range motivates the exploration of higher frequency bands in supporting statistical delay-bounded QoS provisioning. Towards this end, researchers have proposed THz-band communications and wireless networks for supporting provide an unprecedentedly large bandwidth, while satisfying diverse mURLLC requirements.

However, the large pathloss and molecular noise introduced by the THz wireless systems may produce transmission errors during the data transmissions, resulting in distorted multimedia signals received. There are a few studies in the literature which investigate the THz-band communications in supporting various QoS requirements for delay-sensitive wireless applications. Previous works have presented a holistic vision of 6G systems for the 6G-driven applications, performance metrics, and new service classes such as THz, mURLLC, QoS metrics, etc. [15]. However, previous works mainly focus on analyzing specific QoS requirements, while the statistical QoS provisioning based THz-band communications in supporting mURLLC have neither been well understood nor thoroughly studied.

By leveraging the advantages of nanomaterials, THz wireless networks with nano-architectures can alleviate the spectrum scarcity and feasibly achieve ultra-high data-rates up to 1 Tbps, while taking into account constraints of scalability, dimension, topology, processing-power, storage, energy capacities, etc. One of the major constraints of wireless nano-networks is the severely limited energy that can be accessed by nano devices. As a result, researchers have investigated the EH techniques over THz band wireless nano-networks. However, the conventional EH techniques,

such as solar and wind power, cannot be utilized in wireless nano-networks due to technology limitations. Novel nano-scale EH techniques have been investigated to harvest energy from various resources, such as vibration and blood sugar, to address the energy scarcity problem for nano devices. The authors of [109] have conducted detailed studies of EH techniques, energy sources, storage technologies, and the examples of applications and network deployments for EH based nano sensors. Optimal energy management policies for EH based sensor nodes have been proposed in [110]. Although there are some studies of the EH and energy consumption models for nano-scale communications, how to accurately model and characterize the relationships among THz-band wireless channel, energy consumption, and EH models employing FBC based nano-communication still remains as a major challenge in the THz band while supporting both delay and error-rate bounded QoS provisioning.

To effectively overcome the above-mentioned challenges, in this chapter we develop FBC-EH based optimal resource allocation policies for *self-powered* nano devices in the THz band over wireless nano-networks under statistical delay and error-rate bounded QoS constraints. Particularly, we establish THz-band wireless communications model, EH model, and FBC based channel-coding model. Then, we analyze the interference, channel capacity, and channel dispersion functions in the THz band using FBC. Considering statistical delay and error-rate bounded QoS provisioning, we formulate and solve the ϵ-effective capacity maximization problem for our proposed statistical delay and error-rate bounded QoS provisioning in supporting mURLLC over FBC-EH based 6G THz wireless nano-networks. Simulations are conducted, which evaluate and validate our proposed schemes in the THz band over FBC-EH-based wireless nano-networks.

The rest of this chapter is organized as follows: Section 5.2 establishes THz-band nano communication system models. Section 5.3 characterizes the interference, channel capacity, and channel dispersion in the THz band using FBC. Section 5.4 formulates and solves the ϵ-effective capacity maximization problem under statistical delay and error-rate bounded QoS provisioning in the finite blocklength regime in the THz band. Section 5.5 evaluates the system performance for our proposed schemes in the THz band in the finite blocklength regime. The chapter concludes with

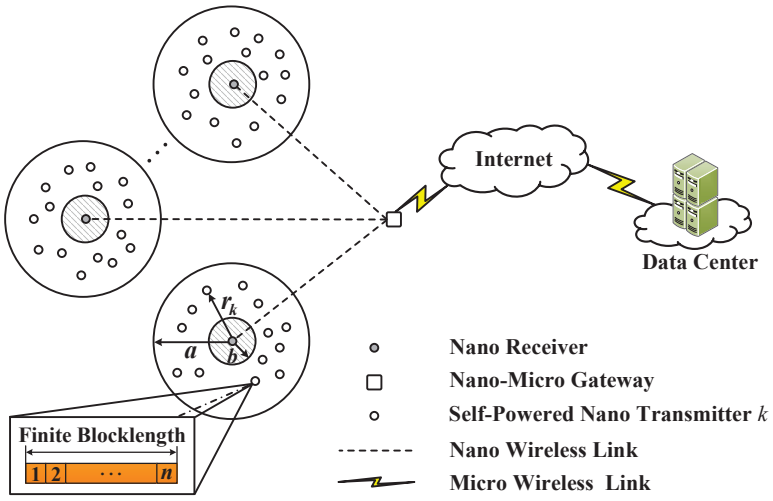

Figure 5.1: The system architecture model for our proposed FBC-EH-based wireless nano-networks in the THz band, where a is the radius of the THz-band covered region, b is the radius of the blind area, and n is the codeword blocklength used in FBC.

Section 5.6.

5.2 The System Models

Fig. 5.1 shows the system architecture model for our proposed FBC-EH-based wireless nano-networks in the THz band, where for each THz-band covered region in a circled area, a is the radius of the THz-band covered region and b is the radius of a very small blind area ($b \ll a$), and there is one nano receiver and $(K+1)$ self-powered nano transmitters, without the use of nano-batteries, randomly distributed within the THz-band covered region, which follows a spatial Poisson process with an arrival-rate intensity equal to λ nodes/cm^2 [111]. Consider the THz-band covered region, denoted by $A(a) \subseteq \mathbb{R}^2$, with radius a. Without loss of generality, we consider that the nano receiver is located at the center of the THz-band covered region $A(a)$. We can derive the probability of finding $(K+1)$ nano transmitters in the THz-band covered region $A(a)$ as follows:

$$\Pr\{(K+1) \text{ nano transmitters in } A(a)\} = \frac{[\lambda \|A(a)\|_\phi]^{(K+1)}}{(K+1)!} \exp\left[-\lambda \|A(a)\|_\phi\right] \tag{5.1}$$

where $\|A(a)\|_{\phi}$ denotes the area of the THz-band covered region $A(a)$. Denote by r_k $(k = 1, \ldots, (K+1))$ the transmission distance from the self-powered nano transmitter k, as shown in Fig. 5.1, to its assigned nano receiver within the THz-band covered region, which is a random variable. Then, we can formulate the PDF of the distribution of transmission distance r_k, denoted by $f_D(r_k)$, from the nano transmitter k to its nano receiver of interest within the THz-band covered region as follows [112]:

$$f_D(r_k) = \begin{cases} \frac{2r_k}{a^2-b^2}, & \text{for } b < r_k < a; \\ 0, & \text{otherwise.} \end{cases} \tag{5.2}$$

5.2.1 THz-Band Channel Model

5.2.1.1 Path Loss Model

In our proposed THz-band channel model, both the spreading loss and shadow fading characteristics of the transmission medium are considered as the main sources of signal attenuation. In the THz band, the path-loss is mainly characterized by the spreading loss and the molecular absorption loss [59]. The total path loss, denoted by $H_k\,(f, r_k)$, in the THz band for nano device k can be derived as follows [59]:

$$H_k\,(f, r_k) = H_{k,\text{spread}}(f, r_k) H_{k,\text{abs}}(r_k) \tag{5.3}$$

where $H_{k,\text{spread}}(f, r_k)$ and $H_{k,\text{abs}}(r_k)$ represent the spreading loss and molecular absorption attenuation, respectively, at transmission distance r_k and operating frequency f, which are defined as follows:

$$\begin{cases} H_{k,\text{spread}}(f, r_k) = \frac{c}{4\pi f r_k}; \\ H_{k,\text{abs}}(r_k) = \exp\left(-\frac{\alpha_{\text{abs}} r_k}{2}\right), \end{cases} \tag{5.4}$$

where c is the speed of light in free space and α_{abs} is the medium absorption coefficient, which depends on the molecular composition in the channel along the transmission path. Then, we can derive the received power, denoted by $\mathcal{P}_{\text{pathloss,r}}(r_k)$, at the nano receiver with the transmission

distance r_k due to pathloss as follows:

$$\mathcal{P}_{\text{pathloss,r}}(r_k) = S(f) \left(\frac{c}{4\pi f r_k} \right)^2 e^{-\alpha_{\text{abs}} r_k} \tag{5.5}$$

where $S(f)$ is the power spectral density of the transmitted pulse. In addition, we can derive the received power, denoted by $\mathcal{P}_{\text{shadow,r}}(r_k)$, from nano transmitter k to its nano receiver with the transmission distance r_k due to shadowing as follows [113]:

$$\mathcal{P}_{\text{shadow,r}}(r_k) = (r_k)^{-\eta} G 10^{\frac{\xi_k}{10}} \tag{5.6}$$

where G denotes the channel gain constant, η is the path loss exponent, ξ_k is a random variable which represents the shadow fading characteristics of the transmission medium. Note that the parameters of the path-loss and shadowing models can be extracted based on empirical measurements or Monte Carlo simulations. According to the Central Limit Theorem, the shadow fading variable ξ_k can be considered as a normal distributed random variable with zero mean and standard deviation σ, i.e., $\xi_k \sim \mathcal{N}(0, \sigma^2)$. Then, we can derive the total received power, denoted by $\mathcal{P}_{\text{total}}(r_k)$, at the nano receiver across the transmission distance r_k from the nano transmitter k as follows:

$$\mathcal{P}_{\text{total}}(r_k) = (r_k)^{-\eta} G 10^{\frac{\xi_k}{10}} S(f) \left(\frac{c}{4\pi f r_k} \right)^2 e^{-\alpha_{\text{abs}} r_k}. \tag{5.7}$$

5.2.1.2 Noise Model

The noise in the THz band is mainly contributed by the molecular absorption noise, which is caused by vibrating molecules [59, 114]. The total power of the molecular absorption noise, denoted by $N_k(r_k)$, in the THz band is composed of the background noise, denoted by N_b, and the self-induced noise, denoted by $N_{k,s}(r_k)$, which is given as follows [115]:

$$N_k(r_k) = N_b + N_{k,s}(r_k) \tag{5.8}$$

where

$$\begin{cases} N_b = B(T_0, f)\left(\frac{c}{\sqrt{4\pi} f_0}\right)^2; \\ N_{k,s}(r_k) = S(f)\left(1 - e^{-\alpha_{\text{abs}} r_k}\right)\left(\frac{c}{4\pi f r_k}\right)^2, \end{cases} \tag{5.9}$$

where T_0 is the reference temperature of the medium, f_0 is the design centre frequency, and $B(T_0, f)$ is the Planck's function, which is given by [116]

$$B(T_0, f) = \frac{2h\pi f^3}{c^2}\left(e^{\frac{hf}{k_B T_0}} - 1\right)^{-1} \tag{5.10}$$

where k_B is the Boltzmann's constant and h is the Planck constant. We can observe from Eq. (5.9) that the background noise N_b depends on the temperature and composition of the medium. On the other hand, the self-induced noise $N_{k,s}(r_k)$ depends on the transmitted signal.

We define $\boldsymbol{x}_k^n \sim \mathcal{N}(0, \overline{\mathcal{P}})$ as the transmit signal vector from nano transmitter k, where $\overline{\mathcal{P}}$ is the average transmit power for the nano device, and $\boldsymbol{y}_k^n \triangleq \left[y_k^{(1)}, \ldots, y_k^{(n)}\right]$ as the receive signal vector. Accordingly, we can derive the received signal, denoted by $\boldsymbol{y}_k^n$, for transmitting n data blocks from nano transmitter k to its nano receiver in the THz band in the finite blocklength regime as follows:

$$\boldsymbol{y}_k^n = \sqrt{\mathcal{P}_{\text{total}}(r_k)}\boldsymbol{x}_k^n + \sum_{i=1, i\neq k}^{K+1} \sqrt{\mathcal{P}_{\text{total}}(r_i)}\boldsymbol{x}_i^n + \boldsymbol{n}_k \tag{5.11}$$

where $\mathcal{P}_{\text{total}}(r_k)$ and $\mathcal{P}_{\text{total}}(r_i)$ are the received signal powers at the nano receiver across the transmission distances r_k and r_i from nano transmitters k and i, respectively, as specified by Eq. (5.7), $\boldsymbol{x}_k^n$ and $\boldsymbol{x}_i^n$ represent the transmitted signals from nano transmitter k and i, respectively, r_i is the transmission distance from the nano transmitter i to its assigned nano receiver, and $\boldsymbol{n}_k$ denotes the absorption noise with power given by Eq. (5.8).

5.2.2 EH Model for Piezoelectric Nanogenerators

Recently, researchers have developed the piezoelectric nanogenerators [117] [118] for converting mechanical energy into electrical energy, as shown in Fig. 5.2. Due to the low energy consumption of nano devices over a short distance in the THz band, the energy harvested from

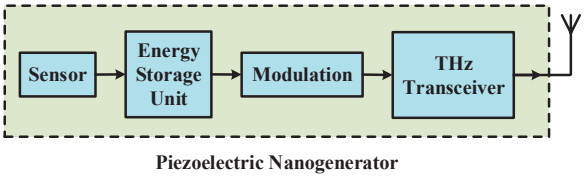

Figure 5.2: The piezoelectric nanogenerator model in the THz band.

the environment should be sufficient to power the nano devices. Without loss of generality, we assume that all harvested energy can be stored in the nanocapacitor. We can derive the stored energy, denoted by E_{cap}, in the nanocapacitor after a number of cycles, denoted by n_{cyc}, as follows [119]:

$$E_{\text{cap}}(n_{\text{cyc}}) = \frac{1}{2} C_{\text{cap}} \left[V_{\text{cap}}(n_{\text{cyc}})\right]^2 \tag{5.12}$$

where C_{cap} and $V_{\text{cap}}(n_{\text{cyc}})$ are the total capacitance and voltage function of the nano-capacitor, respectively. Then, the voltage function $V_{\text{cap}}(n_{\text{cyc}})$ of the charging nanocapacitor can be derived as follows:

$$V_{\text{cap}}(n_{\text{cyc}}) = V_g \left[1 - \exp\left(-\frac{n_{\text{cyc}} t_{\text{cyc}}}{R_g C_{\text{cap}}}\right)\right] = V_g \left[1 - \exp\left(-\frac{n_{\text{cyc}} \Delta Q}{V_g C_{\text{cap}}}\right)\right] \tag{5.13}$$

where V_g represents the generator voltage, R_g is the resistor, t_{cyc} is the time between consecutive cycles, and ΔQ is the amount of electric charge obtained from one cycle. We can derive the maximum energy, denoted by $E_{\text{cap}}^{\max}(n_{\text{cyc}})$, stored in the nanocapacitor as follows:

$$E_{\text{cap}}^{\max}(n_{\text{cyc}}) = \frac{1}{2} C_{\text{cap}} \left(V_g\right)^2. \tag{5.14}$$

Furthermore, the energy harvesting rate, denoted by λ_{eh}, in Joule/second can be computed as a function of the current energy $E_{\text{cap}}(n_{\text{cyc}})$ in the nano-capacitor and the increment in the energy of

the nano-capacitor, denoted by ΔE, which is given as follows [120]:

$$\lambda_{\text{eh}} = \frac{V_g \Delta Q}{t_{\text{cyc}}} \left[\exp\left(-\frac{\Delta Q n_{\text{cyc}}}{V_g C_{\text{cap}}} \right) - \exp\left(-\frac{2\Delta Q n_{\text{cyc}}}{V_g C_{\text{cap}}} \right) \right]. \tag{5.15}$$

5.3 The THz-Band Wireless Channel Modeling in The Finite Blocklength Regime

In this section, we characterize the functions of aggregate interference, channel capacity, channel dispersion, and the ϵ-effective capacity, respectively, in supporting mURLLC over FBC-EH based 6G THz wireless nano-networks.

5.3.1 The Aggregate Interference Modeling for the THz-Band Channels

Using Eqs. (5.7) and (5.8), we can derive the SINR function, denoted by $\gamma_k^{(l)}(\boldsymbol{r})$ $(l = 1, \ldots, n)$, between nano transmitter k and its nano receiver for transmitting the lth data block in the THz band as follows:

$$\gamma_k^{(l)}(\boldsymbol{r}) = \frac{\mathcal{P}_k \mathcal{P}_{\text{total}}(r_k)}{N_{I_k^{(l)}}(\boldsymbol{r}) + N_k(r_k)} \tag{5.16}$$

where $\boldsymbol{r}$ represents the vector of distances r_k $(k = 1, 2, \ldots, (K+1))$ between nano transmitter k and its nano receiver, $N_{I_k^{(l)}}(\boldsymbol{r})$ is the aggregate interference power, and $N_k(r_k)$ is the noise power. To guarantee the successful reception of the transmitted symbol at the nano receiver, the received SINR should be larger than a threshold, denoted by γ_{th}, i.e., $\gamma_k^{(l)}(\boldsymbol{r}) \geq \gamma_{\text{th}}$. We have

$$\frac{\mathcal{P}_k \left(r_k\right)^{-\eta} G 10^{\frac{\xi_k}{10}} S(f) \left(\frac{c}{4\pi f r_k}\right)^2 e^{-\alpha_{\text{abs}} r_k}}{N_k(r_k) + N_{I_k^{(l)}}(\boldsymbol{r})} \geq \gamma_{\text{th}}. \tag{5.17}$$

We can derive the aggregate interference, denoted by $I_k^{(l)}(\boldsymbol{r})$, at the nano receiver for transmitting the lth data block in the THz band as follows:

$$I_k^{(l)}(\boldsymbol{r}) = \sum_{i=1, i\neq k}^{K+1} \sqrt{\mathcal{P}_i \left(r_i\right)^{-\eta} G 10^{\frac{\xi_i}{10}} S(f)} \left(\frac{c}{4\pi f r_i}\right) e^{-\frac{\alpha_{\text{abs}} r_i}{2}} + N_i(r_i). \tag{5.18}$$

Due to the high density of wireless nano-networks, i.e., as $K \to \infty$, we can invoke the Central Limit Theorem and assume that the aggregate interference can be modeled as a Gaussian random process, i.e., $I_k^{(l)}(\boldsymbol{r}) \sim \mathcal{N}\left(\mathbb{E}_{\boldsymbol{r}}[I_k^{(l)}(\boldsymbol{r})], \text{Var}_{I_k^{(l)}}(\boldsymbol{r})\right)$, where $\mathbb{E}_{\boldsymbol{r}}[I_k^{(l)}(\boldsymbol{r})]$ and $\text{Var}_{I_k^{(l)}}(\boldsymbol{r})$ are the mean and variance of the aggregate interference, respectively, and $\mathbb{E}_{\boldsymbol{r}}[\cdot]$ is the expectation operation with respect to $\boldsymbol{r}$. We derive the closed-form expressions for characterizing the mean $\mathbb{E}_{\boldsymbol{r}}[I_k^{(l)}(\boldsymbol{r})]$ and the variance $\text{Var}_{I_k^{(l)}}(\boldsymbol{r})$, respectively, of the aggregate interference in the following theorem.

Theorem 8. ***If*** *the aggregate interference $I_k^{(l)}(\boldsymbol{r})$ is given by Eq.* (5.18) *for our proposed THz-band channel model,* ***then*** *the mean and variance of the aggregate interference between nano transmitter k and its nano receiver in the THz band over wireless nano-networks are characterized by the following two claims, respectively.*

Claim 1. *The mean $\mathbb{E}_{\boldsymbol{r}}[I_k^{(l)}(\boldsymbol{r})]$ of the aggregate interference is accurately estimated by its lower-bound as follows:*

$$\mathbb{E}_{\boldsymbol{r}}[I_k^{(l)}(\boldsymbol{r})] \geq \frac{2\lambda\pi a^2\Lambda\sqrt{\overline{\mathcal{P}}}\left(\frac{2}{\alpha_{abs}}\right)^{1-\frac{\eta}{2}}}{a^2-b^2}\left[\gamma\left(1-\frac{\eta}{2}, \frac{\alpha_{abs}a}{2}\right) - \gamma\left(1-\frac{\eta}{2}, \frac{\alpha_{abs}b}{2}\right)\right] \tag{5.19}$$

where $\gamma(\cdot,\cdot)$ is the lower incomplete Gamma function and

$$\Lambda \triangleq \frac{c\sqrt{GS(f)}}{4\pi f}. \tag{5.20}$$

Claim 2. *The variance $Var_{I_k^{(l)}}(\boldsymbol{r})$ of the aggregate interference is approximated as follows:*

$$\begin{aligned} Var_{I_k^{(l)}}(\boldsymbol{r}) \approx{}& \frac{6\lambda\pi a^2\Lambda^2\overline{\mathcal{P}}(\alpha_{abs})^{-\eta}}{a^2-b^2}\left[\gamma\left(-\eta, a\alpha_{abs}\right) - \gamma\left(-\eta, b\alpha_{abs}\right)\right] + \sum_{i=1, i\neq k}^{K+1} N_{i,b} + \frac{2\lambda\pi a^2\Lambda^2}{a^2-b^2} \\ &\times \left[\log\left(\frac{a}{b}\right) - Ei\left(-\alpha_{abs}a\right) + Ei\left(-\alpha_{abs}b\right)\right] - \left(\frac{2\lambda\pi a^2 C}{a^2-b^2}\right)^2 \overline{\mathcal{P}}\left(\frac{2}{\alpha_{abs}}\right)^{2-\eta} \\ &\times \left[\gamma\left(1-\frac{\eta}{2}, \frac{\alpha_{abs}a}{2}\right) - \gamma\left(1-\frac{\eta}{2}, \frac{\alpha_{abs}b}{2}\right)\right]^2. \end{aligned} \tag{5.21}$$

Proof. The proof is provided in Appendix I. □

Remarks on Theorem 8: The expressions derived in Theorem 8 for the *mean* and *variance* of the aggregate interference play the important roles in modeling the *channel capacity* and *channel dispersion* over our proposed THz-band wireless nano-networks.

5.3.2 The Channel Capacity Modeling Over the THz Band in the Finite Blocklength Regime

Leveraging the Shannon Limit Theorem, we can derive the *channel capacity* $C(r_k, \mathcal{P}_k)$ in terms of the mutual information $I(\boldsymbol{x}_k^n, \boldsymbol{y}_k^n)$ for our proposed statistical delay and error-rate bounded QoS provisioning in supporting mURLLC over FBC-EH based 6G THz wireless nano-networks as follows:

$$C(r_k, \mathcal{P}_k) = \sup_{P_{X_k^n}(\boldsymbol{x}_k^n)} \{I(\boldsymbol{x}_k^n, \boldsymbol{y}_k^n)\} \tag{5.22}$$

where $P_{X_k^n}(\boldsymbol{x}_k^n)$ is the input symbol probability and $I(\boldsymbol{x}_k^n, \boldsymbol{y}_k^n)$ is the *mutual information*, which is given as follows:

$$I(\boldsymbol{x}_k^n, \boldsymbol{y}_k^n) = \mathbb{E}\left[\boldsymbol{i}(\boldsymbol{x}_k^n; \boldsymbol{y}_k^n)\right] = \frac{1}{n}\mathbb{E}\left[\log_2\left(\frac{P_{Y_k^n|X_k^n}(\boldsymbol{y}_k^n|\boldsymbol{x}_k^n)}{Q_{Y_k^n}(\boldsymbol{y}_k^n)}\right)\right]. \tag{5.23}$$

The theorem that follows bellow derives the closed-form expression for the upper-bound to accurately approximate the channel capacity $C(r_k, \mathcal{P}_k)$ given by Eq. (5.22) over the THz band in the finite blocklength regime.

Theorem 9. *The upper-bound on the mutual information $I(\boldsymbol{x}_k^n, \boldsymbol{y}_k^n)$ given by Eq.* (5.23) *for our proposed statistical delay and error-rate bounded QoS provisioning in supporting mURLLC over FBC-EH based 6G THz wireless nano-networks is given as follows:*

$$I(\boldsymbol{x}_k^n, \boldsymbol{y}_k^n) \leq \frac{1}{2}\log_2\left[\frac{\mathcal{P}_k\mathcal{P}_{\textit{total}}(r_k) + N_{I_k^{(l)}}(\boldsymbol{r}) + N_k(r_k)}{N_{I_k^{(l)}}(\boldsymbol{r}) + N_k(r_k)}\right] - (\log_2 e)\left[\frac{\mathcal{P}_k\left[\mathcal{P}_{\textit{total}}(r_k) + 1\right]}{N_{I_k^{(l)}}(\boldsymbol{r}) + N_k(r_k)}\right]. \tag{5.24}$$

Proof. The proof is provided in Appendix J. □

Remarks on Theorem 9: While it is infeasible to derive the exact closed-form expression for the

channel capacity $C(r_k, \mathcal{P}_k)$ in terms of the mutual information for our proposed statistical delay and error-rate bounded QoS provisioning in supporting mURLLC over FBC-EH based 6G THz wireless nano-networks in the finite blocklength regime, Theorem 9 yields the accurate upper-bound for the mutual information $I(\boldsymbol{x}_k^n, \boldsymbol{y}_k^n)$ derived in Eq. (5.24) is an accurate approximation for the channel capacity $C(r_k, \mathcal{P}_k)$ given by Eq. (5.22), which provides with practically very useful designing guidance for engineering, modeling, and evaluating our proposed statistical delay and error-rate bounded QoS provisioning in supporting mURLLC over FBC-EH based 6G THz wireless nano-networks in the finite blocklength regime.

5.3.3 The Channel Dispersion Modeling for the THz Band Communications in the Finite Blocklength Regime

Generally speaking, it is challenging to derive the closed-form expression of the channel dispersion for the nano-communications schemes in the THz band using FBC. However, leveraging some mathematical manipulations, we can obtain the tight upper-bound for the channel dispersion $V(r_k, \mathcal{P}_k)$ for our proposed statistical delay and error-rate bounded QoS provisioning schemes in supporting mURLLC over FBC-EH based 6G THz wireless nano-networks as summarized in the following theorem.

Theorem 10. *The upper-bound on the channel dispersion $V(r_k, \mathcal{P}_k)$ for our proposed statistical delay and error-rate bounded QoS provisioning in supporting mURLLC over FBC-EH based 6G THz wireless nano-networks is given as follows:*

$$V(r_k, \mathcal{P}_k) \leq 8n(\log_2 e)^2 \left[\mathcal{P}_k + N_{I_k^{(l)}}(\boldsymbol{r}) + N_k(r_k)\right]. \tag{5.25}$$

Proof. The proof is provided in Appendix K. □

Remarks on Theorem 10: The upper-bound on the channel dispersion $V(r_k, \mathcal{P}_k)$ given in Eq. (5.25) proved in Theorem 10 is important to derive the maximum achievable coding rate $R(n, r_k, \mathcal{P}_k)$, and thereafter, the ϵ-effective capacity $EC_\epsilon(\theta_k)$, and finally, solve the joint optimization problem for resource allocations to support our proposed statistical delay and error-rate

bounded QoS provisioning for mURLLC over FBC-EH 6G THz wireless nano-networks which are to be investigated in the following section.

5.4 Joint Optimal Resource Allocation for Our Proposed Statistical Delay and Error-Rate Bounded QoS Provisioning for mURLLC Over FBC-EH 6G THz Wireless Nano-Networks

In this section, we derive the optimal resource allocation policies for our proposed statistical delay and error-rate bounded QoS provisioning in supporting mURLLC over FBC-EH based 6G THz wireless nano-networks.

5.4.1 The Set of EH Constraints in the THz Band

5.4.1.1 Transmit Power Constraint

Due to the limitation of the energy harvested at the nanogenerator, we can derive the minimum required energy, denoted by $\mathcal{P}_{\min}$, for transmitting one data packet at each self-powered nano device as follows:

$$\mathcal{P}_{\min} = \zeta_k \mathcal{P}_k + \mathcal{P}_{\text{circuit}} \tag{5.26}$$

where ζ_k is the reciprocal of drain efficiency of power amplifier and $\mathcal{P}_{\text{circuit}}$ consists of two components, i.e., power consumption of the transmitter circuit and the receiver circuit, which is independent of the transmission distance. Then, we can derive the relationship between harvested energy after n_{cyc} cycles and the minimum required energy for transmitting a data packet with length n as follows:

$$\frac{1}{2} C_{\text{cap}} \left[V_{\text{cap}}(n_{\text{cyc}}) \right]^2 \geq n \left(\zeta_k \mathcal{P}_k + \mathcal{P}_{\text{circuit}} \right). \tag{5.27}$$

Plugging Eq. (5.13) into Eq. (5.27), we have

$$\frac{1}{2} C_{\text{cap}} \left\{ V_g \left[1 - \exp\left(-\frac{n_{\text{cyc}} \Delta Q}{V_g C_{\text{cap}}} \right) \right] \right\}^2 \geq n \left(\zeta_k \mathcal{P}_k + \mathcal{P}_{\text{circuit}} \right). \tag{5.28}$$

Accordingly, we can derive a lower bound on the number of cycles n_{cyc} for self-powered nano devices as in the following inequation:

$$n_{\text{cyc}} \geq -\frac{C_{\text{cap}} V_g}{\Delta Q} \log \left[1 - \sqrt{\frac{2n}{C_{\text{cap}} V_g} \left(\zeta_k \mathcal{P}_k + \mathcal{P}_{\text{circuit}} \right)} \right]. \tag{5.29}$$

According to Eq. (5.29), to guarantee the effective value of a lower bound on n_{cyc}, we have

$$\sqrt{\frac{2n}{C_{\text{cap}} V_g} \left(\zeta_k \mathcal{P}_k + \mathcal{P}_{\text{circuit}} \right)} \leq 1. \tag{5.30}$$

Correspondingly, we can derive an upper-bound on the transmit power $\mathcal{P}_k$ for the self-powered nano transmitter k as follows:

$$\mathcal{P}_k \leq \frac{C_{\text{cap}} V_g}{2n\zeta_k} - \frac{P_{\text{circuit}}}{\zeta_k}. \tag{5.31}$$

5.4.1.2 Energy Harvesting Rate Constraint

To derive the EH rate constraint, first we need to calculate the energy consumption rate, denoted by λ_{ec}, of each self-powered nano device as follows:

$$\lambda_{\text{ec}} < \mathcal{P}_k n C(r_k, \mathcal{P}_k). \tag{5.32}$$

As a result, the energy consumption rate λ_{ec} should not be greater than the energy harvesting rate λ_{eh} given in Eq. (5.15), i.e., $\lambda_{\text{ec}} \leq \lambda_{\text{eh}}$. Then, using Eq. (5.15) and (5.32), we can derive an upper-bound on the transmit power $\mathcal{P}_k$ for our proposed statistical delay and error-rate bounded QoS provisioning in supporting mURLLC over FBC-EH based 6G THz wireless nano-networks as follows:

$$\mathcal{P}_k \leq \frac{V_g \Delta Q}{n C(r_k, \mathcal{P}_k) t_{\text{cyc}}} \left[\exp\left(-\frac{\Delta Q n_{\text{cyc}}}{V_g C_{\text{cap}}} \right) - \exp\left(-\frac{2\Delta Q n_{\text{cyc}}}{V_g C_{\text{cap}}} \right) \right]. \tag{5.33}$$

5.4.2 Joint Optimal Resource Allocation for Our Proposed Statistical Delay and Error-Rate Bounded QoS Provisioning for mURLLC Over FBC-EH 6G THz Wireless Nano-Networks

The function of ϵ-effective capacity $EC_{\epsilon}(\theta_k)$ depends on the transmit power $\mathcal{P}_k$ and block-length n. To maximize the ϵ-effective capacity $EC_{\epsilon}(\theta_k)$ while guaranteeing the EH constraints among self-powered nano devices for our proposed statistical delay and error-rate bounded QoS provisioning in supporting mURLLC over FBC-EH based 6G THz wireless nano-networks, we can formulate the optimization problem $\mathbf{P_{15}}$ subject to the EH constraints given by Eqs. (5.31) and (5.33) as follows:

$$\mathbf{P_{15}}: \arg \max_{\{n, \mathcal{P}_k\}} EC_{\epsilon}(\theta_k) \tag{5.34}$$

$$\text{s.t.: } C11: R(n, r_k, \mathcal{P}_k) \approx C(r_k, \mathcal{P}_k) - \sqrt{\frac{V(r_k, \mathcal{P}_k)}{n}} Q^{-1}(\epsilon_k); \tag{5.35}$$

$$C12: \mathcal{P}_k \leq \min\left\{ \frac{C_{\text{cap}} V_g}{2n\zeta_k} - \frac{P_{\text{circuit}}}{\zeta_k}, \frac{V_g \Delta Q}{nC(r_k, \mathcal{P}_k) t_{\text{cyc}}} \left[\exp\left(-\frac{\Delta Q n_{\text{cyc}}}{V_g C_{\text{cap}}} \right) - \exp\left(-\frac{2\Delta Q n_{\text{cyc}}}{V_g C_{\text{cap}}} \right) \right] \right\}; \tag{5.36}$$

$$C13: \mathcal{P}_k \geq \frac{1}{(r_k)^{-\eta} G 10^{\frac{\xi_k}{10}} S(f)} \left[\frac{\gamma_{\text{th}} \left(N_k(r_k) + N_{I_k^{(l)}}(\boldsymbol{r}) \right)}{\left(\frac{c}{4\pi f r_k} \right) e^{-\frac{\alpha_{\text{abs}} r_k}{2}}} \right]^2; \tag{5.37}$$

$$C14: \mathcal{P}_k > 0. \tag{5.38}$$

Equivalently, we can derive a minimization problem $\mathbf{P_{16}}$ as follows:

$$\mathbf{P_{16}}: \arg \min_{\{n, \mathcal{P}_k\}} \mathbb{E}_{r_k} \left\{ \epsilon_k + (1 - \epsilon_k) \exp \left\{ -\theta_k n \left[C(r_k, \mathcal{P}_k) - \sqrt{\frac{V(r_k, \mathcal{P}_k)}{n}} Q^{-1}(\epsilon_k) \right] \right\} \right\} \tag{5.39}$$

subject to the same constraints given in C12, C13, and C14 which are specified by Eqs. (5.36), (5.37), and (5.38), respectively, in optimization problem $\mathbf{P_{15}}$. In order to solve the minimization problem

$\mathbf{P_{16}}$, we define an utility function $F(n, r_k, \mathcal{P}_k)$ as follows:

$$F(n, r_k, \mathcal{P}_k) \triangleq nR(n, r_k, \mathcal{P}_k). \tag{5.40}$$

Then, by plugging Eq. (5.40) back into Eq. (5.39), we can rewrite the ϵ-effective capacity as follows:

$$EC_{\epsilon}(\theta_k) \triangleq -\frac{1}{\theta_k} \log\left(\mathbb{E}_{r_k}\left[\epsilon_k + (1-\epsilon_k)\, e^{-\theta_k F(n, r_k, \mathcal{P}_k)}\right]\right). \tag{5.41}$$

We can formulate a new maximization problem $\mathbf{P_{17}}$, which is equivalent to $\mathbf{P_{16}}$, for our proposed statistical delay and error-rate bounded QoS provisioning in supporting mURLLC over FBC-EH based 6G THz wireless nano-networks as follows:

$$\mathbf{P_{17}} : \arg \max_{\{n, \mathcal{P}_k\}} F(n, r_k, \mathcal{P}_k) \tag{5.42}$$

subject to the same constraints given in C12, C13, and C14 which are specified by Eqs. (5.36), (5.37), and (5.38), respectively, in optimization problem $\mathbf{P_{15}}$. To analyze the monotonicity of problem $\mathbf{P_{17}}$, we investigate the first-order derivative of the function $F(n, r_k, \mathcal{P}_k)$ with respect to the blocklength n when $\epsilon_k \in (0, 0.5)$ as follows:

$$\begin{aligned}
\frac{\partial F(n, r_k, \mathcal{P}_k)}{\partial n} &= \frac{\partial nC(r_k, \mathcal{P}_k)}{\partial n} - \frac{\partial\left[\sqrt{nV(r_k, \mathcal{P}_k)}Q^{-1}(\epsilon_k)\right]}{\partial n} \\
&= C(r_k, \mathcal{P}_k) - \frac{\sqrt{V(r_k, \mathcal{P}_k)}Q^{-1}(\epsilon_k)}{2\sqrt{n}} \\
&= R(n, r_k, \mathcal{P}_k) + \frac{\sqrt{V(r_k, \mathcal{P}_k)}Q^{-1}(\epsilon_k)}{2\sqrt{n}} > 0.
\end{aligned} \tag{5.43}$$

As a result, the optimization problem $\mathbf{P_{17}}$ specified by Eq. (5.42) is a monotonically increasing function of blocklength n when the error probability $\epsilon_k \in (0, 0.5)$. Then, the theorem that follows bellow characterizes the concavity of the optimization problem $\mathbf{P_{17}}$ with respect to the transmit

power $\mathcal{P}_k$.

Theorem 11. *Let the error probability be $\epsilon_k \in (0, 0.5)$ for our proposed statistical delay and error-rate bounded QoS provisioning in supporting mURLLC over FBC-EH based 6G THz wireless nano-networks and define the minimum blocklength, denoted by $n_{\min}$, as the function of ϵ_k, $\mathcal{P}_k$, $\mathcal{P}_{total}(r_k)$, $N_{I_k^{(l)}}(\boldsymbol{r})$, and $N_k(r_k)$ as follows:*

$$n_{\min} \triangleq \frac{2\left[Q^{-1}(\epsilon_k)\right]^2 \left[\mathcal{P}_k + N_{I_k^{(l)}}(\boldsymbol{r}) + N_k(r_k)\right]}{\left[\mathcal{P}_{total}(r_k)\right]^4}. \tag{5.44}$$

If *the blocklength n satisfies following condition for $n_{\min}$ given by Eq.* (5.44)*:*

$$n > n_{\min}, \tag{5.45}$$

then *the optimization problem $\mathbf{P_{17}}$ specified by Eq. (5.42) is strictly concave with respect to the transmit power $\mathcal{P}_k$.*

Proof. To prove this theorem, we need to proceed with the following two steps.

Step 1. We take the first-order derivative over the utility function $F(n, r_k, \mathcal{P}_k)$ specified in Eq. (5.40) with respect to the transmit power $\mathcal{P}_k$ as follows:

$$\begin{aligned}
\frac{\partial F(n, r_k, \mathcal{P}_k)}{\partial \mathcal{P}_k} &= \frac{\partial \left[nC(r_k, \mathcal{P}_k) - \sqrt{nV(r_k, \mathcal{P}_k)}Q^{-1}(\epsilon_k)\right]}{\partial \mathcal{P}_k} \\
&= \frac{\partial [nC(r_k, \mathcal{P}_k)]}{\partial \mathcal{P}_k} - \frac{\partial \left[\sqrt{nV(r_k, \mathcal{P}_k)}Q^{-1}(\epsilon_k)\right]}{\partial \mathcal{P}_k} \\
&= \frac{n\mathcal{P}_{\text{total}}(r_k)}{2(\log 2)\left[\mathcal{P}_k\mathcal{P}_{\text{total}}(r_k) + N_{I_k^{(l)}}(\boldsymbol{r}) + N_k(r_k)\right]} - n(\log_2 e)\left[\frac{\mathcal{P}_{\text{total}}(r_k) + 1}{N_{I_k^{(l)}}(\boldsymbol{r}) + N_k(r_k)}\right] \\
&\quad - \frac{\sqrt{2n}(\log_2 e)Q^{-1}(\epsilon_k)}{\sqrt{\mathcal{P}_k + N_{I_k^{(l)}}(\boldsymbol{r}) + N_k(r_k)}}.
\end{aligned} \tag{5.46}$$

Step 2. We take the second-order derivative of the function $F(n, r_k, \mathcal{P}_k)$ with respect to the

transmit power $\mathcal{P}_k$ as follows:

$$\frac{\partial^2 F(n, r_k, \mathcal{P}_k)}{\partial \mathcal{P}_k^2} = \frac{\sqrt{2n}(\log_2 e) Q^{-1}(\epsilon_k)}{2\left[\mathcal{P}_k + N_{I_k^{(l)}}(\boldsymbol{r}) + N_k(r_k)\right]^{\frac{3}{2}}} - \frac{n\left[\mathcal{P}_{\text{total}}(r_k)\right]^2}{2(\log 2)\left[\mathcal{P}_k \mathcal{P}_{\text{total}}(r_k) + N_{I_k^{(l)}}(\boldsymbol{r}) + N_k(r_k)\right]^2}. \tag{5.47}$$

Applying the fact of $\mathcal{P}_{\text{total}}(r_k) < 1$ into Eq. (5.47), we get:

$$\begin{aligned}
\frac{\partial^2 F(n, r_k, \mathcal{P}_k)}{\partial \mathcal{P}_k^2} =& \frac{\sqrt{2n}(\log_2 e) Q^{-1}(\epsilon_k)}{2\left[\mathcal{P}_k + N_{I_k^{(l)}}(\boldsymbol{r}) + N_k(r_k)\right]^{\frac{3}{2}}} - \frac{n\left[\mathcal{P}_{\text{total}}(r_k)\right]^2}{2(\log 2)\left[\mathcal{P}_k \mathcal{P}_{\text{total}}(r_k) + N_{I_k^{(l)}}(\boldsymbol{r}) + N_k(r_k)\right]^2} \\
\leq& \frac{\sqrt{2n}(\log_2 e) Q^{-1}(\epsilon_k)}{2\left[\mathcal{P}_k + N_{I_k^{(l)}}(\boldsymbol{r}) + N_k(r_k)\right]^{\frac{3}{2}}} - \frac{n\left[\mathcal{P}_{\text{total}}(r_k)\right]^2}{2(\log 2)\left[\mathcal{P}_k + N_{I_k^{(l)}}(\boldsymbol{r}) + N_k(r_k)\right]^2} \\
=& \frac{\sqrt{2n} Q^{-1}(\epsilon_k)\sqrt{\mathcal{P}_k + N_{I_k^{(l)}}(\boldsymbol{r}) + N_k(r_k)} - n\left[\mathcal{P}_{\text{total}}(r_k)\right]^2}{2(\log 2)\left[\mathcal{P}_k + N_{I_k^{(l)}}(\boldsymbol{r}) + N_k(r_k)\right]^2} \\
=& \frac{\left(\sqrt{n n_{\min}} - n\right)\left[\mathcal{P}_{\text{total}}(r_k)\right]^2}{2(\log 2)\left[\mathcal{P}_k + N_{I_k^{(l)}}(\boldsymbol{r}) + N_k(r_k)\right]^2}
\end{aligned} \tag{5.48}$$

where $n_{\min}$ is given by Eq. (5.44). Applying the condition: $n > n_{\min}$ specified by Eq. (5.45) into Eq. (5.48), which implies that $(\sqrt{n n_{\min}} - n) < 0$, and thus we can obtain the following equation:

$$\frac{\partial^2 F(n, r_k, \mathcal{P}_k)}{\partial \mathcal{P}_k^2} < 0. \tag{5.49}$$

Therefore, we complete the proof for Theorem 11. □

Remarks on Theorem 11: Theorem 11 implies that if the finite blocklength is lower-bounded by the minimum blocklength $n_{\min}$ given by Eq. (5.44), then there exists the unique optimal power allocation policy that maximizes the ϵ-effective capacity in the THz band in the finite blocklength regime. Note that $n_{\min}$ is proportional to noise and interference power, and the decoding error probability ϵ_k but inversely proportional to the total received power $\mathcal{P}_{\text{total}}(r_k)$. These observations are expected because the more noisy and interfered channels warrant the longer coding block-

length for the more powerful channel-coding error-control performance. Then, the theorem that follows bellow derives the closed-form expressions of the optimal transmit power for our proposed schemes.

Theorem 12. ***If*** *the blocklength $n > n_{\min}$, which is given by Eq.* (5.44)*, for our proposed statistical delay and error-rate bounded QoS provisioning in supporting mURLLC over FBC-EH based 6G THz wireless nano-networks,* ***then*** *depending on whether the SINR falls into the high-SINR, medium-SINR, and low-SINR regimes, the optimal transmit power policies are given by the following three claims, respectively.*

Claim 1. ***If*** *the SINR falls into a high-SINR regime, which is defined as follows:*

$$\mathcal{P}_k \mathcal{P}_{\textit{total}}(r_k) \gg N_{I_k^{(l)}}(\boldsymbol{r}) + N_k(r_k), \tag{5.50}$$

then *the optimal power allocation policy for the high-SINR regime, denoted by $\mathcal{P}_k^{\textit{OPT,H}}$, at nano transmitter k is given as follows:*

$$\mathcal{P}_k^{\textit{OPT,H}} = \frac{n}{2}\left\{ Q^{-1}(\epsilon_k) + \left\{ \left[Q^{-1}(\epsilon_k)\right]^2 + (\log 2)\left(\lambda_1 - \lambda_2\right) + n\left[\frac{\mathcal{P}_{\textit{total}}(r_k) + 1}{N_{I_k^{(l)}}(\boldsymbol{r}) + N_k(r_k)}\right] \right\}^{\frac{1}{2}} \right\}^{-2}. \tag{5.51}$$

Claim 2. ***If*** *the SINR falls into a low-SINR regime, which is defined as follows:*

$$\mathcal{P}_k \mathcal{P}_{\textit{total}}(r_k) \ll N_{I_k^{(l)}}(\boldsymbol{r}) + N_k(r_k), \tag{5.52}$$

then *the optimal power allocation policy for the low-SINR regime, denoted by $\mathcal{P}_k^{\textit{OPT,L}}$, at nano transmitter k is given as follows:*

$$\mathcal{P}_k^{\textit{OPT,L}} = \frac{2nQ^{-1}(\epsilon_k)}{\left\{ (\log 2)\left(\lambda_2 - \lambda_1\right) - \frac{2n + n\mathcal{P}_{\textit{total}}(r_k)}{2\left[N_{I_k^{(l)}}(\boldsymbol{r}) + N_k(r_k)\right]} \right\}^2} - N_{I_k^{(l)}}(\boldsymbol{r}) - N_k(r_k). \tag{5.53}$$

Claim 3. ***If*** *the SINR falls into the medium-SINR regime between the high-SINR and low-SINR regimes specified by Eqs. (5.50) and (5.52), respectively,* ***then*** *the optimal power allocation policy for the medium-SINR regime, denoted by $\mathcal{P}_k^{OPT,M}$, at nano transmitter k is given as follows:*

$$\mathcal{P}_k^{OPT,M} = \frac{n}{2}\Bigg\{Q^{-1}(\epsilon_k) + \Bigg\{\left[Q^{-1}(\epsilon_k)\right]^2 + (\log 2)\,(\lambda_1 - \lambda_2) + n\left[\frac{\mathcal{P}_{total}(r_k)+1}{N_{I_k^{(l)}}(\boldsymbol{r}) + N_k(r_k)}\right]\Bigg\}^{\frac{1}{2}}\Bigg\}^{-2} - \frac{N_{I_k^{(l)}}(\boldsymbol{r}) + N_k(r_k)}{\mathcal{P}_{total}(r_k)}. \tag{5.54}$$

Proof. The proof is provided in Appendix L. □

Remarks on Theorem 12: Conditioning on blocklength n is lower-bounded by n_{min} and depending on whether the SINR falling into which one of the three high-regime, medium-regime, or low-regime, Theorem 12 derives the three closed-forms solutions for the three corresponding optimal transmit power policies, respectively, for our proposed statistical delay and error-rate bounded QoS provisioning in supporting mURLLC over FBC-EH based 6G THz wireless nano-networks.

To ensure the optimality of the resource allocation policy for the optimization problem $\mathbf{P_{17}}$, we also need to update the Lagrange multipliers λ_1 and λ_2 through iteration. In this chapter, we employ the gradient projection method [121] to achieve the renewal of shadow prices due to its faster convergence towards a local extremum compared with other nongradient methods. We define

$$\begin{cases} \mathcal{P}_k^{\max} \triangleq \min\left\{\frac{C_{\text{cap}}V_g}{2n\zeta_k} - \frac{P_{\text{circuit}}}{\zeta_k}, \frac{V_g\Delta Q}{nC(r_k,\mathcal{P}_k)t_{\text{cyc}}}\left[\exp\left(-\frac{\Delta Q n_{\text{cyc}}}{V_g C_{\text{cap}}}\right) - \exp\left(-\frac{2\Delta Q n_{\text{cyc}}}{V_g C_{\text{cap}}}\right)\right]\right\}; \\ \mathcal{P}_k^{\min} \triangleq \frac{1}{(r_k)^{-\eta}G10^{\frac{\xi_k}{10}}S(f)}\left[\frac{\gamma_{\text{th}}\left(N_k(r_k)+N_{I_k^{(l)}}(\boldsymbol{r})\right)}{\left(\frac{c}{4\pi f r_k}\right)e^{-\frac{\alpha_{\text{abs}}r_k}{2}}}\right]^2. \end{cases} \tag{5.55}$$

Denote by l the number of current iteration and consider $\lambda_1^{(l)}$ and $\lambda_2^{(l)}$ the Lagrange multipliers at the lth iteration, respectively. To be specific, the Lagrange multipliers $\lambda_1^{(l)}$ and $\lambda_2^{(l)}$ can be updated

Algorithm 3 FBC-EH Based Joint Optimal Resource Allocation Policy

Input: $a, b, B, K, t_{\text{cyc}}, \Delta Q, V_g, C_{\text{cap}}, L_{\max}, P_{\text{circuit}}, \lambda$, and γ_{th}

Initialization: $l = 0$ and $\mathcal{P}_k^{(0)} = \overline{\mathcal{P}}$

for $l = 1, l \leq L_{\max}$ **do**

Step 1: Calculate the energy consumption rate by using Eq. (5.32)

if $n > n_{\min}$ **then**

if $\mathcal{P}_k \mathcal{P}_{\text{total}}(r_k) \gg N_{I_k^{(l)}}(\boldsymbol{r}) + N_k(r_k)$ **then**

Calculate the transmit power $\mathcal{P}_k^{(l)}$ that maximize the function $F(n, r_k, \mathcal{P}_k)$ in the high-SINR regime by using Eq. (5.51)

else if $\mathcal{P}_k \mathcal{P}_{\text{total}}(r_k) \ll N_{I_k^{(l)}}(\boldsymbol{r}) + N_k(r_k)$ **then**

Calculate the transmit power $\mathcal{P}_k^{(l)}$ that maximize the function $F(n, r_k, \mathcal{P}_k)$ in the low-SINR regime by using Eq. (5.53)

else

Calculate the transmit power $\mathcal{P}_k^{(l)}$ that maximize the function $F(n, r_k, \mathcal{P}_k)$ by using Eq. (5.54)

end if

end if

Step 2: Determine $n^{(l)}$ to increase the FBC-based ϵ-effective capacity $EC_{\epsilon}^{(l)}(\theta_k)$

if $l = L_{\max}$ **then**

$\mathcal{P}_k^{\text{OPT}} \leftarrow \mathcal{P}_k^{(l)}$ and $n_k^{\text{OPT}} \leftarrow n_k^{(l)}, \forall \mathcal{P}_k^{\text{OPT}} \in \left\{\mathcal{P}_k^{\text{OPT,H}}, \mathcal{P}_k^{\text{OPT,M}}, \mathcal{P}_k^{\text{OPT,L}}\right\}$

end if

Update the Lagrange multipliers $\lambda_1^{(l)}$ and $\lambda_2^{(l)}$ as specified by Eq. (5.56) $l \leftarrow (l+1)$

end for

as follows:

$$\begin{cases} \lambda_1^{(l+1)} = \left[\lambda_1^{(l)} + \tau_1 \left(\mathcal{P}_k^{\max} - \mathcal{P}_k\right)\right]^+; \\ \lambda_2^{(l+1)} = \left[\lambda_2^{(l)} + \tau_2 \left(\mathcal{P}_k - \mathcal{P}_k^{\min}\right)\right]^+, \end{cases} \tag{5.56}$$

where $[a]^+ = \max\{a, 0\}$ and τ_1 and τ_2 are the positive step sizes. Define $L_{\max}$ as the maximum iteration number. Denote by $n^{(l)}$, $\mathcal{P}_k^{(l)}$, and $EC_\epsilon^{(l)}(\theta_k)$ the blocklength, transmit power, and ϵ-effective capacity at the lth iteration, respectively. Define n_k^{OPT} as the optimal blocklength and also we define $\mathcal{P}_k^{\text{OPT}} \in \left\{\mathcal{P}_k^{\text{OPT,H}}, \mathcal{P}_k^{\text{OPT,M}}, \mathcal{P}_k^{\text{OPT,L}}\right\}$ as the general notation of the optimal power allocation policy for nano transmitter k in the THz band. To solve the optimization problem $\mathbf{P_{15}}$, we develop the FBC-EH based optimal resource allocation policy as shown in **Algorithm 3** for our proposed statistical delay and error-rate bounded QoS provisioning in supporting mURLLC over FBC-EH based 6G THz wireless nano-networks.

5.5 Performance Evaluations

We use MATLAB-based simulations to validate and evaluate our proposed FBC-EH based 6G THz wireless nano-networks under statistical delay and error-rate bounded QoS provisioning. Throughout our simulations, we set the bandwidth $B = 1$ THz, the radius of the THz-band covered region $a = 5$ m, the radius of the blind area $b = 5$ mm, the reference temperature $T_0 = 310K$, and the SINR threshold $\gamma_{\text{th}} = 10$ dB. In light of the state-of-the-art in molecular-electronics, we set the total signal energy to be 500 pJ, which is independent of the power spectral distribution. For our proposed THz-band FBC-EH-based nano-communication schemes, we set the generator voltage $V_g = 0.42$ V, total capacitance $C_{\text{cap}} = 176$ μF, the amount of electric charge per cycle $\Delta Q = 3.63$ nC, and the average time between vibrations $t_{\text{cyc}} = 0.02$ sec [119] [120].

Figure 5.3 plots the aggregate interference power as a function of the nano node density λ for our proposed schemes. We can observe from Fig. 5.3 that the aggregate interference first increases and finally converges to a certain value as the node density λ increases. This implies that compared to the interference, the effect of molecular absorption noise is of the secondary importance for our proposed THz-band wireless nano-networks as $K \to \infty$. Fig. 5.3 also shows that given the same

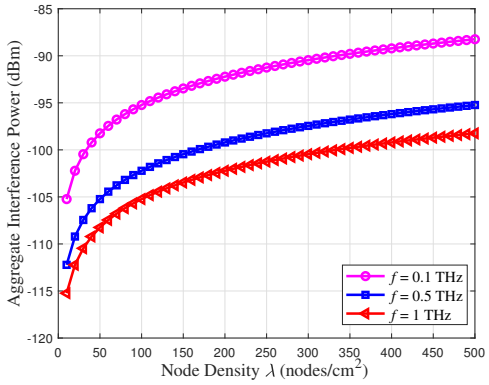

Figure 5.3: The aggregate interference power (dBm) vs. node density λ in the THz band.

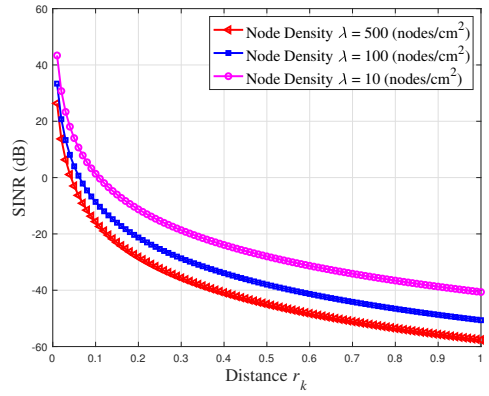

Figure 5.4: The SINR (dB) vs. transmission distance r_k in the THz band in the finite blocklength regime.

node density λ, the aggregate interference decreases at higher frequency f. This implies that the path loss is proportional to the square of frequency f and the absorption coefficients are usually larger at higher frequency in the THz band.

Setting the frequency $f = 1$ THz, using Eq. (5.16), Fig. 5.4 plots the SINR $\gamma_k^{(l)}(\boldsymbol{r})$ as a function of the transmission distance r_k for our proposed schemes. We can observe from Fig. 5.4 that the SINR $\gamma_k^{(l)}(\boldsymbol{r})$ first decreases and then converges to a certain value as the transmission distance r_k increases. This implies that with a shorter transmission distance, we have a lower path loss, which leads to a larger value of the SINR. Fig. 5.4 shows that the SINR $\gamma_k^{(l)}(\boldsymbol{r})$ decreases as the node

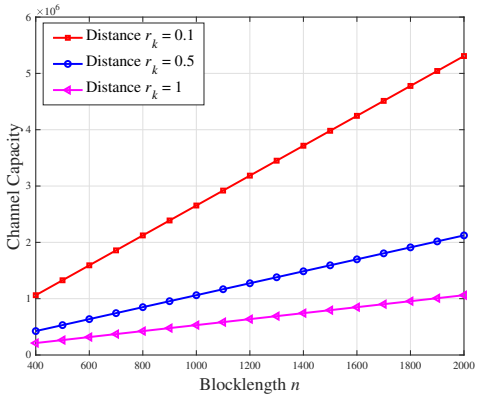

Figure 5.5: The channel capacity $C(r_k, \mathcal{P}_k)$ vs. blocklength n in the THz band in the finite blocklength regime.

density λ increases, indicating that the node density is limited for the practical applications of wireless nano-networks.

Using Eqs. (5.22) and (5.24), Fig. 5.5 depicts the channel capacity $C(r_k, \mathcal{P}_k)$ with different blocklengths n in the THz band for our proposed schemes. As shown in Fig. 5.5, the channel capacity $C(r_k, \mathcal{P}_k)$ increases as the blocklength n increases. Fig. 5.5 also shows that the channel capacity $C(r_k, \mathcal{P}_k)$ decreases as the transmission distance r_k increases.

Figure 5.6 depicts the ϵ-effective capacity $EC_\epsilon(\theta_k)$ as a function of both transmit power $\mathcal{P}_k$ (pJ) and transmission distance r_k in the THz band. We can observe from Fig. 5.6 that there exists an optimal transmit power $\mathcal{P}_k^{\text{OPT}}$ that maximizes the ϵ-effective capacity $EC_\epsilon(\theta_k)$. Fig. 5.6 also shows that the optimal transmit power $\mathcal{P}_k^{\text{OPT}}$ depends on the transmission distance r_k. With the increase of the transmission distance, the value of the optimal transmit power $\mathcal{P}_k^{\text{OPT}}$ decreases in order to achieve the maximum ϵ-effective capacity $EC_\epsilon(\theta_k)$. In addition, setting the frequency $f = 0.1$ THz and the transmission distance $r_k = 0.5$, Fig. 5.7 plots the ϵ-effective capacity $EC_\epsilon(\theta_k)$ as a function of both blocklength n and QoS exponent θ_k for our proposed schemes. We can observe from Fig. 5.7 that a smaller QoS exponent θ_k achieves a larger value of ϵ-effective capacity $EC_\epsilon(\theta_k)$ in the THz band. This implies that a smaller QoS exponent $\theta_k \to 0$ and a larger QoS exponent $\theta_k \to \infty$ set an upper bound and lower bound on the ϵ-effective capacity, respectively.

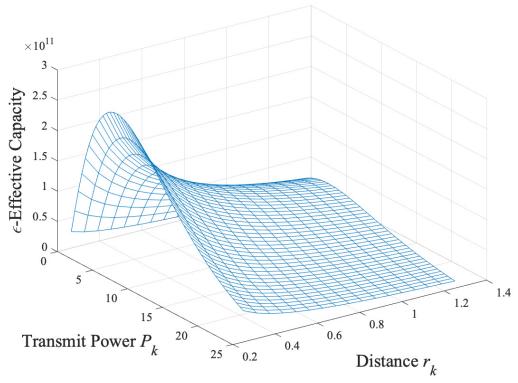

Figure 5.6: The ϵ-effective capacity $EC_\epsilon(\theta_k)$ vs. transmit power $\mathcal{P}_k$ and transmission distance r_k in the THz band in the finite blocklength regime.

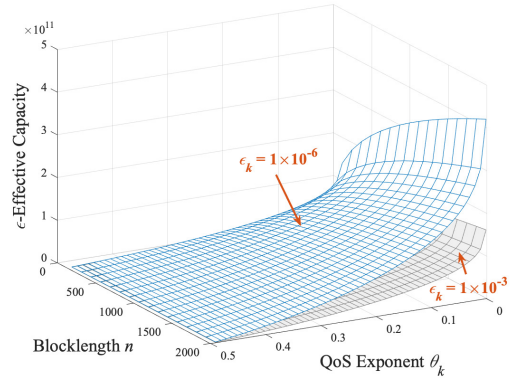

Figure 5.7: The ϵ-effective capacity $EC_\epsilon(\theta_k)$ vs. blocklength n and QoS exponent θ_k in the THz band in the finite blocklength regime.

5.6 Summary

We have developed the optimal resource allocation policies to maximize the ϵ-effective capacity in the THz band over EH-based wireless nano-networks in the finite blocklength regime for statistical delay and error-rate bounded QoS provisioning. In particular, we have established EH-based THz-band nano-communication system models in the finite blocklength regime. Then, we have analyzed the THz-band aggregate interference, channel capacity, and channel dispersion functions using FBC. Considering statistical delay and error-rate bounded QoS provisioning, we

have formulated and solved the ϵ-effective capacity maximization problem for our proposed statistical delay and error-rate bounded QoS provisioning in supporting mURLLC over FBC-EH based 6G THz wireless nano-networks. Simulation results are included, which validate and evaluate our proposed schemes in the THz band over wireless nano-networks.

6. CONCLUSIONS

To support the unprecedented wireless applications with extremely diverse and challenging QoS requirements, the statistical delay and error-rate bounded QoS provisioning emerge as one of the key promising techniques to characterize queueing behaviors for guaranteeing stringent 6G mURLLC requirements. The objective of this dissertation was to design and analyze the analytical modeling frameworks and controlling mechanisms for statistical delay and error-rate bounded QoS provisioning over 6G mobile wireless networks in the non-asymptotic regime. This chapter summarizes the achieved research contributions of this dissertation and proposes some future research directions.

6.1 Summary of the Dissertation

In Chapter 1, we have introduced and motivated the problems. We have considered the problems of the statistical delay and error-rate bounded QoS provisioning for next generation mobile wireless communications and networks in the finite blocklength regime. In Chapter 2, we have developed analytical modeling schemes to precisely characterize the delay and error-rate bounded QoS performances considering non-vanishing decode error probability over 6G CF m-MIMO mobile wireless networks in the finite blocklength regime. In particular, we have developed FBC-based system models and applied the Mellin transform to characterize both arrival and service processes for our proposed CF m-MIMO modeling schemes. Then, we have formulated and solved the delay violation probability minimization problem and obtain the closed-form solution of the optimal rate adaptation policy, which plays the important roles in system design and performance analyses for statistical delay and error-rate bounded QoS provisioning over 6G CF m-MIMO mobile wireless networks.

In Chapter 3, we have proposed statistical delay and error-rate bounded QoS provisioning architectures/schemes over mmWave user-centric CF m-MIMO and FBC-HARQ based 6G wireless mobile networks. In particular,we establish the comprehensive mmWave user-centric CF m-MIMO

based system models. We also apply HARQ-IR protocol to determine the channel capacity and characterize the QoS metrics in terms of error probability. Based on the information theoretic results in QoS theory, we have derived QoS metrics in terms of error probability and corresponding effective capacity function for our proposed FBC-HARQ based mmWave cell-free m-MIMO schemes.

In Chapter 4, we have proposed and developed statistical delay and error-rate bounded QoS provisioning schemes over SWIPT-enabled CF m-MIMO 6G wireless networks in the finite blocklength regime. In particular, we have established SWIPT-enabled CF m-MIMO based system models by using FBC. Taking into account both the harvested energy and transmit power constraints, we have formulated and solved the optimization problems for the tradeoff between the ϵ-effective capacity and harvested energy for both downlink SWIPT and uplink data transfer phases under statistical delay and error rate bounded QoS provisioning in supporting mURLLC.

In Chapter 5, we have proposed optimal resource allocation policies to achieve the maximum ϵ-effective capacity in the THz band over FBC-EH-based nano-networks. Particularly, we establish nanoscale system models and characterize wireless channel models in the THz band using FBC. We have also analyzed the THz-band aggregate interference, channel capacity, and channel dispersion functions using FBC. Considering statistical delay and error-rate bounded QoS provisioning, we formulate and solve the ϵ-effective capacity maximization problem under several different EH constraints for our proposed schemes in supporting mURLLC over FBC-EH based 6G THz wireless nano-networks.

6.2 Further Works

6.2.1 Statistical Delay and Error-Rate Bounded QoS Provisioning in Finite Blocklength Regime

There are still many challenges on how to characterize and model the queuing/reliability performance over various wireless fading channels in guaranteeing statistical delay and error-rate bounded QoS constraints in the finite blocklength regime. The relationship between the maximum

achievable coding rate and the FBC-based outage capacity function over the wireless fading channels considering different 6G architecture models is still an open problem in the finite blocklength regime. To overcome these problems, the novel FBC-based statistical delay and error-rate bounded QoS system frameworks and architectures need to be developed for analyzing the relationship between delay violation probability and decoding error probability in the finite blocklength regime. It is also needed to reformulate and solve the cross-layer ϵ-effective capacity maximization problem and derive optimal resource allocation policies using FBC. Further possible difficulties include the non-convexity issues for various optimization problems, which may need convert non-convex optimization problems into convex optimization problems, before obtaining the closed-form expressions for the maximum ϵ-effective capacity, either in the forms of approximation or performance-bound expressions if the accurate closed-form solutions are not feasible.

6.2.2 Promising Candidate Techniques for Beyond 5G and Future-Generation Multimedia Mobile Wireless Networks

As the technical pillar foundations of 5G and beyond multimedia mobile wireless networks, the emerging advances, evolutions, and developments of key promising techniques continue as time goes. This is because there are always new challenges coming up with each advance and progress of beyond 5G multimedia mobile wireless networks, which need to be overcome by developing new candidate techniques and frameworks. The state-of-the-art techniques and frameworks keep on advancing every day, which are also creating a great deal of new research areas, topics, and realms, and may also yield new research funding opportunities for the future generations of multimedia mobile wireless networks. As it is hard to discuss all possible emerging techniques and frameworks due to lack of space in this research proposal, I would like to pin-point some of these beyond 5G promising candidate techniques and frameworks which I believe need our immediate research attention from both academic and industry standpoints. I plan to continue tackling the following new or emerging techniques (in fact, I have already obtained some initial research results in some of them): (1) CF m-MIMO, (2) edge computing, (3) WiFi and D2D offloading, (4) THz-band wireless communications, (5) intelligent reflection surface (IRS)-assisted unmanned aerial vehicle

(UAV) communications, (6) SWIPT, (7) big data and information-centric multimedia mobile wireless networks, etc. My research endeavours in the above areas will include: developing wireless fading channel model, designing the proposed network architectures, characterizing cross-layer design and optimization policies, establishing test-beds and simulation packages to validate and evaluate the newly proposed and developed research schemes, models, and architectures, etc.

6.2.3 Machine Learning and Deep Learning Based Mobile Wireless Networks

Machine learning is the adaptive computational methodologies for improving computer-controlled decision system's performance by detecting and describing consistencies and patterns in training data. On the other hand, mobile wireless networks have to be predictive, proactive, and anticipatory to ensure URLLC requirements. However, the growing diversity and complexity of mobile network architectures has made it difficult to monitor, allocate, and manage wireless network resources. During the last decades, embedding various machine learning techniques into upcoming mobile wireless networks is drawing significant research attention. However, due to the dynamically changing environments and stochastic mobility patterns of each mobile user, it is challenging to model machine-learning based wireless network architectures. To overcome these problems, I plan to apply machine learning/deep learning into various 5G and beyond promising candidate techniques to bridge the gap between communities of machine learning/deep learning algorithms, mathematical solutions, and 5G and beyond candidate techniques, frameworks, and applications. Instead of using centralized machine learning, I plan to continue further developing the collaborative-learning based system architecture models, which enables distributed servers with storing and computing capabilities to collaboratively learn the CSI, user demands, and mobility patterns of the mobile devices, while guaranteeing the statistical delay and error-rate bounded QoS provisioning. I also plan to design the collaborative-learning based algorithms for optimizing the resource allocations of the mobile devices and WiFi APs.

REFERENCES

[1] X. Zhang, J. Tang, H.-H. Chen, S. Ci, and M. Guizani, "Cross-layer-based modeling for quality of service guarantees in mobile wireless networks," *IEEE Comm. Magazine*, vol. 44, no. 1, pp. 100–106, 2006.

[2] J. Tang and X. Zhang, "Quality-of-service driven power and rate adaptation over wireless links," *IEEE Transactions on Wireless Comm.*, vol. 6, no. 8, pp. 3058–3068, 2007.

[3] J. Tang and X. Zhang, "Cross-layer resource allocation over wireless relay networks for quality of service provisioning," *IEEE Journal on Selected Areas in Communications*, vol. 25, no. 4, pp. 645–656, May 2007.

[4] X. Zhang and J. Tang, "Power-delay tradeoff over wireless networks," *IEEE Transactions on Communications*, vol. 61, no. 9, pp. 3673–3684, 2013.

[5] J. Tang and X. Zhang, "Cross-layer-model based adaptive resource allocation for statistical QoS guarantees in mobile wireless networks," *IEEE Transactions on Wireless Communications*, vol. 7, no. 6, pp. 2318–2328, 2008.

[6] J. Tang and X. Zhang, "Cross-layer modeling for quality of service guarantees over wireless links," *IEEE Transactions on Wireless Communications*, vol. 6, no. 12, pp. 4504–4512, 2007.

[7] J. Tang and X. Zhang, "Quality-of-service driven power and rate adaptation for multichannel communications over wireless links," *IEEE Transactions on Wireless Communications*, vol. 6, no. 12, pp. 4349–4360, 2007.

[8] H. Su and X. Zhang, "Cross-layer based opportunistic MAC protocols for QoS provisionings over cognitive radio wireless networks," *IEEE Journal on Selected Areas in Communications*, vol. 26, no. 1, pp. 118–129, Jan. 2008.

[9] X. Zhang and Q. Du, "Adaptive low-complexity erasure-correcting code-based protocols for QoS-driven mobile multicast services over wireless networks," *IEEE Transactions on Vehicular Technology*, vol. 55, no. 5, pp. 1633–1647, 2006.

[10] Q. Du and X. Zhang, "QoS-aware base-station selections for distributed MIMO links in broadband wireless networks," *IEEE Journal on Selected Areas in Communications*, vol. 29, no. 6, pp. 1123–1138, 2011.

[11] X. Zhang, W. Cheng, and H. Zhang, "Heterogeneous statistical QoS provisioning over airborne mobile wireless networks," *IEEE Journal on Selected Areas in Communications*, vol. 36, no. 9, pp. 2139–2152, 2018.

[12] X. Zhang, W. Cheng, and H. Zhang, "Heterogeneous statistical QoS provisioning over 5G mobile wireless networks," *IEEE Network Magazine*, vol. 28, no. 6, pp. 46–53, Nov. 2014.

[13] W. Cheng, X. Zhang, and H. Zhang, "Statistical-QoS driven energy-efficiency optimization over green 5G mobile wireless networks," *IEEE Journal on Selected Areas in Communications*, vol. 34, no. 12, pp. 3092–3107, 2016.

[14] X. Zhang and J. Wang, *Heterogeneous Statistical QoS Provisioning Over Cognitive-Radio Based 5G Mobile Wireless Networks*. One Chapter in the Book of "Handbook of Cognitive Radio", Springer, ISBN: 978-981-10-1389-8, New York, USA, First Edition, April 2017.

[15] W. Saad, M. Bennis, and M. Chen, "A vision of 6G wireless systems: applications, trends, technologies, and open research problems," *IEEE Network*, vol. 34, no. 3, pp. 134–142, May/June 2020.

[16] K. B. Letaief, W. Chen, Y. Shi, J. Zhang, and Y. A. Zhang, "The roadmap to 6G: AI empowered wireless networks," *IEEE Communications Magazine*, vol. 57, no. 8, pp. 84–90, August 2019.

[17] Z. Zhang, Y. Xiao, Z. Ma, M. Xiao, Z. Ding, X. Lei, G. K. Karagiannidis, and P. Fan, "6G wireless networks: vision, requirements, architecture, and key technologies," *IEEE Vehicular Technology Magazine*, vol. 14, no. 3, pp. 28–41, September 2019.

[18] X. Zhang, W. Cheng, and H. Zhang, "Heterogeneous statistical QoS provisioning over airborne mobile wireless networks," *IEEE Journal on Selected Areas in Communications*, vol. 36, no. 9, pp. 2139–2152, 2018.

[19] X. Zhang, J. Wang, and H. V. Poor, "Heterogeneous statistical-QoS driven resource al-

location over MmWave massive-MIMO based 5G mobile wireless networks in the non-asymptotic regime," *IEEE Journal on Selected Areas in Communications (J-SAC)*, vol. 37, no. 12, pp. 2727–2743, Dec. 2019.

[20] X. Zhang, J. Wang, and H. V. Poor, "Optimal resource allocation for statistical QoS provisioning in supporting mURLLC over FBC-driven 6G terahertz wireless nano-networks," in *Proceedings of IEEE INFOCOM*, 2021.

[21] X. Zhang, J. Wang, and H. V. Poor, "Optimal resource allocations for statistical QoS provisioning in supporting mURLLC over FBC-EH based 6G THz wireless nano-networks," *IEEE Journal on Selected Areas in Communications (J-SAC)*, vol. 39, no. 6, pp. 1544–1560, June 2021.

[22] X. Zhang, J. Wang, and H. V. Poor, "AoI-driven statistical delay and error-rate bounded QoS provisioning for 6G mURLLC over UAV-enabled mobile wireless networks," *IEEE Journal on Selected Areas in Communications (J-SAC)*, vol. 39, no. 11, pp. 3425–3443, Nov. 2021.

[23] H. Ji, S. Park, J. Yeo, Y. Kim, J. Lee, and B. Shim, "Ultra-reliable and low-latency communications in 5G downlink: physical layer aspects," *IEEE Wireless Communications*, vol. 25, no. 3, pp. 124–130, June 2018.

[24] X. Chen, D. W. K. Ng, W. Yu, E. G. Larsson, N. Al-Dhahir, and R. Schober, "Massive access for 5G and beyond," *IEEE Journal on Selected Areas in Communications*, vol. 39, no. 3, pp. 615–637, 2021.

[25] E. Yaacoub and M. Alouini, "A key 6G challenge and opportunityâĂŤconnecting the base of the pyramid: a survey on rural connectivity," *Proceedings of the IEEE*, vol. 108, no. 4, pp. 533–582, 2020.

[26] X. Zhang, J. Wang, and H. V. Poor, "Statistical delay and error-rate bounded QoS provisioning over mmWave cell-free m-MIMO and FBC-HARQ-IR based 6G wireless networks," *IEEE Journal on Selected Areas in Communications (J-SAC)*, vol. 38, no. 8, pp. 1661–1677, 2020.

[27] X. Chen, D. W. K. Ng, W. Yu, E. G. Larsson, N. Al-Dhahir, and R. Schober, "Massive access

for 5G and beyond," *IEEE Journal on Selected Areas in Communications*, Feb. 2020.

[28] W. Yang, G. Durisi, T. Koch, and Y. Polyanskiy, "Quasi-static multiple-antenna fading channels at finite blocklength," *IEEE Transactions on Information Theory*, vol. 60, no. 7, pp. 4232–4265, 2014.

[29] G. Durisi, T. Koch, and P. Popovski, "Toward massive, ultrareliable, and low-latency wireless communication with short packets," *Proceedings of the IEEE*, vol. 104, no. 9, pp. 1711–1726, 2016.

[30] Y. Polyanskiy, H. V. Poor, and S. Verdú, "Channel coding rate in the finite blocklength regime," *IEEE Transactions on Information Theory*, vol. 56, no. 5, pp. 2307–2359, May 2010.

[31] Y. Polyanskiy and S. Verdú, "Empirical distribution of good channel codes with non-vanishing error probability," *IEEE transactions on information theory*, vol. 60, no. 1, pp. 5–21, 2013.

[32] M. Bennis, M. Debbah, and H. V. Poor, "Ultrareliable and low-latency wireless communication: tail, risk, and scale," *Proceedings of the IEEE*, vol. 106, no. 10, pp. 1834–1853, Oct. 2018.

[33] Y. Polyanskiy, H. V. Poor, and S. Verdú, "Feedback in the non-asymptotic regime," *IEEE Transactions on Information Theory*, vol. 57, no. 8, pp. 4903–4925, Aug. 2011.

[34] P. Mary, J. Gorce, A. Unsal, and H. V. Poor, "Finite blocklength information theory: what is the practical impact on wireless communications?," in *Proceedings of IEEE Globecom Workshops*, pp. 1–6, 2016.

[35] W. Yang, G. Durisi, T. Koch, and Y. Polyanskiy, "Quasi-static multiple-antenna fading channels at finite blocklength," *IEEE Transactions on Information Theory*, vol. 60, no. 7, pp. 4232–4265, July 2014.

[36] H. Q. Ngo, A. Ashikhmin, H. Yang, E. G. Larsson, and T. L. Marzetta, "Cell-free massive MIMO versus small cells," *IEEE Transactions on Wireless Communications*, vol. 16, no. 3, pp. 1834–1850, Mar. 2017.

[37] M. Alonzo, S. Buzzi, A. Zappone, and C. D'Elia, "Energy-efficient power control in cell-free and user-centric massive MIMO at millimeter wave," *IEEE Transactions on Green Communications and Networking*, vol. 3, no. 3, pp. 651–663, Sep. 2019.

[38] X. Zhang, J. Wang, and H. V. Poor, "Statistical delay and error-rate bounded QoS provisioning for SWIPT over CF M-MIMO 6G wireless networks using FBC," *IEEE Journal on Selected Topics in Signal Processing (J-STSP)*, vol. 39, no. 3, pp. 1272–1287, Aug. 2021.

[39] M. Varasteh, B. Rassouli, and B. Clerckx, "On capacity-achieving distributions for complex AWGN channels under nonlinear power constraints and their applications to SWIPT," *IEEE Transactions Information Theory*, vol. 66, no. 10, pp. 6488–6508, 2020.

[40] Z. Wang, H. Zhao, S. Wang, J. Zhang, and M. Alouini, "Secrecy analysis in SWIPT systems over generalized-k fading channels," *IEEE Commun. Lett.*, vol. 23, no. 5, pp. 834–837, 2019.

[41] I. Akyildiz, J. Jornet, and C. Han, "Terahertz band: next frontier for wireless communications," *Physical Communication*, vol. 12, pp. 16–32, 2014.

[42] J. M. Jornet and I. F. Akyildiz, "Low-weight channel coding for interference mitigation in electromagnetic nanonetworks in the Terahertz band," in *Proc. 2011 IEEE International Conference on Communications (ICC)*, pp. 1–6, 2011.

[43] E. Nayebi, A. Ashikhmin, T. L. Marzetta, H. Yang, and B. D. Rao, "Precoding and power optimization in cell-free massive MIMO systems," *IEEE Transactions on Wireless Communications*, vol. 16, no. 7, pp. 4445–4459, 2017.

[44] E. Björnson and L. Sanguinetti, "Scalable cell-free massive MIMO systems," *IEEE Transactions on Communications*, pp. 1–15, 2020.

[45] G. Interdonato, P. Frenger, and E. G. Larsson, "Scalability aspects of cell-free massive MIMO," in *2019 IEEE International Conference on Communications (ICC)*, pp. 1–6, 2019.

[46] T. D. Ponnimbaduge Perera, D. N. K. Jayakody, S. K. Sharma, S. Chatzinotas, and J. Li, "Simultaneous wireless information and power transfer (SWIPT): recent advances and future challenges," *IEEE Communications Surveys Tutorials*, vol. 20, no. 1, pp. 264–302, 2018.

[47] L. R. Varshney, "Transporting information and energy simultaneously," in *2008 IEEE International Symposium on Information Theory*, pp. 1612–1616, 2008.

[48] O. L. Alcaraz López, E. M. G. Fernández, R. D. Souza, and H. Alves, "Ultra-reliable cooperative short-packet communications with wireless energy transfer," *IEEE Sensors Journal*, vol. 18, no. 5, pp. 2161–2177, 2018.

[49] T. Kürner and S. Priebe, "Towards THz communications-status in research, standardization and regulation," *Journal of Infrared, Millimeter, and Terahertz Waves*, vol. 35, no. 1, pp. 53–62, 2014.

[50] M. Božanić and S. Sinha, *Millimeter-Wave Integrated Circuits: methodologies for Research, Design and Innovation*, vol. 658. Springer Nature, 2020.

[51] H. Song and T. Nagatsuma, "Present and future of Terahertz communications," *IEEE Transactions on Terahertz Science and Technology*, vol. 1, no. 1, pp. 256–263, Sep. 2011.

[52] K. S. Novoselov, L. C. V. Fal, P. Gellert, M. Schwab, and K. Kim, "A roadmap for graphene," *Nature*, vol. 490, no. 7419, pp. 192–200, 2012.

[53] H. A. Hafez, S. Kovalev, J.-C. Deinert, Z. Mics, B. Green, N. Awari, M. Chen, S. Germanskiy, U. Lehnert, J. Teichert, Z. Wang, K.-J. Tielrooij, Z. Liu, Z. Chen, A. Narita, K. MÃijllen, M. Bonn, M. Gensch, and D. Turchinovich, "Extremely efficient Terahertz high-harmonic generation in graphene by hot dirac fermions," *Nature*, vol. 561, no. 7724, pp. 507–511, 2018.

[54] I. F. Akyildiz and J. M. Jornet, "The Internet of nano-things," *IEEE Wireless Communications*, vol. 17, no. 6, pp. 58–63, 2010.

[55] Q. H. Abbasi, H. El Sallabi, N. Chopra, K. Yang, K. A. Qaraqe, and A. Alomainy, "Terahertz channel characterization inside the human skin for nano-scale body-centric networks," *IEEE Transactions on Terahertz Science and Technology*, vol. 6, no. 3, pp. 427–434, 2016.

[56] Q. H. Abbasi, K. Yang, N. Chopra, J. M. Jornet, N. A. Abuali, K. A. Qaraqe, and A. Alomainy, "Nano-communication for biomedical applications: A review on the state-of-the-art from physical layers to novel networking concepts," *IEEE Access*, vol. 4, pp. 3920–3935,

2016.

[57] F. Dressler and S. Fischer, "Connecting in-body nano communication with body area networks: challenges and opportunities of the internet of nano things," *Nano Communication Networks*, vol. 6, no. 2, pp. 29–38, 2015.

[58] F. Afsana, M. Asif-Ur-Rahman, M. R. Ahmed, M. Mahmud, and M. S. Kaiser, "An energy conserving routing scheme for wireless body sensor nanonetwork communication," *IEEE Access*, vol. 6, pp. 9186–9200, 2018.

[59] J. M. Jornet and I. F. Akyildiz, "Channel modeling and capacity analysis for electromagnetic wireless nanonetworks in the Terahertz band," *IEEE Transactions on Wireless Communications*, vol. 10, no. 10, pp. 3211–3221, Oct. 2011.

[60] J. M. Jornet and I. F. Akyildiz, "Channel capacity of electromagnetic nanonetworks in the Terahertz band," in *Proc. 2010 IEEE International Conference on Communications*, pp. 1–6, 2010.

[61] Z. Xu, X. Dong, and J. Bornemann, "Design of a reconfigurable MIMO system for THz communications based on graphene antennas," *IEEE Transactions on Terahertz Science and Technology*, vol. 4, no. 5, pp. 609–617, 2014.

[62] Z. Xu, X. Dong, and J. Bornemann, "Spectral efficiency of carbon nanotube antenna based MIMO systems in the Terahertz band," *IEEE Wireless Communications Letters*, vol. 2, no. 6, pp. 631–634, 2013.

[63] Y. Liu and Y. Jiang, *Stochastic Network Calculus*. London: Springer, 2008.

[64] M. Kang and M. S. Alouini, "Capacity of MIMO Rician channels," *IEEE Transactions on Wireless Communications*, vol. 5, no. 1, pp. 112–122, Jan. 2006.

[65] G. Caire and S. Shamai, "On the achievable throughput of a multiantenna Gaussian broadcast channel," *IEEE Transactions on Information Theory*, vol. 49, no. 7, pp. 1691–1706, July 2003.

[66] B. M. Hochwald., T. L. Marzetta, and V. Tarokh, "Multiple-antenna channel hardening and its implications for rate feedback and scheduling," *IEEE Transactions on Information The-*

ory, vol. 50, no. 9, pp. 1893–1909, Sep. 2006.

[67] H. Al-Zubaidy, J. Liebeherr, and A. Burchard, "Network-layer performance analysis of multihop fading channels," *IEEE/ACM Transactions on Networking*, vol. 24, no. 1, pp. 204–217, Feb. 2016.

[68] B. Davies, *Integral Transforms and Their Applications*. New York, NY, USA: Springer-Verlag, 1978.

[69] C.-S. Chang, "Stability, queue length, and delay of deterministic and stochastic queueing networks," *IEEE Transactions on Automatic Control*, vol. 39, no. 5, pp. 913–931, May 1994.

[70] S. K. Jayaweera and H. V. Poor, "On the capacity of multiple-antenna systems in Rician fading," *IEEE Transactions on Wireless Communications*, vol. 4, no. 3, pp. 1102–1111, May 2005.

[71] W. Cheng, X. Zhang, and H. Zhang, "Heterogeneous statistical QoS provisioning for downlink transmissions over mobile wireless cellular networks," in *Proceedings of IEEE GLOBECOM 2014*, pp. 4757–4763, 2014.

[72] S. Lin and P. Yu, "A hybrid ARQ scheme with parity retransmission for error control of satellite channels," *IEEE Transactions on Communications*, vol. 30, no. 7, pp. 1701–1719, July 1982.

[73] D. To, H. X. Nguyen, Q. Vien, and L. Huang, "Power allocation for HARQ-IR systems under QoS constraints and limited feedback," *IEEE Transactions on Wireless Communications*, vol. 14, no. 3, pp. 1581–1594, Mar. 2015.

[74] Jung-Fu Cheng, "Coding performance of hybrid arq schemes," *IEEE Transactions on Communications*, vol. 54, no. 6, pp. 1017–1029, June 2006.

[75] P. Frenger, S. Parkvall, and E. Dahlman, "Performance comparison of HARQ with chase combining and incremental redundancy for HSDPA," in *IEEE 54th Vehicular Technology Conference. VTC Fall 2001. Proceedings (Cat. No.01CH37211)*, vol. 3, pp. 1829–1833, Oct. 2001.

[76] Y. Li, M. C. Gursoy, and S. Velipasalar, "On the throughput of hybrid-ARQ under statistical queuing constraints," *IEEE Transactions on Vehicular Technology*, vol. 64, no. 6, pp. 2725–2732, June 2015.

[77] H. Q. Ngo, L. Tran, T. Q. Duong, M. Matthaiou, and E. G. Larsson, "On the total energy efficiency of cell-free massive MIMO," *IEEE Transactions on Green Communications and Networking*, vol. 2, no. 1, pp. 25–39, Mar. 2018.

[78] S. Buzzi and C. DâĂŹAndrea, "Cell-free massive MIMO: User-centric approach," *IEEE Wireless Communications Letters*, vol. 6, no. 6, pp. 706–709, Dec. 2017.

[79] E. Nayebi, A. Ashikhmin, T. L. Marzetta, H. Yang, and B. D. Rao, "Precoding and power optimization in cell-free massive MIMO systems," *IEEE Transactions on Wireless Communications*, vol. 16, no. 7, pp. 4445–4459, July 2017.

[80] A. Alkhateeb, G. Leus, and R. W. Heath, "Limited feedback hybrid precoding for multi-user millimeter wave systems," *IEEE Transactions on Wireless Communications*, vol. 14, no. 11, pp. 6481–6494, Nov. 2015.

[81] Y. Ding and B. D. Rao, "Dictionary learning-based sparse channel representation and estimation for FDD massive MIMO systems," *IEEE Transactions on Wireless Communications*, vol. 17, no. 8, pp. 5437–5451, Aug. 2018.

[82] M. Aharon, M. Elad, and A. Bruckstein, "K-SVD: An algorithm for designing overcomplete dictionaries for sparse representation," *IEEE Transactions on Signal Processing*, vol. 54, no. 11, pp. 4311–4322, Nov. 2006.

[83] L. D. Nguyen, T. Q. Duong, H. Q. Ngo, and K. Tourki, "Energy efficiency in cell-free massive MIMO with zero-forcing precoding design," *IEEE Communications Letters*, vol. 21, no. 8, pp. 1871–1874, Aug. 2017.

[84] M. Alonzo and S. Buzzi, "Cell-free and user-centric massive MIMO at millimeter wave frequencies," in *2017 IEEE 28th Annual International Symposium on Personal, Indoor, and Mobile Radio Communications (PIMRC)*, pp. 1–5, Oct. 2017.

[85] M. Alonzo, S. Buzzi, and A. Zappone, "Energy-efficient downlink power control in

mmwave cell-free and user-centric massive MIMO," in *2018 IEEE 5G World Forum (5GWF)*, pp. 493–496, July 2018.

[86] O. E. Ayach, R. W. Heath, S. Abu-Surra, S. Rajagopal, and Z. Pi, "Low complexity precoding for large millimeter wave MIMO systems," in *2012 IEEE International Conference on Communications (ICC)*, pp. 3724–3729, 2012.

[87] J. A. Tropp, "Greed is good: algorithmic results for sparse approximation," *IEEE Transactions on Information Theory*, vol. 50, no. 10, pp. 2231–2242, Oct. 2004.

[88] S. L. Fong, V. Y. F. Tan, and J. Yang, "Non-asymptotic achievable rates for energy-harvesting channels using save-and-transmit," *IEEE Journal on Selected Areas in Communications*, vol. 34, no. 12, pp. 3499–3511, Dec. 2016.

[89] W. Feller, *An Introduction to Probability Theory and Its Applications (2nd ed.)*, vol. 2. New York: Wiley, 1971.

[90] B. L. Mark and G. Ramamurthy, "Real-time estimation and dynamic renegotiation of UPC parameters for arbitrary traffic sources in ATM networks," *IEEE/ACM Transactions on Networking*, vol. 6, no. 6, pp. 811–827, Dec. 1998.

[91] D. Wu and R. Negi, "Effective capacity: a wireless link model for support of quality of service," *IEEE Transactions on Wireless Communications*, vol. 2, no. 4, pp. 630–643, July 2003.

[92] M. Ozmen and M. C. Gursoy, "Wireless throughput and energy efficiency with random arrivals and statistical queuing constraints," *IEEE Transactions on Information Theory*, vol. 62, no. 3, pp. 1375–1395, Mar. 2016.

[93] C.-S. Chang and J. A. Thomas, "Effective bandwidth in high-speed digital networks," *IEEE Journal on Selected Areas in Communications*, vol. 13, no. 6, pp. 1091–1100, Aug. 1995.

[94] B. Soret, M. C. Aguayo-torres, and J. T. Entrambasaguas, "Capacity with explicit delay guarantees for generic sources over correlated Rayleigh channel," *IEEE Transactions on Wireless Communications*, vol. 9, no. 6, pp. 1901–1911, June 2010.

[95] W. Tan, M. Matthaiou, S. Jin, and X. Li, "Spectral efficiency of DFT-based processing

hybrid architectures in massive MIMO," *IEEE Wireless Communications Letters*, vol. 6, no. 5, pp. 586–589, Oct. 2017.

[96] A. Alkhateeb, O. E. Ayach, G. Leus, and R. W. Heath, "Channel estimation and hybrid precoding for millimeter wave cellular systems," *IEEE Journal of Selected Topics in Signal Processing*, vol. 8, no. 5, pp. 831–846, Oct. 2014.

[97] G. Amarasuriya, E. G. Larsson, and H. V. Poor, "Wireless information and power transfer inÂămultiway massive MIMO relay networks," *IEEE Transactions on Wireless Comm.*, vol. 15, no. 6, pp. 3837–3855, 2016.

[98] A. Agarwal, A. K. Jagannatham, and L. Hanzo, "Finite blocklength non-orthogonal cooperative communication relying on SWIPT-enabled energy harvesting relays," *IEEE Transactions on Comm.*, vol. 68, no. 6, pp. 3326–3341, 2020.

[99] O. L. Alcaraz López, E. M. G. Fernández, R. D. Souza, and H. Alves, "Wireless powered communications with finite battery and finite blocklength," *IEEE Transactions on Comm.*, vol. 66, no. 4, pp. 1803–1816, 2018.

[100] S. M. Perlaza, A. Tajer, and H. V. Poor, "Simultaneous information and energy transmission: a finite block-length analysis," in *2018 IEEE 19th International Workshop on Signal Processing Advances in Wireless Communications (SPAWC)*, pp. 1–5, 2018.

[101] I. Kim, D. I. Kim, and J. Kang, "Rate-energy tradeoff and decoding error probability-energy tradeoff for SWIPT in finite code length," *IEEE Transactions on Wireless Comm.*, vol. 16, no. 12, pp. 8220–8234, 2017.

[102] S. Kusaladharma, W. P. Zhu, W. Ajib, and G. A. A. Baduge, "Stochastic geometry based performance characterization of SWIPT in cell-free massive MIMO," *IEEE Transactions on Vehicular Technology*, vol. 69, no. 11, pp. 13357–13370, 2020.

[103] R. Shrestha and G. Amarasuriya, "SWIPT in cell-free massive MIMO," in *2018 IEEE Global Communications Conference (GLOBECOM)*, pp. 1–7, 2018.

[104] M. Alageli, A. Ikhlef, F. Alsifiany, M. A. M. Abdullah, G. Chen, and J. Chambers, "Optimal downlink transmission for cell-free SWIPT massive MIMO systems with active eavesdrop-

ping," *IEEE Transactions on Information Forensics and Security*, vol. 15, pp. 1983–1998, 2020.

[105] X. Zhou, R. Zhang, and C. K. Ho, "Wireless information and power transfer: architecture design and rate-energy tradeoff," *IEEE Transactions on Comm.*, vol. 61, no. 11, pp. 4754–4767, 2013.

[106] D. S. Michalopoulos, H. A. Suraweera, and R. Schober, "Relay selection for simultaneous information transmission and wireless energy transfer: a tradeoff perspective," *IEEE Journal on Selected Areas in Comm.*, vol. 33, no. 8, pp. 1578–1594, 2015.

[107] P. Grover and A. Sahai, "Shannon meets Tesla: wireless information and power transfer," in *2010 IEEE International Symposium on Information Theory*, pp. 2363–2367, 2010.

[108] B. Clerckx, R. Zhang, R. Schober, D. W. K. Ng, D. I. Kim, and H. V. Poor, "Fundamentals of wireless information and power transfer: from RF energy harvester models to signal and system designs," *IEEE Journal on Selected Areas in Comm.*, vol. 37, no. 1, pp. 4–33, 2019.

[109] S. Sudevalayam and P. Kulkarni, "Energy harvesting sensor nodes: survey and implications," *IEEE Communications Surveys Tutorials*, vol. 13, no. 3, pp. 443–461, 2011.

[110] V. Sharma, U. Mukherji, V. Joseph, and S. Gupta, "Optimal energy management policies for energy harvesting sensor nodes," *IEEE Transactions on Wireless Communications*, vol. 9, no. 4, pp. 1326–1336, 2010.

[111] A. Baddeley, I. Bárány, and R. Schneider, *Stochastic Geometry: lectures Given at the CIME Summer School Held in Martina Franca, Italy, September 13-18, 2004*. Springer, 2006.

[112] V. Petrov, D. Moltchanov, and Y. Koucheryavy, "Interference and SINR in dense terahertz networks," in *2015 IEEE 82nd Vehicular Technology Conference (VTC2015-Fall)*, pp. 1–5, 2015.

[113] F. Afsana, S. A. Mamun, M. S. Kaiser, and M. R. Ahmed, "Outage capacity analysis of cluster-based forwarding scheme for body area network using nano-electromagnetic communication," in *Proc. 2015 2nd International Conference on Electrical Information and Communication Technologies (EICT)*, pp. 383–388, 2015.

[114] I. Llatser, A. Cabellos-Aparicio, E. AlarcÃşn, J. M. Jornet, A. Mestres, H. Lee, and J. Solé-Pareta, "Scalability of the channel capacity in graphene-enabled wireless communications to the nanoscale," *IEEE Transactions on Communications*, vol. 63, no. 1, pp. 324–333, Jan. 2015.

[115] R. Zhang, K. Yang, Q. Abbasi, K. Qaraqe, and A. Alomainy, "Analytical modelling of the effect of noise on the Terahertz in-vivo communication channel for body-centric nano-networks," *Nano Communication Networks*, vol. 15, pp. 59–68, May 2017.

[116] S. Chandrasekhar, *Radiative Transfer*. Courier Corporation, 2013.

[117] S. Xu, B. J. Hansen, and Z. L. Wang, "Piezoelectric-nanowire-enabled power source for driving wireless microelectronics," *Nature Communications*, vol. 1, no. 7, pp. 1–5, Oct. 2010.

[118] S. Xu, Y. Qin, C. Xu, Y. Wei, R. Yang, and Z. L. Wang, "Self-powered nanowire devices," *Nature Nanotechnology*, vol. 5, pp. 366–373, 2010.

[119] J. M. Jornet and I. F. Akyildiz, "Joint energy harvesting and communication analysis for perpetual wireless nanosensor networks in the Terahertz band," *IEEE Transactions on Nanotechnology*, vol. 11, no. 3, pp. 570–580, 2012.

[120] J. M. Jornet, "A joint energy harvesting and consumption model for self-powered nano-devices in nanonetworks," in *Proc. 2012 IEEE International Conference on Communications (ICC)*, pp. 6151–6156, 2012.

[121] S. Boyd, L. Xiao, and A. Mutapcic, "Subgradient methods," *lecture notes of EE392o, Stanford University, Autumn Quarter*, pp. 2004–2005, 2003.

[122] S. Schiessl, J. Gross, and H. Al-Zubaidy, "Delay analysis for wireless fading channels with finite blocklength channel coding," in *Proceedings of the 18th ACM International Conference on Modeling, Analysis and Simulation of Wireless and Mobile Systems*, pp. 13–22, 2015.

[123] I. Gradshteyn and I. Ryzhik, *Table of Integrals, Series, and Products*. New York, NY, USA: Academic Press, 8th ed., 2007.

[124] B. Makki, T. Svensson, and M. Zorzi, "Finite block-length analysis of the incremental redundancy HARQ," *IEEE Wireless Communications Letters*, vol. 3, no. 5, pp. 529–532, Oct. 2014.

[125] S. Boyd and L. Vandenberghe, *Convex Optimization*. Cambridge, U.K.: Cambridge University Press, 2004.

[126] R. M. Corless, G. H. Gonnet, D. E. G. Hare, D. J. Jeffrey, and D. E. Knuth, "On the Lambert W function," *Advances in Computational mathematics*, vol. 5, no. 1, pp. 329–359, 1996.

[127] A. Lapidoth and S. M. Moser, "Capacity bounds via duality with applications to multiple-antenna systems on flat-fading channels," *IEEE Transactions on Information Theory*, vol. 49, no. 10, pp. 2426–2467, Oct. 2003.

[128] X. Li, E. BjÃűrnson, S. Zhou, and J. Wang, "Massive MIMO with multi-antenna users: When are additional user antennas beneficial?," in *2016 23rd International Conference on Telecommunications (ICT)*, pp. 1–6, 2016.

[129] V. Petrov, D. Moltchanov, and Y. Koucheryavy, "Interference and SINR in dense Terahertz networks," in *Proc. 2015 IEEE 82nd Vehicular Technology Conference (VTC2015-Fall)*, pp. 1–5, 2015.

APPENDIX A

PROOF OF THEOREM 1

Considering the decoding error at the receiver, we can derive the Mellin transform over service process as follows:

$$\begin{aligned}\mathcal{M}_{\mathcal{S}_m}(1-\theta_m) &= \mathbb{E}_{\gamma_m}\left[\epsilon_m + (1-\epsilon_m)e^{-\theta_m n_{\mathrm{d}} R_m(n_{\mathrm{d}},\epsilon_m)}\right] \\ &= \int_0^{\infty}\left[\epsilon_m + (1-\epsilon_m)e^{-\theta_m n_{\mathrm{d}} R_m(n_{\mathrm{d}},\epsilon_m)}\right] f_{\gamma_m}(\gamma_m)d\gamma_m \end{aligned} \tag{A.1}$$

where $\mathbb{E}_{\gamma_m}[\cdot]$ is the expectation operation with respect to γ_m. We define

$$f_m(n_{\mathrm{d}},\epsilon_m) \triangleq \frac{1+\gamma_m}{\exp\left(\sqrt{\frac{V(\gamma_m)}{n_{\mathrm{d}}}}Q^{-1}(\epsilon_m)\right)}. \tag{A.2}$$

Given the decoding error probability ϵ_m, the data rate $R_m(n_{\mathrm{d}},\epsilon_m)$ could become smaller than zero when the SINR is below a certain threshold γ_{th} [122]. As a result, the achievable data rate can be rewritten as follows:

$$R_m(n_{\mathrm{d}},\epsilon_m) = \max\left\{\log_2\left(f_m(n_{\mathrm{d}},\epsilon_m)\right), 0\right\}. \tag{A.3}$$

Accordingly, we can obtain the following equation:

$$\begin{aligned}\mathcal{M}_{\mathcal{S}_m}(1-\theta_m) &= (1-\epsilon_m)\left\{\int_0^{\infty}\left[f_m(n_{\mathrm{d}},\epsilon_m)\right]^{-\frac{\theta_m n_{\mathrm{d}}}{(\log 2)}} f_{\gamma_m}(\gamma_m)d\gamma_m + F_0(\gamma_m)\right\} + \epsilon_m \\ &= (1-\epsilon_m)\left\{\int_{\gamma_0}^{\infty}\left[\frac{1+\gamma_m}{\exp\left\{\sqrt{\frac{V(\gamma_m)}{n_{\mathrm{d}}}}Q^{-1}(\epsilon_m)\right\}}\right]^{-\frac{\theta_m n_{\mathrm{d}}}{(\log 2)}} f_{\gamma_m}(\gamma_m)d\gamma_m + F_0(\gamma_0)\right\} + \epsilon_m \end{aligned} \tag{A.4}$$

where

$$F_0(\gamma_0) \triangleq \int_0^{\gamma_0} 2(1+\kappa)\gamma_m e^{-(1+\kappa)\gamma_m-\kappa} I_0\left[2\sqrt{\kappa(1+\kappa)}\gamma_m\right] d\gamma_m. \tag{A.5}$$

Then, we can expand the Bessel function into an infinite series and obtain the following equation [123]:

$$\begin{aligned} F_0(\gamma_0) &= 2e^{-\kappa}\int_0^{\gamma_0} \gamma_m e^{-(1+\kappa)\gamma_m} \sum_{i=0}^{\infty} \frac{\kappa^i(\kappa+1)^{i+1}\left(\gamma_m\right)^i}{(i!)^2} d\gamma_m \\ &= \frac{2e^{-\kappa}}{\kappa+1}\sum_{i=0}^{\infty}\frac{\kappa^i}{(i!)^2}\gamma\left(i+2,(1+\kappa)\gamma_0\right). \end{aligned} \tag{A.6}$$

We define the following equation:

$$\begin{aligned} F_1(\gamma_0) &\triangleq \int_{\gamma_0}^{\infty} \left[\frac{1+\gamma_m}{e^{\sqrt{\frac{V(\gamma_m)}{n_{\mathrm{d}}}}Q^{-1}(\epsilon_m)}}\right]^{-\frac{\theta_m n_{\mathrm{d}}}{(\log 2)}} 2(1+\kappa)\gamma_m e^{-(1+\kappa)\gamma_m-\kappa} I_0\left[2\sqrt{\kappa(1+\kappa)}\gamma_m\right] d\gamma_m \\ &= 2e^{-\kappa}\int_{\gamma_0}^{\infty} \left[\frac{1+\gamma_m}{e^{\sqrt{\frac{V(\gamma_m)}{n_{\mathrm{d}}}}Q^{-1}(\epsilon_m)}}\right]^{-\frac{\theta_m n_{\mathrm{d}}}{(\log 2)}} \gamma_m e^{-(1+\kappa)\gamma_m} \sum_{i=0}^{\infty}\frac{\kappa^i(\kappa+1)^{i+1}\left(\gamma_m\right)^i}{(i!)^2} d\gamma_m. \end{aligned} \tag{A.7}$$

In the high-end SNR region ($\gamma_m \gg 1$), the channel dispersion $V(\gamma_m) \to 1$. Correspondingly, we can rewrite Eq. (A.7) as follows:

$$\begin{aligned} F_1(\gamma_0) &= 2e^{-\kappa}\sum_{i=0}^{\infty}\frac{\kappa^i(\kappa+1)^{i+1}}{(i!)^2}\int_{\gamma_0}^{\infty}\left(\gamma_m\right)^{i+1-\frac{\theta_m n_{\mathrm{d}}}{(\log 2)}} e^{-(1+\kappa)\gamma_m} d\gamma_m \\ &= 2e^{-\kappa}\left[e^{-\sqrt{n_{\mathrm{d}}}}Q^{-1}(\epsilon_m)\right]^{\frac{\theta_m n_{\mathrm{d}}}{(\log 2)}}\sum_{i=0}^{\infty}\frac{\kappa^i(\kappa+1)^{\frac{\theta_m n_{\mathrm{d}}}{(\log 2)}-1}}{(i!)^2}\Gamma\left(i+2-\frac{\theta_m n_{\mathrm{d}}}{(\log 2)},(1+\kappa)\gamma_0\right). \end{aligned} \tag{A.8}$$

Therefore, by substituting Eqs. (A.6) and (A.8) back into Eq. (A.4), we can obtain the results in Eq. (2.30), which completes the proof of Theorem 1.

APPENDIX B

PROOF OF THEOREM 2

To derive the average decoding error probability function, first we introduce an approximation of the Q-function as follows:

$$Q\left(\frac{C\left(\gamma_m\right)-R_m}{\sqrt{V\left(\gamma_m\right)/n_{\mathrm{d}}}}\right)\approx\Psi(\gamma_m) \tag{B.1}$$

where the function $\Psi(\gamma_m)$ is given as follows [124]:

$$\Psi(\gamma_m)=\begin{cases}1, & \gamma_m\leq\zeta_{m,\mathrm{l}};\\ \frac{1}{2}-\vartheta_m\sqrt{n_{\mathrm{d}}}\left(\gamma_m-2^{R_m-1}\right), & \zeta_{m,\mathrm{l}}<\gamma_m<\zeta_{m,\mathrm{u}};\\ 0, & \gamma_m\geq\zeta_{m,\mathrm{u}},\end{cases} \tag{B.2}$$

where $\vartheta_m\triangleq\frac{1}{2\pi\sqrt{2^{2R_m-1}}}$, $\zeta_{m,\mathrm{l}}\triangleq 2^{R_m-1}-\frac{1}{2\vartheta_m\sqrt{n_{\mathrm{d}}}}$, and $\zeta_{m,\mathrm{u}}\triangleq 2^{R_m-1}+\frac{1}{2\vartheta_m\sqrt{n_{\mathrm{d}}}}$. Taking expectation over Eqs. (2.37) and (B.2), we can obtain the following equation:

$$\begin{aligned}\mathbb{E}_{\gamma_m}\left[\epsilon_m\left(n_{\mathrm{d}},\gamma_m\right)\right]\approx F_{\gamma_m}\left(2^{R_m-1}-\frac{1}{2\vartheta_m\sqrt{n_{\mathrm{d}}}}\right)+\left[\frac{1}{2}+\vartheta_m\sqrt{n_{\mathrm{d}}}\left(e^{R_m}-1\right)\right]\left[F_{\gamma_m}\left(2^{R_m-1}+\frac{1}{2\vartheta_m\sqrt{n_{\mathrm{d}}}}\right)\right.\\ \left.-F_{\gamma_m}\left(2^{R_m-1}-\frac{1}{2\vartheta_m\sqrt{n_{\mathrm{d}}}}\right)\right]-\vartheta_m\sqrt{n_{\mathrm{d}}}\int_{2^{R_m-1}-\frac{1}{2\vartheta_m\sqrt{n_{\mathrm{d}}}}}^{2^{R_m-1}+\frac{1}{2\vartheta_m\sqrt{n_{\mathrm{d}}}}}\gamma_m f_{\gamma_m}(\gamma_m)d\gamma_m\end{aligned} \tag{B.3}$$

where $F_{\gamma_m}(\gamma_m)$ is the cumulative probability function (CDF) of SINR γ_m. Using Eqs. (2.35) and (2.36), we can derive the CDF of SINR as follows:

$$F_{\gamma_m}(\gamma_m)=1-\sum_{k=1}^{K_{\mathrm{a}}}\left(1-e^{-\xi_{k,m}\gamma_m}\right). \tag{B.4}$$

Plugging Eq. (B.4) back into Eq. (B.3), we obtain:

$$\begin{aligned}\mathbb{E}_{\gamma_m}\left[\epsilon_m\left(n_{\mathrm{d}},\gamma_m\right)\right] \approx & 1-\sum_{k=1}^{K_{\mathrm{a}}}\left[1-e^{-\xi_{k,m}\left(2^{R_m-1}-\frac{1}{2\vartheta_m\sqrt{n_{\mathrm{d}}}}\right)}\right]+\left[\frac{1}{2}+\vartheta_m\sqrt{n_{\mathrm{d}}}\left(e^{R_m}-1\right)\right] \\ & \times\left[\sum_{k=1}^{K_{\mathrm{a}}} e^{-\xi_{k,m}\left(2^{R_m-1}-\frac{1}{2\vartheta_m\sqrt{n_{\mathrm{d}}}}\right)}-\sum_{k=1}^{K_{\mathrm{a}}} e^{-\xi_{k,m}\left(2^{R_m-1}+\frac{1}{2\vartheta_m\sqrt{n_{\mathrm{d}}}}\right)}\right]-\vartheta_m\sqrt{n_{\mathrm{d}}} \\ & \times\left\{\left(2^{R_m-1}-\frac{1}{2\vartheta_m\sqrt{n_{\mathrm{d}}}}\right)\left[\sum_{k=1}^{K_{\mathrm{a}}} e^{-\xi_{k,m}\left(2^{R_m-1}-\frac{1}{2\vartheta_m\sqrt{n_{\mathrm{d}}}}\right)}\right]-\left(2^{R_m-1}+\frac{1}{2\vartheta_m\sqrt{n_{\mathrm{d}}}}\right)\right. \\ & \left.\times\left[\sum_{k=1}^{K_{\mathrm{a}}} e^{-\xi_{k,m}\left(2^{R_m-1}+\frac{1}{2\vartheta_m\sqrt{n_{\mathrm{d}}}}\right)}\right]+\sum_{k=1}^{K_{\mathrm{a}}}\int_{2^{R_m-1}-\frac{1}{2\vartheta_m\sqrt{n_{\mathrm{d}}}}}^{2^{R_m-1}+\frac{1}{2\vartheta_m\sqrt{n_{\mathrm{d}}}}} \frac{e^{-\xi_{k,m}\gamma_m}}{\gamma_m} d\gamma_m\right\}.\end{aligned} \tag{B.5}$$

Then, using the definition of exponential integral function, we can obtain Eq. (2.39), completing the proof of Theorem 2.

APPENDIX C

PROOF OF LEMMA 2

Using the Chernoff bound, we have $Q(x) \leq \frac{1}{2}e^{-\frac{x^2}{2}}$ if $x \geq 0$. We can derive an upper bound on the average decoding error probability function $\mathbb{E}_{\gamma_m}\left[\epsilon_m\left(n_{\mathrm{d}}, \gamma_m\right)\right]$ for mobile user m in the high-end SNR regime as follows:

$$\begin{aligned}\mathbb{E}_{\gamma_m}\left[\epsilon_m\left(n_{\mathrm{d}}, \gamma_m\right)\right] &= \int_0^{\infty} \mathbb{E}_{\gamma_m}\left[Q\left(\widetilde{\Phi}\left(n_{\mathrm{d}}, \gamma_m\right)\right)\right] f_{\gamma_m}(\gamma_m) d\gamma_m \\ &\leq \frac{1}{2}\int_0^{\infty} \mathbb{E}_{\gamma_m}\left[e^{-\frac{\widetilde{\Phi}^2\left(n_{\mathrm{d}}, \gamma_m\right)}{2}}\right] f_{\gamma_m}(\gamma_m) d\gamma_m \end{aligned} \tag{C.1}$$

where $f_{\gamma_m}(\gamma_m)$ is the PDF of the SINR γ_m over Rayleigh wireless fading channels, which is given as follows:

$$f_{\gamma_m}(\gamma_m) = \sum_{k=1}^{K_{\mathrm{a}}} \xi_{k,m} e^{-\xi_{k,m}\gamma_m}. \tag{C.2}$$

Then, using Eq. (2.20), we can obtain:

$$\mathbb{E}_{\gamma_m}\left[e^{-\frac{\widetilde{\Phi}^2\left(n_{\mathrm{d}}, \gamma_m\right)}{2}}\right] = \mathbb{E}_{\gamma_m}\left[e^{-\frac{n_{\mathrm{d}}\left(\log_2(\gamma_m+1)-R_m\right)^2}{2}}\right] = \int_0^{\infty} e^{-\frac{n_{\mathrm{d}}\left(\log_2(\gamma_m+1)-R_m\right)^2}{2}} f_{\gamma_m}(\gamma_m) d\gamma_m. \tag{C.3}$$

Since we can easily show that $\widetilde{\Phi}\left(n_{\mathrm{d}}, \gamma_m\right)$ is concave in γ_m. As a result, we can derive a lower bound on the function $\mathbb{E}_{\gamma_m}\left[e^{-\frac{\widetilde{\Phi}^2\left(n_{\mathrm{d}}, \gamma_m\right)}{2}}\right]$ when $\widetilde{\Phi}\left(n_{\mathrm{d}}, \gamma_m\right)$ is replaced by its Taylor expansion at any point. Using the Taylor expansion of $\widetilde{\Phi}\left(n_{\mathrm{d}}, \gamma_m\right)$ at $\gamma_m = \nu_m$, we can obtain the following equation:

$$\mathbb{E}_{\gamma_m}\left[e^{-\frac{\widetilde{\Phi}^2\left(n_{\mathrm{d}}, \gamma_m\right)}{2}}\right] \geq \int_0^{\infty} \sum_{k=1}^{K_{\mathrm{a}}} e^{-\frac{n_{\mathrm{d}}}{2}\left(\gamma_m-\nu_m\right)^2} \xi_{k,m} e^{-\xi_{k,m}\gamma_m} d\gamma_m. \tag{C.4}$$

Letting $t_m \triangleq \sqrt{\frac{n_\mathrm{d}}{2}}\left(\gamma_m - \nu_m\right)$, we have

$$\begin{aligned}\mathbb{E}_{\gamma_m}\left[e^{-\frac{\tilde{\Phi}^2(n_\mathrm{d},\gamma_m)}{2}}\right] &\geq \sqrt{\frac{2}{n_\mathrm{d}}}\sum_{k=1}^{K_\mathrm{a}}\xi_{k,m}e^{-\xi_{k,m}\nu_m}\int_{-\frac{\sqrt{n_\mathrm{d}}}{\sqrt{2}}\nu_m}^{\infty} e^{-(t_m)^2}e^{-\frac{\sqrt{2}\xi_{k,m}}{\sqrt{n_\mathrm{d}}}t_m}dt_m \\ &= \sqrt{\frac{2}{n_\mathrm{d}}}\sum_{k=1}^{K_\mathrm{a}}\xi_{k,m}e^{-\xi_{k,m}\nu_m}\int_{-\frac{\sqrt{n_\mathrm{d}}}{\sqrt{2}}\nu_m}^{\infty} e^{\frac{\left(\xi_{k,m}\right)^2}{2n_\mathrm{d}}}e^{-\left(t_m+\frac{\xi_{k,m}}{\sqrt{2n_\mathrm{d}}}\right)^2}dt_m. \end{aligned} \tag{C.5}$$

Letting $\widetilde{t}_m \triangleq t_m + \frac{\xi_{k,m}}{\sqrt{2n_\mathrm{d}}}$, we can derive a lower bound on the function $\mathbb{E}_{\gamma_m}\left[e^{-\frac{\tilde{\Phi}^2(n_\mathrm{d},\gamma_m)}{2}}\right]$ as follows:

$$\begin{aligned}\mathbb{E}_{\gamma_m}\left[e^{-\frac{\tilde{\Phi}^2(n_\mathrm{d},\gamma_m)}{2}}\right] &\geq \sqrt{\frac{2}{n_\mathrm{d}}}\sum_{k=1}^{K_\mathrm{a}}\xi_{k,m}\exp\left\{\frac{\left(\xi_{k,m}\right)^2}{2n_\mathrm{d}} - \xi_{k,m}\nu_m\right\}\int_{\frac{\xi_{k,m}}{\sqrt{2n_\mathrm{d}}}-\frac{\sqrt{n_\mathrm{d}}}{\sqrt{2}}\nu_m}^{\infty} e^{-\left(\widetilde{t}_m\right)^2}d\widetilde{t}_m \\ &= \frac{\sqrt{\pi}}{2\sqrt{2n_\mathrm{d}}}\sum_{k=1}^{K_\mathrm{a}}\left\{\xi_{k,m}\exp\left\{\frac{\left(\xi_{k,m}\right)^2}{2n_\mathrm{d}} - \xi_{k,m}\nu_m\right\}\left[1-\mathrm{erf}\left(\frac{\xi_{k,m}}{\sqrt{2n_\mathrm{d}}} - \frac{\sqrt{n_\mathrm{d}}}{\sqrt{2}}\nu_m\right)\right]\right\}\end{aligned} \tag{C.6}$$

where $\mathrm{erf}(x) \triangleq \frac{2}{\sqrt{\pi}}\int_0^x e^{-t^2}dt$ is the error function. As a result, by plugging Eq. (C.6) back into Eq. (C.1), we can obtain Eq. (2.41), which completes the proof of Lemma 2.

APPENDIX D

PROOF OF THEOREM 3

For presenting convenience, we start with Claim 2.

Claim 2. To analyze the convexity of the minimization problem $\mathbf{P_2}$, we apply the chain rule for second-order derivative and obtain the following equation:

$$\frac{\partial^2 \mathcal{M}_{\mathcal{S}_m}(1-\theta_m)}{\partial R_m^2} = \frac{\partial^2 \mathcal{M}_{\mathcal{S}_m}(1-\theta_m)}{\partial \epsilon_m^2\left(n_{\mathrm{d}}, \gamma_m\right)} \left[\frac{\partial \epsilon_m\left(n_{\mathrm{d}}, \gamma_m\right)}{\partial R_m}\right]^2 + \frac{\partial \mathcal{M}_{\mathcal{S}_m}(1-\theta_m)}{\partial \epsilon_m\left(n_{\mathrm{d}}, \gamma_m\right)} \frac{\partial^2 \epsilon_m\left(n_{\mathrm{d}}, \gamma_m\right)}{\partial R_m^2}. \tag{D.1}$$

To analyze the convexity of the Mellin transform over service process $\mathcal{M}_{\mathcal{S}_m}(1-\theta_m)$, first we need to investigate the following equations when $\theta_m > 0$:

$$\begin{cases} \frac{\partial \mathcal{M}_{\mathcal{S}_m}(1-\theta_m)}{\partial \epsilon_m(n_{\mathrm{d}}, \gamma_m)} = 1 - e^{-\theta_m n_{\mathrm{d}} R_m} > 0; \\ \frac{\partial^2 \mathcal{M}_{\mathcal{S}_m}(1-\theta_m)}{\partial \epsilon_m^2(n_{\mathrm{d}}, \gamma_m)} = 0. \end{cases} \tag{D.2}$$

Then, using Eq. (2.47) and (D.2), we can show that $\frac{\partial^2 \mathcal{M}_{\mathcal{S}_m}(1-\theta_m)}{\partial R_m^2} > 0$, completing the proof of Claim 2 in Theorem 2.

Claim 1. Applying the sufficient conditions for convexity, we can prove that the Mellin transform function $\mathcal{M}_{\mathcal{S}_m}(1-\theta_m)$ is strictly convex with respect to the achievable data rate R_m for $\theta_m > 0$, completing the proof of Claim 1 in Theorem 2.

Claim 3. Due to the property of strict convexity and uniqueness of optimal solutions [125], there exists the unique optimal rate adaptation policy R_m^{opt} that minimizes problem $\mathbf{P_2}$ for each mobile user m when $\theta_m > 0$. Taking the first-order derivative of the Mellin transform function

$\mathcal{M}_{\mathcal{S}_m}$ with respect to R_m, we can obtain the following equation:

$$\frac{\partial \mathcal{M}_{\mathcal{S}_m}(1-\theta_m)}{\partial R_m} = \frac{\partial \mathbb{E}_{\gamma_m}\left[\epsilon_m\left(n_{\mathrm{d}},\gamma_m\right)\right]}{\partial R_m} - \frac{\partial \mathbb{E}_{\gamma_m}\left[\epsilon_m\left(n_{\mathrm{d}},\gamma_m\right)\right]}{\partial R_m} e^{-\theta_m n_{\mathrm{d}} R_m} - \left\{1 - \mathbb{E}_{\gamma_m}\left[\epsilon_m\left(n_{\mathrm{d}},\gamma_m\right)\right]\right\} \times \theta_m n_{\mathrm{d}} e^{-\theta_m n_{\mathrm{d}} R_m}. \tag{D.3}$$

Setting $\frac{\partial \mathcal{M}_{\mathcal{S}_m}(1-\theta_m)}{\partial R_m} = 0$, we have

$$\frac{\partial \mathbb{E}_{\gamma_m}\left[\epsilon_m\left(n_{\mathrm{d}},\gamma_m\right)\right]}{\partial R_m}\left(1 - e^{-\theta_m n_{\mathrm{d}} R_m}\right) - \left\{1 - \mathbb{E}_{\gamma_m}\left[\epsilon_m\left(n_{\mathrm{d}},\gamma_m\right)\right]\right\}\theta_m n_{\mathrm{d}} e^{-\theta_m n_{\mathrm{d}} R_m} = 0. \tag{D.4}$$

We can rewrite Eq. (D.4) as follows:

$$e^{\theta_m n_{\mathrm{d}} R_m} - 1 = \frac{\theta_m n_{\mathrm{d}}\left(1 - \mathbb{E}_{\gamma_m}\left[\epsilon_m\left(n_{\mathrm{d}},\gamma_m\right)\right]\right)}{\frac{\partial \mathbb{E}_{\gamma_m}\left[\epsilon_m\left(n_{\mathrm{d}},\gamma_m\right)\right]}{\partial R_m}}. \tag{D.5}$$

Using Eqs. (2.44) and (2.45), we can obtain the following equation:

$$\begin{aligned} R_m &= \frac{1}{\theta_m n_{\mathrm{d}}} \log\left\{1 + \frac{\theta_m n_{\mathrm{d}}\left(1 - \mathbb{E}_{\gamma_m}\left[\epsilon_m\left(n_{\mathrm{d}},\gamma_m\right)\right]\right)}{\frac{\partial \mathbb{E}_{\gamma_m}\left[\epsilon_m\left(n_{\mathrm{d}},\gamma_m\right)\right]}{\partial R_m}}\right\} \\ &= \frac{1}{\theta_m n_{\mathrm{d}}} \log\left\{1 + \frac{\theta_m \sqrt{2\pi n_{\mathrm{d}}}\left\{1 - \mathbb{E}_{\gamma_m}\left[\epsilon_m\left(n_{\mathrm{d}},\gamma_m\right)\right]\right\}}{\mathbb{E}_{\gamma_m}\left[e^{-\frac{\Phi^2(n_{\mathrm{d}},\gamma_m)}{2}}\left(\frac{1}{\sqrt{1-\frac{1}{(1+\gamma_m)^2}}}\right)\right]}\right\} \end{aligned} \tag{D.6}$$

where $\mathbb{E}_{\gamma_m}\left[\epsilon_m\left(n_{\mathrm{d}},\gamma_m\right)\right]$ is given by Eq. (2.39). In the high-end SNR regime, we have $V\left(\gamma_m\right) = 1 - \left(1+\gamma_m\right)^{-2} \to 1$. Using the Chernoff bound, we have $Q(x) \leq \frac{1}{2}e^{-\frac{x^2}{2}}$ when $x \geq 0$. Applying

Eq. (D.6), we can obtain the following equation:

$$
\begin{aligned}
R_m &= \frac{1}{\theta_m n_{\mathrm{d}}} \log \left\{ 1 + \frac{\theta_m \sqrt{2\pi n_{\mathrm{d}}} \left\{ 1 - \mathbb{E}_{\gamma_m} \left[Q \left(\widetilde{\Phi} \left(n_{\mathrm{d}}, \gamma_m \right) \right) \right] \right\}}{\mathbb{E}_{\gamma_m} \left[e^{-\frac{\widetilde{\Phi}^2 (n_{\mathrm{d}}, \gamma_m)}{2}} \right]} \right\} \\
&\geq \frac{1}{\theta_m n_{\mathrm{d}}} \log \left\{ 1 + \frac{\theta_m \sqrt{2\pi n_{\mathrm{d}}} \left(1 - \mathbb{E}_{\gamma_m} \left[\frac{1}{2} e^{-\frac{\widetilde{\Phi}^2 (n_{\mathrm{d}}, \gamma_m)}{2}} \right] \right)}{\mathbb{E}_{\gamma_m} \left[e^{-\frac{\widetilde{\Phi}^2 (n_{\mathrm{d}}, \gamma_m)}{2}} \right]} \right\} \\
&= \frac{1}{\theta_m n_{\mathrm{d}}} \log \left\{ 1 + \theta_m \sqrt{2\pi n_{\mathrm{d}}} \left\{ \frac{1}{\mathbb{E}_{\gamma_m} \left[e^{-\frac{\widetilde{\Phi}^2 (n_{\mathrm{d}}, \gamma_m)}{2}} \right]} - \frac{1}{2} \right\} \right\}.
\end{aligned} \tag{D.7}
$$

Then, plugging Eq. (C.6) back into Eq. (D.7), we have:

$$
\begin{aligned}
R_m \approx \frac{1}{\theta_m n_{\mathrm{d}}} \log \Bigg\{ 1 + \theta_m \sqrt{2\pi n_{\mathrm{d}}} \Bigg\{ & - \frac{1}{2} + \frac{\sqrt{2n_{\mathrm{d}}}}{\sqrt{\pi}} \left[\sum_{k=1}^{K_{\mathrm{a}}} \xi_{k,m} \exp \left\{ \frac{\left(\xi_{k,m} \right)^2}{2n_{\mathrm{d}}} - \xi_{k,m} \nu_m \right\} \right. \\
& \left. \times \left\{ 1 - \mathrm{erf} \left(\frac{\xi_{k,m}}{\sqrt{2n_{\mathrm{d}}}} - \frac{\sqrt{n_{\mathrm{d}}}}{\sqrt{2}} \nu_m \right) \right\} \right]^{-1} \Bigg\} \Bigg\}.
\end{aligned} \tag{D.8}
$$

Since the error function $-1 \leq \mathrm{erf}(x) \leq 1$, we can remove the error function from Eq. (D.8) and obtain the following equation:

$$
e^{\theta_m n_{\mathrm{d}} R_m} \approx 1 - \frac{\theta_m \sqrt{2\pi n_{\mathrm{d}}}}{2} + \frac{2\theta_m n_{\mathrm{d}}}{\sum_{k=1}^{K_{\mathrm{a}}} \xi_{k,m}} \left\{ \exp \left\{ \frac{\left(\xi_{k,m} \right)^2}{2n_{\mathrm{d}}} - \xi_{k,m} \nu_m \right\} \right\}^{-1}. \tag{D.9}
$$

Substituting $\nu_m = 2^{R_m} - 1$ back into Eq. (D.9), we have

$$
e^{\theta_m n_{\mathrm{d}} R_m} - \sum_{k=1}^{K_{\mathrm{a}}} \left[\frac{2\theta_m n_{\mathrm{d}} e^{\xi_{k,m} 2^{R_m}}}{\xi_{k,m} \exp \left\{ \frac{\left(\xi_{k,m} \right)^2}{2n_{\mathrm{d}}} + \xi_{k,m} \right\}} \right] \approx 1 - \frac{\theta_m \sqrt{2\pi n_{\mathrm{d}}}}{2} \tag{D.10}
$$

where $\xi_{k,m}$ is given by Eq. (2.36). Let $z_m \triangleq \sum_{k=1}^{K_\mathrm{a}} \xi_{k,m} 2^{R_m}$. We have

$$\left(\sum_{k=1}^{K_\mathrm{a}} \xi_{k,m} \right)^{-\frac{\theta_m n_\mathrm{d}}{(\log 2)}} (z_m)^{\frac{\theta_m n_\mathrm{d}}{(\log 2)}} - 2\theta_m n_\mathrm{d} e^{z_m} \left\{ \sum_{k=1}^{K_\mathrm{a}} \left[\xi_{k,m} \exp\left\{ \frac{(\xi_{k,m})^2}{2n_\mathrm{d}} + \xi_{k,m} \right\} \right] \right\}^{-1}$$
$$\approx 1 - \frac{\theta_m \sqrt{2\pi n_\mathrm{d}}}{2}. \tag{D.11}$$

Then, solving for the $\frac{\theta_m n_\mathrm{d}}{(\log 2)}$th root on both sides of Eq. (D.11), we can obtain:

$$\left(\sum_{k=1}^{K_\mathrm{a}} \xi_{k,m} \right)^{-1} z_m - e^{z_m \frac{(\log 2)}{\theta_m n_\mathrm{d}}} \left[\frac{2\theta_m n_\mathrm{d}}{\sum_{k=1}^{K_\mathrm{a}} \xi_{k,m} \exp\left\{ \frac{(\xi_{k,m})^2}{2n_\mathrm{d}} + \xi_{k,m} \right\}} \right]^{\frac{(\log 2)}{\theta_m n_\mathrm{d}}} \approx \left[1 - \frac{\theta_m \sqrt{2\pi n_\mathrm{d}}}{2} \right]^{\frac{(\log 2)}{\theta_m n_\mathrm{d}}}. \tag{D.12}$$

Let $\widetilde{z}_m \triangleq z_m \frac{(\log 2)}{\theta_m n_\mathrm{d}}$. After some algebra manipulations, we have

$$\frac{(\log 2) \sum_{k=1}^{K_\mathrm{a}} \xi_{k,m}}{\theta_m n_\mathrm{d}} \left[\frac{2\theta_m n_\mathrm{d}}{\sum_{k=1}^{K_\mathrm{a}} \xi_{k,m} \exp\left\{ \frac{(\xi_{k,m})^2}{2n_\mathrm{d}} + \xi_{k,m} \right\}} \right]^{\frac{(\log 2)}{\theta_m n_\mathrm{d}}} e^{\widetilde{z}_m}$$
$$\approx \widetilde{z}_m - \frac{(\log 2)}{\theta_m n_\mathrm{d}} \left(\sum_{k=1}^{K_\mathrm{a}} \xi_{k,m} \right) \left[1 - \frac{\theta_m \sqrt{2\pi n_\mathrm{d}}}{2} \right]^{\frac{(\log 2)}{\theta_m n_\mathrm{d}}}. \tag{D.13}$$

Then, multiplying the following expression on both sides of Eq. (D.13):

$$\left[e^{-\widetilde{z}_m} + \frac{(\log 2)}{\theta_m n_\mathrm{d}} \left(\sum_{k=1}^{K_\mathrm{a}} \xi_{k,m} \right) \left[1 - \frac{\theta_m \sqrt{2\pi n_\mathrm{d}}}{2(\log 2)} \right]^{\frac{(\log 2)}{\theta_m n_\mathrm{d}}} \right], \tag{D.14}$$

we can obtain:

$$\begin{aligned}
&\frac{(\log 2)\sum_{k=1}^{K_{\mathrm{a}}}\xi_{k,m}}{\theta_m n_{\mathrm{d}}}\left[\frac{2\theta_m n_{\mathrm{d}}}{\sum_{k=1}^{K_{\mathrm{a}}}\xi_{k,m}\exp\left\{\frac{\left(\xi_{k,m}\right)^2}{2n_{\mathrm{d}}}+\xi_{k,m}\right\}}\right]^{\frac{(\log 2)}{\theta_m n_{\mathrm{d}}}}\exp\left\{\frac{(\log 2)}{\theta_m n_{\mathrm{d}}}\left(\sum_{k=1}^{K_{\mathrm{a}}}\xi_{k,m}\right)\right.\\
&\quad\left.\times\left(1-\frac{\theta_m\sqrt{2\pi n_{\mathrm{d}}}}{2}\right)^{\frac{(\log 2)}{\theta_m n_{\mathrm{d}}}}\right\}\\
&\approx\left[\widetilde{z}_m-\frac{(\log 2)}{\theta_m n_{\mathrm{d}}}\left(\sum_{k=1}^{K_{\mathrm{a}}}\xi_{k,m}\right)\left(1-\frac{\theta_m\sqrt{2\pi n_{\mathrm{d}}}}{2}\right)^{\frac{(\log 2)}{\theta_m n_{\mathrm{d}}}}\right]\exp\left\{-\widetilde{z}_m+\frac{(\log 2)}{\theta_m n_{\mathrm{d}}}\left(\sum_{k=1}^{K_{\mathrm{a}}}\xi_{k,m}\right)\right.\\
&\quad\left.\times\left(1-\frac{\theta_m\sqrt{2\pi n_{\mathrm{d}}}}{2}\right)^{\frac{(\log 2)}{\theta_m n_{\mathrm{d}}}}\right\}.
\end{aligned}\tag{D.15}$$

Therefore, using the Lambert W function [126], we can derive the approximate optimal rate adaptation policy R_m^{opt} for our proposed FBC based CF m-MIMO schemes in the high-end SNR region as follows:

$$\begin{aligned}
R_m^{\mathrm{opt}}\approx&\log_2\left\{\frac{\theta_m n_{\mathrm{d}}}{(\log 2)\sum_{k=1}^{K_{\mathrm{a}}}\xi_{k,m}}\left[\frac{(\log 2)}{\theta_m n_{\mathrm{d}}}\left(\sum_{k=1}^{K_{\mathrm{a}}}\xi_{k,m}\right)\left(1-\frac{\theta_m\sqrt{2\pi n_{\mathrm{d}}}}{2}\right)^{\frac{(\log 2)}{\theta_m n_{\mathrm{d}}}}\right.\right.\\
&-\mathcal{W}\left(-\frac{(\log 2)\sum_{k=1}^{K_{\mathrm{a}}}\xi_{k,m}}{\theta_m n_{\mathrm{d}}}\left[\frac{2\theta_m n_{\mathrm{d}}}{\sum_{k=1}^{K_{\mathrm{a}}}\xi_{k,m}\exp\left\{\frac{\left(\xi_{k,m}\right)^2}{2n_{\mathrm{d}}}+\xi_{k,m}\right\}}\right]^{\frac{(\log 2)}{\theta_m n_{\mathrm{d}}}}\right.\\
&\left.\left.\left.\times\exp\left\{\frac{(\log 2)}{\theta_m n_{\mathrm{d}}}\left(\sum_{k=1}^{K_{\mathrm{a}}}\xi_{k,m}\right)\left(1-\frac{\theta_m\sqrt{2\pi n_{\mathrm{d}}}}{2}\right)^{\frac{(\log 2)}{\theta_m n_{\mathrm{d}}}}\right\}\right)\right]\right\}.
\end{aligned}\tag{D.16}$$

Thus, we complete the proof of Claim 3 in Theorem 3.

APPENDIX E

PROOF OF LEMMA 5

To derive a lower bound on the channel capacity, we first need to analyze the mutual information $I\left(\mathbf{X}_m^{\widehat{n}l}; \boldsymbol{y}_m^{\widehat{n}l} | \widetilde{\boldsymbol{h}}_{k,m}\right)$ as follows [127]:

$$I\left(\mathbf{X}_m^{\widehat{n}l}; \boldsymbol{y}_m^{\widehat{n}l} | \widetilde{\boldsymbol{h}}_{k,m}\right) = H\left(\mathbf{X}_m^{\widehat{n}l} | \widetilde{\boldsymbol{h}}_{k,m}\right) - H\left(\mathbf{X}_m^{\widehat{n}l} | \boldsymbol{y}_m^{\widehat{n}l}, \widetilde{\boldsymbol{h}}_{k,m}\right) \tag{E.1}$$

where $H(\cdot)$ represents the function of information entropy. We can derive $H\left(\mathbf{X}_m^{\widehat{n}l} | \widetilde{\boldsymbol{h}}_{k,m}\right)$ in Eq. (E.1) as follows:

$$H\left(\mathbf{X}_m^{\widehat{n}l} | \widetilde{\boldsymbol{h}}_{k,m}\right) = \log_2\left(\pi e \mathbf{I}_{N_T}\right). \tag{E.2}$$

Then, define $\widehat{\mathbf{X}}_m^{\widehat{n}l}$ as the linear MMSE estimate of $\mathbf{X}_m^{\widehat{n}l}$ given $\boldsymbol{y}_m^{\widehat{n}l}$ and $\widetilde{\boldsymbol{h}}_{k,m}$. Correspondingly, using the suboptimal beam-training precoders $\mathbf{F}_{k,m}^{\mathrm{R}}$ and $\mathbf{F}_{k,m}^{\mathrm{B}}$ derived in **Algorithm 1**, we can obtain the following equation:

$$\widehat{\mathbf{X}}_m^{\widehat{n}l} = \left(\widetilde{\boldsymbol{h}}_{k,m}\right)^{\dagger} \boldsymbol{\Xi}_{k,m} \boldsymbol{y}_m^{\widehat{n}l} \tag{E.3}$$

where

$$\boldsymbol{\Xi}_{k,m} \triangleq \left(\mathbb{E}_{\widetilde{\boldsymbol{h}}_{k,m}} \left[\boldsymbol{h}_{k,m} \sum_{m'=1}^{K_{\mathrm{u}}} \sum_{k \in \mathcal{K}(m')} \mathbf{F}_{k,m'}^{\mathrm{R}} \mathbf{F}_{k,m'}^{\mathrm{B}} \boldsymbol{\Omega}_{k,m'} \times \left(\mathbf{F}_{k,m'}^{\mathrm{R}} \mathbf{F}_{k,m'}^{\mathrm{B}}\right)^{\dagger} \left(\boldsymbol{h}_{k,m}\right)^{\dagger} \right] + \sigma^2 \right)^{-1}. \tag{E.4}$$

Correspondingly, we can derive an upper bound on the conditional entropy $H\left(\mathbf{X}_m^{\widehat{n}l} | \boldsymbol{y}_m^{\widehat{n}l}, \widetilde{\boldsymbol{h}}_{k,m}\right)$ as in the following equation:

$$\begin{aligned} H\left(\mathbf{X}_m^{\widehat{n}l} | \boldsymbol{y}_m^{\widehat{n}l}, \widetilde{\boldsymbol{h}}_{k,m}\right) &\leq \mathbb{E}_{\widetilde{\boldsymbol{h}}_{k,m}} \left[\left(\mathbf{X}_m^{\widehat{n}l} - \widehat{\mathbf{X}}_m^{\widehat{n}l}\right) \left(\mathbf{X}_m^{\widehat{n}l} - \widehat{\mathbf{X}}_m^{\widehat{n}l}\right)^{\dagger} \right] \\ &= \log_2\left(\pi e \det\left(\mathbf{I}_{N_T} - \left(\widetilde{\boldsymbol{h}}_{k,m}\right)^{\dagger} \boldsymbol{\Xi}_{k,m} \widetilde{\boldsymbol{h}}_{k,m} \right) \right). \end{aligned} \tag{E.5}$$

Then, plugging Eqs. (E.2) and (E.5) back into Eq. (E.1), we can derive a lower bound on the mutual information $I\left(\mathbf{X}_m^{\widehat{n}l}; \boldsymbol{y}_m^{\widehat{n}l}|\widetilde{\boldsymbol{h}}_{k,m}\right)$ as follows [128]:

$$\begin{aligned} I\left(\mathbf{X}_m^{\widehat{n}l}; \boldsymbol{y}_m^{\widehat{n}l}|\widetilde{\boldsymbol{h}}_{k,m}\right) &\geq \log_2\left(\pi e \mathbf{I}_{N_T}\right) - \log_2\left(\pi e \det\left(\mathbf{I}_{N_T} - \left(\widetilde{\boldsymbol{h}}_{k,m}\right)^{\dagger} \boldsymbol{\Xi}_{k,m} \widetilde{\boldsymbol{h}}_{k,m}\right)\right) \\ &\geq \log_2\left(\det\left(\mathbf{I}_{N_T} + \left(\widetilde{\boldsymbol{h}}_{k,m}\right)^{\dagger}\left(\left(\boldsymbol{\Xi}_{k,m}\right)^{-1} - \widetilde{\boldsymbol{h}}_{k,m}\left(\widetilde{\boldsymbol{h}}_{k,m}\right)^{\dagger}\right)^{-1} \widetilde{\boldsymbol{h}}_{k,m}\right)\right). \end{aligned} \tag{E.6}$$

Accordingly, we can derive a lower bound on the channel capacity as follows:

$$\begin{aligned} C_m\left(\widetilde{\boldsymbol{h}}_{k,m}\right) &= \mathbb{E}_{\widetilde{\boldsymbol{h}}_{k,m}}\left[\max_{p_{\mathbf{X}_m^{\widehat{n}l}|\widetilde{\boldsymbol{h}}_{k,m}}} \left\{I\left(\mathbf{X}_m^{\widehat{n}l}; \boldsymbol{y}_m^{\widehat{n}l}|\widetilde{\boldsymbol{h}}_{k,m}\right)\right\}\right] \\ &\geq \mathbb{E}_{\widetilde{\boldsymbol{h}}_{k,m}}\left[\log_2\left(\det\left(\mathbf{I}_{N_T} + \left(\widetilde{\boldsymbol{h}}_{k,m}\right)^{\dagger}\left(\left(\boldsymbol{\Xi}_{k,m}\right)^{-1} - \widetilde{\boldsymbol{h}}_{k,m}\left(\widetilde{\boldsymbol{h}}_{k,m}\right)^{\dagger}\right)^{-1} \widetilde{\boldsymbol{h}}_{k,m}\right)\right)\right] \\ &= \mathbb{E}_{\widetilde{\boldsymbol{h}}_{k,m}}\left[\log_2\left(\det\left(\left(\left(\boldsymbol{\Xi}_{k,m}\right)^{-1} - \widetilde{\boldsymbol{h}}_{k,m}\left(\widetilde{\boldsymbol{h}}_{k,m}\right)^{\dagger}\right) + \left(\widetilde{\boldsymbol{h}}_{k,m}\right)^{\dagger}\widetilde{\boldsymbol{h}}_{k,m}\right)\right)\right] \\ &\quad - \mathbb{E}_{\widetilde{\boldsymbol{h}}_{k,m}}\left[\log_2\left(\det\left(\left(\boldsymbol{\Xi}_{k,m}\right)^{-1} - \widetilde{\boldsymbol{h}}_{k,m}\left(\widetilde{\boldsymbol{h}}_{k,m}\right)^{\dagger}\right)\right)\right] \end{aligned} \tag{E.7}$$

which is a lower bound on the channel capacity $C_m\left(\widetilde{\boldsymbol{h}}_{k,m}\right)$ as shown in Eq. (3.27). Therefore, we complete the proof of Lemma 5.

APPENDIX F

PROOF OF THEOREM 4

To derive an upper bound on the channel dispersion $V\left(\widehat{n}N_l\right)$, we need to proceed with the following steps. First, we start with variance as in the following equation:

$$\begin{aligned}\text{Var}\left[\boldsymbol{i}\left(\mathbf{X}_m^{\widehat{n}l};\boldsymbol{y}_m^{\widehat{n}l},\widetilde{\boldsymbol{h}}_{k,m}\right)\right] &= \text{Var}\left[\log\left(\frac{P_{\boldsymbol{y}_m^{\widehat{n}l}|\widetilde{\boldsymbol{h}}_{k,m},\mathbf{X}_m^{\widehat{n}l}}\left(\boldsymbol{y}_m^{\widehat{n}l}|\widetilde{\boldsymbol{h}}_{k,m},\mathbf{X}_m^{\widehat{n}l}\right)}{P_{\boldsymbol{y}_m^{\widehat{n}l}|\widetilde{\boldsymbol{h}}_{k,m}}\left(\boldsymbol{y}_m^{\widehat{n}l}|\widetilde{\boldsymbol{h}}_{k,m}\right)}\right)\right] \\ &\leq 2\Big(\text{Var}\left[\log\left(P_{\boldsymbol{y}_m^{\widehat{n}l}|\widetilde{\boldsymbol{h}}_{k,m},\mathbf{X}_m^{\widehat{n}l}}\left(\boldsymbol{y}_m^{\widehat{n}l}|\widetilde{\boldsymbol{h}}_{k,m},\mathbf{X}_m^{\widehat{n}l}\right)\right)\right] \\ &\quad + \text{Var}\left[\log\left(P_{\boldsymbol{y}_m^{\widehat{n}l}|\widetilde{\boldsymbol{h}}_{k,m}}\left(\boldsymbol{y}_m^{\widehat{n}l}|\widetilde{\boldsymbol{h}}_{k,m}\right)\right)\right]\Big) \end{aligned} \tag{F.1}$$

where Var$[\cdot]$ represents the variance. Second, using the beam-training precoder $\mathbf{F}_{k,m}^{\mathsf{B}}$ derived in **Algorithm 1**, we can apply the Poincará inequality to derive the following equation:

$$\begin{aligned}&\text{Var}\left[\log\left(P_{\boldsymbol{y}_m^{\widehat{n}l}|\widetilde{\boldsymbol{h}}_{k,m}}\left(\boldsymbol{y}_m^{\widehat{n}l}|\widetilde{\boldsymbol{h}}_{k,m}\right)\right)\right] \\ &\leq \mathbb{E}_{\widetilde{\boldsymbol{h}}_{k,m}}\left[\left\|\nabla\log\left(P_{\boldsymbol{y}_m^{\widehat{n}l}|\widetilde{\boldsymbol{h}}_{k,m}}\left(\boldsymbol{y}_m^{\widehat{n}l}|\widetilde{\boldsymbol{h}}_{k,m}\right)\right)\right\|^2\middle|\mathbf{X}_m^{\widehat{n}l}\right] \\ &= \frac{1}{\sigma^2}\mathbb{E}_{\widetilde{\boldsymbol{h}}_{k,m}}\left[\left\|\mathbb{E}_{\widetilde{\boldsymbol{h}}_{k,m}}\left[\sum_{m'=1}^{K_{\mathsf{u}}}\sum_{k\in\mathcal{K}(m')}\widetilde{\boldsymbol{h}}_{k,m}\mathbf{F}_{k,m'}^{\mathsf{B}}\left(\boldsymbol{\Omega}_{k,m'}\right)^{\frac{1}{2}}\mathbf{X}_{m'}^{\widehat{n}l}\middle|\boldsymbol{y}_m^{\widehat{n}l}\right] - \boldsymbol{y}_m^{\widehat{n}l}\right\|^2\middle|\mathbf{X}_m^{\widehat{n}l}\right]. \end{aligned} \tag{F.2}$$

Third, we define

$$\mathbb{E}_{\widetilde{\boldsymbol{h}}_{k,m}}\left[\sum_{m'=1}^{K_{\mathsf{u}}}\sum_{k\in\mathcal{K}(m')}\widetilde{\boldsymbol{h}}_{k,m}\mathbf{F}_{k,m'}^{\mathsf{B}}\left(\boldsymbol{\Omega}_{k,m'}\right)^{\frac{1}{2}}\widehat{\mathbf{X}}_{m'}^{\widehat{n}l}\right] \triangleq \mathbb{E}_{\widetilde{\boldsymbol{h}}_{k,m}}\left[\sum_{m'=1}^{K_{\mathsf{u}}}\sum_{k\in\mathcal{K}(m')}\widetilde{\boldsymbol{h}}_{k,m}\mathbf{F}_{k,m'}^{\mathsf{B}}\left(\boldsymbol{\Omega}_{k,m'}\right)^{\frac{1}{2}}\mathbf{X}_{m'}^{\widehat{n}l}\middle|\boldsymbol{y}_m^{\widehat{n}l}\right]. \tag{F.3}$$

Accordingly, we can have:

$$
\begin{aligned}
&\mathrm{Var}\left[\log\left(P_{\boldsymbol{y}_m^{\widehat{n}l}|\widetilde{\boldsymbol{h}}_{k,m}}\left(\boldsymbol{y}_m^{\widehat{n}l}|\widetilde{\boldsymbol{h}}_{k,m}\right)\right)\right] \\
&\leq \frac{1}{\sigma^2}\mathbb{E}_{\widetilde{\boldsymbol{h}}_{k,m}}\left[\left\|\boldsymbol{y}_m^{\widehat{n}l}-\sum_{m'=1}^{K_{\mathrm{u}}}\sum_{k\in\mathcal{K}(m')}\widetilde{\boldsymbol{h}}_{k,m}\mathbf{F}_{k,m'}^{\mathrm{B}}\left(\boldsymbol{\Omega}_{k,m'}\right)^{\frac{1}{2}}\widehat{\mathbf{X}}_{m'}^{\widehat{n}l}\right\|^2\middle|\mathbf{X}_m^{\widehat{n}l}\right] \\
&\leq \frac{2}{\sigma^2}\mathbb{E}_{\widetilde{\boldsymbol{h}}_{k,m}}\left[\left\|\boldsymbol{y}_m^{\widehat{n}l}\middle|\mathbf{X}_m^{\widehat{n}l}\right\|^2\middle|\mathbf{X}_m^{\widehat{n}l}\right]+\frac{2}{\sigma^2}\mathbb{E}_{\widetilde{\boldsymbol{h}}_{k,m}}\left[\left\|\sum_{m'=1}^{K_{\mathrm{u}}}\sum_{k\in\mathcal{K}(m')}\widetilde{\boldsymbol{h}}_{k,m}\mathbf{F}_{k,m'}^{\mathrm{B}}\left(\boldsymbol{\Omega}_{k,m'}\right)^{\frac{1}{2}}\widehat{\mathbf{X}}_{m'}^{\widehat{n}l}\right\|^2\middle|\mathbf{X}_m^{\widehat{n}l}\right] \\
&\leq \frac{6\widehat{n}l\overline{\mathcal{P}}_m}{\sigma^4}\mathbb{E}_{\widetilde{\boldsymbol{h}}_{k,m}}\left[\left\|\sum_{m'=1}^{K_{\mathrm{u}}}\sum_{k\in\mathcal{K}(m')}\widetilde{\boldsymbol{h}}_{k,m}\mathbf{F}_{k,m'}^{\mathrm{B}}\left(\boldsymbol{\Omega}_{k,m'}\right)^{\frac{1}{2}}\right\|^2\right]+4\mathbb{E}_{\widetilde{\boldsymbol{h}}_{k,m}}\left[\left\|\frac{\boldsymbol{n}_m}{\sigma^2}\right\|^2\middle|\mathbf{X}_m^{\widehat{n}l}\right] \\
&= \frac{6\widehat{n}l\overline{\mathcal{P}}_m}{\sigma^4}\mathbb{E}_{\widetilde{\boldsymbol{h}}_{k,m}}\left[\left\|\sum_{m'=1}^{K_{\mathrm{u}}}\sum_{k\in\mathcal{K}(m')}\widetilde{\boldsymbol{h}}_{k,m}\mathbf{F}_{k,m'}^{\mathrm{B}}\left(\boldsymbol{\Omega}_{k,m'}\right)^{\frac{1}{2}}\right\|^2\right]+4\widehat{n}l. \qquad \text{(F.4)}
\end{aligned}
$$

Following the similar procedures for obtaining $\mathrm{Var}\left[\log\left(P_{\boldsymbol{y}_m^{\widehat{n}l}|\widetilde{\boldsymbol{h}}_{k,m}}\left(\boldsymbol{y}_m^{\widehat{n}l}|\widetilde{\boldsymbol{h}}_{k,m}\right)\right)\right]$ in Eq. (F.4), we can derive an upper bound on $\mathrm{Var}\left[\log\left(P_{\boldsymbol{y}_m^{\widehat{n}l}|\widetilde{\boldsymbol{h}}_{k,m},\mathbf{X}_m^{\widehat{n}l}}\left(\boldsymbol{y}_m^{\widehat{n}l}|\widetilde{\boldsymbol{h}}_{k,m},\mathbf{X}_m^{\widehat{n}l}\right)\right)\right]$ for all $\mathbf{X}_m^{\widehat{n}l}\in\mathcal{M}_m$ as follows:

$$
\begin{aligned}
\mathrm{Var}\left[\log\left(P_{\boldsymbol{y}_m^{\widehat{n}l}|\widetilde{\boldsymbol{h}}_{k,m},\mathbf{X}_m^{\widehat{n}l}}\left(\boldsymbol{y}_m^{\widehat{n}l}|\widetilde{\boldsymbol{h}}_{k,m},\mathbf{X}_m^{\widehat{n}l}\right)\right)\right] &\leq \frac{6\widehat{n}l\overline{\mathcal{P}}_m}{\sigma^4}\mathbb{E}_{\widetilde{\boldsymbol{h}}_{k,m}}\left[\left\|\sum_{m'=1}^{K_{\mathrm{u}}}\sum_{k\in\mathcal{K}(m')}\widetilde{\boldsymbol{h}}_{k,m}\mathbf{F}_{k,m'}^{\mathrm{B}}\left(\boldsymbol{\Omega}_{k,m'}\right)^{\frac{1}{2}}\right\|^2\right] \\
&\quad+4\widehat{n}l \qquad \text{(F.5)}
\end{aligned}
$$

Finally, substituting Eqs. (F.4) and (F.5) back into Eqs. (F.1), we can derive an upper bound on the channel dispersion $V_m\left(\widetilde{\boldsymbol{h}}_{k,m}\right)$ as follows:

$$
V_m\left(\widetilde{\boldsymbol{h}}_{k,m}\right)\leq 8\widehat{n}l\left(\frac{3\overline{\mathcal{P}}_m}{\sigma^4}\mathbb{E}_{\widetilde{\boldsymbol{h}}_{k,m}}\left[\left\|\sum_{m'=1}^{K_{\mathrm{u}}}\sum_{k\in\mathcal{K}(m')}\widetilde{\boldsymbol{h}}_{k,m}\mathbf{F}_{k,m'}^{\mathrm{B}}\left(\boldsymbol{\Omega}_{k,m'}\right)^{\frac{1}{2}}\right\|^2\right]+2\right) \qquad \text{(F.6)}
$$

which is Eq. (3.29), completing the proof of Theorem 4.

APPENDIX G

PROOF OF THEOREM 6

We proceed with the proof by showing Claim 1, Claim 2, and Claim 3, respectively.

Claim 1. To characterize the convexity of the objective function in $\mathbf{P_{10}}$ given by Eq. (4.20) with respect to the TS factor α, first we define two auxiliary functions as follows:

$$\begin{cases} F\left(\gamma_{\mathrm{d},m}\right) \triangleq \mathbb{E}_{\gamma_{\mathrm{d},m}}\left[\epsilon_{\mathrm{d},m} + \left(1-\epsilon_{\mathrm{d},m}\right) e^{-\theta_m(1-\alpha)n_{\mathrm{d}}T_s R_{\mathrm{d},m}}\right]; \\ F_1(\gamma_{\mathrm{d},m}) \triangleq (1-\alpha)R_{\mathrm{d},m} = (1-\alpha)C\left(\gamma_{\mathrm{d},m}\right) - \sqrt{\frac{(1-\alpha)V\left(\gamma_{\mathrm{d},m}\right)}{n_{\mathrm{d}}}}Q^{-1}(\epsilon_{\mathrm{d},m}). \end{cases} \tag{G.1}$$

Thus, we have

$$F\left(\gamma_{\mathrm{d},m}\right) = \mathbb{E}_{\gamma_{\mathrm{d},m}}\left[\epsilon_{\mathrm{d},m} + \left(1-\epsilon_{\mathrm{d},m}\right) e^{-\theta_m n_{\mathrm{d}}T_s F_1(\gamma_{\mathrm{d},m})}\right]. \tag{G.2}$$

Second, we can derive the first-order derivative of the auxiliary function $F\left(\gamma_{\mathrm{d},m}\right)$ with respect to the TS factor α as in the following equation:

$$\frac{\partial F\left(\gamma_{\mathrm{d},m}\right)}{\partial \alpha} = \frac{\partial F\left(\gamma_{\mathrm{d},m}\right)}{\partial F_1(\gamma_{\mathrm{d},m})}\frac{\partial F_1(\gamma_{\mathrm{d},m})}{\partial \alpha} \tag{G.3}$$

where

$$\frac{\partial F\left(\gamma_{\mathrm{d},m}\right)}{\partial F_1(\gamma_{\mathrm{d},m})} = \mathbb{E}_{\gamma_{\mathrm{d},m}}\left[-\left(1-\epsilon_{\mathrm{d},m}\right) e^{-\theta_m(1-\alpha)n_{\mathrm{d}}T_s R_{\mathrm{d},m}}\theta_m n_{\mathrm{d}}T_s\right] < 0 \tag{G.4}$$

and

$$\frac{\partial F_1(\gamma_{\mathrm{d},m})}{\partial \alpha} = -C\left(\gamma_{\mathrm{d},m}\right) + \sqrt{\frac{V\left(\gamma_{\mathrm{d},m}\right)}{n_{\mathrm{d}}}}\frac{Q^{-1}(\epsilon_{\mathrm{d},m})\left(1-\alpha\right)^{-\frac{1}{2}}}{2}. \tag{G.5}$$

Third, using chain rule, we derive the second-order derivative of $F\left(\gamma_{\mathrm{d},m}\right)$ with respect to the

TS factor α as follows:

$$\frac{\partial^2 F\left(\gamma_{\mathrm{d},m}\right)}{\partial \alpha^2} = \frac{\partial^2 F\left(\gamma_{\mathrm{d},m}\right)}{\partial \left[F_1(\gamma_{\mathrm{d},m})\right]^2} \left[\frac{\partial F_1(\gamma_{\mathrm{d},m})}{\partial \alpha}\right]^2 + \frac{\partial F\left(\gamma_{\mathrm{d},m}\right)}{\partial F_1(\gamma_{\mathrm{d},m})} \frac{\partial^2 F_1(\gamma_{\mathrm{d},m})}{\partial \alpha^2} \tag{G.6}$$

where

$$\frac{\partial^2 F\left(\gamma_{\mathrm{d},m}\right)}{\partial \left[F_1(\gamma_{\mathrm{d},m})\right]^2} = \mathbb{E}_{\gamma_{\mathrm{d},m}}\left[\left(1-\epsilon_{\mathrm{d},m}\right) e^{-\theta_m(1-\alpha)n_{\mathrm{d}}T_s R_{\mathrm{d},m}} \left(\theta_m n_{\mathrm{d}} T_s\right)^2\right] > 0 \tag{G.7}$$

and

$$\frac{\partial^2 F_1(\gamma_{\mathrm{d},m})}{\partial \alpha^2} = \sqrt{\frac{V\left(\gamma_{\mathrm{d},m}\right)}{n_{\mathrm{d}}}} \frac{Q^{-1}(\epsilon_{\mathrm{d},m})\left(1-\alpha\right)^{-\frac{3}{2}}}{4}. \tag{G.8}$$

Since when $Q^{-1}(\epsilon_{\mathrm{d},m}) > 0$ for $\epsilon_{\mathrm{d},m} \in (0, 0.5)$, we can obtain $\partial^2 F_1(\gamma_{\mathrm{d},m})/\partial\alpha^2 > 0$.

Then, by plugging Eqs. (G.7) and (G.8) back into Eq. (G.6), we have

$$\begin{aligned}
\frac{\partial^2 F\left(\gamma_{\mathrm{d},m}\right)}{\partial \alpha^2} =& \theta_m n_{\mathrm{d}} T_s \left[-C\left(\gamma_{\mathrm{d},m}\right) + \sqrt{\frac{V\left(\gamma_{\mathrm{d},m}\right)}{n_{\mathrm{d}}}} \frac{Q^{-1}(\epsilon_{\mathrm{d},m})}{2} \left(1-\alpha\right)^{-\frac{1}{2}} \right]^2 \\
& - \sqrt{\frac{V\left(\gamma_{\mathrm{d},m}\right)}{n_{\mathrm{d}}}} \frac{Q^{-1}(\epsilon_{\mathrm{d},m})\left(1-\alpha\right)^{-\frac{3}{2}}}{4} \\
=& \theta_m n_{\mathrm{d}} T_s \Bigg\{ \left[C\left(\gamma_{\mathrm{d},m}\right)\right]^2 + \frac{V\left(\gamma_{\mathrm{d},m}\right)\left[Q^{-1}(\epsilon_{\mathrm{d},m})\right]^2}{4n_{\mathrm{d}}\left(1-\alpha\right)} - C\left(\gamma_{\mathrm{d},m}\right) \sqrt{\frac{V\left(\gamma_{\mathrm{d},m}\right)}{n_{\mathrm{d}}}} Q^{-1}(\epsilon_{\mathrm{d},m}) \\
& \times \left(1-\alpha\right)^{-\frac{1}{2}} \Bigg\} - \sqrt{\frac{V\left(\gamma_{\mathrm{d},m}\right)}{n_{\mathrm{d}}}} \frac{Q^{-1}(\epsilon_{\mathrm{d},m})\left(1-\alpha\right)^{-\frac{3}{2}}}{4} \\
> & \theta_m n_{\mathrm{d}} T_s \Bigg\{ \left[C\left(\gamma_{\mathrm{d},m}\right)\right]^2 - C\left(\gamma_{\mathrm{d},m}\right) \sqrt{\frac{V\left(\gamma_{\mathrm{d},m}\right)}{n_{\mathrm{d}}}} Q^{-1}(\epsilon_{\mathrm{d},m}) \left(1-\alpha\right)^{-\frac{1}{2}} \Bigg\} \\
& - \sqrt{\frac{V\left(\gamma_{\mathrm{d},m}\right)}{n_{\mathrm{d}}}} \frac{Q^{-1}(\epsilon_{\mathrm{d},m})\left(1-\alpha\right)^{-\frac{3}{2}}}{4}.
\end{aligned} \tag{G.9}$$

Using Eq. (2.19), we get

$$\sqrt{\frac{V\left(\gamma_{\mathrm{d},m}\right)}{(1-\alpha)n_{\mathrm{d}}}} Q^{-1}(\epsilon_{\mathrm{d},m}) = C\left(\gamma_{\mathrm{d},m}\right) - R_{\mathrm{d},m}. \tag{G.10}$$

Thus, plugging Eq. (G.10) back into Eq. (G.9), we can obtain the following equation:

$$\begin{aligned}\frac{\partial^2 F\left(\gamma_{\mathrm{d},m}\right)}{\partial \alpha^2} &> \theta_m n_{\mathrm{d}} T_s \left\{ \left[C\left(\gamma_{\mathrm{d},m}\right)\right]^2 - C\left(\gamma_{\mathrm{d},m}\right)\left[C\left(\gamma_{\mathrm{d},m}\right) - R_{\mathrm{d},m}\right]\right\} - \frac{C\left(\gamma_{\mathrm{d},m}\right) - R_{\mathrm{d},m}}{4(1-\alpha)} \\ &= \theta_m n_{\mathrm{d}} T_s C\left(\gamma_{\mathrm{d},m}\right) R_{\mathrm{d},m} - \frac{C\left(\gamma_{\mathrm{d},m}\right) - R_{\mathrm{d},m}}{4(1-\alpha)} \\ &= \frac{1}{R_{\mathrm{d},m}}\left[\theta_m n_{\mathrm{d}} T_s C\left(\gamma_{\mathrm{d},m}\right) + \frac{1}{4(1-\alpha)} - \frac{C\left(\gamma_{\mathrm{d},m}\right)}{4(1-\alpha)R_{\mathrm{d},m}}\right] \end{aligned} \tag{G.11}$$

Based on Eq. (2.19), we can obtain that

$$\frac{C\left(\gamma_{\mathrm{d},m}\right)}{R_{\mathrm{d},m}} < \frac{C\left(\gamma_{\mathrm{d},m}\right)}{C\left(\gamma_{\mathrm{d},m}\right) - \sqrt{\frac{1}{(1-\alpha)n_{\mathrm{d}}}} Q^{-1}(\epsilon_{\mathrm{d},m})}. \tag{G.12}$$

Thus, plugging Eq. (G.12) back into Eq. (G.11), we have

$$\begin{aligned}\frac{\partial^2 F\left(\gamma_{\mathrm{d},m}\right)}{\partial \alpha^2} &> \frac{4(1-\alpha)}{R_{\mathrm{d},m}}\left\{4(1-\alpha)\theta_m n_{\mathrm{d}} T_s C\left(\gamma_{\mathrm{d},m}\right) + 1 - \frac{C\left(\gamma_{\mathrm{d},m}\right)}{C\left(\gamma_{\mathrm{d},m}\right) - \sqrt{\frac{1}{(1-\alpha)n_{\mathrm{d}}}} Q^{-1}(\epsilon_{\mathrm{d},m})}\right\} \\ &= \frac{4(1-\alpha)}{R_{\mathrm{d},m}}\left\{\frac{C\left(\gamma_{\mathrm{d},m}\right)}{C\left(\gamma_{\mathrm{d},m}\right) - \sqrt{\frac{1}{(1-\alpha)n_{\mathrm{d,th}}^{\mathrm{TS}}}} Q^{-1}(\epsilon_{\mathrm{d},m})} - \frac{C\left(\gamma_{\mathrm{d},m}\right)}{C\left(\gamma_{\mathrm{d},m}\right) - \sqrt{\frac{1}{(1-\alpha)n_{\mathrm{d}}}} Q^{-1}(\epsilon_{\mathrm{d},m})}\right\} \end{aligned} \tag{G.13}$$

where $n_{\mathrm{d,th}}^{\mathrm{TS}}$ is given by Eq. (4.21). Applying the condition: $n_{\mathrm{d}} > n_{\mathrm{d,th}}^{\mathrm{TS}}$ into Eq. (G.13), which implies that $\left[(1-\alpha)n_{\mathrm{d,th}}^{\mathrm{TS}}\right]^{-\frac{1}{2}} > \left[(1-\alpha)n_{\mathrm{d}}\right]^{-\frac{1}{2}}$, and thus we can obtain the following equation:

$$\frac{\partial^2 F\left(\gamma_{\mathrm{d},m}\right)}{\partial \alpha^2} > 0. \tag{G.14}$$

Therefore, the objective function in $\mathbf{P_{10}}$ specified by Eq. (4.20) is convex with respect to the TS factor α when $\epsilon_{\mathrm{d},m} \in (0, 0.5)$ and the constraint $n_{\mathrm{d}} > n_{\mathrm{d,th}}^{\mathrm{TS}}$ is satisfied, which completes the proof of Claim 1 in Theorem 6.

Claim 2. To characterize the convexity of the objective function in $\mathbf{P_{10}}$ given by Eq. (4.20) with respect to the downlink data blocklength n_{d}, first we define the auxiliary function, denoted by

$F_2(\gamma_{\mathrm{d},m})$, as follows:

$$F_2(\gamma_{\mathrm{d},m}) \triangleq n_{\mathrm{d}} R_{\mathrm{d},m} = n_{\mathrm{d}} C\left(\gamma_{\mathrm{d},m}\right) - \sqrt{\frac{n_{\mathrm{d}} V\left(\gamma_{\mathrm{d},m}\right)}{1-\alpha}} Q^{-1}(\epsilon_{\mathrm{d},m}). \tag{G.15}$$

Second, we derive the first-order derivative of the auxiliary function $F\left(\gamma_{\mathrm{d},m}\right)$ with respect to the downlink data blocklength n_{d} as follows:

$$\frac{\partial F\left(\gamma_{\mathrm{d},m}\right)}{\partial n_{\mathrm{d}}} = \frac{\partial F\left(\gamma_{\mathrm{d},m}\right)}{\partial F_2(\gamma_{\mathrm{d},m})} \frac{\partial F_2(\gamma_{\mathrm{d},m})}{\partial n_{\mathrm{d}}} \tag{G.16}$$

where

$$\frac{\partial F\left(\gamma_{\mathrm{d},m}\right)}{\partial F_2(\gamma_{\mathrm{d},m})} = \mathbb{E}_{\gamma_{\mathrm{d},m}}\left[-\left(1-\epsilon_{\mathrm{d},m}\right) e^{-\theta_m (1-\alpha) n_{\mathrm{d}} T_s R_{\mathrm{d},m}} \theta_m (1-\alpha) T_s \right] < 0 \tag{G.17}$$

and

$$\frac{\partial F_2(\gamma_{\mathrm{d},m})}{\partial n_{\mathrm{d}}} = C\left(\gamma_{\mathrm{d},m}\right) - \sqrt{\frac{V\left(\gamma_{\mathrm{d},m}\right)}{1-\alpha}} \frac{Q^{-1}(\epsilon_{\mathrm{d},m}) \left(n_{\mathrm{d}}\right)^{-\frac{1}{2}}}{2}. \tag{G.18}$$

Third, using chain rule, we derive the second-order derivative of $F\left(\gamma_{\mathrm{d},m}\right)$ with respect to n_{d} as follows:

$$\frac{\partial^2 F\left(\gamma_{\mathrm{d},m}\right)}{\partial (n_{\mathrm{d}})^2} = \frac{\partial^2 F\left(\gamma_{\mathrm{d},m}\right)}{\partial \left[F_2(\gamma_{\mathrm{d},m})\right]^2} \left[\frac{\partial F_2(\gamma_{\mathrm{d},m})}{\partial n_{\mathrm{d}}}\right]^2 + \frac{\partial F\left(\gamma_{\mathrm{d},m}\right)}{\partial F_2(\gamma_{\mathrm{d},m})} \frac{\partial^2 F_2(\gamma_{\mathrm{d},m})}{\partial (n_{\mathrm{d}})^2} \tag{G.19}$$

where

$$\frac{\partial^2 F\left(\gamma_{\mathrm{d},m}\right)}{\partial \left[F_2(\gamma_{\mathrm{d},m})\right]^2} = \mathbb{E}_{\gamma_{\mathrm{d},m}}\left[\left(1-\epsilon_{\mathrm{d},m}\right) e^{-\theta_m (1-\alpha) n_{\mathrm{d}} T_s R_{\mathrm{d},m}} \left[\theta_m (1-\alpha) T_s\right]^2 \right] > 0 \tag{G.20}$$

and

$$\frac{\partial^2 F_2(\gamma_{\mathrm{d},m})}{\partial (n_{\mathrm{d}})^2} = -\sqrt{\frac{V\left(\gamma_{\mathrm{d},m}\right)}{1-\alpha}} \frac{Q^{-1}(\epsilon_{\mathrm{d},m}) \left(n_{\mathrm{d}}\right)^{-\frac{3}{2}}}{4}. \tag{G.21}$$

Since when $Q^{-1}(\epsilon_{\mathrm{d},m}) > 0$ for $\epsilon_{\mathrm{d},m} \in (0, 0.5)$, we can obtain $\partial^2 F_2(\gamma_{\mathrm{d},m})/\partial(n_{\mathrm{d}})^2 > 0$. Therefore, we can obtain $\partial^2 F\left(\gamma_{\mathrm{d},m}\right)/\partial(n_{\mathrm{d}})^2 > 0$, implying that the objective function in $\mathbf{P_{10}}$ specified by Eq. (4.20) is convex with respect to the downlink data blocklength n_{d} when $\epsilon_{\mathrm{d},m} \in (0, 0.5)$, which completes the proof of Claim 2 in Theorem 6.

Claim 3. Similar to the proof of Claim 2, we can easily show that the second-order derivative $\partial^2 F\left(\gamma_{\mathrm{d},m}\right)/\partial(\eta_{k,m})^2 > 0$, implying that the objective function in $\mathbf{P_{10}}$ specified by Eq. (4.20) is convex with respect to the downlink power allocation coefficient $\eta_{k,m}$ when $\epsilon_{\mathrm{d},m} \in (0, 0.5)$. Thus, we complete the proof of Claim 3 in Theorem 6.

APPENDIX H

PROOF OF THEOREM 7

To characterize the convexity of the objective function in $\mathbf{P_{12}}$ specified in Eq. (4.25) with respect to the PS factor ρ, first we can derive the first-order derivative of the auxiliary function $F\left(\gamma_{\mathrm{d},m}\right)$ with respect to the PS factor ρ as follows:

$$\frac{\partial F\left(\gamma_{\mathrm{d},m}\right)}{\partial \rho} = \frac{\partial F\left(\gamma_{\mathrm{d},m}\right)}{\partial R_{\mathrm{d},m}} \frac{\partial R_{\mathrm{d},m}}{\partial \rho} \tag{H.1}$$

where

$$\frac{\partial F\left(\gamma_{\mathrm{d},m}\right)}{\partial R_{\mathrm{d},m}} = \mathbb{E}_{\gamma_{\mathrm{d},m}}\left[-\left(1-\epsilon_{\mathrm{d},m}\right) e^{-\theta_m n_{\mathrm{d}} T_s R_{\mathrm{d},m}} \theta_m n_{\mathrm{d}} T_s \right] < 0 \tag{H.2}$$

and

$$\frac{\partial R_{\mathrm{d},m}}{\partial \rho} = \frac{\partial C\left(\gamma_{\mathrm{d},m}\right)}{\partial \rho} - \frac{Q^{-1}(\epsilon_{\mathrm{d},m})}{2\sqrt{n_{\mathrm{d}} V\left(\gamma_{\mathrm{d},m}\right)}} \frac{\partial V\left(\gamma_{\mathrm{d},m}\right)}{\partial \rho}. \tag{H.3}$$

Second, using chain rule, we derive the second-order derivative of $F\left(\gamma_{\mathrm{d},m}\right)$ with respect to the PS factor ρ as follows:

$$\frac{\partial^2 F\left(\gamma_{\mathrm{d},m}\right)}{\partial \rho^2} = \frac{\partial^2 F\left(\gamma_{\mathrm{d},m}\right)}{\partial \left[R_{\mathrm{d},m}\right]^2} \left[\frac{\partial R_{\mathrm{d},m}}{\partial \rho}\right]^2 + \frac{\partial F\left(\gamma_{\mathrm{d},m}\right)}{\partial R_{\mathrm{d},m}} \frac{\partial^2 R_{\mathrm{d},m}}{\partial \rho^2} \tag{H.4}$$

where

$$\frac{\partial^2 F\left(\gamma_{\mathrm{d},m}\right)}{\partial \left[R_{\mathrm{d},m}\right]^2} = \left(1-\epsilon_{\mathrm{d},m}\right)\left(\theta_m n_{\mathrm{d}} T_s\right)^2 e^{-\theta_m n_{\mathrm{d}} T_s R_{\mathrm{d},m}} > 0. \tag{H.5}$$

Since $\partial^2 F\left(\gamma_{\mathrm{d},m}\right)/\partial\left[R_{\mathrm{d},m}\right]^2 > 0$ and $\partial F\left(\gamma_{\mathrm{d},m}\right)/\partial R_{\mathrm{d},m} < 0$, to determine whether $\partial^2 F\left(\gamma_{\mathrm{d},m}\right)/\partial \rho^2 > 0$ in Eq. (H.4), it is equivalent to determine whether $\partial^2 R_{\mathrm{d},m}/\partial \rho^2 < 0$.

In addition, to determine whether $\frac{\partial^2 R_{\mathrm{d},m}}{\partial \rho^2} < 0$, first we obtain the second-order derivatives of the downlink channel capacity $C\left(\gamma_{\mathrm{d},m}\right)$ and channel dispersion $V\left(\gamma_{\mathrm{d},m}\right)$ with respect to the PS

factor ρ, respectively, as follows:

$$\frac{\partial^2 C\left(\gamma_{\mathrm{d},m}\right)}{\partial \rho^2} = -\frac{1}{\left(\log 2\right)\left(1+\gamma_{\mathrm{d},m}\right)^2}\left(\frac{\partial \gamma_{\mathrm{d},m}}{\partial \rho}\right)^2 + \frac{\partial^2 \gamma_{\mathrm{d},m}}{\partial \rho^2}\frac{1}{\left(\log 2\right)\left(1+\gamma_{\mathrm{d},m}\right)} \tag{H.6}$$

and

$$\frac{\partial^2 V\left(\gamma_{\mathrm{d},m}\right)}{\partial \rho^2} = -6\left(1+\gamma_{\mathrm{d},m}\right)^{-4}\left(\frac{\partial \gamma_{\mathrm{d},m}}{\partial \rho}\right)^2 + 2\left(1+\gamma_{\mathrm{d},m}\right)^{-3}\frac{\partial^2 \gamma_{\mathrm{d},m}}{\partial \rho^2}. \tag{H.7}$$

Then, using Eqs. (H.6) and (H.7), we obtain the second-order derivative of $R_{\mathrm{d},m}$ with respect to the PS factor ρ as follows:

$$\begin{aligned}
&\frac{\partial^2 R_{\mathrm{d},m}}{\partial \rho^2} \\
&= \frac{\partial^2 C\left(\gamma_{\mathrm{d},m}\right)}{\partial \rho^2} + \frac{Q^{-1}(\epsilon_{\mathrm{d},m})}{4\sqrt{n_{\mathrm{d}}}}\left[V\left(\gamma_{\mathrm{d},m}\right)\right]^{-\frac{3}{2}}\left[\frac{\partial V\left(\gamma_{\mathrm{d},m}\right)}{\partial \rho}\right]^2 - \frac{Q^{-1}(\epsilon_{\mathrm{d},m})}{2\sqrt{n_{\mathrm{d}}}}\left[V\left(\gamma_{\mathrm{d},m}\right)\right]^{-\frac{1}{2}}\frac{\partial^2 V\left(\gamma_{\mathrm{d},m}\right)}{\partial \rho^2} \\
&= -\frac{1}{\left(\log 2\right)\left(1+\gamma_{\mathrm{d},m}\right)^2}\left(\frac{\partial \gamma_{\mathrm{d},m}}{\partial \rho}\right)^2 + \frac{1}{\left(\log 2\right)\left(1+\gamma_{\mathrm{d},m}\right)}\frac{\partial^2 \gamma_{\mathrm{d},m}}{\partial \rho^2} + \frac{Q^{-1}(\epsilon_{\mathrm{d},m})}{4\sqrt{n_{\mathrm{d}}}}\left[V\left(\gamma_{\mathrm{d},m}\right)\right]^{-\frac{3}{2}} \\
&\quad \times \left[-6\left(1+\gamma_{\mathrm{d},m}\right)^{-4}\left(\frac{\partial \gamma_{\mathrm{d},m}}{\partial \rho}\right)^2 + 2\left(1+\gamma_{\mathrm{d},m}\right)^{-3}\frac{\partial^2 \gamma_{\mathrm{d},m}}{\partial \rho^2}\right]^2 - \frac{Q^{-1}(\epsilon_{\mathrm{d},m})}{2\sqrt{n_{\mathrm{d}}}} \\
&\quad \times \left[V\left(\gamma_{\mathrm{d},m}\right)\right]^{-\frac{1}{2}}\left[-6\left(1+\gamma_{\mathrm{d},m}\right)^{-4}\left(\frac{\partial \gamma_{\mathrm{d},m}}{\partial \rho}\right)^2 + \frac{\partial^2 \gamma_{\mathrm{d},m}}{\partial \rho^2}2\left(1+\gamma_{\mathrm{d},m}\right)^{-3}\right] \\
&= -\frac{1}{\left(\log 2\right)\left(1+\gamma_{\mathrm{d},m}\right)^2}\left(\frac{\partial \gamma_{\mathrm{d},m}}{\partial \rho}\right)^2 + \frac{1}{\left(\log 2\right)\left(1+\gamma_{\mathrm{d},m}\right)}\frac{\partial^2 \gamma_{\mathrm{d},m}}{\partial \rho^2} - \frac{Q^{-1}(\epsilon_{\mathrm{d},m})}{2\sqrt{n_{\mathrm{d}}}}\left[V\left(\gamma_{\mathrm{d},m}\right)\right]^{-\frac{1}{2}} \\
&\quad \times \left[-6\left(1+\gamma_{\mathrm{d},m}\right)^{-4}\left(\frac{\partial \gamma_{\mathrm{d},m}}{\partial \rho}\right)^2 + 2\left(1+\gamma_{\mathrm{d},m}\right)^{-3}\frac{\partial^2 \gamma_{\mathrm{d},m}}{\partial \rho^2}\right]\left\{1 - \frac{1}{2V\left(\gamma_{\mathrm{d},m}\right)}\right. \\
&\quad \times \left.\left[-6\left(1+\gamma_{\mathrm{d},m}\right)^{-4}\left(\frac{\partial \gamma_{\mathrm{d},m}}{\partial \rho}\right)^2 + 2\left(1+\gamma_{\mathrm{d},m}\right)^{-3}\frac{\partial^2 \gamma_{\mathrm{d},m}}{\partial \rho^2}\right]\right\}.
\end{aligned} \tag{H.8}$$

Second, we can rewrite the SNR function given by Eq. (4.13) as follows:

$$\gamma_{\mathrm{d},m} = \frac{(1-\rho)\gamma_{1,m}}{(1-\rho)\gamma_{2,m}+1} \tag{H.9}$$

where

$$\begin{cases} \gamma_{1,m} = \mathcal{P}_{\mathrm{d}} \left| \mathbb{E}\left[\sum\limits_{k=1}^{K_{\mathrm{a}}} \sqrt{\eta_{k,m}} (\boldsymbol{h}_{k,m})^H \boldsymbol{b}_{k,m} \right] \right|^2; \\ \gamma_{2,m} = \mathcal{P}_{\mathrm{d}} \sum\limits_{m'=1}^{K_{\mathrm{u}}} \mathbb{E}\left[\left| \sum_{k=1}^{K_{\mathrm{a}}} \sqrt{\eta_{k,m'}} (\boldsymbol{h}_{k,m'})^H \boldsymbol{b}_{k,m} \right|^2 \right] - \mathcal{P}_{\mathrm{d}} \left| \mathbb{E}\left[\sum\limits_{k=1}^{K_{\mathrm{a}}} \sqrt{\eta_{k,m}} (\boldsymbol{h}_{k,m})^H \boldsymbol{b}_{k,m} \right] \right|^2. \end{cases} \tag{H.10}$$

Using Eq. (4.13), we characterize the first-order and second-order derivatives of $\gamma_{\mathrm{d},m}$ with respect to the PS factor ρ as follows:

$$\begin{cases} \frac{\partial \gamma_{\mathrm{d},m}}{\partial \rho} = \frac{-\gamma_{1,m}}{\left[(1-\rho)\gamma_{2,m}+1\right]^2}; \\ \frac{\partial^2 \gamma_{\mathrm{d},m}}{\partial \rho^2} = \frac{-2\gamma_{1,m}\gamma_{2,m}}{\left[(1-\rho)\gamma_{2,m}+1\right]^3}. \end{cases} \tag{H.11}$$

Plugging Eq. (H.11) back into Eq. (H.8), we can obtain:

$$\begin{aligned} \frac{\partial^2 R_{\mathrm{d},m}}{\partial \rho^2} < & - \frac{1}{(\log 2)\left(1+\gamma_{\mathrm{d},m}\right)^2} \left(\frac{\partial \gamma_{\mathrm{d},m}}{\partial \rho} \right)^2 + \frac{1}{(\log 2)\left(1+\gamma_{\mathrm{d},m}\right)} \frac{\partial^2 \gamma_{\mathrm{d},m}}{\partial \rho^2} - \frac{Q^{-1}(\epsilon_{\mathrm{d},m})}{2\sqrt{n_{\mathrm{d}}}} \left[V\left(\gamma_{\mathrm{d},m}\right) \right]^{-\frac{1}{2}} \\ & \times \left[-6\left(1+\gamma_{\mathrm{d},m}\right)^{-4} \left(\frac{\partial \gamma_{\mathrm{d},m}}{\partial \rho} \right)^2 + 2\left(1+\gamma_{\mathrm{d},m}\right)^{-3} \frac{\partial^2 \gamma_{\mathrm{d},m}}{\partial \rho^2} \right]. \end{aligned} \tag{H.12}$$

Then, in order to guarantee $\frac{\partial^2 R_{\mathrm{d},m}}{\partial \rho^2} < 0$, it is sufficient to have

$$\begin{aligned} & - \frac{1}{(\log 2)\left(1+\gamma_{\mathrm{d},m}\right)^2} \left(\frac{\partial \gamma_{\mathrm{d},m}}{\partial \rho} \right)^2 + \frac{1}{(\log 2)\left(1+\gamma_{\mathrm{d},m}\right)} \frac{\partial^2 \gamma_{\mathrm{d},m}}{\partial \rho^2} \\ & < \frac{Q^{-1}(\epsilon_{\mathrm{d},m})}{2\sqrt{n_{\mathrm{d}}}} \left[V\left(\gamma_{\mathrm{d},m}\right) \right]^{-\frac{1}{2}} \left[-6\left(1+\gamma_{\mathrm{d},m}\right)^{-4} \left(\frac{\partial \gamma_{\mathrm{d},m}}{\partial \rho} \right)^2 + 2\left(1+\gamma_{\mathrm{d},m}\right)^{-3} \frac{\partial^2 \gamma_{\mathrm{d},m}}{\partial \rho^2} \right] \end{aligned} \tag{H.13}$$

which leads to the following inequality:

$$\begin{aligned} & \frac{1}{(\log 2)\left(1+\gamma_{\mathrm{d},m}\right)} \frac{\partial^2 \gamma_{\mathrm{d},m}}{\partial \rho^2} - \frac{Q^{-1}(\epsilon_{\mathrm{d},m})}{\sqrt{n_{\mathrm{d}} V\left(\gamma_{\mathrm{d},m}\right)}} \left(1+\gamma_{\mathrm{d},m}\right)^{-3} \frac{\partial^2 \gamma_{\mathrm{d},m}}{\partial \rho^2} \\ & < \frac{1}{(\log 2)\left(1+\gamma_{\mathrm{d},m}\right)^2} \left(\frac{\partial \gamma_{\mathrm{d},m}}{\partial \rho} \right)^2 - \frac{3Q^{-1}(\epsilon_{\mathrm{d},m})}{\sqrt{n_{\mathrm{d}} V\left(\gamma_{\mathrm{d},m}\right)}} \left(1+\gamma_{\mathrm{d},m}\right)^{-4} \left(\frac{\partial \gamma_{\mathrm{d},m}}{\partial \rho} \right)^2 \end{aligned} \tag{H.14}$$

Then, we get

$$\left[\frac{1}{(\log 2)\left(1+\gamma_{\mathrm{d},m}\right)}-\frac{Q^{-1}(\epsilon_{\mathrm{d},m})}{\sqrt{n_{\mathrm{d}}V\left(\gamma_{\mathrm{d},m}\right)}}\left(1+\gamma_{\mathrm{d},m}\right)^{-3}\right]\frac{\partial^2\gamma_{\mathrm{d},m}}{\partial\rho^2}$$
$$<\left[\frac{1}{(\log 2)\left(1+\gamma_{\mathrm{d},m}\right)^2}-\frac{3Q^{-1}(\epsilon_{\mathrm{d},m})}{\sqrt{n_{\mathrm{d}}V\left(\gamma_{\mathrm{d},m}\right)}}\left(1+\gamma_{\mathrm{d},m}\right)^{-4}\right]\left(\frac{\partial\gamma_{\mathrm{d},m}}{\partial\rho}\right)^2. \tag{H.15}$$

Since $\partial^2\gamma_{\mathrm{d},m}/\partial\rho^2<0$ and $Q^{-1}(\epsilon_{\mathrm{d},m})$ when $\epsilon_{\mathrm{d},m}\in(0,0.5)$, to guarantee Eq. (H.15) holds, it is equivalent to show that the following inequalities hold:

$$\begin{cases}\frac{1}{(\log 2)\left(1+\gamma_{\mathrm{d},m}\right)}-\frac{Q^{-1}(\epsilon_{\mathrm{d},m})}{\sqrt{n_{\mathrm{d}}V\left(\gamma_{\mathrm{d},m}\right)}}\left(1+\gamma_{\mathrm{d},m}\right)^{-3}>0;\\ \frac{1}{(\log 2)\left(1+\gamma_{\mathrm{d},m}\right)^2}-\frac{3Q^{-1}(\epsilon_{\mathrm{d},m})}{\sqrt{n_{\mathrm{d}}V\left(\gamma_{\mathrm{d},m}\right)}}\left(1+\gamma_{\mathrm{d},m}\right)^{-4}>0.\end{cases} \tag{H.16}$$

which leads to the following inequalities:

$$\begin{cases}\sqrt{n_{\mathrm{d}}V\left(\gamma_{\mathrm{d},m}\right)}>\frac{Q^{-1}(\epsilon_{\mathrm{d},m})(\log 2)}{\left(1+\gamma_{\mathrm{d},m}\right)^2};\\ \sqrt{n_{\mathrm{d}}V\left(\gamma_{\mathrm{d},m}\right)}>\frac{3Q^{-1}(\epsilon_{\mathrm{d},m})(\log 2)}{\left(1+\gamma_{\mathrm{d},m}\right)^2}.\end{cases} \tag{H.17}$$

Thus, using Eq. (H.17), we can obtain the lower bound on the downlink data blocklength to guarantee $\partial^2 R_{\mathrm{d},m}/\partial\rho^2<0$ as follows:

$$n_{\mathrm{d}}>\frac{9}{V\left(\gamma_{\mathrm{d},m}\right)}\left[\frac{Q^{-1}(\epsilon_{\mathrm{d},m})(\log 2)}{\left(1+\gamma_{\mathrm{d},m}\right)^2}\right]^2. \tag{H.18}$$

Finally, we can obtain $\frac{\partial^2 R_{\mathrm{d},m}}{\partial\rho^2}<0$. Therefore, we obtain $\partial^2 F\left(\gamma_{\mathrm{d},m}\right)/\partial\rho^2>0$, implying that the objective function in $\mathbf{P_{12}}$ specified by Eq. (4.25) is convex with respect to the PS factor ρ when $\epsilon_{\mathrm{d},m}\in(0,0.5)$. Thus, we complete the proof of Theorem 7.

APPENDIX I

PROOF OF THEOREM 8

To derive the closed-form expressions for the mean and variance of the aggregate interference, we prove **Claim 1** and **Claim 2**, respectively, for this theorem as follows.

Claim 1. We can derive the mean of aggregate interference $\mathbb{E}_{\boldsymbol{r}}[I_k^{(l)}(\boldsymbol{r})]$ between nano node k and its nano receiver in the THz band over wireless nano-networks as follows:

$$\mathbb{E}_{\boldsymbol{r}}[I_k^{(l)}(\boldsymbol{r})] = \mathbb{E}_{\boldsymbol{r}}\left[\sum_{i=1,i\neq k}^{K+1}\sqrt{\mathcal{P}_i\mathcal{P}_{\text{total}}(r_i)}\right]. \tag{I.1}$$

Then, in order to calculate the mean of aggregate interference $\mathbb{E}_{\boldsymbol{r}}[I_k^{(l)}(\boldsymbol{r})]$, first we need to calculate the expression function given in the right-hand-side of Eq. (I.1) as follows:

$$\begin{aligned}\mathbb{E}_{\boldsymbol{r}}\left[\sum_{i=1,i\neq k}^{K+1}\sqrt{\mathcal{P}_i\mathcal{P}_{\text{total}}(r_i)}\right] &= \mathbb{E}_{\boldsymbol{r}}\left[\sum_{i=1,i\neq k}^{K+1}\sqrt{\mathcal{P}_i\left(r_i\right)^{-\eta}G10^{\frac{\xi_i}{10}}S(f)}\left(\frac{c}{4\pi f r_i}\right)e^{-\frac{\alpha_{\text{abs}}r_i}{2}}\right]\\ &= \Lambda\mathbb{E}_{\boldsymbol{r}}\left[\sum_{i=1,i\neq k}^{K+1}\sqrt{\mathcal{P}_i 10^{\frac{\xi_i}{10}}}F(r_i)\right]\end{aligned} \tag{I.2}$$

where Λ is given by Eq. (5.20) and

$$F(r_i) \triangleq r_i^{-\frac{\eta}{2}-1}e^{-\frac{\alpha_{\text{abs}}r_i}{2}}. \tag{I.3}$$

Then, we need to calculate the function $\mathbb{E}_{\boldsymbol{r}}\left[\sum_{i=1,i\neq k}^{K+1}\sqrt{\mathcal{P}_i 10^{\frac{\xi_i}{10}}}F(r_i)\right]$. Assuming that random number $\mathcal{K}$ interfering nano nodes (transmitters) is equal to κ, we can obtain the conditional expectation

function as follows [129]:

$$\mathbb{E}_{\boldsymbol{r}}\left[\sum_{i=1,i\neq k}^{K+1}\sqrt{\mathcal{P}_i 10^{\frac{\xi_i}{10}}}F(r_i)\middle|\mathcal{K}=\kappa\right]=\sum_{i=1,i\neq k}^{K+1}\mathbb{E}_{\boldsymbol{r}}\left[\sqrt{\mathcal{P}_i 10^{\frac{\xi_i}{10}}}F(r_i)\middle|\mathcal{K}=\kappa\right]=\kappa\mathbb{E}_{r_i}\left[\sqrt{\mathcal{P}_i 10^{\frac{\xi_i}{10}}}F(r_i)\right]$$
$$\geq\kappa\mathbb{E}_{r_i}\left[\sqrt{\mathcal{P}_i 10^{\frac{\xi_i}{10}}}\right]\mathbb{E}_{r_i}\left[F(r_i)\right]=\kappa\sqrt{\overline{\mathcal{P}}}\mathbb{E}_{r_i}\left[F(r_i)\right] \tag{I.4}$$

where $\mathbb{E}_{r_i}[\cdot]$ is the expectation operation with respect to r_i and

$$\begin{aligned}\mathbb{E}_{r_i}\left[F(r_i)\right]&=\int_b^a r_i^{-\frac{\eta}{2}-1}e^{-\frac{\alpha_{\text{abs}}r_i}{2}}f_D(r_i)dr_i=\frac{2}{a^2-b^2}\int_b^a r_i^{-\frac{\eta}{2}}e^{-\frac{\alpha_{\text{abs}}r_i}{2}}dr_i\\&=\frac{2\left(\frac{2}{\alpha_{\text{abs}}}\right)^{1-\frac{\eta}{2}}}{a^2-b^2}\int_{\frac{\alpha_{\text{abs}}b}{2}}^{\frac{\alpha_{\text{abs}}a}{2}}r_i^{-\frac{\eta}{2}}e^{-r_i}dr_i\\&=\frac{2\left(\frac{2}{\alpha_{\text{abs}}}\right)^{1-\frac{\eta}{2}}}{a^2-b^2}\left[\gamma\left(1-\frac{\eta}{2},\frac{\alpha_{\text{abs}}a}{2}\right)-\gamma\left(1-\frac{\eta}{2},\frac{\alpha_{\text{abs}}b}{2}\right)\right].\end{aligned} \tag{I.5}$$

In addition, using the spatial Poisson process, we can obtain the mean and variance of the number of interfering nano nodes $\mathcal{K}$ as follows:

$$\begin{cases}\mathbb{E}[\mathcal{K}]=\lambda\pi a^2;\\ \text{Var}(\mathcal{K})=\lambda\pi a^2,\end{cases} \tag{I.6}$$

where $\mathbb{E}[\cdot]$ and $\text{Var}(\cdot)$ are the standard expectation and variance operations, respectively. Correspondingly, using Eqs. (I.5) and (I.6), we can obtain the following equation:

$$\begin{aligned}\mathbb{E}_{\boldsymbol{r}}\left[\sum_{i=1,i\neq k}^{K+1}\sqrt{\mathcal{P}_i 10^{\frac{\xi_i}{10}}}F(r_i)\right]&\geq\mathbb{E}\left[\mathcal{K}\right]\sqrt{\overline{\mathcal{P}}}\mathbb{E}_{r_i}\left[F(r_i)\right]\\&=\frac{2\lambda\pi a^2\sqrt{\overline{\mathcal{P}}}\left(\frac{2}{\alpha_{\text{abs}}}\right)^{1-\frac{\eta}{2}}}{a^2-b^2}\left[\gamma\left(1-\frac{\eta}{2},\frac{\alpha_{\text{abs}}a}{2}\right)-\gamma\left(1-\frac{\eta}{2},\frac{\alpha_{\text{abs}}b}{2}\right)\right].\end{aligned} \tag{I.7}$$

As a result, by plugging Eq. (I.7) back into Eq. (I.2), we can characterize the mean of aggregate

interference $\mathbb{E}_{\boldsymbol{r}}[I_k^{(l)}(\boldsymbol{r})]$ as follows:

$$\mathbb{E}_{\boldsymbol{r}}[I_k^{(l)}(\boldsymbol{r})] \geq \frac{2\lambda\pi a^2\Lambda\sqrt{\overline{\mathcal{P}}}\left(\frac{2}{\alpha_{\text{abs}}}\right)^{1-\frac{\eta}{2}}}{a^2-b^2}\left[\gamma\left(1-\frac{\eta}{2},\frac{\alpha_{\text{abs}}a}{2}\right)-\gamma\left(1-\frac{\eta}{2},\frac{\alpha_{\text{abs}}b}{2}\right)\right] \tag{I.8}$$

which is Eq. (5.19). Thus, we complete the proof for **Claim 1** in Theorem 8.

Claim 2. We can derive the variance of the aggregate interference $\text{Var}_{I_k^{(l)}}(\boldsymbol{r})$ for our proposed THz-band nano-communication schemes as follows:

$$\text{Var}_{I_k^{(l)}}(\boldsymbol{r}) = \mathbb{E}_{\boldsymbol{r}}\left[\left(I_k^{(l)}(\boldsymbol{r})\right)^2\right] - \left(\mathbb{E}_{\boldsymbol{r}}[I_k^{(l)}(\boldsymbol{r})]\right)^2 \tag{I.9}$$

where

$$\mathbb{E}_{\boldsymbol{r}}\left[\left(I_k^{(l)}(\boldsymbol{r})\right)^2\right] = \mathbb{E}_{\boldsymbol{r}}\left[\sum_{i=1,i\neq k}^{K+1}\mathcal{P}_i\mathcal{P}_{\text{total}}(r_i)+N_i(r_i)\right]+2\mathbb{E}_{\boldsymbol{r}}\left[\sum_{i=1,i\neq k}^{K+1}\sum_{j=1}^{i-1}\sqrt{\mathcal{P}_i\mathcal{P}_j\mathcal{P}_{\text{total}}(r_i)\mathcal{P}_{\text{total}}(r_j)}\right]. \tag{I.10}$$

To obtain the variance of aggregate interference by $\text{Var}_{I_k^{(l)}}(\boldsymbol{r})$, first we need to obtain the following equation:

$$\begin{aligned}\mathbb{E}_{\boldsymbol{r}}\left[\sum_{i=1,i\neq k}^{K+1}\mathcal{P}_i\mathcal{P}_{\text{total}}(r_i)\right] &= \mathbb{E}_{\boldsymbol{r}}\left[\sum_{i=1,i\neq k}^{K+1}\mathcal{P}_i\left(r_i\right)^{-\eta}G10^{\frac{\xi_i}{10}}S(f)\left(\frac{c}{4\pi f r_i}\right)^2 e^{-\alpha_{\text{abs}}r_i}\right] \\ &= \Lambda^2\mathbb{E}_{\boldsymbol{r}}\left[\sum_{i=1,i\neq k}^{K+1}\mathcal{P}_i 10^{\frac{\xi_i}{10}}\widetilde{F}(r_i)\right]\end{aligned} \tag{I.11}$$

where

$$\widetilde{F}(r_i) \triangleq (r_i)^{-\eta-2}e^{-\alpha_{\text{abs}}r_i}. \tag{I.12}$$

Since the transmission power $\mathcal{P}_i$ is upper-bounded by $\overline{\mathcal{P}}$, we can then obtain the conditional ex-

pectation function as follows:

$$\mathbb{E}_{\boldsymbol{r}}\left[\sum_{i=1,i\neq k}^{K+1}\mathcal{P}_i 10^{\frac{\xi_i}{10}}\widetilde{F}(r_i)\middle|\mathcal{K}=\kappa\right]=\kappa\mathbb{E}_{r_i}\left[\mathcal{P}_i 10^{\frac{\xi_i}{10}}\widetilde{F}(r_i)\right]$$
$$\geq \kappa\mathbb{E}_{r_i}\left[\mathcal{P}_i 10^{\frac{\xi_i}{10}}\right]\mathbb{E}_{r_i}\left[\widetilde{F}(r_i)\right]=\kappa\overline{\mathcal{P}}\mathbb{E}_{r_i}\left[\widetilde{F}(r_i)\right] \tag{I.13}$$

where

$$\begin{aligned}\mathbb{E}_{r_i}\left[\widetilde{F}(r_i)\right]&=\int_b^a (r_i)^{-\eta-2}e^{-\alpha_{\text{abs}}r_i}f_D(r_i)dr_i\\&=\frac{2}{a^2-b^2}\int_b^a (r_i)^{-\eta-1}e^{-\alpha_{\text{abs}}r_i}dr_i=\frac{2(\alpha_{\text{abs}})^{-\eta}}{a^2-b^2}\int_{b\alpha_{\text{abs}}}^{a\alpha_{\text{abs}}}(r_i)^{-\eta-1}e^{-r_i}dr_i\\&=\frac{2(\alpha_{\text{abs}})^{-\eta}}{a^2-b^2}\left[\gamma\left(-\eta,a\alpha_{\text{abs}}\right)-\gamma\left(-\eta,b\alpha_{\text{abs}}\right)\right].\end{aligned} \tag{I.14}$$

Using Eqs. (I.6), (I.11), and (I.14), we can obtain the following inequation:

$$\mathbb{E}_{\boldsymbol{r}}\left[\sum_{i=1,i\neq k}^{K+1}\mathcal{P}_i\mathcal{P}_{\text{total}}(r_i)\right]\geq\frac{2\lambda\pi a^2\Lambda^2\overline{\mathcal{P}}(\alpha_{\text{abs}})^{-\eta}}{a^2-b^2}\left[\gamma\left(-\eta,a\alpha_{\text{abs}}\right)-\gamma\left(-\eta,b\alpha_{\text{abs}}\right)\right]. \tag{I.15}$$

We also need to show that the following equations hold true:

$$\begin{aligned}\mathbb{E}_{\boldsymbol{r}}\left[\sum_{i=1,i\neq k}^{K+1}N_i(r_i)\right]&=\mathbb{E}_{\boldsymbol{r}}\left[\sum_{i=1,i\neq k}^{K+1}\left(N_{i,b}+N_{i,s}(r_i)\right)\right]=\sum_{i=1,i\neq k}^{K+1}N_{i,b}+\mathbb{E}_{\boldsymbol{r}}\left[\sum_{i=1,i\neq k}^{K+1}N_{i,s}(r_i)\right]\\&=\sum_{i=1,i\neq k}^{K+1}N_{i,b}+\mathbb{E}_{\boldsymbol{r}}\left[\sum_{i=1,i\neq k}^{K+1}S(f)\left(1-e^{-\alpha_{\text{abs}}r_i}\right)\left(\frac{c}{4\pi f r_i}\right)^2\right]\\&=\sum_{i=1,i\neq k}^{K+1}N_{i,b}+\Lambda^2\mathbb{E}_{\boldsymbol{r}}\left[\sum_{i=1,i\neq k}^{K+1}\widehat{F}(r_i)\right]\end{aligned} \tag{I.16}$$

where

$$\widehat{F}(r_i)\triangleq(r_i)^{-2}\left(1-e^{-\alpha_{\text{abs}}r_i}\right). \tag{I.17}$$

Similarly, we can obtain the conditional expectation function as follows:

$$\mathbb{E}_{\boldsymbol{r}|\mathcal{K}}\left[\sum_{i=1,i\neq k}^{K+1}\widehat{F}(r_i)\middle|\mathcal{K}=\kappa\right]=\kappa\mathbb{E}_{r_i}\left[\widehat{F}(r_i)\right] \tag{I.18}$$

where $\mathbb{E}_{\boldsymbol{r}|\mathcal{K}}[\cdot]$ represents conditional expectation operations and

$$\begin{aligned}\mathbb{E}_{r_i}\left[\widehat{F}(r_i)\right]&=\int_b^a (r_i)^{-2}\left(1-e^{-\alpha_{\text{abs}}r_i}\right)f_D(r_i)dr_i\\&=\frac{2}{a^2-b^2}\int_b^a\frac{1-e^{-\alpha_{\text{abs}}r_i}}{r_i}dr_i\\&=\frac{2}{a^2-b^2}\left[\log\left(\frac{a}{b}\right)-\text{Ei}\left(-\alpha_{\text{abs}}a\right)+\text{Ei}\left(-\alpha_{\text{abs}}b\right)\right].\end{aligned} \tag{I.19}$$

Similar to Eq. (I.15), we can obtain the following equation:

$$\mathbb{E}_{\boldsymbol{r}}\left[\sum_{i=1,i\neq k}^{K+1}\widehat{F}(r_i)\right]=\frac{2\lambda\pi a^2}{a^2-b^2}\left[\log\left(\frac{a}{b}\right)-\text{Ei}\left(-\alpha_{\text{abs}}a\right)+\text{Ei}\left(-\alpha_{\text{abs}}b\right)\right]. \tag{I.20}$$

Furthermore, due to the high density of wireless nano-networks, we assume that the distances r_i $(i=1,\ldots,K+1$ and $i\neq k)$ between its nano receiver and all interfering nano nodes are approximately the same. As a result, we get

$$\begin{aligned}\mathbb{E}_{\boldsymbol{r}}\left[\sum_{i=1,i\neq k}^{K+1}\sum_{j=1}^{i-1}\sqrt{\mathcal{P}_i\mathcal{P}_j\mathcal{P}_{\text{total}}(r_i)\mathcal{P}_{\text{total}}(r_j)}\right]&\geq\Lambda^2\mathbb{E}\left[\mathcal{K}\right]\mathbb{E}_{r_i}\left[\mathcal{P}_i 10^{\frac{\xi_i}{10}}\widetilde{F}(r_i)\right]\\&\geq\frac{2\lambda\pi a^2\Lambda^2\overline{\mathcal{P}}(\alpha_{\text{abs}})^{-\eta}}{a^2-b^2}\left[\gamma\left(-\eta,a\alpha_{\text{abs}}\right)-\gamma\left(-\eta,b\alpha_{\text{abs}}\right)\right].\end{aligned} \tag{I.21}$$

Therefore, plugging Eqs. (I.15) and (I.21) back into Eq. (I.10), we can obtain the following equa-

tion:

$$\mathbb{E}_{\boldsymbol{r}}\left[\left(I_k^{(l)}(\boldsymbol{r})\right)^2\right] \approx \frac{6\lambda\pi a^2\Lambda^2\overline{\mathcal{P}}(\alpha_{\text{abs}})^{-\eta}}{a^2-b^2}\left[\gamma\left(-\eta, a\alpha_{\text{abs}}\right) - \gamma\left(-\eta, b\alpha_{\text{abs}}\right)\right] + \sum_{i=1, i\neq k}^{K+1} N_{i,b} + \frac{2\lambda\pi a^2\Lambda^2}{a^2-b^2} \times \left[\log\left(\frac{a}{b}\right) - \text{Ei}\left(-\alpha_{\text{abs}}a\right) + \text{Ei}\left(-\alpha_{\text{abs}}b\right)\right]. \tag{I.22}$$

Consequently, substituting Eq. (I.22) back into Eq. (I.9), we can derive the approximate variance of aggregate interference $\text{Var}_{I_k^{(l)}}(\boldsymbol{r})$ as follows:

$$\text{Var}_{I_k^{(l)}}(\boldsymbol{r}) \approx \frac{6\lambda\pi a^2\Lambda^2\overline{\mathcal{P}}(\alpha_{\text{abs}})^{-\eta}}{a^2-b^2}[\gamma(-\eta, a\alpha_{\text{abs}}) - \gamma(-\eta, b\alpha_{\text{abs}})] + \sum_{i=1, i\neq k}^{K+1} N_{i,b} + \frac{2\lambda\pi a^2\Lambda^2}{a^2-b^2}\left[\log\left(\frac{a}{b}\right) - \text{Ei}\left(-\alpha_{\text{abs}}a\right) + \text{Ei}\left(-\alpha_{\text{abs}}b\right)\right] - \left(\frac{2\lambda\pi a^2 C}{a^2-b^2}\right)^2 \overline{\mathcal{P}}\left(\frac{2}{\alpha_{\text{abs}}}\right)^{2-\eta} \times \left[\gamma\left(1-\frac{\eta}{2}, \frac{\alpha_{\text{abs}}a}{2}\right) - \gamma\left(1-\frac{\eta}{2}, \frac{\alpha_{\text{abs}}b}{2}\right)\right]^2 \tag{I.23}$$

which is Eq. (5.21). Thus, we complete the proof for **Claim 2** in Theorem 8.

APPENDIX J

PROOF OF THEOREM 9

To derive the upper-bound given by Eq. (5.24) on the mutual information $I(\boldsymbol{x}_k^n, \boldsymbol{y}_k^n)$ given by Eq. (5.23) to accurately approximate the channel capacity $C(r_k, \mathcal{P}_k)$ given by Eq. (5.22), we need to proceed with the following four steps.

Step 1. We need to derive the conditional distribution function $P_{Y_k^n|X_k^n}\left(\boldsymbol{y}_k^n|\boldsymbol{x}_k^n\right)$ as follows:

$$P_{Y_k^n|X_k^n}\left(\boldsymbol{y}_k^n|\boldsymbol{x}_k^n\right) = \frac{1}{\left[2\pi\left(N_{I_k^{(l)}}(\boldsymbol{r}) + N_k(r_k)\right)\right]^{\frac{n}{2}}} \exp\left\{-\frac{\left\|\boldsymbol{y}_k^n - \mathbb{E}\left[I_k^{(l)}(\boldsymbol{r})\right]\mathbf{I}_n - \boldsymbol{x}_k^n\right\|^2}{2\left[N_{I_k^{(l)}}(\boldsymbol{r}) + N_k(r_k)\right]}\right\} \quad \text{(J.1)}$$

where $\|\cdot\|$ is the Euclidean norm and $\mathbf{I}_n$ is the identity matrix with size n.

Step 2. To derive the modified information density $\boldsymbol{i}(\boldsymbol{x}_k^n; \boldsymbol{y}_k^n)$, we apply the mean and variance of interference derived in Eqs. (5.19) and (5.21) and select the reference output distribution for the THz wireless channel as $Q_{Y_k^n}\left(\boldsymbol{y}_k^n\right) \sim \mathcal{N}\left(\mathbb{E}\left[I_k^{(l)}(\boldsymbol{r})\right]\mathbf{I}_n, \left(\mathcal{P}_k\mathcal{P}_{\text{total}}(r_k) + N_{I_k^{(l)}}(\boldsymbol{r}) + N_k(r_k)\right)\mathbf{I}_n\right)$.

Step 3. Using Eqs. (5.23) and (J.1), we derive the *modified information density* $\boldsymbol{i}(\boldsymbol{x}_k^n; \boldsymbol{y}_k^n)$ as

follows:

$$
\begin{aligned}
\boldsymbol{i}(\boldsymbol{x}_k^n;\boldsymbol{y}_k^n) = & \frac{1}{n}\log_2\Bigg\{\frac{\left[2\pi\left(\mathcal{P}_k\mathcal{P}_{\text{total}}(r_k)+N_{I_k^{(l)}}(\boldsymbol{r})+N_k(r_k)\right)\right]^{\frac{n}{2}}}{\left[2\pi\left(N_{I_k^{(l)}}(\boldsymbol{r})+N_k(r_k)\right)\right]^{\frac{n}{2}}}\exp\Bigg\{-\frac{\left\|\boldsymbol{y}_k^n-\mathbb{E}\left[I_k^{(l)}(\boldsymbol{r})\right]\mathbf{I}_n-\boldsymbol{x}_k^n\right\|^2}{2\left[N_{I_k^{(l)}}(\boldsymbol{r})+N_k(r_k)\right]}\Bigg\} \\
& \times\exp\Bigg\{\frac{\left\|\boldsymbol{y}_k^n-\mathbb{E}\left[I_k^{(l)}(\boldsymbol{r})\right]\mathbf{I}_n\right\|^2}{2\left[\mathcal{P}_k\mathcal{P}_{\text{total}}(r_k)+N_{I_k^{(l)}}(\boldsymbol{r})+N_k(r_k)\right]}\Bigg\}\Bigg\} \\
= & \frac{1}{n}\log_2\Bigg\{\frac{\left[2\pi\left(\mathcal{P}_k\mathcal{P}_{\text{total}}(r_k)+N_{I_k^{(l)}}(\boldsymbol{r})+N_k(r_k)\right)\right]^{\frac{n}{2}}}{\left[2\pi\left(N_{I_k^{(l)}}(\boldsymbol{r})+N_k(r_k)\right)\right]^{\frac{n}{2}}}\Bigg\}+\Bigg[\frac{\left\|\boldsymbol{y}_k^n-\mathbb{E}\left[I_k^{(l)}(\boldsymbol{r})\right]\mathbf{I}_n\right\|^2}{\mathcal{P}_k\mathcal{P}_{\text{total}}(r_k)+N_{I_k^{(l)}}(\boldsymbol{r})+N_k(r_k)} \\
& -\frac{\left\|\boldsymbol{y}_k^n-\mathbb{E}\left[I_k^{(l)}(\boldsymbol{r})\right]\mathbf{I}_n-\boldsymbol{x}_k^n\right\|^2}{N_{I_k^{(l)}}(\boldsymbol{r})+N_k(r_k)}\Bigg]\frac{(\log_2 e)}{2n} \\
= & \frac{1}{2}\log_2\left[\frac{\mathcal{P}_k\mathcal{P}_{\text{total}}(r_k)+N_{I_k^{(l)}}(\boldsymbol{r})+N_k(r_k)}{N_{I_k^{(l)}}(\boldsymbol{r})+N_k(r_k)}\right]+\frac{(\log_2 e)}{2n}\Bigg[\frac{\left\|\boldsymbol{y}_k^n-\mathbb{E}\left[I_k^{(l)}(\boldsymbol{r})\right]\mathbf{I}_n\right\|^2}{\mathcal{P}_k\mathcal{P}_{\text{total}}(r_k)+N_{I_k^{(l)}}(\boldsymbol{r})+N_k(r_k)} \\
& -\frac{\left\|\boldsymbol{y}_k^n-\mathbb{E}\left[I_k^{(l)}(\boldsymbol{r})\right]\mathbf{I}_n-\boldsymbol{x}_k^n\right\|^2}{N_{I_k^{(l)}}(\boldsymbol{r})+N_k(r_k)}\Bigg]. \qquad \text{(J.2)}
\end{aligned}
$$

Using Eq. (5.11), we obtain the following equation:

$$
\begin{aligned}
\boldsymbol{i}(\boldsymbol{x}_k^n;\boldsymbol{y}_k^n) = & \frac{1}{2}\log_2\left[\frac{\mathcal{P}_k\mathcal{P}_{\text{total}}(r_k)+N_{I_k^{(l)}}(\boldsymbol{r})+N_k(r_k)}{N_{I_k^{(l)}}(\boldsymbol{r})+N_k(r_k)}\right]+\frac{(\log_2 e)}{2n}\Bigg[\Bigg\|\sqrt{\mathcal{P}_{\text{total}}(r_k)}\boldsymbol{x}_k^n \\
& +\sum_{i=1,i\neq k}^{K+1}\sqrt{\mathcal{P}_{\text{total}}(r_i)}\boldsymbol{x}_i^n+\boldsymbol{n}_k-\mathbb{E}\left[I_k^{(l)}(\boldsymbol{r})\right]\mathbf{I}_n\Bigg\|^2\Bigg\{\mathcal{P}_k\mathcal{P}_{\text{total}}(r_k)+N_{I_k^{(l)}}(\boldsymbol{r})+N_k(r_k)\Bigg\}^{-1} \\
& -\left\|\sqrt{\mathcal{P}_{\text{total}}(r_k)}\boldsymbol{x}_k^n+\sum_{i=1,i\neq k}^{K+1}\sqrt{\mathcal{P}_{\text{total}}(r_i)}\boldsymbol{x}_i^n+\boldsymbol{n}_k-\mathbb{E}\left[I_k^{(l)}(\boldsymbol{r})\right]\mathbf{I}_n-\boldsymbol{x}_k^n\right\|^2 \\
& \times\Bigg\{N_{I_k^{(l)}}(\boldsymbol{r})+N_k(r_k)\Bigg\}^{-1}\Bigg]. \qquad \text{(J.3)}
\end{aligned}
$$

Step 4. Using Eqs. (5.23) and (J.3), we can derive an *upper-bound* on the mutual information

$I(\boldsymbol{x}_k^n, \boldsymbol{y}_k^n)$ as follows:

$$
\begin{aligned}
I(\boldsymbol{x}_k^n, \boldsymbol{y}_k^n) =& \mathbb{E}\left[\frac{1}{2}\log_2\left[\frac{\mathcal{P}_k\mathcal{P}_{\text{total}}(r_k)+N_{I_k^{(l)}}(\boldsymbol{r})+N_k(r_k)}{N_{I_k^{(l)}}(\boldsymbol{r})+N_k(r_k)}\right]+\frac{(\log_2 e)}{2n}\left\{\left\|\sqrt{\mathcal{P}_{\text{total}}(r_k)}\boldsymbol{x}_k^n\right.\right.\right.\\
&+\sum_{i=1,i\neq k}^{K+1}\sqrt{\mathcal{P}_{\text{total}}(r_i)}\boldsymbol{x}_i^n+\boldsymbol{n}_k-\mathbb{E}\left[I_k^{(l)}(\boldsymbol{r})\right]\mathbf{I}_n\Big\|^2\left\{\mathcal{P}_k\mathcal{P}_{\text{total}}(r_k)+N_{I_k^{(l)}}(\boldsymbol{r})+N_k(r_k)\right\}^{-1}\\
&-\left\|\sqrt{\mathcal{P}_{\text{total}}(r_k)}\boldsymbol{x}_k^n+\sum_{i=1,i\neq k}^{K+1}\sqrt{\mathcal{P}_{\text{total}}(r_i)}\boldsymbol{x}_i^n+\boldsymbol{n}_k-\mathbb{E}\left[I_k^{(l)}(\boldsymbol{r})\right]\mathbf{I}_n-\boldsymbol{x}_k^n\right\|^2\\
&\left.\left.\times\left\{N_{I_k^{(l)}}(\boldsymbol{r})+N_k(r_k)\right\}^{-1}\right\}\right]\\
\leq& \frac{1}{2}\log_2\left[\frac{\mathcal{P}_k\mathcal{P}_{\text{total}}(r_k)+N_{I_k^{(l)}}(\boldsymbol{r})+N_k(r_k)}{N_{I_k^{(l)}}(\boldsymbol{r})+N_k(r_k)}\right]+\frac{(\log_2 e)}{n}\left\{\mathbb{E}\left[\left\|\sqrt{\mathcal{P}_{\text{total}}(r_k)}\boldsymbol{x}_k^n\right\|^2\right.\right.\\
&+\left\|\sum_{i=1,i\neq k}^{K+1}\sqrt{\mathcal{P}_{\text{total}}(r_i)}\boldsymbol{x}_i^n-\mathbb{E}\left[I_k^{(l)}(\boldsymbol{r})\right]\mathbf{I}_n\right\|^2+\|\boldsymbol{n}_k\|^2\Big]\left\{\mathcal{P}_k\mathcal{P}_{\text{total}}(r_k)+N_{I_k^{(l)}}(\boldsymbol{r})+N_k(r_k)\right\}^{-1}\\
&-\mathbb{E}\left[\left\|\sqrt{\mathcal{P}_{\text{total}}(r_k)}\boldsymbol{x}_k^n\right\|^2+\left\|\sum_{i=1,i\neq k}^{K+1}\sqrt{\mathcal{P}_{\text{total}}(r_i)}\boldsymbol{x}_i^n-\mathbb{E}\left[I_k^{(l)}(\boldsymbol{r})\right]\mathbf{I}_n\right\|^2+\|\boldsymbol{n}_k\|^2+\|\boldsymbol{x}_k^n\|^2\right]\\
&\left.\times\left\{N_{I_k^{(l)}}(\boldsymbol{r})+N_k(r_k)\right\}^{-1}\right\}\\
=& \frac{1}{2}\log_2\left[\frac{\mathcal{P}_k\mathcal{P}_{\text{total}}(r_k)+N_{I_k^{(l)}}(\boldsymbol{r})+N_k(r_k)}{N_{I_k^{(l)}}(\boldsymbol{r})+N_k(r_k)}\right]-(\log_2 e)\left[\frac{\mathcal{P}_k\left[\mathcal{P}_{\text{total}}(r_k)+1\right]}{N_{I_k^{(l)}}(\boldsymbol{r})+N_k(r_k)}\right] \qquad \text{(J.4)}
\end{aligned}
$$

which is Eq. (5.24), completing the proof for Theorem 9.

APPENDIX K

PROOF OF THEOREM 10

To derive the upper-bound on the channel dispersion $V(r_k, \mathcal{P}_k)$, we need to proceed with the following two steps.

Step 1. We start with variance of the modified information density $\boldsymbol{i}(\boldsymbol{x}_k^n; \boldsymbol{y}_k^n)$ as in the following equation:

$$V(r_k, \mathcal{P}_k) = \text{Var}\left[\boldsymbol{i}(\boldsymbol{x}_k^n; \boldsymbol{y}_k^n)\right] = \frac{1}{n}\text{Var}\left[\log_2\left(\frac{P_{Y_k^n|X_k^n}\left(\boldsymbol{y}_k^n|\boldsymbol{x}_k^n\right)}{Q_{Y_k^n}\left(\boldsymbol{y}_k^n\right)}\right)\right]$$
$$\leq \frac{2}{n}\Big\{\text{Var}\left[\log_2\left(P_{Y_k^n|X_k^n}\left(\boldsymbol{y}_k^n|\boldsymbol{x}_k^n\right)\right)\right] + \text{Var}\left[\log_2\left(Q_{Y_k^n}\left(\boldsymbol{y}_k^n\right)\right)\right]\Big\} \tag{K.1}$$

where Var$[\cdot]$ represents the variance operation.

Step 2. We can apply the Poincará inequality to derive the following equation:

$$\text{Var}\left[\log_2\left(P_{Y_k^n|X_k^n}\left(\boldsymbol{y}_k^n|\boldsymbol{x}_k^n\right)\right)\right] \leq \mathbb{E}\left[\left\|\nabla \log_2\left(P_{Y_k^n|X_k^n}\left(\boldsymbol{y}_k^n|\boldsymbol{x}_k^n\right)\right)\right\|^2\right] \tag{K.2}$$

where ∇ is the Nabla operator. Then, to calculate the function $\nabla \log_2 \left(P_{Y_k^n|X_k^n}\left(\boldsymbol{y}_k^n|\boldsymbol{x}_k^n\right)\right)$, we have

$$\begin{aligned}
\nabla \log_2 \left(P_{Y_k^n|X_k^n}\left(\boldsymbol{y}_k^n|\boldsymbol{x}_k^n\right)\right) &= \frac{(\log_2 e)}{P_{Y_k^n|X_k^n}\left(\boldsymbol{y}_k^n|\boldsymbol{x}_k^n\right)} \nabla P_{Y_k^n|X_k^n}\left(\boldsymbol{y}_k^n|\boldsymbol{x}_k^n\right) \\
&= \frac{(\log_2 e)}{P_{Y_k^n|X_k^n}\left(\boldsymbol{y}_k^n|\boldsymbol{x}_k^n\right)} \sum_{m=1}^{M} \Bigg\{ \frac{1}{M} \left[2\pi \left(N_{I_k^{(l)}}(\boldsymbol{r}) + N_k(r_k)\right)\right]^{-\frac{n}{2}} \\
&\quad \times \nabla \exp\left\{ -\frac{\|\boldsymbol{y}_k^n - \mathbb{E}\left[I_k^{(l)}(\boldsymbol{r})\right] \mathbf{I}_n - \boldsymbol{x}_k^n(m)\|^2}{2\left[N_{I_k^{(l)}}(\boldsymbol{r}) + N_k(r_k)\right]} \right\} \Bigg\} \\
&= \frac{(\log_2 e)}{P_{Y_k^n|X_k^n}\left(\boldsymbol{y}_k^n|\boldsymbol{x}_k^n\right)} \sum_{m=1}^{M} \Bigg\{ \frac{1}{M} \left[2\pi \left(N_{I_k^{(l)}}(\boldsymbol{r}) + N_k(r_k)\right)\right]^{-\frac{n}{2}} \\
&\quad \times \left(\boldsymbol{x}_k^n(m) + \mathbb{E}\left[I_k^{(l)}(\boldsymbol{r})\right] \mathbf{I}_n - \boldsymbol{y}_k^n\right) \\
&\quad \times \exp\left\{ -\frac{\left\|\boldsymbol{y}_k^n - \mathbb{E}\left[I_k^{(l)}(\boldsymbol{r})\right] \mathbf{I}_n - \boldsymbol{x}_k^n(m)\right\|^2}{2\left[N_{I_k^{(l)}}(\boldsymbol{r}) + N_k(r_k)\right]} \right\} \Bigg\} \\
&= (\log_2 e) \left\{ \mathbb{E}\left[\boldsymbol{x}_k^n|\boldsymbol{y}_k^n\right] + \mathbb{E}\left[I_k^{(l)}(\boldsymbol{r})\right] \mathbf{I}_n - \boldsymbol{y}_k^n \right\} \qquad \text{(K.3)}
\end{aligned}$$

where $\boldsymbol{x}_k^n(m)$ is the encoded signal from message $m \in \mathcal{M}$ with length n at nano transmitter k. Let us define:

$$\widehat{\boldsymbol{x}}_k^n \triangleq \mathbb{E}\left[\boldsymbol{x}_k^n|\boldsymbol{y}_k^n\right]. \qquad \text{(K.4)}$$

Accordingly, using the average power constraint, we can obtain the following equation:

$$\begin{aligned}
\text{Var}\left[\log_2 \left(P_{Y_k^n|X_k^n}\left(\boldsymbol{y}_k^n|\boldsymbol{x}_k^n\right)\right)\right] &\leq (\log_2 e)^2 \mathbb{E}\left[\left\|\widehat{\boldsymbol{x}}_k^n + \mathbb{E}\left[I_k^{(l)}(\boldsymbol{r})\right] \mathbf{I}_n - \boldsymbol{y}_k^n\right\|^2\right] \\
&\leq 2(\log_2 e)^2 \left\{ \mathbb{E}\left[\|\widehat{\boldsymbol{x}}_k^n\|^2\right] + \mathbb{E}\left[\left\|\boldsymbol{y}_k^n - \mathbb{E}\left[I_k^{(l)}(\boldsymbol{r})\right]\right\|^2\right] \right\} \\
&= 2(\log_2 e)^2 \left\{ n\mathcal{P}_k + n\left[N_{I_k^{(l)}}(\boldsymbol{r}) + N_k(r_k)\right] \right\} \\
&= 2n(\log_2 e)^2 \left[\mathcal{P}_k + N_{I_k^{(l)}}(\boldsymbol{r}) + N_k(r_k)\right]. \qquad \text{(K.5)}
\end{aligned}$$

Similarly, we can derive the function Var $\left[\log_2\left(Q_{Y_k^n}\left(\boldsymbol{y}_k^n\right)\right)\right]$ as follows:

$$\text{Var}\left[\log_2\left(Q_{Y_k^n}\left(\boldsymbol{y}_k^n\right)\right)\right] \leq 2n(\log_2 e)^2\left[\mathcal{P}_k + N_{I_k^{(l)}}(\boldsymbol{r}) + N_k(r_k)\right]. \tag{K.6}$$

Therefore, plugging Eqs. (K.5) and (K.6) back into Eq. (K.1), we get:

$$V(r_k, \mathcal{P}_k) \leq 8n(\log_2 e)^2\left[\mathcal{P}_k + N_{I_k^{(l)}}(\boldsymbol{r}) + N_k(r_k)\right] \tag{K.7}$$

which is Eq. (5.25), completing the proof for Theorem 10.

APPENDIX L

PROOF OF THEOREM 12

To derive the closed-form solutions to the optimization problem $\mathbf{P_{17}}$, we can formulate its Lagrange function, denoted by J, as follows:

$$J = n\left[C(r_k,\mathcal{P}_k) - \sqrt{\frac{V(r_k,\mathcal{P}_k)}{n}}Q^{-1}(\epsilon_k)\right] + \lambda_1\left(\mathcal{P}_k^{\max} - \mathcal{P}_k\right) + \lambda_2\left(\mathcal{P}_k - \mathcal{P}_k^{\min}\right) \tag{L.1}$$

where λ_1 and λ_2 are the Lagrange multipliers associated with the EH constraints C12 and C13 which are specified by Eqs. (5.36) and (5.37), respectively, in optimization problem $\mathbf{P_{15}}$. Then, we can obtain the following Karush-Kuhn-Tucker (KKT) conditions:

$$\begin{cases} \frac{\partial J}{\partial \mathcal{P}_k} = \frac{n\mathcal{P}_{\text{total}}(r_k)}{2(\log 2)\left[\mathcal{P}_k\mathcal{P}_{\text{total}}(r_k)+N_{I_k^{(l)}}(\boldsymbol{r})+N_k(r_k)\right]} - n(\log_2 e)\left[\frac{\mathcal{P}_{\text{total}}(r_k)+1}{N_{I_k^{(l)}}(\boldsymbol{r})+N_k(r_k)}\right] - \frac{\sqrt{2n}(\log_2 e)Q^{-1}(\epsilon_k)}{\sqrt{\mathcal{P}_k+N_{I_k^{(l)}}(\boldsymbol{r})+N_k(r_k)}} - \lambda_1+\lambda_2 \\ \qquad = 0; \\ \lambda_1, \lambda_2 > 0. \end{cases} \tag{L.2}$$

Using the first part of Eq. (L.2), we can obtain the following equation:

$$\begin{aligned} &\frac{n\mathcal{P}_{\text{total}}(r_k)}{2\left[\mathcal{P}_k\mathcal{P}_{\text{total}}(r_k) + N_{I_k^{(l)}}(\boldsymbol{r}) + N_k(r_k)\right]} - \frac{\sqrt{2n}Q^{-1}(\epsilon_k)}{\sqrt{\mathcal{P}_k + N_{I_k^{(l)}}(\boldsymbol{r}) + N_k(r_k)}} \\ &\quad = (\log 2)(\lambda_1 - \lambda_2) + n\left[\frac{\mathcal{P}_{\text{total}}(r_k)+1}{N_{I_k^{(l)}}(\boldsymbol{r}) + N_k(r_k)}\right]. \end{aligned} \tag{L.3}$$

To derive the optimal power allocation policy for nano transmitter k, we prove **Claim 1**, **Claim 2**, and **Claim 3**, respectively, for this theorem as follows.

Claim 1. Considering the high-SINR regime, we have $\mathcal{P}_k\mathcal{P}_{\text{total}}(r_k) \gg N_{I_k^{(l)}}(\boldsymbol{r}) + N_k(r_k)$. Since

$\mathcal{P}_{\text{total}}(r_k) < 1$, we can obtain:

$$\mathcal{P}_k \gg N_{I_k^{(l)}}(\boldsymbol{r}) + N_k(r_k). \tag{L.4}$$

As a result, we can convert Eq. (L.3) in the high-SINR regime into the following equation:

$$\frac{n}{2\mathcal{P}_k} - \frac{\sqrt{2n}Q^{-1}(\epsilon_k)}{\sqrt{\mathcal{P}_k}} = (\log 2)\,(\lambda_1 - \lambda_2) + n\left[\frac{\mathcal{P}_{\text{total}}(r_k)+1}{N_{I_k^{(l)}}(\boldsymbol{r}) + N_k(r_k)}\right]. \tag{L.5}$$

By solving Eq. (L.5), we obtain the optimal power allocation policy $\mathcal{P}_k^{\text{OPT,H}}$ for the high-SINR regime as given in Eq. (5.51).

Claim 2. In the low-SINR regime, we have $\mathcal{P}_k\mathcal{P}_{\text{total}}(r_k) \ll N_{I_k^{(l)}}(\boldsymbol{r}) + N_k(r_k)$. As a result, we can convert Eq. (L.3) in the low-SINR regime into the following equation:

$$\frac{n\mathcal{P}_{\text{total}}(r_k)}{2\left[N_{I_k^{(l)}}(\boldsymbol{r}) + N_k(r_k)\right]} - \frac{\sqrt{2n}Q^{-1}(\epsilon_k)}{\sqrt{\mathcal{P}_k + N_{I_k^{(l)}}(\boldsymbol{r}) + N_k(r_k)}} = (\log 2)\,(\lambda_1-\lambda_2)+n\left[\frac{\mathcal{P}_{\text{total}}(r_k)+1}{N_{I_k^{(l)}}(\boldsymbol{r})+N_k(r_k)}\right]. \tag{L.6}$$

By solving Eq. (L.6), we can obtain the optimal power allocation policy $\mathcal{P}_k^{\text{OPT,L}}$ for the low-SINR regime as given in Eq. (5.53).

Claim 3. If the SINR falls into the medium-SINR regime between the high-SINR and low-SINR regimes, specified by Eqs. (5.50) and (5.52), respectively, then using Eq. (L.3), we can obtain the following equation:

$$\begin{aligned}&\frac{n\mathcal{P}_{\text{total}}(r_k)}{2\left[\mathcal{P}_k\mathcal{P}_{\text{total}}(r_k) + N_{I_k^{(l)}}(\boldsymbol{r}) + N_k(r_k)\right]} - \frac{\sqrt{2n\mathcal{P}_{\text{total}}(r_k)}Q^{-1}(\epsilon_k)}{\sqrt{\mathcal{P}_k\mathcal{P}_{\text{total}}(r_k) + N_{I_k^{(l)}}(\boldsymbol{r}) + N_k(r_k)}}\\ &\quad= (\log 2)\,(\lambda_1 - \lambda_2) + n\left[\frac{\mathcal{P}_{\text{total}}(r_k)+1}{N_{I_k^{(l)}}(\boldsymbol{r}) + N_k(r_k)}\right].\end{aligned} \tag{L.7}$$

By solving the above Eq. (L.7), we can obtain the optimal power allocation policy for the medium-SINR regime $\mathcal{P}_k^{\text{OPT,M}}$ as given in Eq. (5.54). Therefore, we complete the proof for Theorem 12.